M. Stive

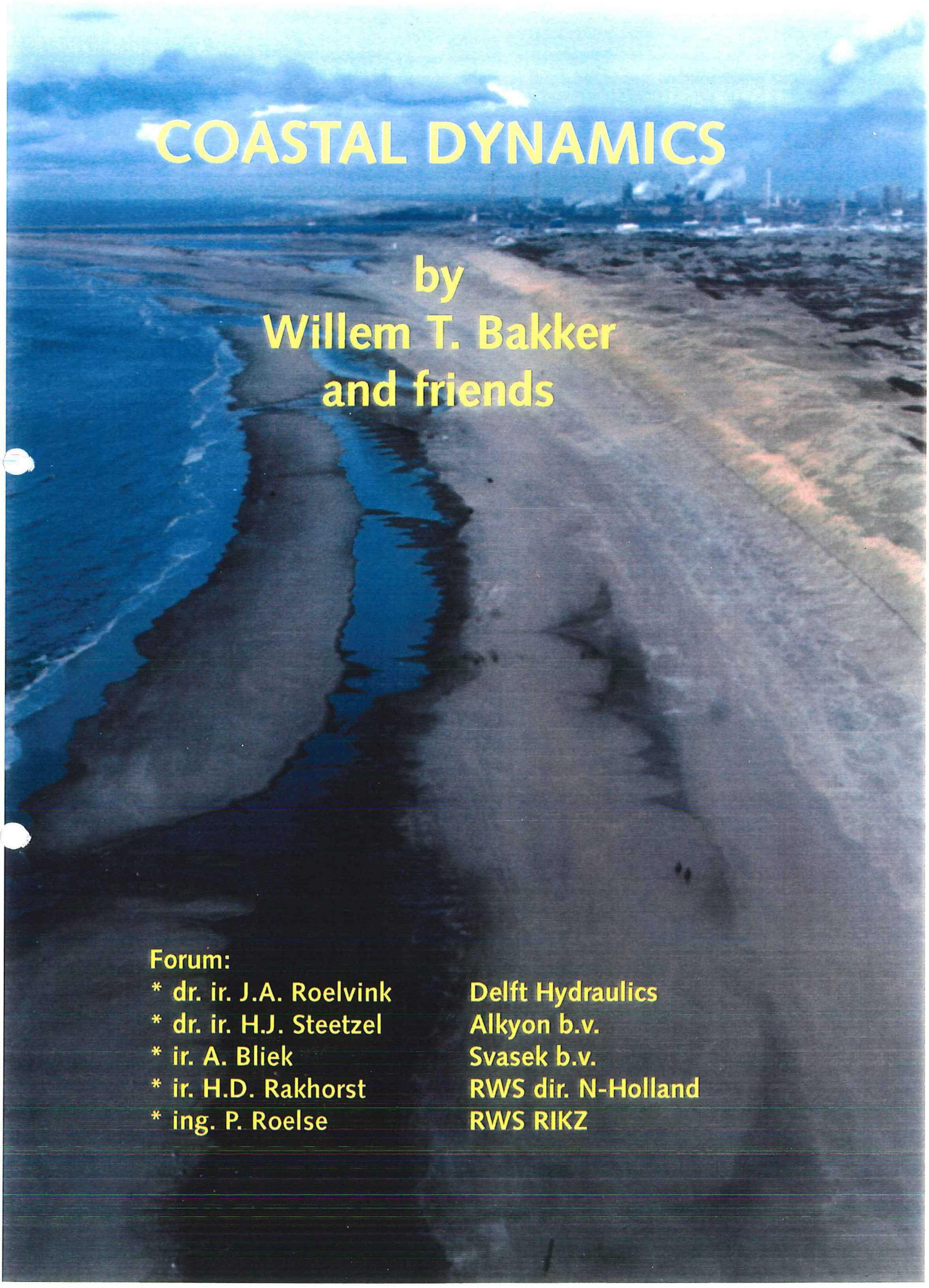

COASTAL DYNAMICS

by Willem T. Bakker and friends

Forum:

* dr. ir. J.A. Roelvink	Delft Hydraulics
* dr. ir. H.J. Steetzel	Alkyon b.v.
* ir. A. Bliek	Svasek b.v.
* ir. H.D. Rakhorst	RWS dir. N-Holland
* ing. P. Roelse	RWS RIKZ

Table of Contents

Preface

When Lord created Man, he created two species:
The kind which listens to you;
The kind which does not listen to you.

Maybe your feeling is the same as mine, that species A is rather rare compared to B and your joy when you meet the A-kind can be compared with the one of an ornithologist, finding a rare species. Still, reviewing a human life time, I think I may be grateful for the number of findings.

Mostly, when they met, they said: "Listen, Wim, explaining something to someone is like showing your house to some people. You should take your guest by his hand, showing him the entrance first, and then...".
After that, muttering they moved to their desk and started to write; they wrote about what they thought I thought, or about what they thought I should think on things, if I had the time to think about those things. And, because they were intelligent people (per definition) what they wrote was always better than I could have thought.
In this way species A and I wrote many papers together.

Given the opportunity to organize a meeting for the A-species (mostly new findings; young people) and to tell them about the thoughts their predecessors and I had together, I decided to staple a number of former papers.
I edited those in this way, that I tried to filter out duplications. and that I made links.
In fact, all my friends together built a house for me, in which I felt myself very much at home. The aim of the present book is to show this house rather than their individual performances. Whether correct or not, whether outdated or not, it has one definite characteristic, in plain European: "Es ist aus einem Guss".
I remember a frowning remark on the title of these notes: "Coastal Dynamics? Can't you be more specific?"
The answer is: "This is Coastal Dynamics by Willem T.Bakker and friends". In the Introduction I shall try to show the limitations more verbalistic.

I should give the builders the credit they owe. I really tried to: at the end of this preface I made an alphabetic list of first-authors or co-authors of the stapled papers.
However, not everything is co-production and these notes contain as well information not published before.

- Still, acknowledgment to the authors is not enough. Part of the A-species is A-species by appointment or by profession.
Writing on Coastal Engineering as an engineer of Rijkswaterstaat means interference with many people and your work could not be carried out without the support of many, mostly unnamed people. The same is the case at Universities. There is the direct support of the people, who make drawings for you or mark your lips.
I should name the whole staff of the former Department of Coastal Research of the former Directorate for Water Management and Hydraulic Research of the Rijkswaterstaat.
Many of the drawings in this booklet, Mr.Dofferhoff, originate from their work. I still remember the precious writing of my many formulas in my former reports by Ellen Brans; those reports are at the basis of the present lectures.
Part of this book consists of class notes made during my stay as Visiting Professor at the University of Hawaii. Thank you, Warren Bucher; thank you Gary Mocke, thank you Edith Katada and your staff for the work you did.
And how could I have delivered this work without the help of Edwin Elias (doing the Word processing) and Linda van Veen (translating some parts in English) and of Mark Voorendt, a super wizard spelling all the Word Wizards. Those Word Wizards put things on my laserprinter I never wanted to.

But I should like to honor as well the numerous skippers and observers on the measuring vessels and behind the water leveling apparatus. Names like Glim, Vonk, Blokland, Scheers, Goedegebuure [1] cross my mind.

Figure 1 is to honor people like them: generally the brand of, what I would call "Rijkswaterstaat people": sturdy, reliable, no fuss [2].

Figure 1

Chapter 2 is derived from three papers [2.37],[2.57.] and [2.61]. Ch.3 (translated by Gary Mocke) originates from the Dutch text of the course "De Dynamica van Kusten" on Delft Univ. of Technology, given by me, apart from sect 3.4 (refer to Smit [3.42]). Ch.4 has been published in [4.37]; (cf. [4.20.] and [4.36] as well). Sect 5.1 is a report of Delft Hydraulics (special thanks to Kees Hulsbergen) [5.1]) . Refer to [.] with respect to Sect.5.2.2 and to [.] concerning subsect. 5.2.3 and 5.2.4. Subsect.5.2.5 originates from ICCE'90 [.] and 5.2.6 from the NOURTEC study [.]. The evaluation of the line theories (ch 6) is new. Ch.7 gives background concepts for ch.8 and 9, last-mentioned chapters being a publication on the Plymouth conference on Coastal Dynamics [.].. The background , ch.7 (coastal dynamics as a diffusion problem) has not been published before. Chapter 10 again contains three papers, i.e. [.], [.] and [.]..

Putting the co-authors of the various papers quoted above in alphabetic order, the result is:
Agema; V.d.Biezen; Bilse; V Bochove; Dijkman; Heemink; Hulsbergen; Joustra; V.d.Kerk; Kersting; Klein Breteler; Knaapen; Niemeyer; v.Overeem; Pylarczyk; Roos; Smit; Speekenbrink; v.Veghel; de Vroeg.; de Vriend, (last but not least).
Still, this list does unjustice to a number of people, who had either an essential part in underlying reports, or by papers, not directly cited here. I would like to mention specially Edelman [.], Svasek [.], V.d.Meulen [.], ten Hoopen [.], Casteleyn [.], Opdam [.], Jallah [.], Bult [.], Dijkstra [.]

Finally, I would like to stress, that this report and this lecture series would not have been possible without the logistic and financial support of the Rijkswaterstaat (prof.dr.ir. J.Dronkers) and Delft University of Technology (prof. ir. K.d'Angremond).

[1] Apologies to the many people, which were in my mind when I wrote "Unnamed People" and which will be still remain unnamed after the publishing of this book.
[2] Figure 1 is a drawing from Elsevier (by Bantzinger) from many years ago.

1. Introduction

The solving of coastal problems will remain for years rather an art than a knowledge, with the slogan: 'the art of engineering is to get sufficient conclusions from insufficient data". However also art needs skill, and a mathematical theory; which clarifies in an exact way the implications of several schematizations of reality, may provide a part of this skill. At the moment only several aspects of the processes, which occur in nature can be schematized and translated into a mathematical theory. In the transition of the real prototype to the mathematical model the danger is hidden, to concentrate on an insignificant feature, which gives pseudo exact results. This can be avoided by active knowledge of the prototype and carrying out measurements in prototype and hydraulic models , from which a "smoothing of data" can result. It is cheaper and faster to consider only one of the three aspects: prototype, theory and laboratory, however, often only a combination of all of these aspects reveals the truth. The theory indicates pertinent contradictions in the measurements, but measurements in prototype are necessary to keep the attention on invalid schematization.

This book deals on "Coastal Dynamics", which will be defined in a narrow sense as a mathematical theory, which starts from given equations of motion for the sediment, which leads with the continuity equation and given boundary conditions to a calculated (eventually schematized) coastal topography, which is generally a function of time. This is clearly analogous to aero- and hydrodynamics, thermo-dynamics, hydrology and other related fields. The subject of this book, however, covers only a specific part of the Coastal Dynamics. It is based upon the notion of old masters, that for a manager the back-side of a cigar-box should be large enough to evaluate all the information and anti-information which is poured over him. For instance: statements, based upon high-tech number-crunching can find a sad end when those do not match large-scale continuity. Think for instance of tidal computations, in which time-varying boundary conditions (shoals which emerge above water level during a part of the tide) are not reproduced accurately enough.

The positive role of refined numerical techniques on solving problems in coastal dynamics should be stressed. However, one will not find much about it in this book. Emphasis is on physics, rather than on mathematics. It is meant for coastal managers, to inspire them, to enable them to put sensible questions and, if necessary, to say: "Oh, no sir".
The theory would be sterile without a consideration about the validity of the equation of motion, so much the more, while these equations of motion are not as evident, straight-forward and single- valued as for instance the Euler - equations in hydrodynamics.
The Newtonian laws are not quite sufficient for the computation of the sediment motion, because the motion of grains is subject to stochastic processes as the shape of the grains, the shape of the granular bed surface, turbulence, irregular wave motion etc.
In modern sophisticated computermodels a physical approach going far into details is possible, this includes the consideration of water and sand apart from each other, investigation of turbulent and viscous forces on the grains, and calculation of the sediment motion.

This is a difficult and tiresome way, which has to be followed and will give finally the best results. However, the building of constructions cannot wait for that, as it has not done in the past and therefore a short-cut from theory to practice has to be made, which involves the use of experimental data. This includes entirely the loss of the paradise of exactness. As the accuracy of the experimental data is very poor, this is a serious draw-back. Instead of the real equations of motion substitutes have- to be chosen and when it is not carefully examined, if and when these assumed equations of motion are valid, the mathematical theory is just an escape from reality.

In the mathematical theory, all constants and variables are indicated by symbols and it is suggested, that the numerical value of many of these constants can be found from prototype data. Without a discussion about at least the order of magnitude of these constants. the theory is no more than a start for future research.

Under coastal dynamics in a broader sense also these discussions about the validity of the equations of motion and the order of magnitude of the assumed constants will be included. In this book the sediment transport formulae which are used are not thoroughly discussed. The coastal dynamics, as presented in this course provides a far from complete theory.

The aim is threefold:

- It is a start for future research;
- it leads to qualitative conclusions about the effect of coastal constructions;
- some of the results are already available for practical computations.

Although based upon universal physics, applications treated are more or less tailor made for Dutch circumstances. The same holds for schematizations used.
Chapter 2 gives an overview of the Dutch coast. The papers, on which it is based upon, are written for a broad public and thus sometimes might give more basics than necessary for most of the present readers.
Chapter 3 gives (at this moment more or less classical) line theory. Ch.4 to 6 (determination coastal constants; experimental verification (laboratory and nature) and evaluation) try to expose, whether nature knows coastal dynamics.
In ch.7 theory is generalized, by taking line theory as a specific case of diffusitivity theory. Ch.8 deals with modern ways of data-assimilation in theory. In ch.9 the ideas on longshore and cross-shore diffusitivity are summarized.
Where the former chapters mainly deal with uninterrupted coasts (apart from single discontinuities like harbor moles or groins, in ch.10 some ideas are exposed concerning interaction of delta's and tidal basins: an important subject for the Netherlands, as a large part of the coast consists of tidal lagoons and estuaries (ch.2.1)..

As mentioned in the preface, in this book coastal dynamics is considered from one viewpoint. Thus the attention should be drawn on the appendix, in which a number of Dutch coastal specialists give additional information and thus can deliver the three-dimensional view.

2. The Dutch coast: a coastal engineering view

2.1 General

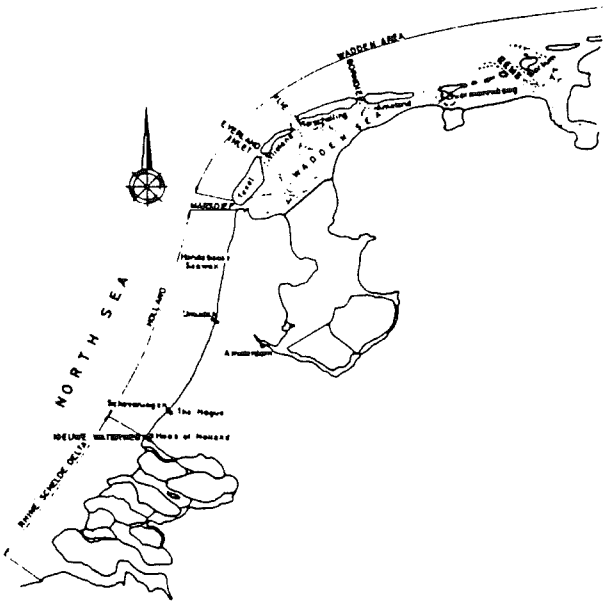

The dutch coast can be divided into three parts (fig 2-1)

- the Rine-Scheldt Delta
- the uninterrupted coast of Holland
- the Wadden area

Figure 2-1: The Dutch coast

It is a sandy coast ($D_m \approx 200\ \mu$); the tidal range varies between 4m near the Belgian border, down to 1.5 m near Hook of Holland, to 1.3 m near Den Helder and up to 2.2 m near the German Island Borkum. The tidal channel systems in the Rhine-Scheldt delta and that of the inlets between the Wadden Islands in the North have quite a different shape, since the tidal bassins are quite different. In the south the basins are rectangular with an open short side towards the sea and in the North they are rectangular with the long side parallel with the coast-line; this side is bordered by the Wadden Islands with narrow inlets in between. Therefore the Wadden coast can be compared with lagoon coasts, as those occur in many parts of the world. The Wadden Sea is a tidal flat, which is submerged during every high tide.

The main purpose of this chapter is to supply data, to enable international comparison. This chapter gives a summary of many reports of regional study departments of Rijkswaterstaat, made over a period of about 50 years. Amongst the former papers, covering the same subject, special attention should be given to Wentholt (1912) [2], who investigated in particular the effect of groynes, Van Veen (1936) [3], [4], who dealt with the origin of the Dutch coast and the shape of the tidal channels, Van Bendegom [5], who investigated the hydraulic laws for the motion of the tidal channels, Van Straaten [6], who considered the directional effects of winds, waves and currents, and concluded that the sand drift must be strong (west to east) along the northern barrier islands and small between Katwijk and Texel, Edelman and Eggink [7], who drew morphological conclusions from the curvature of the coast. Per Bruun and Gerritsen [8] dealt with the cross section of gullies and the stability of coastal inlets. Bijker and Svasek [9]gave a treatise about IJmuiden harbour. The present chapter gives more recent data than Wentholt. The conclusions of Van Veen, Van Straaten, Edelman and Eggink are reviewed in the light of "modern" theories about sand transport of CERC, Bijker and Svasek, making use of tidal computations.

The eldest Dutch coastal data is data concerning the site of the coastline, measured since 1850 already. The measurements are discussed in sect.2.2. Especially is focused on the effect of harbor moles (sect. 2.2.1) and on the effect of groins (2.2..2)
Since ca. 1960 yearly the whole coastal topography is monitored; as described in sect. 2.3. Apart from the morphological behavior of harbor moles, also the behavior of breaker bars

can be investigated in this way. Also, the order of magnitude of the cross-shore transport can be estimated. The magnitude of the longshore transport (also taking the effect of tides into consideration) along the Holland coast is treated in sect.2.4. A quite different effect of tides may be expected near an inlet. The general idea will be exposed in sect 2.5; an elaboration for the Wadden area is given in sect.2.6. and for the Delta area in sect.2.7..

2.2 150 years of beach measurements

Figure 2-2 and 2-3 show the erosion and accretion of the low-tide line, the high-tide line and the dune foot in periods of 10 year. First the 10-year average of each of these lines was determined, for instance 1856-1865; the distance between two successive 10-year averages is plotted in fig. 2-2 and 2-3. The positions of groynes, seawalls or harbour moles are shown and their dates of construction are also indicated.

2.2.1 The effect of harbor moles

The area of the Holland coast (fig. 2-2) has been highly influenced by the building of the harbour moles of Hook of Holland and IJmuiden in 1870. The low-tide line shows the influence of climatologic changes [6]; the overall picture is a large amount of erosion between 1860 and 1880 and accretion between 1880 and 1900. These periodical changes very strongly attenuate in the line of the dune foot and here one finds the general trend as indicated by Edelman and Eggink [7] , i.e. a general accretion of ½ m/year, with erosion near Hook of Holland and Den Helder (fig. 4). The Hondbossche Seawall at the moment lies much further seaward than the adjacent dunes because of the erosion of these dunes.

The influence of the harbour moles (original length 1400 m) at IJmuiden, built in 1870 is shown in detail in fig. 2-5. Fig. 2-2 shows that the low-tide line and high-tide line near IJmuiden reach a point of stability about 1900, but that the dune foot changes up to 1930. Fig. 2-5 gives a plan view of the 5-years average of the low-tide and high-tide lines (seaward scale exaggerated with respect to the longshore scale). The total gain of sand was $9 \cdot 10^6$ m^3 to the North and $6 \cdot 10^6$ m^3 to the South of the IJmuiden harbour moles [9]. In 1965 the harbour moles were lengthened to 3000 m. On the right hand side of fig. 2-5 the change of the mean of the low-tide and high-tide lime since 1965 is shown. Now the accretion on the South side is more than on the North side. Although a changing of the wave climate may have had an effect[6], [9], the fact that at the moment an extensive area with only small currents prevents the entrainment of material from the surf zone around the head of the mole, must be important.

The changes of the Wadden Islands are shown in fig. 2-3. The change at the ends are large compared to the changes is the middle of the island., partly due to the changes in the channel-systems in the inlets; the (total) sedimenttation of a channel may sometimes have the effect that a shoal grows onto the end of an island. After that, a sandwave along the coast is generated subsect. 5.2.2. The relatively large erosion on both ends of Texel is obvious. We shall return to this subject.

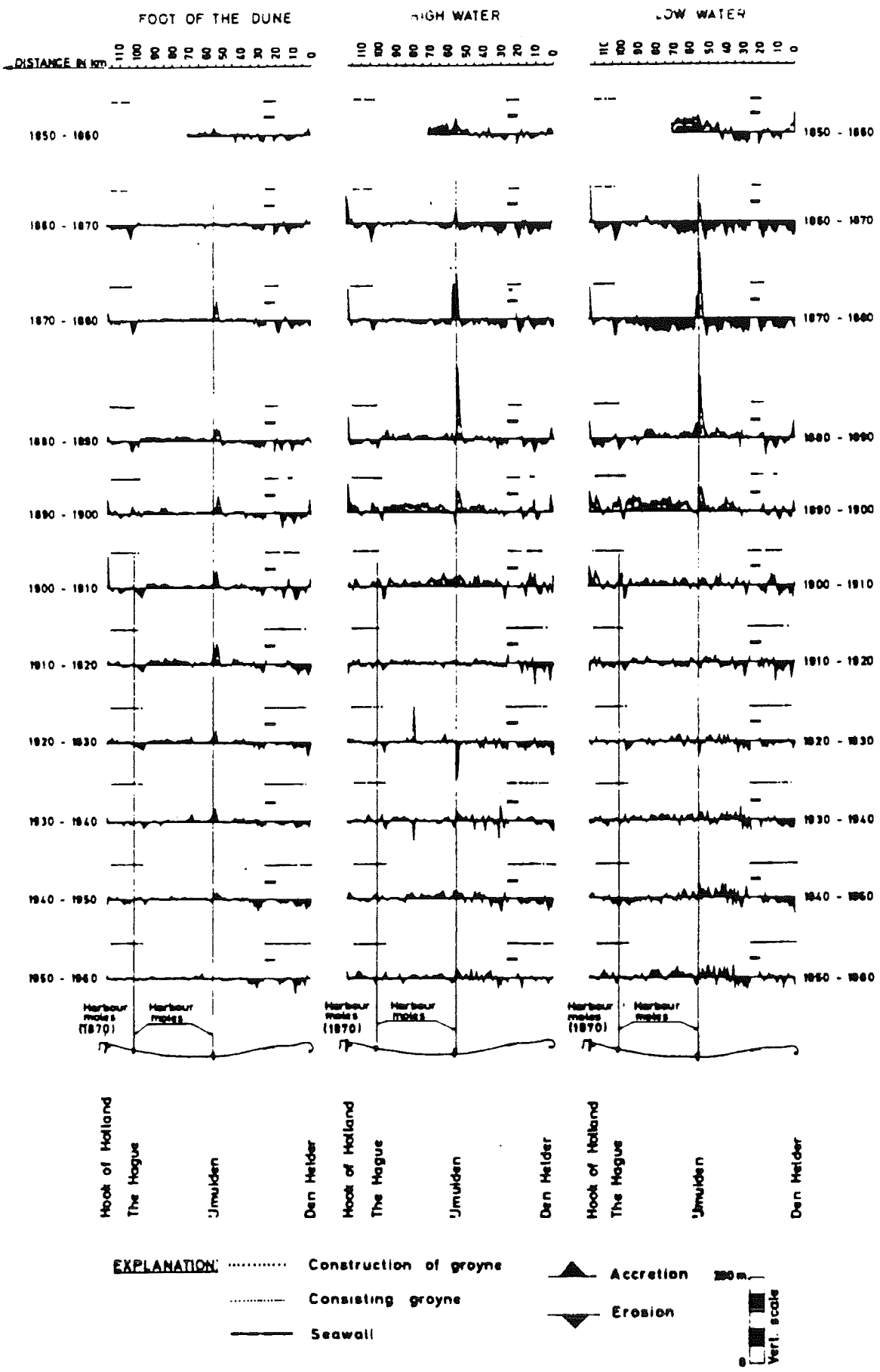

Figure 2-2: Accretion and erosion of the coast of Holland

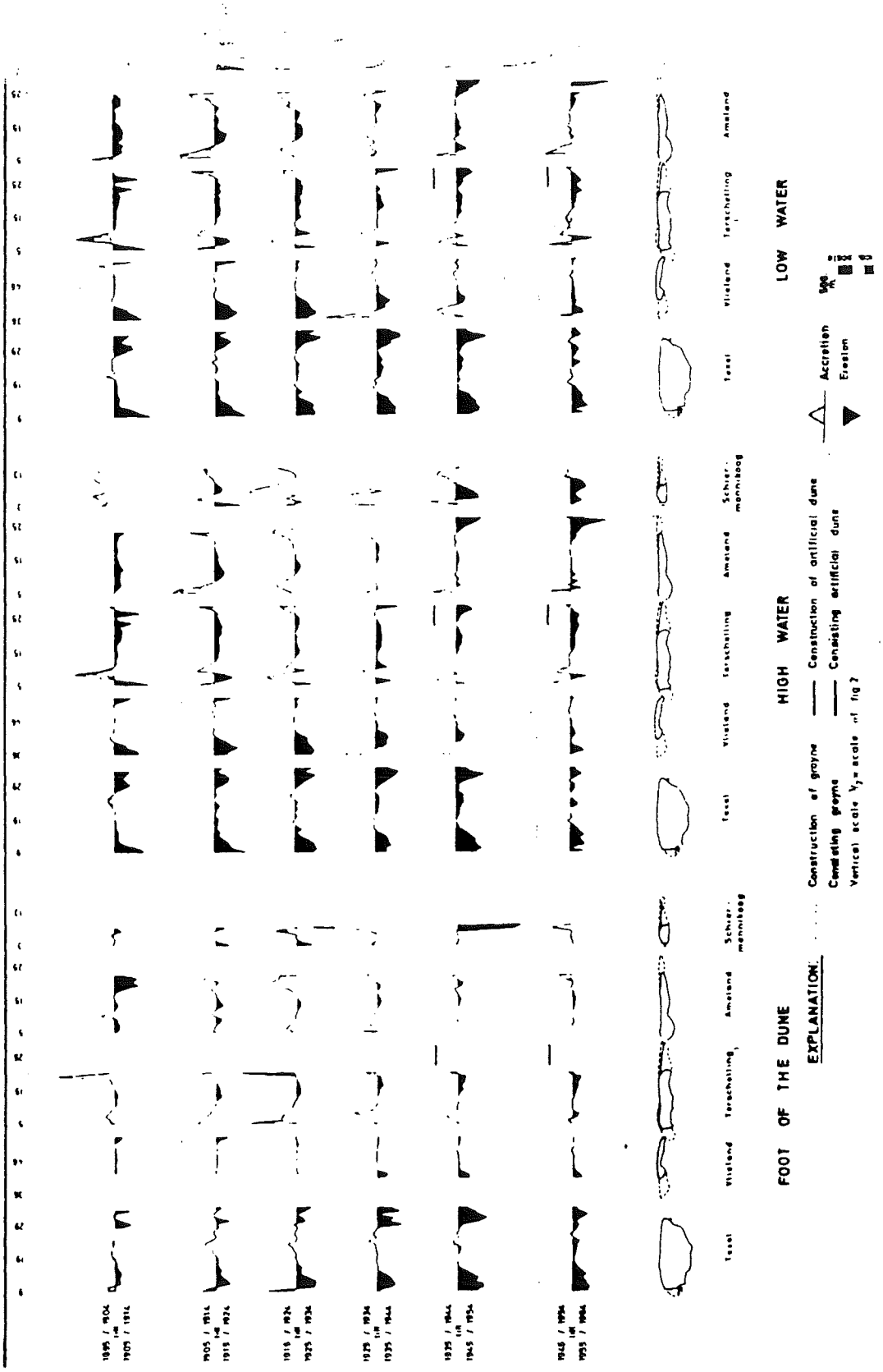

Figure 2-3: Aceccretion and erosion of the Wadden islands

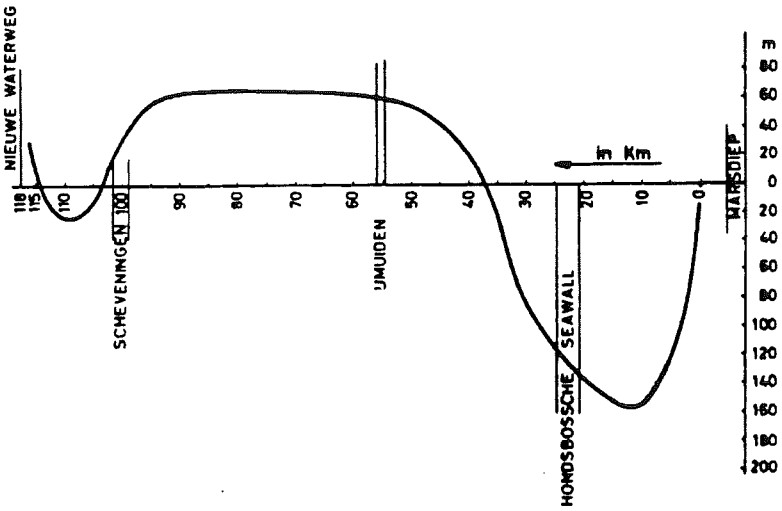

Figure 2-4: Mean dune-foot movements from 1860 till 1960 between Nieuwe Waterweg and Marsdiep (from Edelman & eggink).

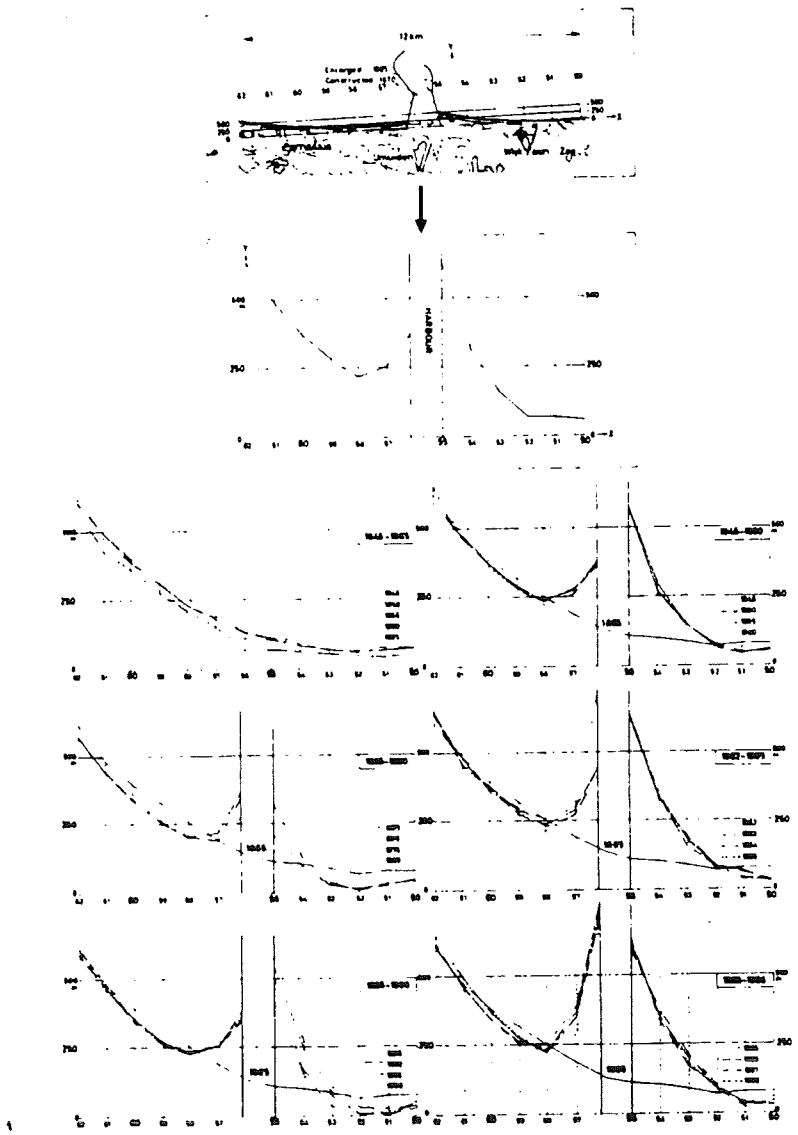

Figure 2-5: Development of the waterline near IJmuiden

2.2.2 The effect of groins

The Dutch groynes have a length of about 200 m. The distance between the successive groynes can be found from fig. 2-6 to 2-8 (about 200 m). In the considered area they are broad-crested stone structures, lying at about mean sea-level. In order to investigate the behaviour of groynes in practice three areas were considered, on which groynes were constructed during the period of the measurements: South-Holland km 97 to 105 (fig. 2-6). North-Holland km 8 to 20 (fig. 2-7, derived from [11])) and Vlieland km 41 to 52 (fig. 2-8). In the figures 2-6, 2-7 and 2-8, the 5-year averages of the low water line have been shown (for instance 1858 to 1862 for 1860). The scale perpendicular to the reference line is exaggerated with respect to the longshore direction by 10 times in fig. 2-8 and by 20 times in fig. 2-6 and 2-7. In each figure two successive lines are plotted together, the black areas show the erosion in 10 years, the grey areas the accretion. The groynes built from 1853-1862 are plotted through the line of 1860, and so on. The hatched area gives the protected coastal area.

Fig. 2-8 seems a striking proof of the benefit of groynes. The erosion near km 47 to 51 in 1860/70 can hardly be ascribed to the groynes 5 km away. The reduction of the erosion after the building of the groynes is quite clear. Of course, this does met mean that groynes are the most economic way of coastal protection. The same kind of effect can be seen in fig. 2-6, 1860/70, although less convincingly. The influence of the lee-side scour also plays a big role here. A rough estimation of this lee-side scour (giving also a measure for the net littoral drift in this sons) would be about 100,000 m^3/year (i.e. erosion of about 2 m/year over 3 km). Less clear still is fig. 2-7.
The Northern part of this area is subject to the movement of the Schulpengat, the Southern branch of the inlet of Texel. The lee-side scour on the Northern side can be observed clearly (km 20, 21; 1860 to 1880 etc.), and also the inverse: the accretion near km 13, 14 between 1900 and 1910 on the luff-side.

Analysis of the effect of the groynes is very difficult. Comparison with unprotected parts of the beach is senseless, since groynes are constructed only on eroding beaches. A before- and after-comparison will be obscured by climatological changes (cf fig. 2-2 and 2-3, low-waterline): We chose the areas of fig. 2-6, 2-7 and 2-8 for comparison (all eroding beaches, gradually more and more protected with groynes) and computed for each area for each 10-year period the mean erosion/year of the protected part and of the unprotected part (fig. 9a, b, c) . Thus the erosion on the same area could be compared for when this area was protected (later on), and for when it was not (in the beginning). In order to eliminate local influences all three areas were put together and again the mean erosion per year of the protected and of the unprotected areas was computed (fig. 2-9d). an impression of the climatological changes given fig. 2-9e. in which the mean regression and progression per 10-year period of the low-tide line of the uninterrupted coast of Holland is shown. Only the relative changes are of importance. Finally in fig. 2-9f the erosion of the protected part of fig. 2-9d is plotted against the erosion of the unprotected part, from which a considerable reduction of the erosion can be concluded. Although nearly all the considered unprotected areas were subect to lee-side scour, fig. 2-8 shows that the reduction is not mainly caused by that, but that the building of groynes reduced the erosion.

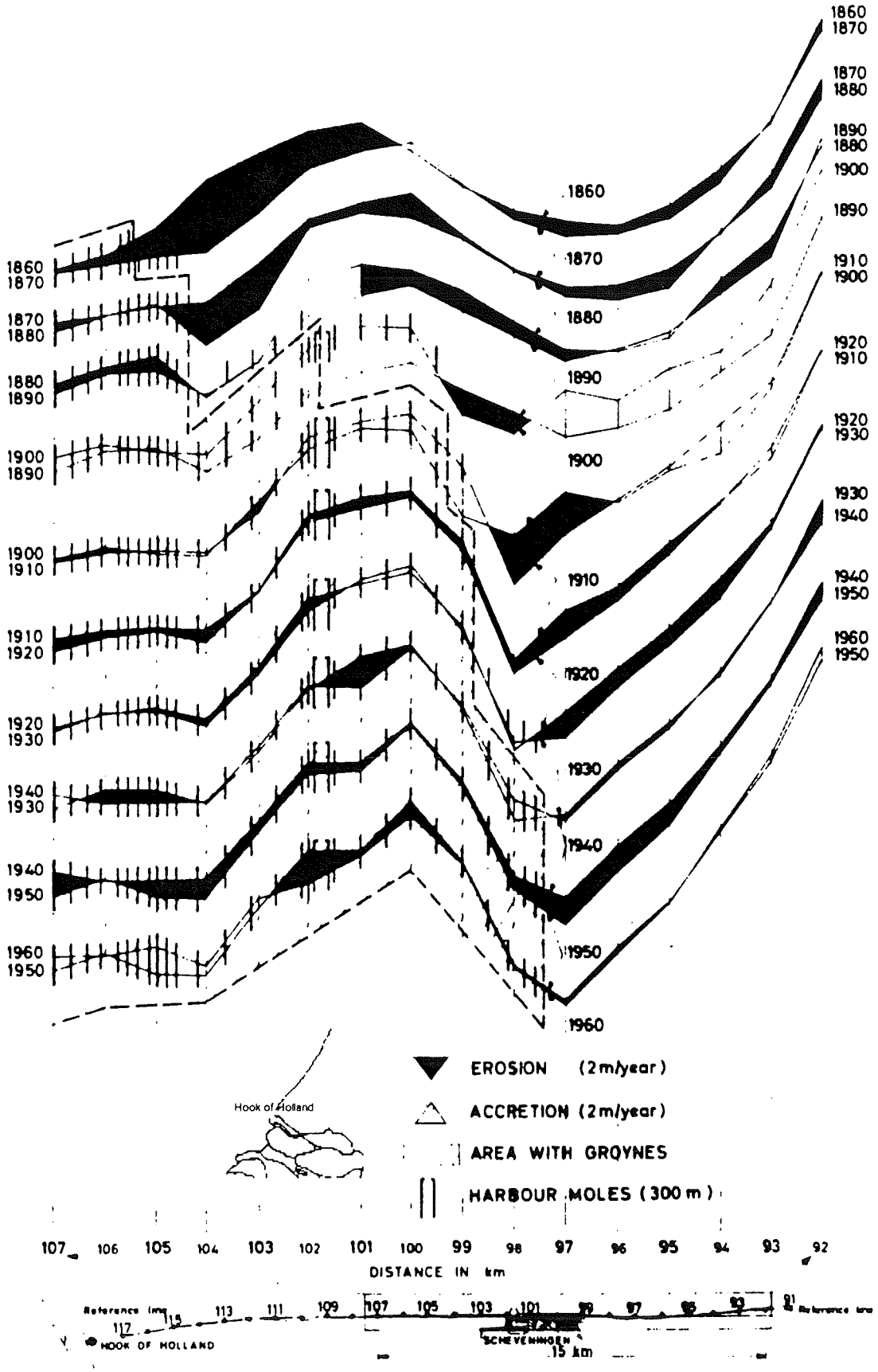

Figure 2-6: Erosion and accretion low water line South Holland

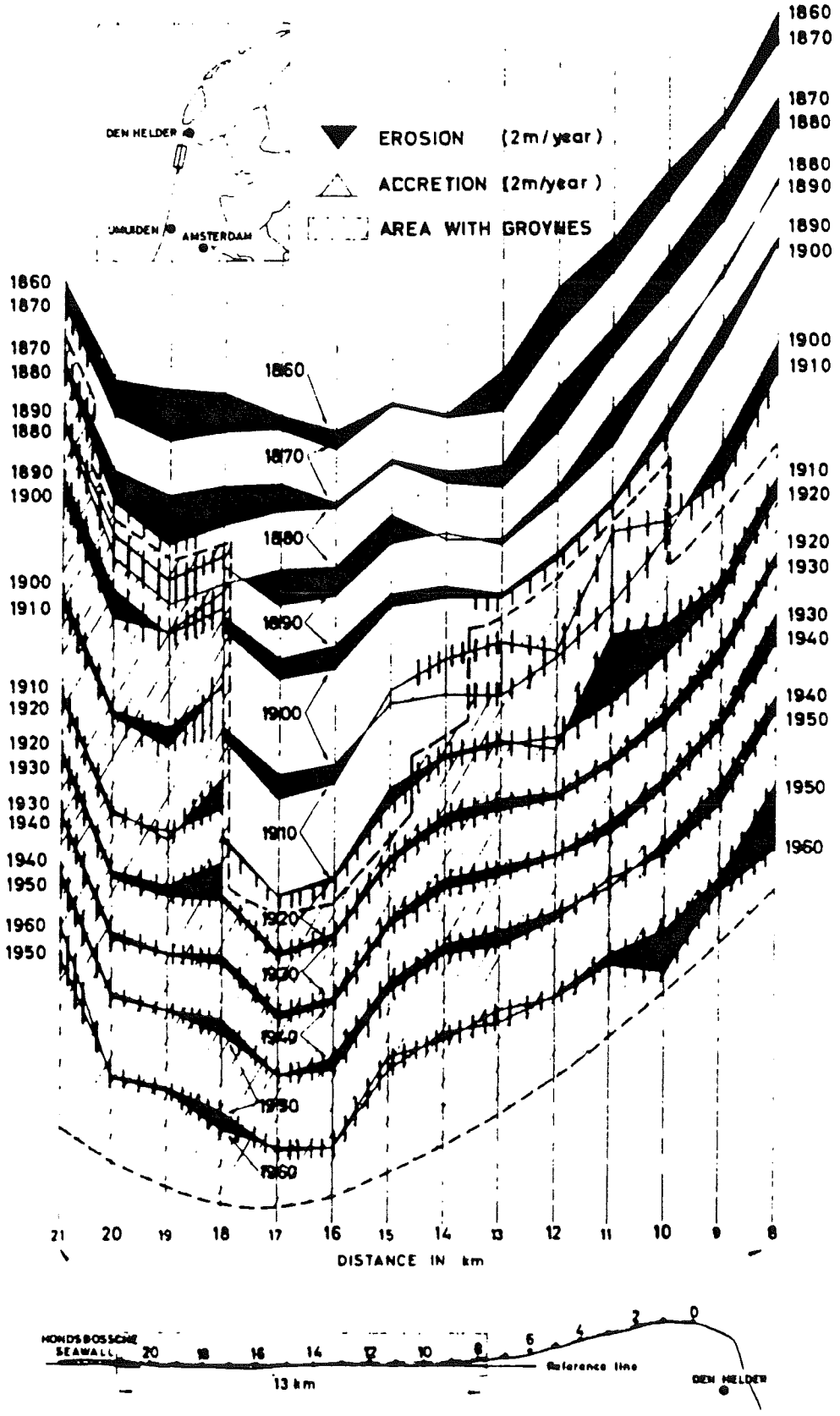

Figure 2-7: Erosion and accretion low water line North-Holland

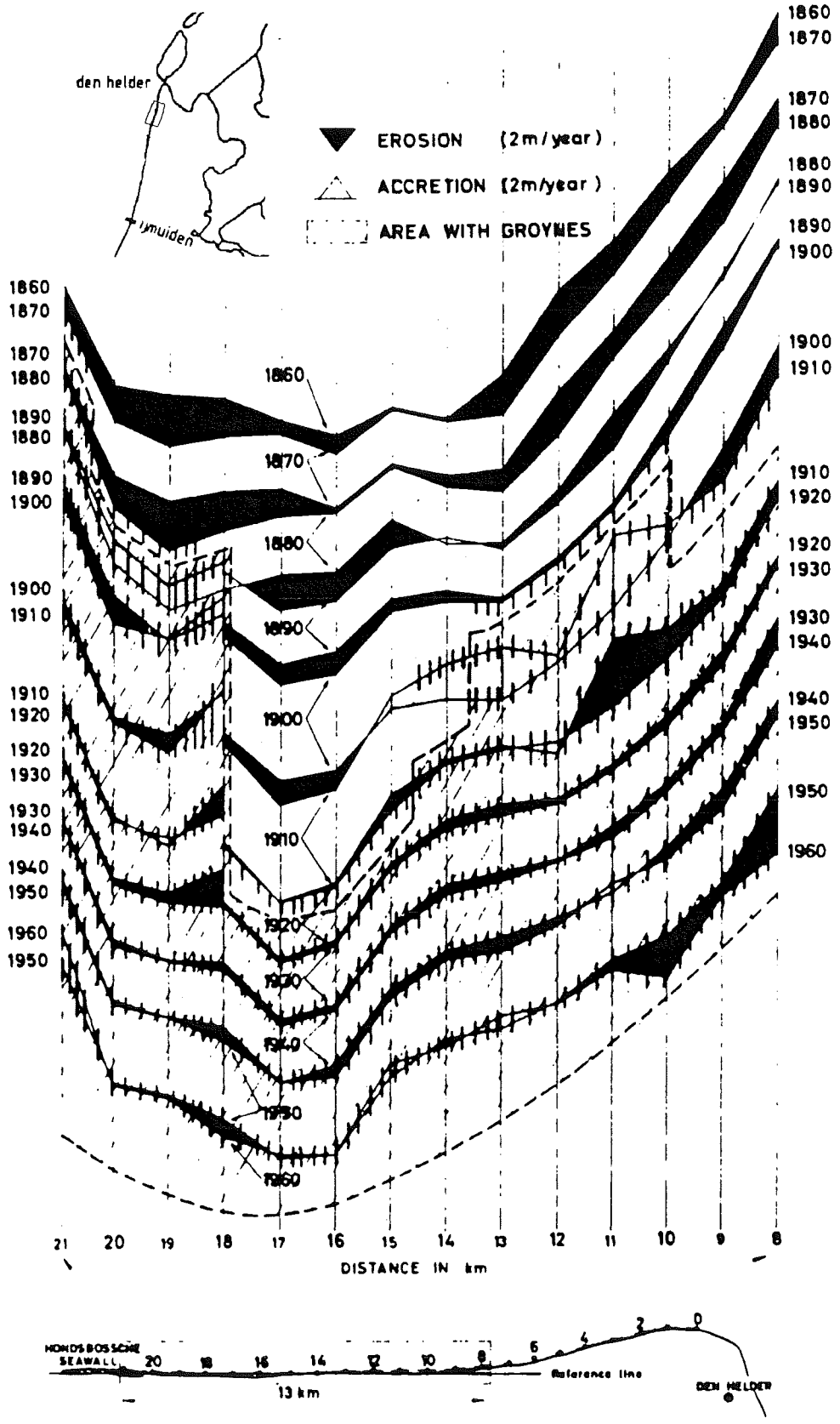

Figure 2-8: Erosion and accretion low water line of Vlieland

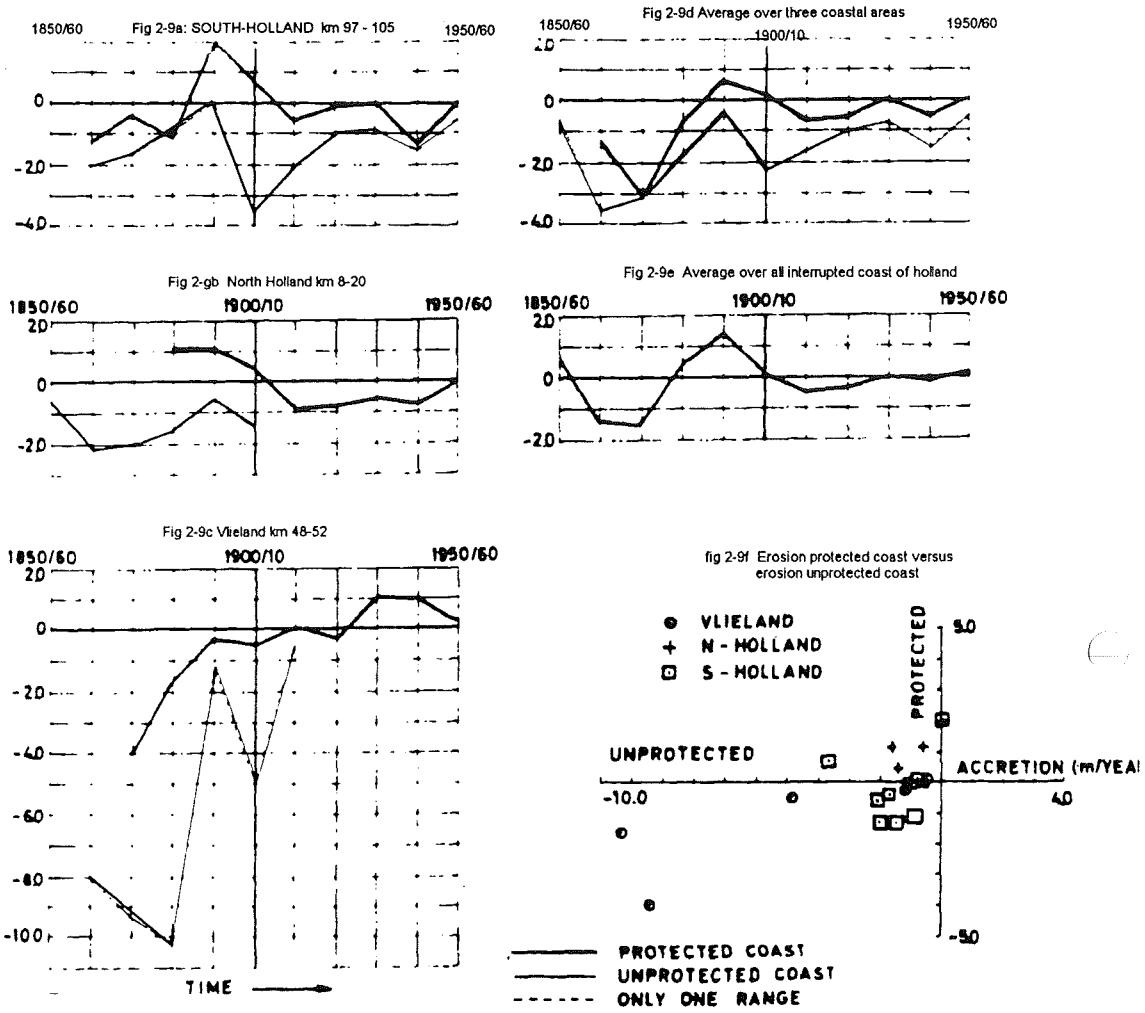

Figure 2-9: Comparison of erosion in m/year of protected and unprotected areas

2.3 The JARKUS measurements (Holland coast)

2.3.1 General remarks on the topography

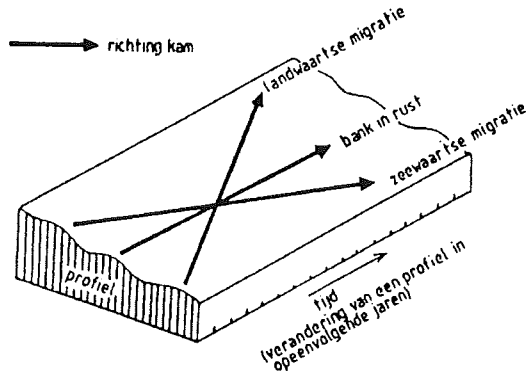

Figure 2-10: Principeschets 3D-tijd figuur

For the investigation of the bottomtopography between den Helder and Hook of Holland use has been made of the yearly coastal measurements, which have been carried out by Rijkswaterstaat and the local regional boards ("waterschappen"). In seaward direction measurements extend to appr. 800 m from the waterline. Ranges of the measured grid have a mutual distance of 200 to 250 m longshore; measuring points being at a mutual distance of 10 tot 20 m cross-shore.
In this subsection, the results of the measurements are displayed in two ways, According to the first kind of display (3D-space , fig 2-11a,b) the measurements of a year are displayed according to a three-dimensional pattern in oblique parallel projection; this results in a realistic picture of the bottom topography in the year considered. However, the reference line of the coordinates of the displayed picture is straight, which in reality it should be curvilinear.

For this reason the Southern part shows a distortion with respect of the Northern part of the order of 45 degrees.
The second type of display (3D-time) shows the cross-sections, measured in one range for all the successive years (cf. fig. 13a,b), in which the site of the ranges in question are shown in an inset map. This results in a three-dimensional figure. If, in this kind of figure, the site of the top of a breakerbar keeps a constant distance to the time-axis, this indicates, that the breaker bar is stable in the course of time. Deviations (to the left or right) with respect to the time axis of the line through the top of the crests indicates a seaward, c.q. a landward motion. The principle is shown in the sketch of fig. 2-10.
Fig. 2-11a shows a three-dimensional picture of the coast of North-Holland between Den Helder and IJmuiden, as measured in 1984. The landward boundary is near the dune foot (or somewhat more landward, as near Callantsoog); the area considered has a width of ca.800 m. The distance Den Helder-IJmuiden is 55 km; so the length scale shown is reduced with respect to the width.
Near Den Helder the coastal protection is heavily under attack of the Nieuwe Schulpengat (depth ca 25 m), the most southern branch of the channel system of the Texel inlet. For long this area of the coast at the position of the northern point, the so-called "Kaaphoofd", has been defended by an ongoing revetment. At least till RSP (governmental range system) km 10.00 the influence of the inlet can be felt. The depth of the seaward boundary of the area considered decreases in Southward direction until a minimum of NAP - 7.5 m near RSP km 16.88. One might presume a high elevated boundary of an outer delta at this site, but its position would be extremely southward. Although this area defended by groins shows since long times an erosion of 1 to 1.5 m/year, the shape of the coastal profile is surprisingly stable the last 20 years, cf. fig 2-13a where among others the 3D-time figures for the ranges RSP km 9.94 and 20.15 are shown: in these ranges the lines through the tops of the bars are parallel to the time-axis.
The three-dimensional figure 2-11a depicting the coastal area shows between RSP km 20 and km 26 an omission at the landward side; over here the Hondsbossche Seawall is situated, which protuberates into sea over ca. 200 m in seaward direction.

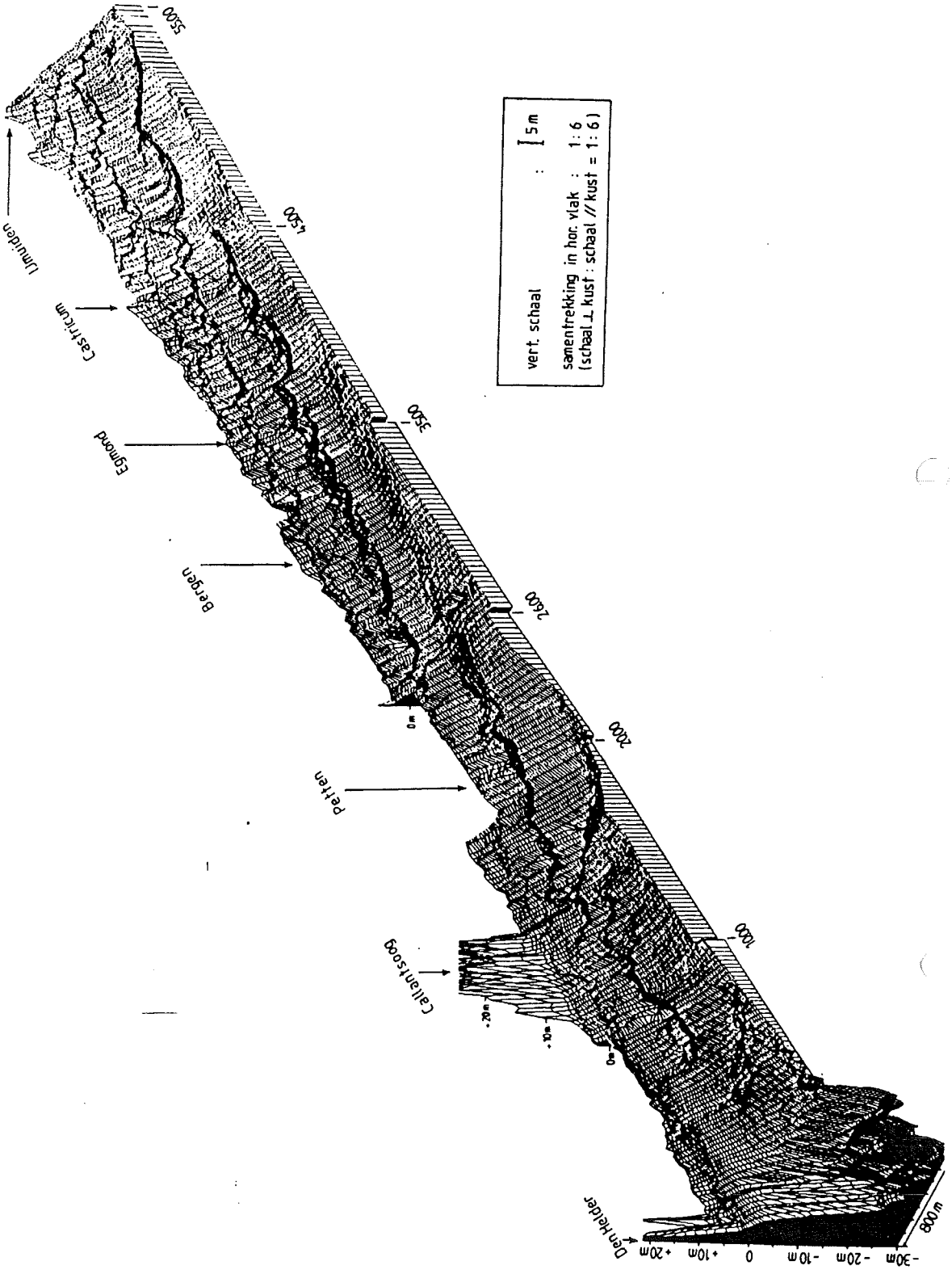

Figure 2-11a: Drie-dimensionale weergave Noordhollandse kust

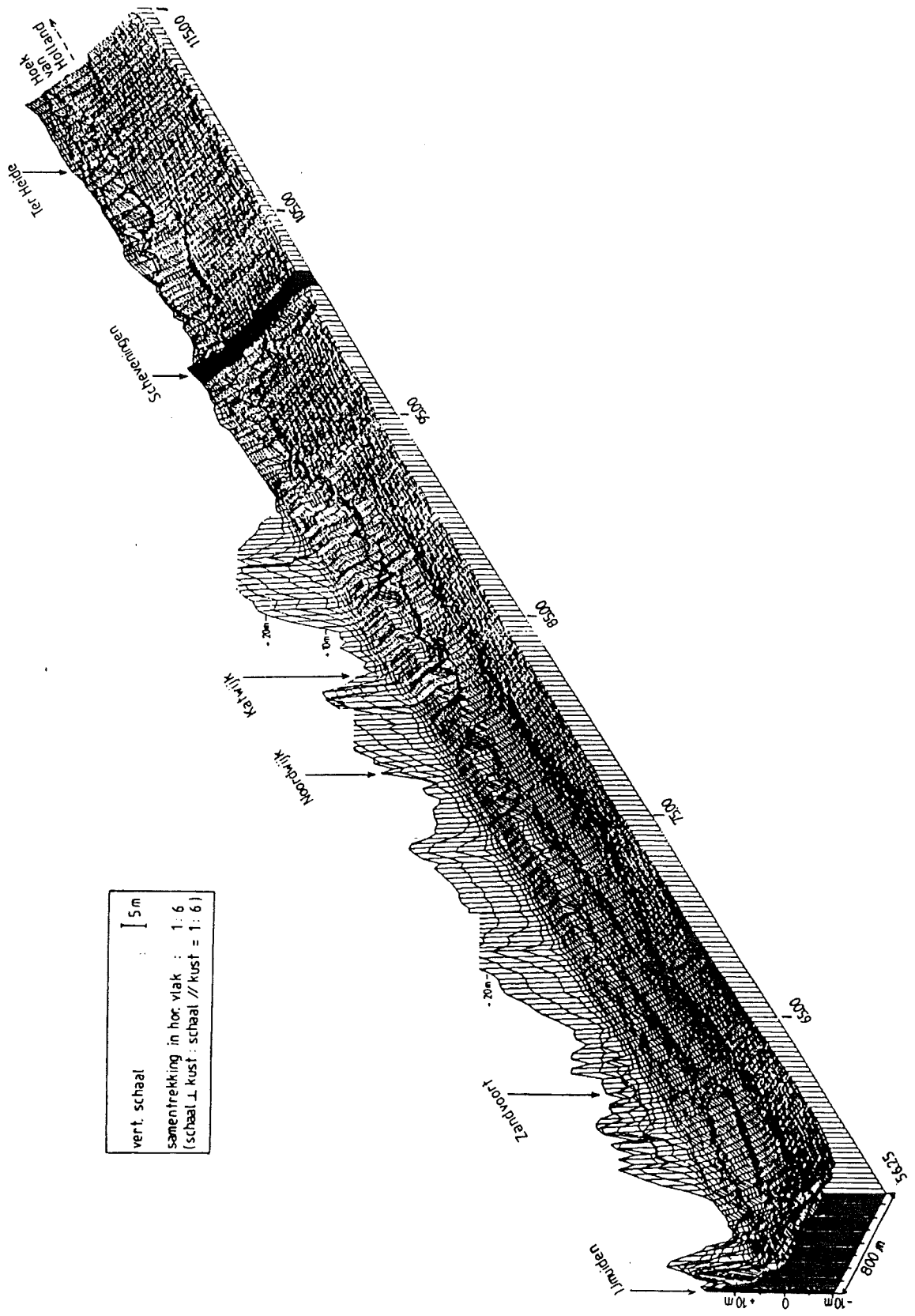

Figure 2-:11b Drie-dimensionale weergave Zuidhollandse kust

Considering the breaker bars: in the whole area between Callantsoog and IJmuiden these show -despite of the small scale muddled patterns - a surprisingly regularity at a larger scale of space. Over a distance of 30 km the bars are "lined up" in a way a Dutch army sergeant with soldiers (being member of the trade union), would be proud of. Yet these features are no "fossilized" geological structures. In particular South of Petten the bars are clearly moving. This shows from the 3D-time presentations of the ranges km 30.00, 40.00 and 50.00, given in fig. 2-13a, from which clearly a seaward propagation can be observed. This does not imply a priori seaward transport of sand, averaged over the period of the bar motion: just oscillating transport is also a possibility.

For comparison of the behavior of bars and foot of the dunes, see fig 2-10, taken from [31], in which the behavior of the dune foot, averaged over a period of 100 years is depicted. This shows that the dunes of for example Katwijk tend to accrete, while the breaker bars move seaward.

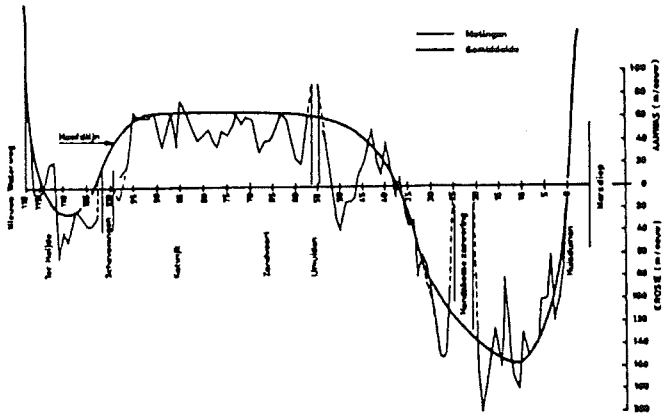

Figure 2-12-2: Erosion and accretion of the Dutch Coast (dune foot) according to Edelman [31]. Calculated from measurments of the dune foot position between 1860 and 1960

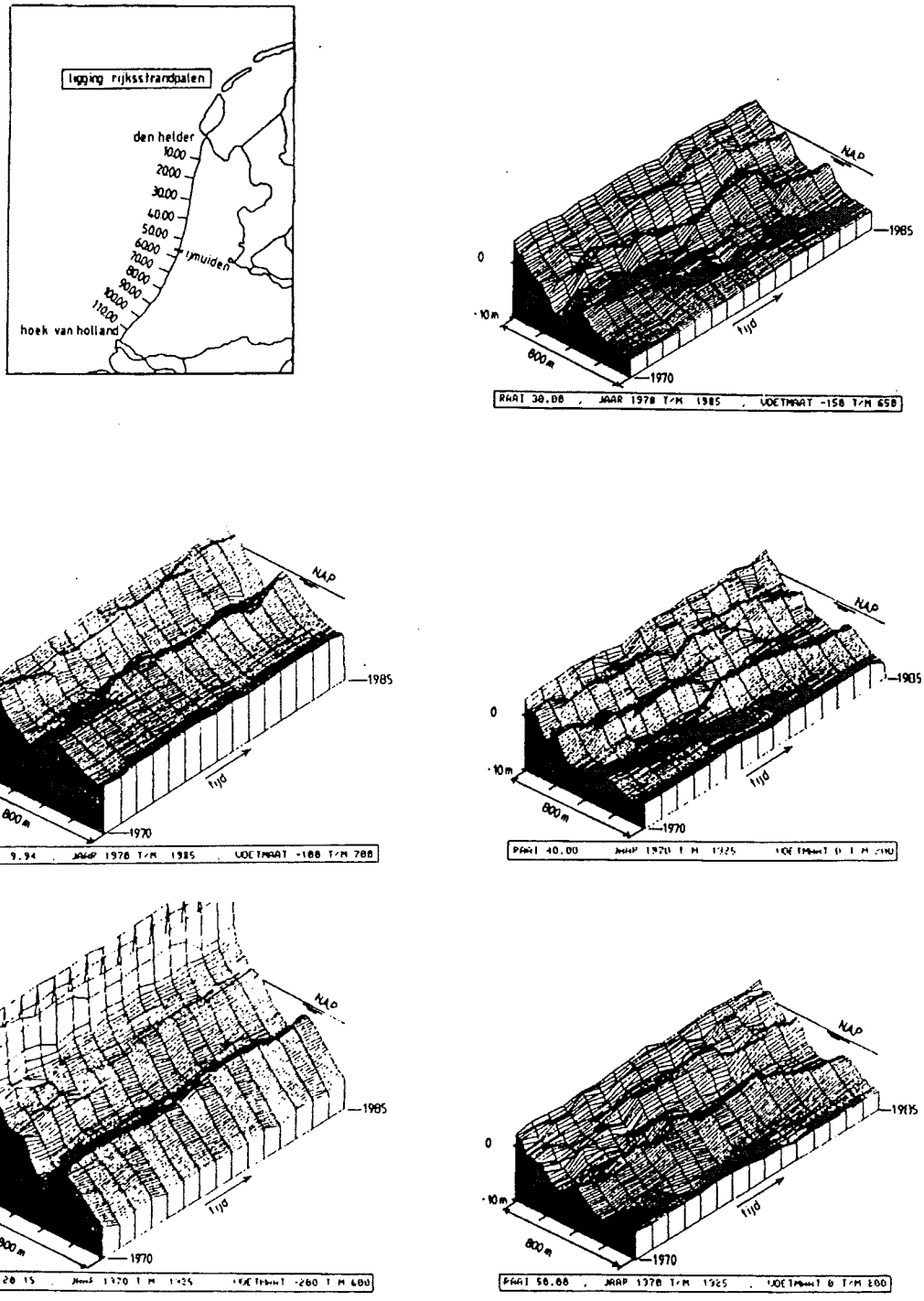

Figure 2-13a: 3D-tijd diagramman van Noord- Holland

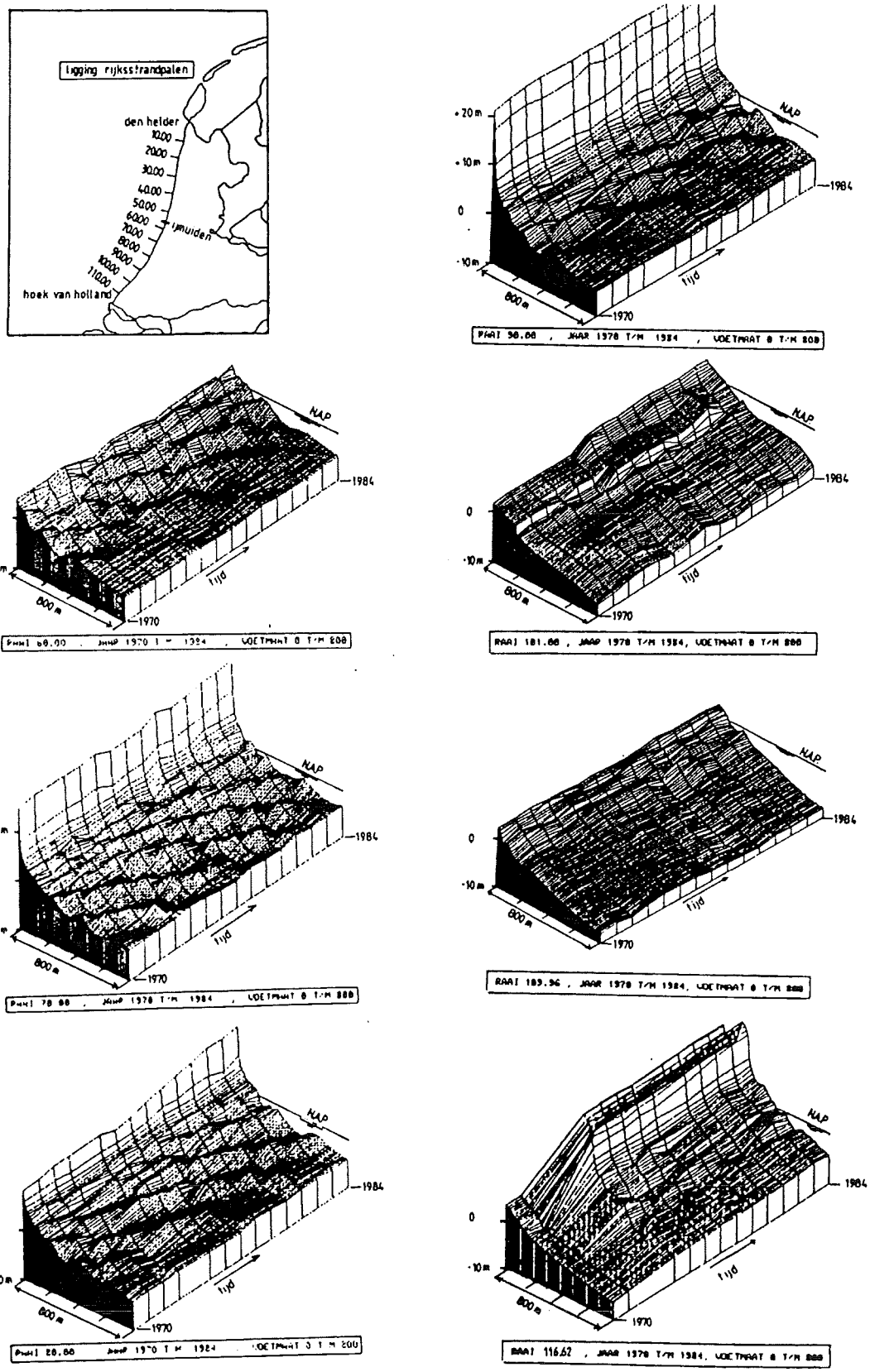

Figure 2-13b: 3D-tijd diagramman van Zuid-Holland

2.3.2 Breaker bars

2.3.2.1 Phenomenological description of breaker bars

Depending on the site of the breaker bars troughs may occur relatively near to the dunes or further away. This affectes the amount of dune-erosion during storms and because of this there are "safe" and "dangerous" years. This raises the question, whether from the position of these breaker bars in the past the "safe" and "dangerous" years of the future (which can differ from place to place) can be deduced.
This problem has been investigated by De Vroeg and Bakker ([32]) and 2.3.2.2), who schematize a breaker bar system to seawards propagating sandwaves with straight crests, which in principle are oblique to the coast. In seaward direction the amplitude first increases and then decreases; the wavelength and the propagation velocity of these sandwaves over a coastal area are assumed to be constant. According to this schematization every point in the surf zone oscillates harmonically, however everywhere with a different amplitude and phase.
The mathematical formulation used is a compromise between on one side a reproduction as realistic as possible and on the other side a simple expression. Fig 2-13a, b gives an impression of the mathematical approximation of the coastal behavior to RSP km 60.00 in the shape of a 3D-place and a 3D-time figure. The propagation of the wave is in the figure should be superponed to a time-averaged profile.
With the aid of statistical techniques it is possible to match the constants in the mathematical description as good as possible to reality.
With the use of the model on the Dutch coast is, for the sake of homogenety, the coast divided into pieces of 5 km.

From this some characteristic values for breakerbars can be derived, which for some coastal areas are shown in the table underneath.

Coastal Area	max. ampl. (m)	distance max. ampl. From coastline (m)	period (year)	av.distance between crests (m)	propagation velocity. (m/year) [1] hook
Bergen-Ijmuiden	0,90	400	ca. 20	400	< 28 m/y 0°
Zandvoort-Noortwijk	0,65	330	4	225	57 m/y -3 à +2° [2]
Noordwijk-Scheveningen	0,50	250	5	300	62 m/y 0°

table 2-1: Average characteristic values for breakerbars for some coastal areas

[1] Measured perpendicular to the crest, seaward is positive
[2] positve angle = opening to the South

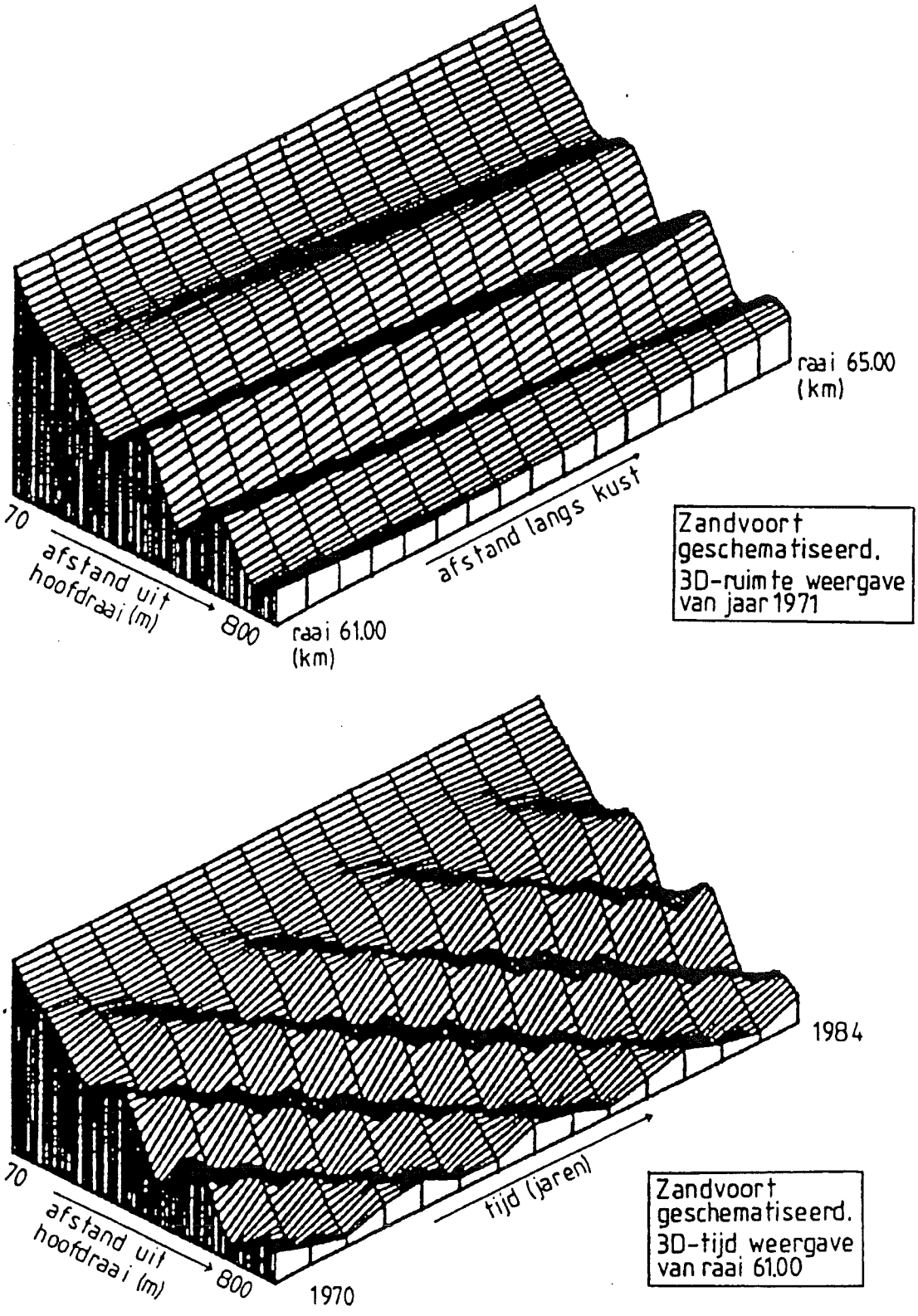

Figure 2-14: Mathematical approximation of the coastal behavior of breaker bars

2.3.2.2 Mathematical description of breaker bars

In the former subsection the next questions were posed:

- Can the coastal behavior be predicted more accurately, if the pre-knowledge is implemented that breaker bars appear?
- How much cross-shore transport is involved with the motion of these bars?

This present subsection explains the mathematical background of the way of treatment of those questions.
De Vroeg [32] answers these questions by approaching the shape and the behavior of a breaker bar system quantitatively. These bars are schematized to seaward propagating sandwaves with straight crests, which in principle are oblique to the coast. (cf. subsect 2.3.2.1). In the present subsection the mathematical description will be given.
A periodic transversal wave motion in an approximately horizontal plane can be simulated mathematically by a harmonic motion, $A \cos(\omega t - k_x x - k_y y)$, where x and y represent the considered coordinates, parallel and perpendicular on the coast, ω is $2\pi/T$, T is the period of the motion, t is the time, (k_x, k_y) are the component of the wave number, i.e., the wavelength in the x- and y- position are resp. $2\pi/k_x$ and $2\pi/k_y$.
A is the amplitude of the wave motion; in the considered case of breaker bars it is assumed to be only a function of y. It first increases and later on decreases in seaward direction In the investigation quoted above the magnitude of the amplitude has been approximated by the function:

$$A = A_1 \cdot (y - y_1) \cdot \exp - \left(\frac{y - y_0}{S} \right)^2$$

where A_1, y_1, y_0 and S are coefficients. In this way it is possible to simulate a wave, propagating in seaward direction, first increasing and later on decreasing. The used formulation is a compromise between on the one hand a simulation as realistic as possible and on the other hand an expression, which is simply to handle . The ratio k_x/k_y represents the tangens of the angle between the breaker bars and the coast. The magnitude of the different constants can by determined by curve-fitting. Fig 14 gives an impression of the mathematical approximation of the coastal behavior near RSP km 60.00 (fig.3a) in the shape of a 3D-site and a 3D-time figure. The propagation of the wave in the figure is superponed on a time-averaged profile.
For application of this model to the Dutch coast the coast has been divided into parts of 5 km in order to warrant homogenuity.

After determination of the parameters it is possible to deduce the values for:

- the maximum amplitude in a cross-section;
- the distance of this maximum related to the site of the coastline;
- the period T of the motion of the bars;
- the average distance $2\pi/k_y$ between the crests
- the propagation speed and direction;
- the orientation of the bars w.r.t. the coastline (+ = opening to the south).

The table 2-1 in subsect 2.3.2.1 gives an overview of the values for some coastal areas. Purpose of the approach shown is that predictions can be made. For this goal the sand-volume (m^3/m') of the coastal zone between the contour lines OD + 1m and OD - 3m, seaward of the main range (parallel to the coast) as a function of time and locaton is compared to the "theoretical" function (fig 15). The drawn line gives for a number of ranges in a coastal stretch of 4 km in the surroundings of Zandvoort (fig.10b) the number of m3/m sand according to the coastal measurements; the interrupted line shows this amount according to the simulation as described above. The fluctuation of volume, caused by the variability of the site of the breaker bars is shown. According to the simulation this fluctuation should shift (because the bars are oblique to the coast) with a period of 4 years and a

propagation velocity of approx. 1.7 km/year in Northernly direction (from km 65 to km 61); The magnitude of this fluctuation is approx. 45 m^3/m'. With the mathematical formulation given it should be possible to predict more precisely the dune erosion during storms. However, although the approximation is not too bad, for the purpose in question it appears to be too inaccurate, in that sense that the "hindcasting" including the periodical fluctuations is not better (in other words: it does not give a smaller standard deviation) than just taking the linear trend into account.

There are two causes for this inaccuracy:

- the position fixing of the bars in location and time by a cosine function is too simple. It suggests, that the bar length (top-top position) is constant over the whole profile, while in the nature the length of the bars increases in seaward direction [1]
- discontinuities, as occur in practice have a strongly negative effect on the results.

To illustrate this, in fig. 16 the measured and simulated crests of the breaker bars at RSP km 60.00 till 65.00 during the years 1971 to1975. Caused by both formerly mentioned symptoms phase differences of 180 degrees may arise between the mathematical approximation and nature, causing a rapid growth of standard deviations between measurement and calculation. To achieve the aim a more precise approach is necessary.
The mathematical approach does give an impression of the amount of cross-shore transport which the phenomenon "breaker bars" involves (fig. 17).
For better understanding, consider some coast which is stable at the long term; refer to subsect. 2.3.2.3 concerning amounts of sand transport linked with long term erosion and accretion.
The mathematical approach enables to express the amount of sand, positioned at a certain moment landward of a given coordinate y in the variables appearing in the formulae like V, y, t, etc. Differentiating this expression to time yields the crossshore transport as a function of time and location. In this concept the cross-shore transport landward of $y = y_1$ (the point where the amplitude of the sandwaves is zero) is supposed to be zero. As can be expected an oscillating transport with frequency ω is found (fig. 17); This yields the location and magnitude of the maximum "amplitude of cross-shore transport". Starting from the characteristics found for the breaker bars near Zandvoort (fig.10b), the result (per m in longshore direction) is approx. 45 m^3/year. [32].

[1] Refer to sect.7.2.1 concerning this matter

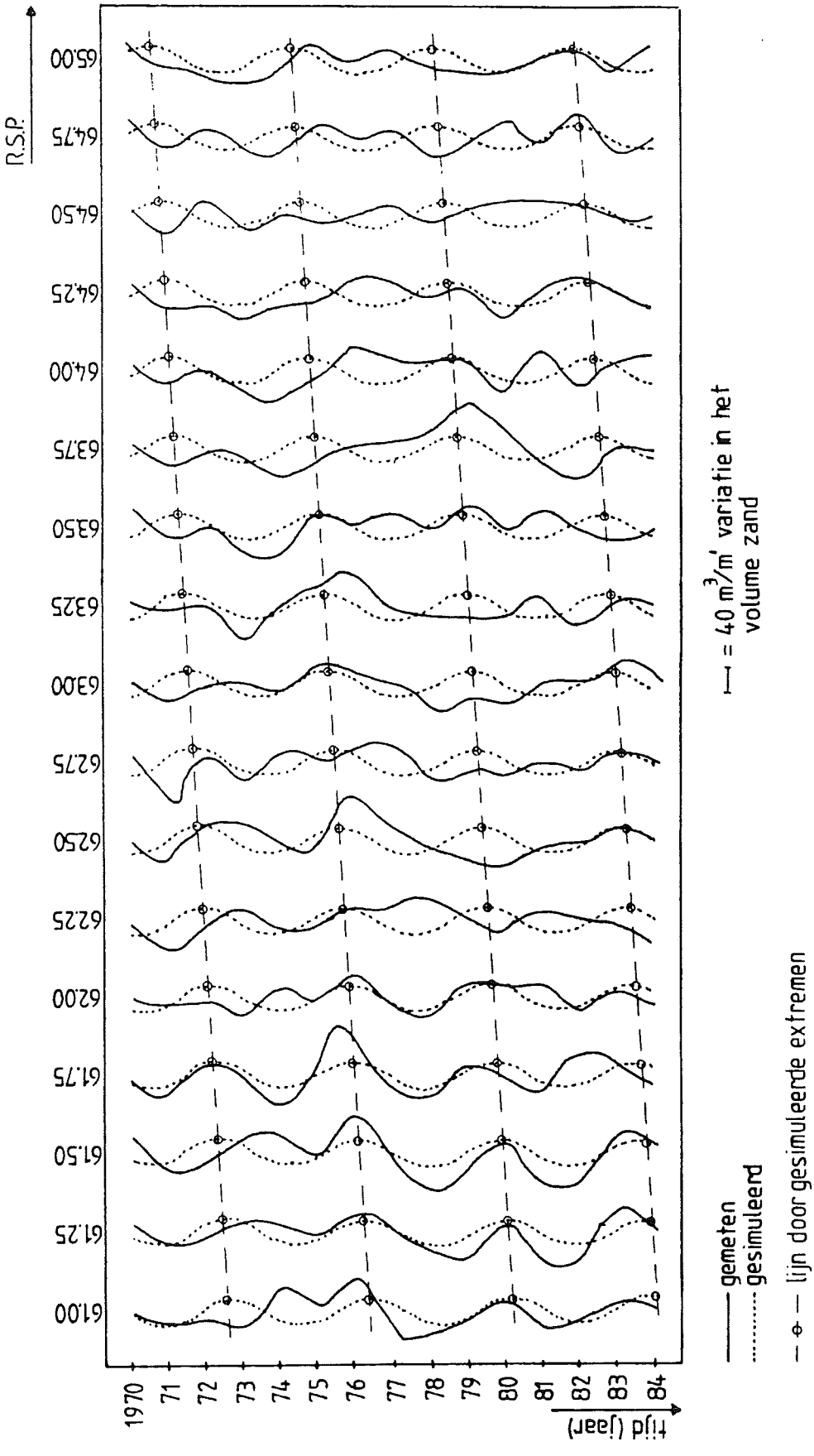

Figure 2-15: Comparisation variation measured and calculated sand volume.

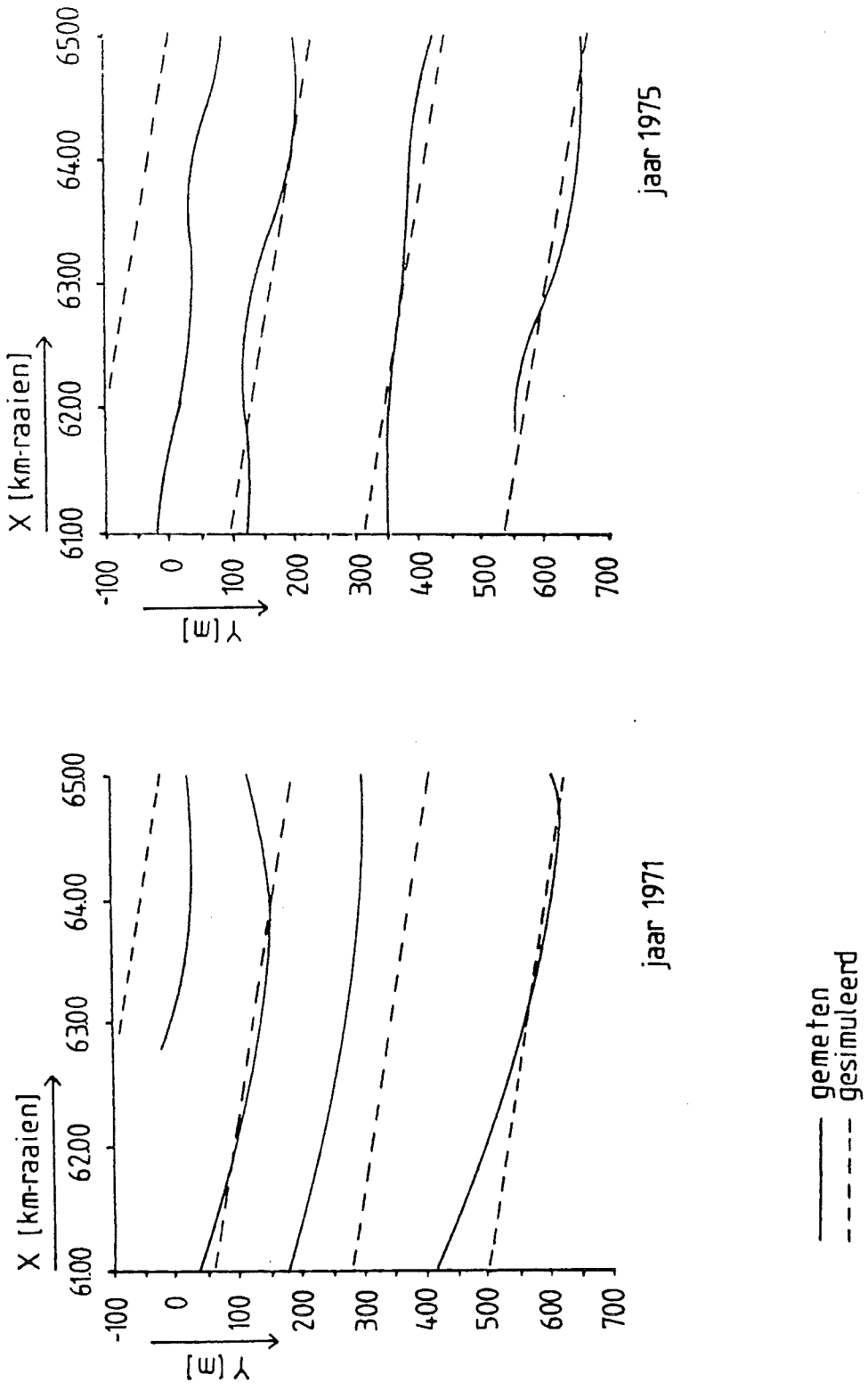

Figure 2-16: Measured and simulated crests of the breaker bars

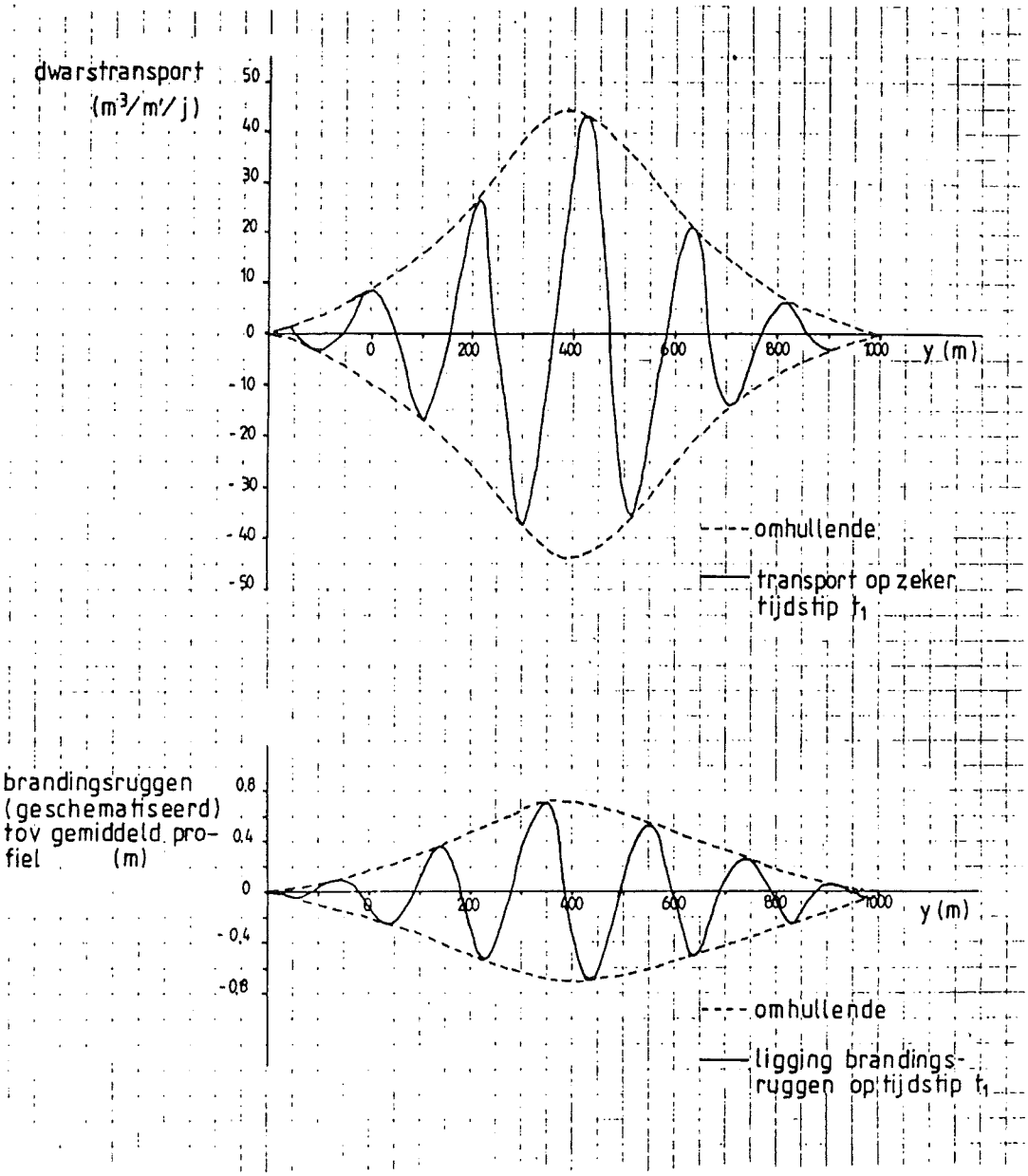

Figure 2-17: Cross-shore transport due to breaker bars

2.3.2.3 The order of magnitude of the cross-shore transport along the dutch coast

In this subsection 2.3.2.3 the amount of cross-shore transport, involved in the propagation of breaker bars is compared with the order of magnitude of the amounts as a consequence of the other morphological features.
The result is depicted in fig. 2-17, which will be explained below. In order to be somewhat specific, there is focused on the area between Zandvoort and Noordwijk (fig. 2-11b), where the breaker bars are developed strongly and have a period of about 4 years; this implies a (semi-)periodical transport of 45 m^3/m/year (subsect. 2.3.2.2).
However, the yearly coastal accretion of the coastal stretch in question has been kept out of consideration. If it may be assumed, that the coastal area to be considered extends from OD -5m to OD +15 m, the yearly accretion of 0.5 m/year,occurring at this site (fig.2-4) implies a landward transport of 10 m^3/m/year.
One may compare this magnitude with the amount of dune erosion during a sturdy storm, which can be (in cross-shore direction) approx. 30 m^3/storm/m. Often during more quiet circumstances this amount is transported dune-ward again.
How to compare this amount with the cross-shore transport, which is linked with sea level rise and with the transport alongshore?
In this investigation a coastal strip is considered with a width of approx. 1 km. During a sea level rise of 2 mm/year an amount of 2 m^3 per meter coastal length is necessary to maintain the local depth of this strip constant with respect to mean sea level.

Compared with the gross littoral drift along the coast this amount pales into insignificance.

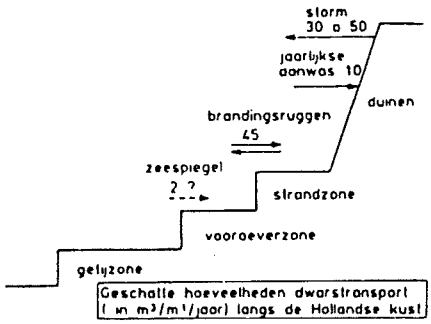

Figure 2-18: estimated transports along the coast as a result of the wave-driven longshore current and tide

Fig. 2-18, made on the basis of calculations, mentioned in [33] (see as well sect.2.4 and fig.2-19), gives the estimated transports along the coast as a result of the wave-driven longshore current and tide. Breaking waves, oblique to the coast generate wave-driven longshore currents, which even with a small angle of wave incidence will dominate the tide (sect.2.4).

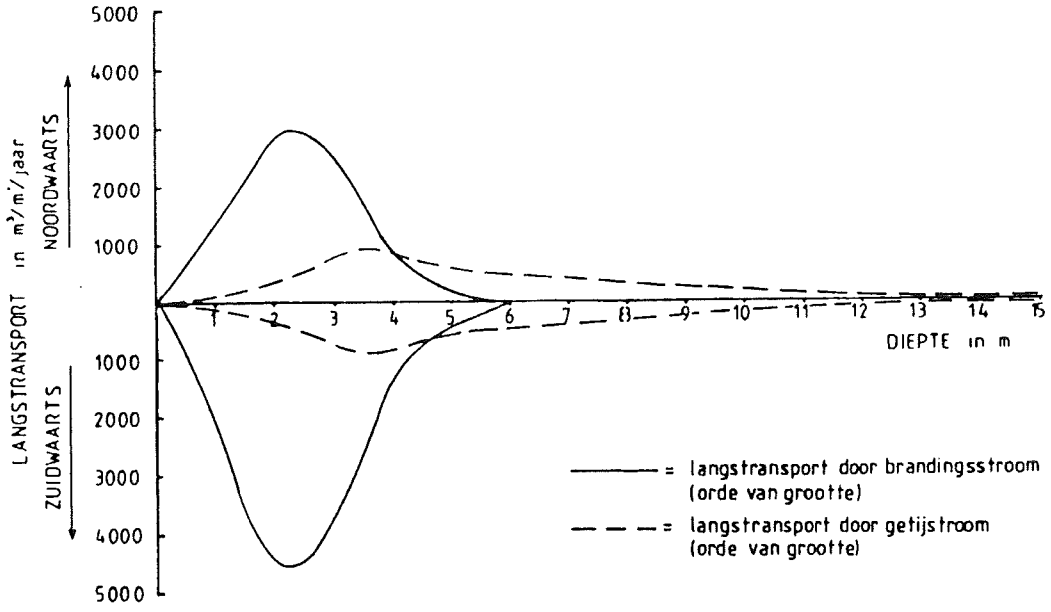

Fig 2-19: Order of magnitude of the yearly transport along the coast as a result of the wave-driven longshore current and tide

The drawn lines in fig. 2-19 represent the year-averaged transports per meter coastal width, caused by this wave-driven current.
Herewith the probability of wave conditions (height; period; direction) has been taken into account.
Near Scheveningen the transport Northwards and Southwards appear to be of the same order of magnitude. The calculations are not accurate enough to make statements over the resulting transports; some more information will be given in subsect.5.2.5.
Evidently, outside the surf zone the tide-driven transports dominate although the waves can still boost the transport by stirring effects. There the direction of the waves is only of secondary importance.

With an interrupted line in fig. 2-18 is given, on basis of exploring calculations [35], how this transport is distributed over the depth. Close to the coast the tidal transport decreases, as it is, at this location, mostly replaced with wave-driven transport. Far from the coast it also decreases, because the influence of the waves on the tide-driven transport becomes smaller. Plotted is the calculated transport per flood-(ebb-)period, multiplied by the number of tides per year. Again, probability of wave occurrence has been taken into account. Also in this case inaccuracy of the calculations prohibits statements on the resulting transport[1].
From fig. 2-18 it shows, that the longshore transport is at least a factor 100 larger than the cross-shore transport. However, accretion and erosion arise by local differences in transport. These differences ("gradients") can be of the same order of magnitude for longshore- and cross-shore transport.
The longshore transport is large compared to the cross-shore transport. This means that the "to and fro moving slicer", who smoothens the breaker bars and models it in that way, is directed along the coast. But what "inspires" the coast to form breaker bars [2]?

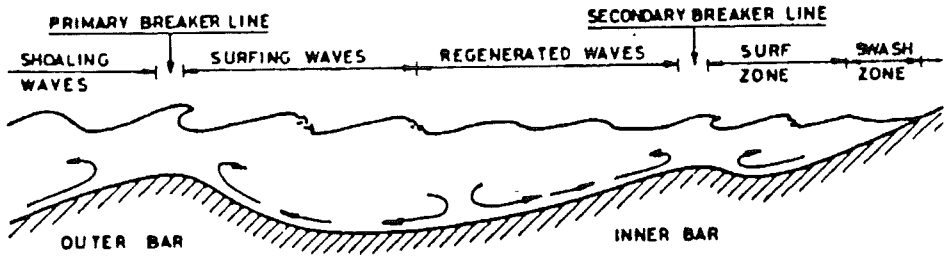

Fig.2-20. Resultant current circulation near the bottom at a coast with 2 breaker bars.
According to Dyhr Nielsen and Sorensen [36]

One could have the following conception in mind: as soon as there is a small irregularity on the profile, this causes wave breaking; the momentum of the breaking and broken waves will be large above the crest of the breaker bar compared with the momentum below the crest, on the landward flank of the breaker bar. This could drive a circulation (fig. 2-20) (an exact formula is given by Dyhr Nielsen and Sorensen [36]). Together with the longshore current in the trough this results in a spiraling current.
The relative distance between the breaker bars is probably being ruled by a subtle mechanism, of where the essence only can be suspected [37 t/m 40].
It is thought, that the relative distance between the breaker bars is regulated by resonance systems of long-periodic waves with wavelengths of hundreds of meters till 1 km (periods of some minutes, amplitudes max. some dm). The principle of these waves, the so-called "surf beat", can by described as follows [39]. Interference often causes grouping of alternately high and low waves. Breaking of those waves results in a shore-ward directed pulse, which varies in strength, because of the variation of higher and lower waves in the wave groups. The water in the surf zone reacts by an oscillation, not with the period of the separate waves, but

[1] Refer to the RWS-Coastal Management Reports of 1990 and 1995 for more daring statements
[2] Since the original version of this text has been written (in dutch) this topic has been subject of many excellent investigations, for instance by Roelvink [.] and Ruessink [.]. Do read the comment by Roelvink (ch.12).!

with the period of the wave group. This generates standing waves, of which the amplitude gradually increases in shore-ward direction. The amplitude of oscillation depends on whether the period of the surfbeat agrees with the "resonance frequency", to which the breaker bar system is "tuned": in the same way as a tuned radio can select from all waves in the ether only one or some frequencies to amplify. One could imagine that the resulting water motion above and between the breaker bars causes sand motion in this way, remoulding these breaker bars in a specific way. Because of the large scale of this phenomenon the remoulding will be very slow, and thus the resonance frequency can adjust itself only very slowly (N.B.: a radio tuning itself!).
Even if the incoming waves differ from day to day, the same resonance frequency would be picked up and the remoulding of the breaker bars would occur in the same way.
This could explain that breaker bars react more to a wave climate than to the instantaneous wave characteristics.
However, as usual the scholars do not agree: this applies as well concerning the importance of surf beat ([40] and ch.12) Evidently, a theory that can accurately predict the height and the propagation of the breaker bars, is not yet at disposal, although investigations of Roelvink [.] are encouraging.
A similar mechanism as being drawn up for the surf beat can be responsible for long-periodic waves, which propagate in longshore direction. Also propagating atmospheric disturbances can by a driving force for this kind of waves. These so-called "edge waves", of which the amplitude mostly decreases as well in seaward direction, could be responsible for the relative distance between the rip-currents perpendicular to the coast [37].

2.3.3 The effect of harbor moles

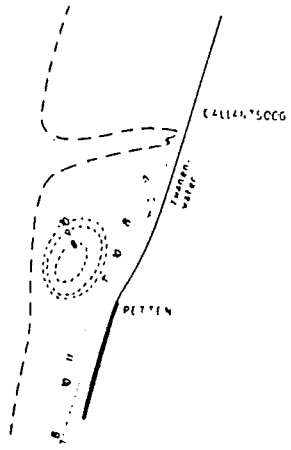

Figure 2-21: Situering Zijpe

North of RSP km 30 the coast is defended by a groin system; this is not the case South of this site. This fact does not seem to affect the shape and site of the breaker bars very much; also the influence of the Hondsbossche Seawall on the breaker bars appears to be very small.
At the North-side of the Hondsbossche Seawall, at the seaward side, fig. 2-11a shows a deep trough, of which the landward side is directed to Callantsoog. The coastal profile in this neighborhood is the steepest of the entire Dutch coast, apart from the vicinity of the Inlet of Texel. Fig. 2-21 (inset of fig. 2-11a) shows once more the situation on this spot, now in the shape of a map. Do we see a relict of former centuries? Does the coast invites to sail the old Zijpe, leading towards the Zwanenwater? The latter is nowadays a nature reserve, landward of the dunes, but in the thirteenth century the entrance of the Zijpe was situated here (see fig. 2-21 after data from Schoorl [55] en De Mulder [54]). At that time the coast extended 3 km seawards. Still now the old remains of the so-called "Pettemer Polder" can be found at a depth of 6 m and at a distance of 2 km from the present coastline (fig. 2-21). According to de Mulder [54] the Pleistocene is situated at the depth of NAP – 8 m. The Pettemer Polder forms a protuberance on a peculiar horizontal plane at a depth of approx. OD – 10 a 12 m, which is located from RSP km 10 to km 20 from approx. 600 m seaward from the coastline unto 3 km from the coastline. Possibly a 4000 year old current resistant clay and peat layer is located here. Bottom corings landward of the Hondsbossche Seawall [54] make this probable and recent geological research could prove this. Although the old reconstruction [55] of the Zijpe channel locates this north of the Petterner Polder, it seems hydraulically and morphologically feasible there is (possibly) a (second) Southern channel. In a clay bottom this channel position could indeed be preserved.

However, one could also attribute the trough in the coastal profile at the north-west side of the Hondsbossche Seawall to this coastal defense as a consequence of stream contraction. The fact that the depth does not adapt itself to that of a "normal" profile points to a hydraulically stable situation, or to a low amount of transport.
Between Bergen and Egmond one could, with some imagination, discover a terrace at the seaside, where the old clay and peat formations (lagunal depositions of more then 6000 years of age) could surface (see for instance Wiersma [29]). However, from the 3D-time diagram of fig. 2-13a it does not show clearly, that the bank at the seaside of the area in question would be solid;: the bottom level varies somewhat at this side.

Now take a look at the immediate surroundings North of IJmuiden (fig. 2-11a).
Ever since the harbor moles of IJmuiden were build in 1870 sand accumulated here. The result is a gentle sloping coastal profile. A gentle sloping profile appears to go together along the Dutch coast with many breaker bars; like here, where the number of breaker bars increases from 2 to 3 (similar to at other places along the Noord-Holland coast) up to 4 or 5. It shows, that along the entire North-Holland coast these bars make a certain angle with the coast.
As appears from the 3D-time diagrams (fig. 2-13a), the behavior of the IJmuiden coast is rather fussy. Possibly this is caused by the fact that short-term climatological influences (accretion North of IJmuiden, if the dominating waves come from the North and erosion in the opposite case) clearly are manifest here, because the longshore transport gradients are large. For the harbor moles completely interrupt the local longshore transport.

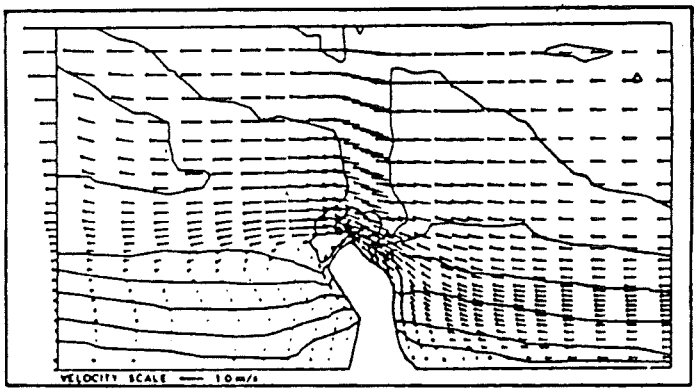

figure 2-22: Flow pattern during ebb near the IJmuiden harbor from. The original harbor moles (before 1970) stretch only to the "crack" in the current southern head.

The immediate surroundings southward of IJmuiden have also been influenced by these harbor moles.
The extension (1970) of the Southern mole makes an angle with respect to the original one: it is more Southward directed compared to the 1870 harbor moles, which were directed westward, fig. 2-22). Thus at the landward side of it a sheltered area emerged, where sand, deposited by the sea during Southwestern storms was able to stay during NW storms, when the area was in the leeside of the harbor mole. Because of this shelter effect, and possibly also by eddies (fig. 2-22), after 1970 behind the harbor mole a rapid expansion of the beach area next to the Southern mole developed; this also shows in fig. 2-11b. The sloping terrace, which is present at the seaward side of the area considered, shows little variation (see fig. 3b, and the 3D- time diagram of RSP km 60.00). The breaker bars, which at this spot clearly propagate in seaward direction attenuate on this terrace. Do resistant layers from geological times show up here as well?
Further southwards the 3D-time diagrams show, that the breaker bars between Zandvoort and Scheveningen also move seaward; however, the amplitude is decreasing much slower compared to RSP km 60.00, causing the bars to extend much further seaward than at RSP km 60.00 (fig. 2-3b and subsect. 2.3.2.1). Here the bars propagate in a regular way, as the 3D- time diagrams depict. The regularity appears to arise above the relative chaos of the

climatological circumstances: it is hard to discover the influence of relatively stormy years in these figures. In subsect. 2.3.2.1 this is treated more extensively.
More to the south the number of breaker bars decreases, while the coastal profile is steepening. At Scheveningen harbor monitoring is interrupted. North of the Scheveningen harbor a channel can be found parallel to the harbor head.
South of Scheveningen, along the Delfland coast a steep foreshore is found combined with at some places an underdeveloped breaker bar.

The movement of the coast near raai RSP km 101.00 (fig. 3b), just north of the harbor head of Scheveningen, is dominated at one side by the wave sheltering by the moles and the effect of the hampering of the littoral drift, however as well by the fact that in 1975 0,7 million m^3 sand has been supplied. Also, according to information of the "Hoogheemraadschap Delfland", periodically sand of the beach south of the harbor heads is removed and dumped on the beach north of these moles, while the groin, directly north of the harbor moles was enlengthened in 1972 to affect the circulation of the tidal current in a positive way. Without thorough research it is hard to distinguish the differences between the various effects. This is even stronger at RSP km 116.62 (fig 2-23b), where during the extension of the Hook of Holland harbor in 1971/1972 the coast also was brought in a more forward position and 18,94 million m^3 sand was deposited in the scope of the Beach Project Hook of Holland (just North of the harbor mole)..

The coast of Delfland (Scheveingen -Hook of Holland; fig.2-23b) erodes already for century's. This is illustrated by fig. 2-12, after Edelman[9], where for the entire coast of Holland the accretion and the erosion of the foot of the dunes between 1860 and 1960 is given. One could imagine, that the sand initially would be withdrawn from deeper water, which would cause steepening.
The shoreface in the immediate vicinity of Hook of Holland is slightly higher, on one hand because of the effect of the Northern mole, constructed in 1870 and enlarged in 1970, making part of the works near the entrance of the Nieuwe Waterweg; on the other hand because of the beach nourishment at Hook of Holland (this took place, at a site, somewhat South of the area, depicted in fig. 2-23b).
Of the coastal area between IJmuiden and Hoek van Holland only the Delfland coast – approx. from the north side of the Scheveningen Boulevard (fig.2.6) - is protected by groins (fig.2-6). The effect of this coastal defense system appears to be modest. Investigation of this area is facilitated thanks to the fact that the Hoogheemraadschap Delfland made profile measurements for this part of the coast during more than 150 years.

2.3.4 Coastal behaviour after averaging the breaker bars

Knowledge of the period of motion of a bar system gives the opportunity to determine the accuracy, with which the coastal trend can be determined. This accuracy depends on the one hand upon the ratio between the period of the breaker bars, compared with the period of observation and on the other hand on the phase of the bar cycle at the start of the observation time. This statement will be elucidated in the next subsect 2.3.5.
Fig 2-23a,b shows those trends over the period 1970 to 1984, however only for those measuring points, in which the series of observations does not show considerable gaps. With the least square method the linear trend of the bottom level rise of each point of the measuring grid has been determined. Depicted are lines of equal bottom level rise (which is expressed in cm/year). These lines separate the area in sections which are about stable (changes of 1 cm/year or less), moderately accreting, c.q. eroding (2 to 10 cm/year) and those changing strongly (10 cm/year or more).
Although the pattern obtained is consistent, it is not easy to interprete. As subsect. 2.3.5 will elucidate, the "pseudo-trend", caused by the breaker bars will play an important role.This pseudo-trend depends as well on the amplitude as on the period of the breaker bars. For instance (table 2-1): the amplitude of the breaker bars is of the order of 1 meter and the period is about 20 years for the coastal stretch Bergen-IJmuiden (fig.2-11a) and 5 years for

IJmuiden-Katwijk (fig.2-11b). Thus, for a period of observation of 20 years one finds a pseudo-trend of ca. 1 dm/year for Bergen-IJmuiden and ca. 2 cm/year for IJmuiden-Katwijk. As a matter of fact, one indeed observes in the picture of fig. 2-23a a strong dominance by the motion of the breaker bars: shifting in parallel belts of alternately sedimentation and erosion. Indeed, this "trend" is of the order of 1 to 2 dm/year. Topographically, those belts coincide rather well with the breaker bars. Visually, the macroscopic consistency of the features is striking (the same trends over a distance of 30 km!)
Near Callantsoog (fig.2-23a) sand was supplied for dune enforcement in 1976/77 (350.000 m3) and in 1979/1980 (470.000 m3). This explains the sedimentation in fig 2-23a at the landward side.
In the vicinity of Den Helder (fig.2-11a and 2-23a; fig 2-40) one observes sedimentation in the shallow part of the Schulpengat. Not enough data was available in the deeper part of the Schulpengat to make statements concerning the trend at that site.
Consider now the part south of IJmuiden (fig23b) Generally, here the trends vary between -9 to +9 cm/yr at the inshore; stronger trends occur in the dunes (order: +/- 20 cm/yr).
Below OD -6m there are large areas (between km 80 and km 90) where the coast is practically stable; however, at some places, for instance between Scheveningen and Hook of Holland (fig 2-11b) also there variations of 5 cm/yr do occur.
Dominating in fig.2-23a,b are the direct or indirect outcomes of human interference. At Hook of Holland, the whole picture is dominated by the local Beach Project Hook of Holland; although less rigorous, the same holds for the coastal behavior North of Scheveningen (the effect of enlargement of the harbor moles; refer to subsect. 2.3.3 for both cases).
Indirect results of human interference can be observed from the sedimentation South of thwe harbor moles of IJmuiden; sheltering effects (5.2.5) probably are dominant. In the direct vicinity of the Southern mole a sedimnetation took place at a rate of ca. 20 cm/year at the inshore and even at a rate of 40 cm/yr in the dune area. At a distance of 3 km Southernly of this mole (near km 59; fig. 2-11b and 2-23b) sedimentation rates are reduced to 1 to 5 cm/yr.
Another indirect outcome of human interference is the formation of a scour hole near the Scheveningen moles, caused by the contraction of the streamlines and local high's of the current velocity[1], In the local bottomtrends (fig.2-23b) this reveals itself by the abrupt transition of some sedimentation into larger erosion, (5-11 cm/year) concentrating itself within a small area (RSP km 100.50). Also in the 3D-picture (fig.2-11b) the scour hole is visible.
Considering fig. 2-23b, as well longshore as cross-shore features are showing off, i.e.: longshore and profile changes. Clearly turns out: the erosion of the coast near Zandvoort; This seduces to ponder, that the sand for the sedimentation near IJmuiden has to come from somewhere. Here (RSP km 59.00-64.00) bottom level changes occur at a rate of -1 to -5 cm/yr [2].
Longshore belts are visible in fig. 2-23b. This leads to think of effects of breaker bars. However, the bar-structure does not show up in the location and orientation of those belts. Furthermore, the feature is present as well near the coast of Delfland (i.e., Scheveningen—Hook of Holland), where (if bars are present anyway) bar activity is of minimal importance.
Excluding the area of the Beach Project Hook of Holland at the seaward end of the area under consideration some offshore erosion can be observed. Seaward of the area considered nearTerheide (fig. 2-11b) one finds a long term dumping site of silt from the Nieuwe Waterweg[3] . Fig. 2-23b does not show coastal accretion at that site (rather: coastal erosion).
Generally speaking, changes in the curvature of the coastal profile show up more explicitely than a general steepening or flattening of the proifile. Adequate explanations are still lacking. A 100-year analysis probably would result in smaller trends than the 20 years considered. For one cannot assign the sky the limit to those trends and furthermore opposite trends in neighboring areas will cause reactive forces. Thus a similar analysis as displayed in this chapter at the turn of each millennium would be advisable.

[1] An example of this kind of process, however valid for IJmuiden, is depicted in fig. 2-22. (subsect. 2.3.3)
[2] Sedimentation being positive, evidently
[3] called "loswal Noord" in Dutch

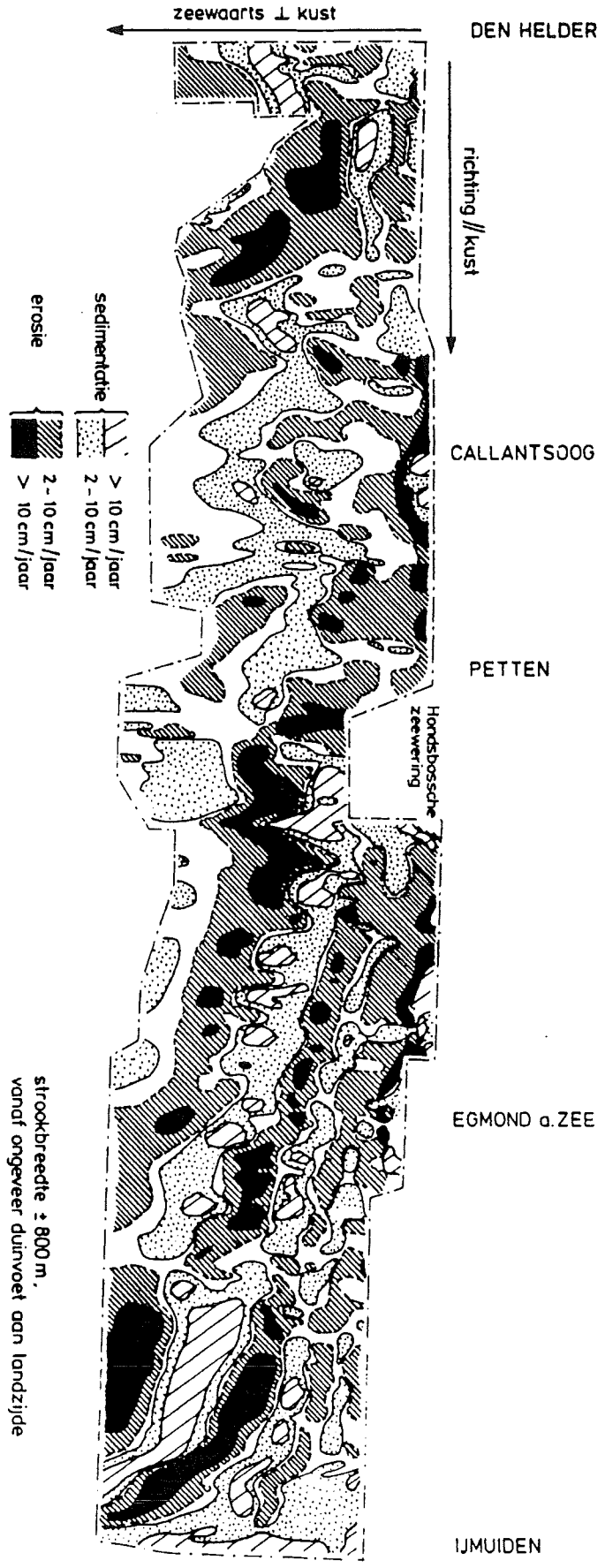

Figure 2-23a: 20 year averaged bodemtrends North-Holland

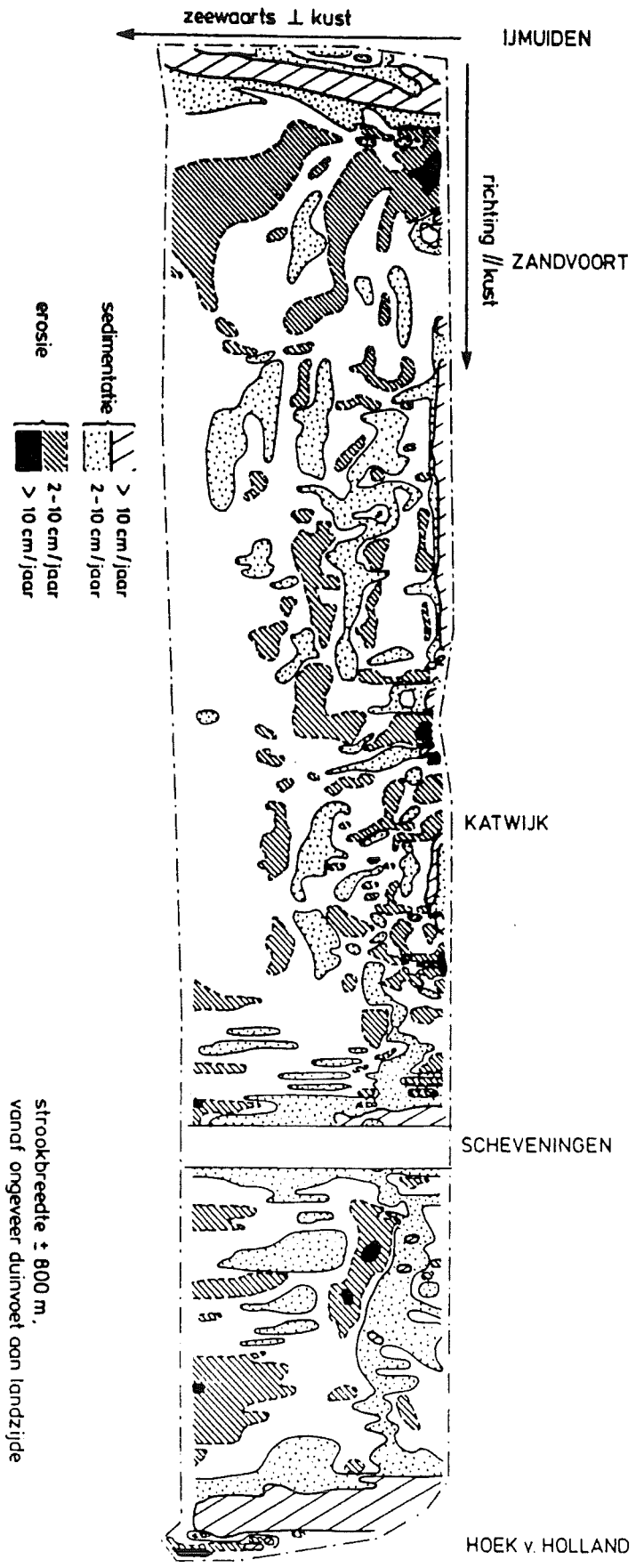

Figure 2-23b: 20 year averaged bodemtrends South-Holland

2.3.5 Philosophy concerning "trend"

Do 20-year averaged linear bottom trends (cf. subsect.2.3.4 and fig.2-23a,b) make sense? This is the topic of this subsect. 2.3.5.

In the first place the question arises, how consistent the measured trends are. For instance, the pattern of fig. 2-23b b is rather mixed-up (in contrast with the one shown in fig. 2-23a, where the 20-year motion of the breaker bars strongly dominates). The consistence appears to be better than fig. 2-23b suggests. This is illustrated with fig. 24, where as a detail of fig. 2-23b the trends in any of the respective measuring points in the surroundings of IJmuiden have been depicted. It shows, that de spatial gradients in the accretion velocity are small and over belts with a width of several hundreds of meters and over the length of 5 to 10 km the same tendencies are found.
Lit. [58] deals with the influence of accidental measurement errors on trends. From the calculations the following result is found. If the standard deviation of the accuracy of sounding in every separate measuring point amounts 20 cm, with annual surveys over a period of 20 years a standard deviation of the trend of approx. 1.4 cm/year is found. This if the deviations from the trend from year to year are not correlated.
But is this the case?
Suppose, a sinusoidal signal is averaged over a certain observation time with the aid of the least square method. This implies the assumption of a linear trend; every deviation from this straight line will be seen as a random fluctuation. With reason statisticians will object to this method; however, if one has to deal with periods of the signal of four years and sample frequencies of once a year with a relatively small observation period, it is hard to distinguish signal and noise.

At first presume, that the observation time is very short compared to the period of the sinus and that at the starting time of observation the signal has the value zero (fig. 2-25). As (pseudo)-trend one will find the tangent to the sine curve. Clearly, this is the maximal pseudo-trend that can be obtained. Fig.2-26 displays the pseudo-trend (as fraction of the earlier mentioned maximum) as a function of the observation period. As mentioned, there was started from the assumption that the signal was zero at the beginning of the observation time and after that it became positive. The calculations are given in [53]. For the area between Zandvoort and Noordwijk (table 2.1, subsect.2.3.2.1) in the longshore belt with maximum breaker bar motion a maximum pseudo trend (small observation period) of 1,14 m/year is found, caused by the periodical motion of the breaker bars. Choosing an observation period of 4 times the period of the breaker bars, i.e. 16 years, still a maximum pseudo trend of 1,9% (fig. 2-26) remains: this means 2 cm/year. In fact the pseudo trend will be somewhat smaller, as at the beginning of the observation period the phase of the oscillation will be different everywhere.
It is a case of philosophy, to which rate one wants to involve the influence of the long period oscillations (like for instance with a period of 30 years) into a 20 year trend. In the first place it will be disputable, if one will be able to recognize those signals as periodic; however, even if this is the case, it is "allowed" that 2 succeeding 20- year trends are different. However, it makes sense to realize, how long period motion affects the trend.
The breaker bars in the surroundings of Egmond for instance, have a period in the order of 20 years; fig. 2-23a is not corrected for this. According to fig.2-25 this can cause "errors" in the order of the trend of 30 to 40 % of the maximum pseudo trend, which has a value of 30 cm/year at this location. In order to give an impression, how the breaker bars affect the accuracy of the trends, in fig. B4 for the area between IJmuiden and Scheveningen has been indicated (according a way of presentation corresponding to fig. 2-23) which pseudo trend would arise due to the breaker bars, as schematized according to description in subsect.2.3.2.1 and as calculated for the area under consideration. At the most an inaccuracy of 3 to 4 cm/year is found. One has to compare this pattern with the data in fig. 2-23b. An other illustration of the non-linearity of the trend is given in fig.2-28, an early version

of fig. 2-23b. South of the Hondsbossche Seawall five extra ranges are taken into account, however this data is only available for the last 7 years (from 1975 to 1985). Because the measurement period differs, these ranges are found to have a completely different trend, than in the surrounding area.

It is in any case useful to realize, how time dependent the calculated 20-year trends (still) are. A trend of 5 cm/year is (mathematically) 5m/century. The area between the Delfland groins accretes with approx. 5 cm/year, however one has to be a very big optimist to expect this to go on for a century.
The 100-year trend of erosion and accretion of the coast of 1 to 2 m/year (fig. 2-12) should, at a average coastal slope of 1:100, be translated to vertical trends of 1 to 2 cm/year. From the previous it shows that the noise of short-term phenomena is to big to monitor those trends. This goes even more for the a sea level rise at 2 mm/year.

2.3.6 General conclusions

1. The Dutch coast is far from uniform (fig. 2-11a, b). The part near Den Helder is determined by the dynamics of the Texel inlet. South of the outer delta occasionally one breaker bar shows up. Farther south the Hondsbossche and Pettemer Seawall dominate the bottom topography. South of this (Egmond) a somewhat tangled pattern of 2 or 3 breaker bars appear somewhat obliquely to the coast (the opening heading south). Continuing in Southward direction, the coastal profile becomes more gentle; this goes together with more breaker bars.
   For example between Bergen and Egmond in the deeper regions bottom changes are restrained by the expose of old clay and peat formations [26].
   The harbor moles of IJmuiden strongly determine the local topography. Further South, away from this influence, a regular pattern of 2 to 3 breaker bars is found. Number and size of the breaker bars decrease in southward direction as the coast tends to steepen. South of Scheveningen no breaker bars are found.

2. South of IJmuiden the breaker bars propagate seawards with a velocity of 60 to 80 m/year (fig. 2-13b); its wavelength is in the order of 200 to 300 m and its period is 3 to 4 years. The influence of storms on the behavior of the breaker bars can hardly be recognized. North of IJmuiden the movements are much smaller and less regular (fig. 2-13a).

3. Probably, "surf beat" and "edge waves" play a big role in the dynamics of breaker bars. These are low-frequent waves with a period in the order of 5 minutes, emerging because the momentum of groups of alternately high and low waves forces resonance of the (total) water mass in the surf zone.

4. The gross longshore transport along the Dutch coast is in the order of a 100 times larger than the cross-shore transport (compare fig. 2-18 and 2-19). However, sedimentation and erosion appear by local differences in transport. These can by of the same size order for the longshore and cross-shore transport.

5. The direct and indirect consequences of human interference as on the one hand the extension of the harbor heads of IJmuiden, Scheveningen and Hook of Holland and on the other hand the large-scale sand supply of the Beach project Hook of Holland are very clearly and these locally dominate the natural changes along the coast (fig. 2-23a,b). Because the breaker bars North of IJmuiden have a period, of the same order of magnitude as the observation period the propagation of these breaker bars is reflected in the linear trend; this results in trends, varying alternately in belts (300m wide; 30 km long) of sedimentation and erosion in the order of 10 to 20 cm/year. The site of those belts coincides with the site of the breaker bars.
   South of IJmuiden, where the period of those breaker bars is considerably less, the motion of these bars averages out (to a large extent) over the observation period,

although the influence of the breaker bars still can not be neglected. In subsect. 2.3.5 this averaging effect is investigated.
South of IJmuiden changes of the underwater topography, remaining after time-averaging the breaker bars, generally vary between + and – 10 cm/year. Spatial gradients in sedimentation velocity are small: over belts with a width of several hundreds of meters and lengths of 5 to 10 km the same tendency is found (fig. 2-23a).

6. Only locally, like between (about) Zandvoort and Scheveningen (fig.2-23b) , the most seaward part of the measured coastal profile (until about 800 m seaward of the coastline) is stable. In front of Monster however an erosion rate between 5 and 10 cm/year is found.

7. Changes in the curvature of the coastal profile (after time-averaging the breaker bars) show off over the last 20 years more clearly than an overall steepening or leveling.

8. Rather much for sure the 20-year trends are still large compared to the 100-year trends, in which even more phenomena are time-averaged.

Many of the causes of the registered coastal behavior is still unknown.
It will be clear, that monitoring the topography of the coastal zone requires a great effort in measuring and processing capacity.
However, this is necessary to maintain the validity of the statement: "the coast is safe".

2.4 Sand transport by waves and tides (uninterrupted coast)

Van Straaten [6] and Edelman and Eggink [7] both give qualitative considerations about the sand transport by waves. Since their publications, so much data has been collected about the relation between the longshore component of the wave energy and the sand transport, that it is worthwhile to apply such formulae to the Dutch coast in order to obtain more quantitative conclusions. However these conclusions cannot be better than the available data; i.e. the visual wave observations made on the Dutch lightvessels (table 2-2). These measurements from 1949 to 1957 have been statistically analyzed by Dorrestein [12], giving the probability of occurrence for each wave condition, (characterized by height period and direction of the waves). Harreveld [13] correlated the visual wave height of the Goeree lightvessel (at 10 km from the coast) with the wave height observed on the step resistance wave gage "Triton" at 3 km from the coast, and concluded from this that the low waves were estimated too low and high waves too high, the (significant) waves of 1 to 2m being estimated correctly. The regression coefficients between lightvessel and wave gage were different for each wave direction, which is clear for the offshore waves because these waves were generated with a different fetch. However, also for the onshore waves there appears to be some influence of site. From the visually measured wave period at the lightvessels an "equivalent wave period" T_{eq} has been derived, according to Battjes [14]

$$T_{eq} = 1.23\, T_m \tag{2.1}$$

in which T_m is the mean period of upward zero-crossings. The equivalent wave period is the period, for which the energy/m^2 and the energy-flux/m of the replacing sinusoidal wave are equal to those in the wave in nature. Harreveld [13] found the visual Goeree lightvessel period T_{vi} about equal to $1.5\, T_m$ from which $T_{eq} = 0.82\, T_{vi}$. The longshore component of the wave energy-flux, P_l has been computed from:

$$P_l = 1380 h_{br}^3 \frac{\sin \varphi_0}{c_0} \qquad (P_l \text{ in W/m', } h_{br} \text{ in m}) \tag{2.2}$$

in which φ_0 and C_0 were the deep-water wave direction and phase velocity, and the breakerdepth h_{br} was found from:

$$h_{br} = \left[\frac{H_{sign}^2\, c_0 \cos \varphi_0}{2(0.4)^2 \sqrt{1.4 g} \cos \varphi_{br}} \right]^{\frac{2}{5}} \tag{2.3}$$

The theoretical basis of these formulae is given in [16]. The way of calculation (however for a more general kind of topography) is explained in ch.4 2.2 as well: eqn.(2.2) is analogous to eqn. (4.3b).The results are given in the next table.

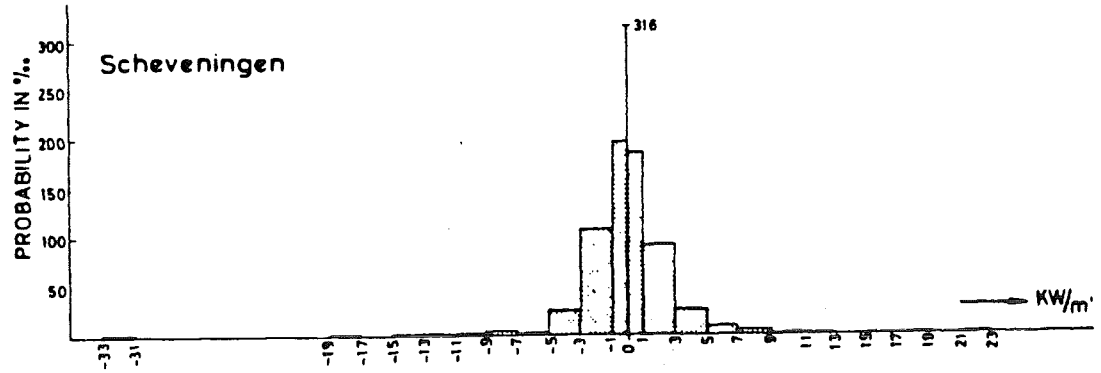

Figure 2-29: The probability distribution of the longshore current af the wave energy-flux near Scheveningen.

Probability (fr. in ‰) the occurrence of a certain value of P_1

site	Vlieland[1]	Texel[2]	IJmuiden[3]	Scheveningen[4]	
The size of P_1 \ orientation of the coast with respect to the North	060°-240°	030°-210°	15°-195°	045°-225°	
$-33 < P_1 < -31$				.13	North
$-31 < P_1 < -29$			.52		
$-25 < P_1 < -23$			.17		
$-23 < P_1 < -21$		.13	.24		
$-19 < P_1 < -17$			.42	.27	
$-17 < P_1 < -15$		.13	.70		
$-15 < P_1 < -13$	.03	.25		.92	
$-13 < P_1 < -11$	.27	.50	1.1	1.6	to
$-11 < P_1 < -9$	.25	.76	3.1	.35	
$-9 < P_1 < -7$	1.2	2.4	8.7	5.6	
$-7 < P_1 < -5$	.82	4.3	3.4	2.0	
$-5 < P_1 < -3$	8.9	19	26	26	South
$-3 < P_1 < -1$	32	56	120	119	
$-1 < P_1 < 0$	166	203	159	200	
$-\infty < P_1 < 0$	210	287	323	355	
$P_1 = 0$	529	401	299	316	
$0 < P_1 < 1$	155	196	272	188	
$1 < P_1 < 3$	53	70	86	92	
$3 < P_1 < 5$	29	31	15	28	South
$5 < P_1 < 7$	11	6.1	4.0	10	
$7 < P_1 < 9$	5.4	4.2	.88	6.0	
$9 < P_1 < 11$	1.4	2.1	1.3	.56	
$11 < P_1 < 13$	1.0	.61	.15	2.9	to
$13 < P_1 < 15$	1.1	.84			
$15 < P_1 < 17$	.84	.47		.56	
$17 < P_1 < 19$	.81	.24		.22	
$21 < P_1 < 23$	.34	.23		.44	North
$23 < P_1 < 25$	.42				
$29 < P_1 < 31$	.12				
$0 < P_1 < +\infty$	261	312	379	329	

1) From data lightvessel.
2) From data lightvessel Texel.
3) Probability of wave characteristics: mean between lightvessels Texel and Goeree.
4) From data lightvessel Goeree.

Table 2-2: The visual wave observations made on the Dutch lightvessels

Fig. 29 gives one of the probability distributions. From this it is easy to compute the mean energy flux and the mean littoral drift S^* (integrated over the surf zone) , using the CERC-formula:

$$S^* = 1.4 \cdot 10^{-2} \frac{P_l}{\frac{1}{16}\rho_w g} \qquad (\rho_w g = \text{specific weight water}) \qquad (2.4)$$

where ρ_w is the specific density of the fluid and g the acceleration of gravity.

$$S^* = 2300\, P_l \qquad (S^* \text{ in } m^3/\text{year}, P_l \text{ in W/m'}) \qquad (2.5)$$

However the used data and formulae are not accurate enough to justify this computation since the probability distributions are about symmetrical. Only along the Vlieland coast the resultant drift is significant (about ½ mln. m^3/year). The resultant net energy-flux was always less than 0.3 KN/m'.
The gross littoral drift (sum of transport in both directions) can be computed from the summations of the products of the absolute value of P_l and the corresponding probability of occurrence (called pr (P_l)).

$$S^*_{gross} = 2300^{-2} \sum_{all\ prob.} \{|P_l| \cdot pr(P_l)\} \qquad (2.6)$$

This gross littoral drift is found to be of the order of 1.5 to 2 rnln m^3 /year (thus about 1 mln m^3 in each direction).
Assuming for a moment no influence of tides, the distribution of the littoral drift over the surf zone has been computed by an adapted method proposed by Svasek [8]; the method of computation is illustrated in [15] and is treated in more detail in [16]; in sect.4,2 a more general case is treated[1]. The result for Scheveningen is shown in fig. 30.

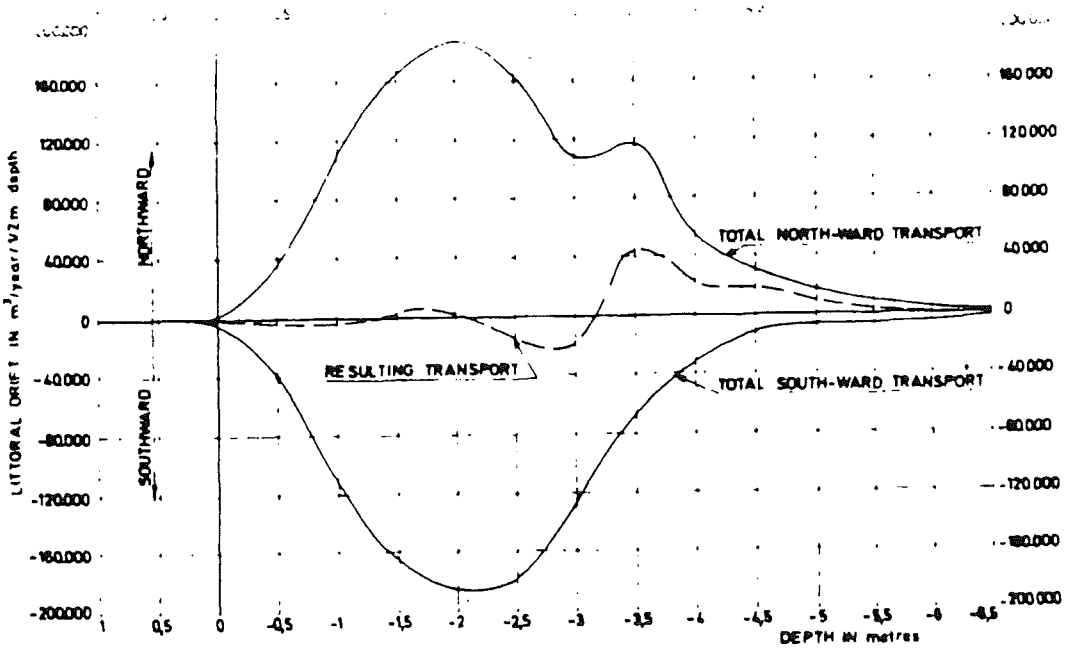

Figure 2-30: Distribution litt. Drift over profile.

[1] If h_1 in eqn. (4.3a) is taken equal to zero, the result is eqn (2.2). Eqn. (2.3) is a specific case of eqn. (4.17a): n_0=0.5; γ=0.4; F_r=√ 1.4

Considering which influence is more important, the one of waves or the one of tides, in [17] and [18] the driving forces of waves and currents are investigated. The total driving force of the longshore current in the surf zone is [19]

$$\frac{1}{2} E_{br} \sin 2\varphi_{br} = \frac{1}{16} \rho g \gamma^2 h_{br}^2 \sin \varphi_{br}, \tag{2.7}$$

in which E_{br} is the wave energy per m^2 in the breaker zone, φ_{br} the angle of wave incidence, h_{br} the breaker depth and γ the ratio between breaker height H_{br} and h_{br}
The driving tidal force over the breaker zone assuming a rigid bottom slope with gradient m is:

$$\frac{1}{2m} h^2 \cdot \rho g \frac{\partial h}{\partial x} \tag{2.8}$$

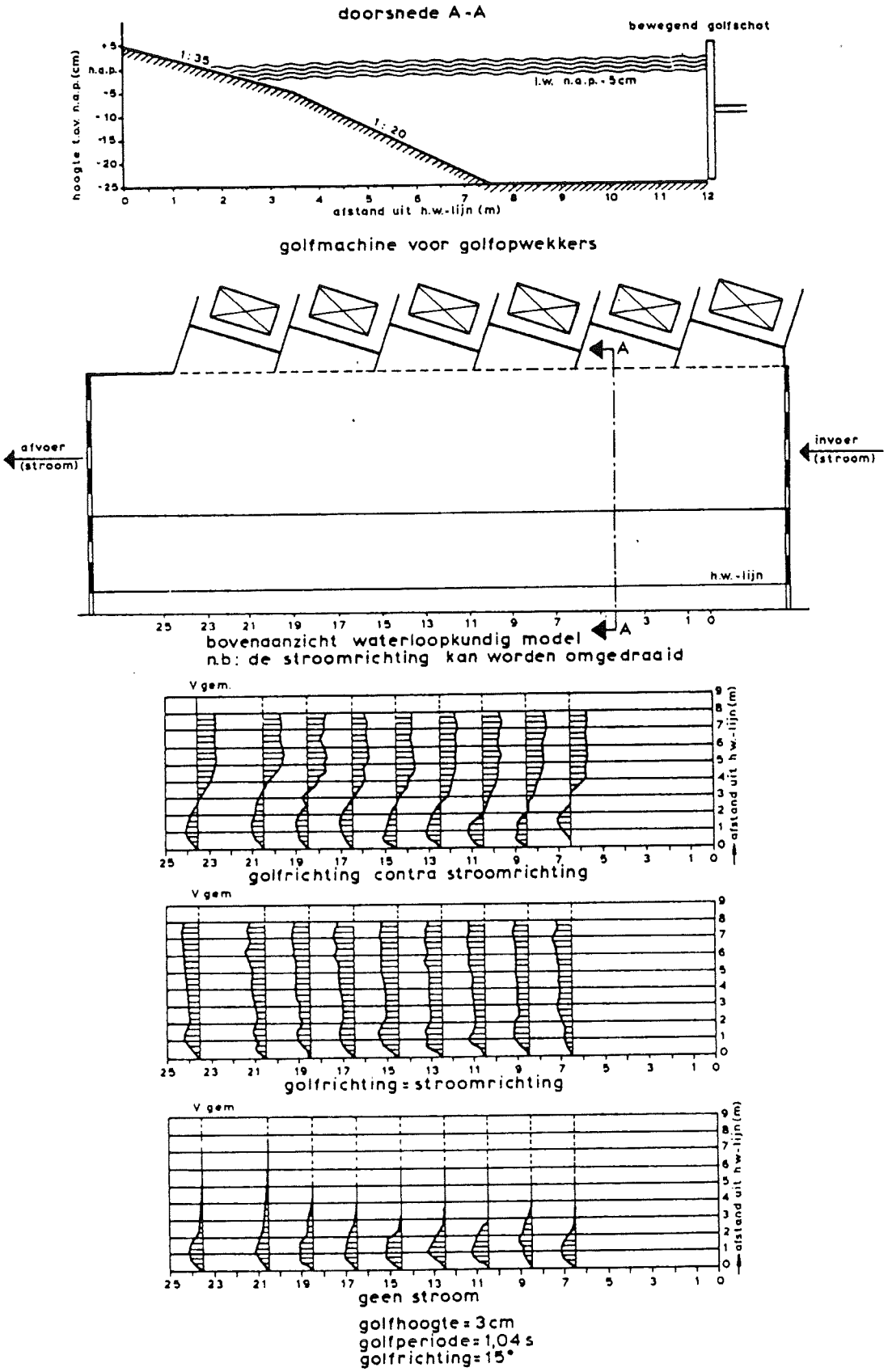

Figure 2-31: Experimental data concerning currents, generated by combination of waves and (tidal) water level gradients.

in which $\frac{\partial h}{\partial x}$ is the gradient of the water level in longshore direction, of which for a sinusoidal tide (a. *cos(ωt-kx)*) is taken the maximum value, i.e. ak. The ratio between the longshore-current force and the tidal force is therefore

$$\frac{1}{8}\frac{m\gamma^2}{ak}\sin 2\varphi_{br} \qquad (2.9)$$

which is mostly large except for very small angles of wave incidence.

This estimate of order of magnitudes can be illustrated with the aid of fig. 31. This figure shows the result of current measurements in a wave basin in Delft Hydraulics Laboratory, in which the current was measured caused by obliquely incident waves, respectively (first alternative:) without a gradient of the water level (then only longshore current results), (second alternative:) with a surface current in the direction of the longshore current and (third:) with a surface gradient counteracting the longshore current. Fig. 31 demonstrates, that the longshore current overrules the tidal current.
Assuming that the waves stir the material and the currents transport it, it thus is reasonable that the transport in the surf zone, according to the former computation, is rather well reproduced, except for the case where zero transport is computed..
In order to get an impression of the influence of the tide a tidal computation has been carried out with the numerical tidal model of which fig. 32 gives the scheme [20]. Assumed is one channel system parallel and another one perpendicular to the coast. At the boundaries (the ends of the coastal-parallel channels) the vertical tide was given; at the junctions the vertical tide was computed and in the channels the horizontal tide. The computer program was developed by Booy according to the explicit leap-frog method; non-linear terms were considered, but Coriolis was neglected. In each channel at every time was computed: $\sum_t B\,v\,h\cdot\Delta t$, in which B is the width of the channel, v the current velocity, h the water depth at the moment and Δt the time step. From this, the resultant currents were found as indicated in the upper part of fig. 31; about 3 cm/sec in the shallow regions and 6 cm/sec in the deeper regions.

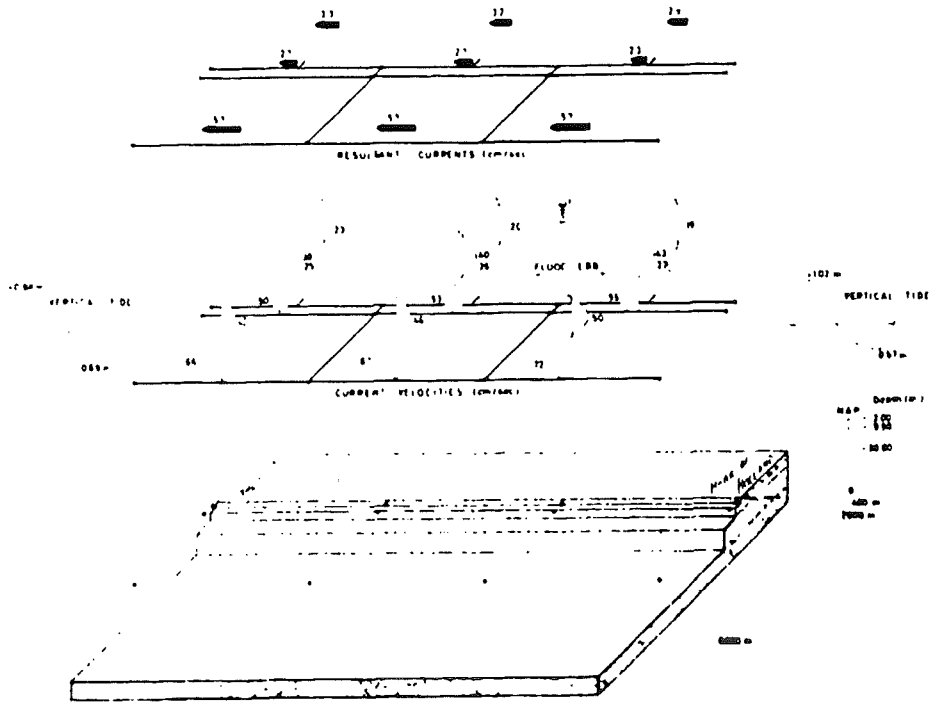

Figure 2-32: Tidal model

2.5 Tides, shaping a coast: lessons from old masters

As one may expect, the effect of waves and tides near tidal inlets will greatly differ from the one along an uninterrupted coast as treated in sect.2.4.
Again, causes of changes are tides, waves, wind, and current, where pilot investigations show, that the influence of wind is relatively small.

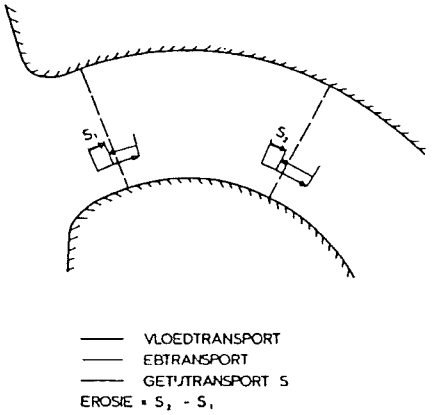

Figure 2-33: Erosion difference between sand transport in two cross sections.

Consider first the tide (fig. 2-33). During the flood period sand is transported in flood direction; during the ebb-tide the inverse Difference between ebb and flood transport is called the tidal transport; this is mostly small compared to ebb- and flood-transports. As its calculation involves the subtraction of two large and relatively inaccurate numbers, the result will be very inaccurate.
As a striking example: Delft Hydraulics (van Rijn & de Leeuw [49]) investigate the accuracy of the calculation of the erosion/sedimentation of the Valkenisse channel in the Western Scheldt (channel 14 in fig. 2-34) and find an estimate of the sedimentation of -0.3 cm/yr with a standard deviation of 35 cm/yr.
Table 2-3a,b,c (fig. 2.34) shows the way of calculation. Mind, that the calculated accuracy of the transport integrated over one flood-tide and one cross-section (i.e., integrated over a number of measuring positions as well) has "only" a standard deviation of the same order of magnitude of the transport itself. The sedimentation really measured in the channel was 20-30 cm/year, which, as the report states: "is within the range of accuracy".
The investigation, quoted above illustrates also, that the existence of tidal transport does not imply, that the tidal channel is subject to changes. For if this transport is uniform, the channel is stable. The same statement holds for the adjacent coasts [1]. Erosion results from a positive spatial transport gradient; sedimentation from the opposite case. As illustrated by the "channel 14"-story, determination of the rate of accretion, c.q. erosion is still more inaccurate than of the transport per tide, because again the difference between two large, inaccurate numbers has to be determined. The example given: "calculated rate of accretion/erosion orders of magnitude less than the standard deviation of the computation" is normative.
Still, despite of all the reserve, qualitatively some statements on the mechanism of tidal transport can be made [2].

The Southern part of the North sea (roughly between Den Helder-Cromer at the Northern side and the English Channel at the Southern side) has a length of about one quarter of the length of the tidal wave. Thus one would expect a system of nodes and anti-nodes with a large vertical tide near Calais and practically no vertical tide near Den Helder-Cromer; however, because of the effect of earth rotation during flood water is pressed to the English coast and during the ebb against the Dutch coast. This has the effect, that the tidal wave turns around in the North Sea: from North to South along the English coast and from South to North along the Belgian and Dutch coast (fig.2-35).
This implies, that in the Netherlands the tidal wave intrudes from the Southside in the estuaries. Fig. 2-36 shows the cotidal lines of HW in de embouchment of the Easter- and Western Scheldt: the "crest" of the tidal wave intrudes from the Southern side in the estuary. In the direction of the crest the water levels at a certain time are equal (by approximation)

[1] If one replaces "transport by current" by "combined transport by waves and currents" in the statement treated (cf. sect. 2.4).
[2] The idea originates from Van Veen [4]: a classical paper, demonstrating the fine-tuned physical feeling of our predecessors and masters. Refer to Edelman [59] as well.

and as, generally speaking, water directs itself to the lower level, current velocities in the direction of the crest are small. In the same way it may be explained, that as the water surface gradient is perpendicular to the tidal wave crest, i.e.: the current direction will be perpendicular to the crest as well. It may be clear that direction of channel scouring coincides with current direction, i.e. (again: generally speaking) perpendicular to the crest of the tidal wave, i.e. to the cotidal lines. This implies, that the main channels in the estuaria are mostly directed in Southward direction. The fact, that in spite of this there still exist channels with another orientation, is caused by the over-simplification of the explanation above. One of the effects neglected is the difference in behavior of ebb and flood (fig. 2-37). The estuary sucks its flood-water from all sides in a funnel, but it spits its ebb-water as a thin jet into sea. More formally: mind the (unidirectional) momentum of the ebb-current. So the main channel (mentioned before) generally will be an ebb-channel, where at the borders of the basin "flood-channels" will emerge (fig.2.38).
If, for a minute, one takes [1] a coastline in North-South direction in mind (inset of fig. 2-39), interrupted by a number of East-West orientated estuaries, then generally the North-West corner will be cut off strongly, where the South-Western corner suffers less current attack (although evidently, the flood channel still will play its role). In this way the coastal shape will look like a kind of a stepping stone See fig 2-38 from Van Veen [4] and fig. 2-39 after Edelman and Eggink [7] and [48].
In the next sections 2.6 with these principles in mind (most of the) Dutch inlets will be considered.

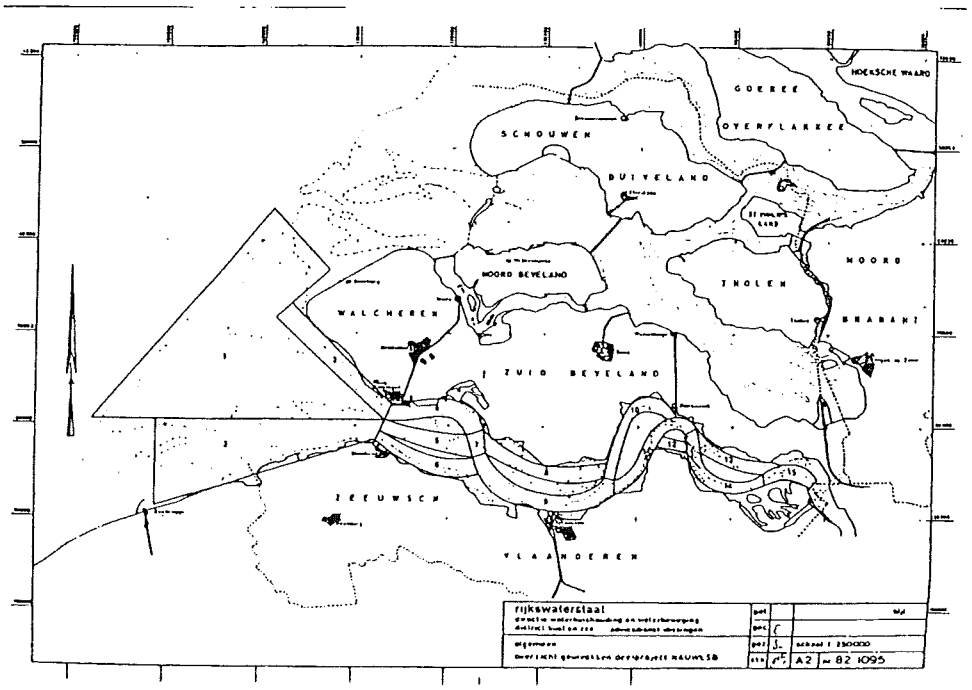

Figuur 2-34: Investigations of the NAUWES-B project (Delft)

Sandtransport integrated over a tideperiod

geul 14, 1981	S_{netto}	Standaartafwijking	
	(kg)	(kg)	%
westrand, vloed	$0{,}813 \times 10^7$	$0{,}848 \times 10^7$	104,3
westrand, eb	$0{,}806 \times 10^7$	$0{,}848 \times 10^7$	105,2
oostrand, vloed	$0{,}482 \times 10^7$	$0{,}470 \times 10^7$	97,5
oostrand, eb	$0{,}465 \times 10^7$	$0{,}470 \times 10^7$	101,1

Sandtransport over a tideperiod in a channel

[1] Dutch tidal conditions

geul 14, 1981	S_{netto}, getijfase (kg)	variantie (kg^2)	standaardafwijking (kg)
eb	$-0{,}341 \times 10^7$	$0{,}798 \times 10^{14}$	$0{,}894 \times 10^7$
vloed	$0{,}331 \times 10^7$	$0{,}798 \times 10^{14}$	$0{,}894 \times 10^7$

In total :

geul 14, 1981	S_{netto}, getijfase (kg)	variantie (kg^2)	standaardafwijking (kg)
eb+vloed	$-0{,}10 \times 10^6$	$0{,}160 \times 10^{15}$	$0{,}126 \times 10^8$

Resulting bottom change: $\Delta z = -0{,}3 \pm 35$ cm/jaar (1981)

Table 2-3a,b,c: Calculation Sandtransport

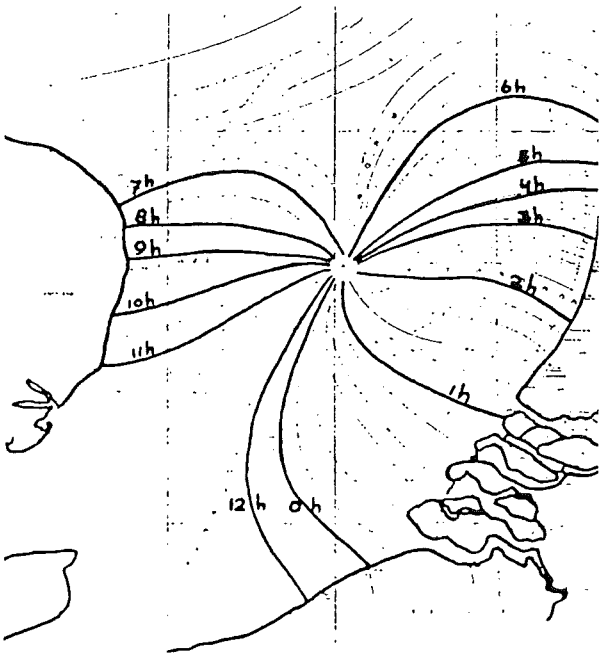

Figure 2-35: Co-tidal lines in the North Sea

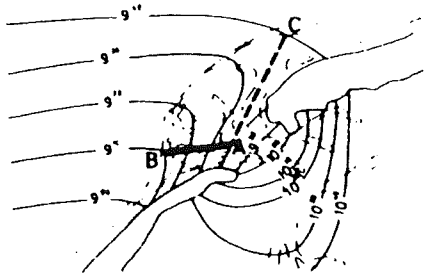

Figure 2-36: Orientation of channels according to van Veen

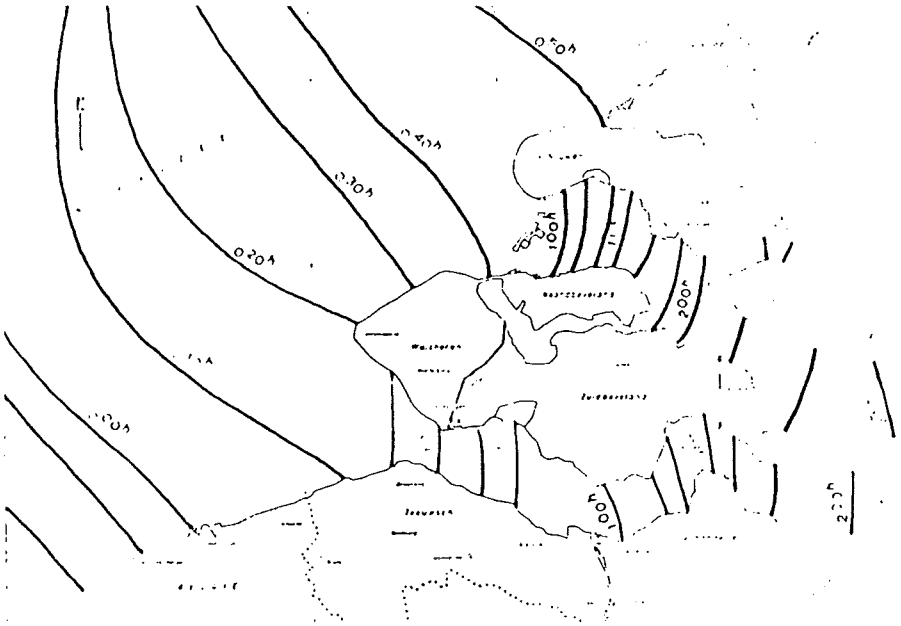

Figure 2-37: Co-tidal lines in the Zeeland area

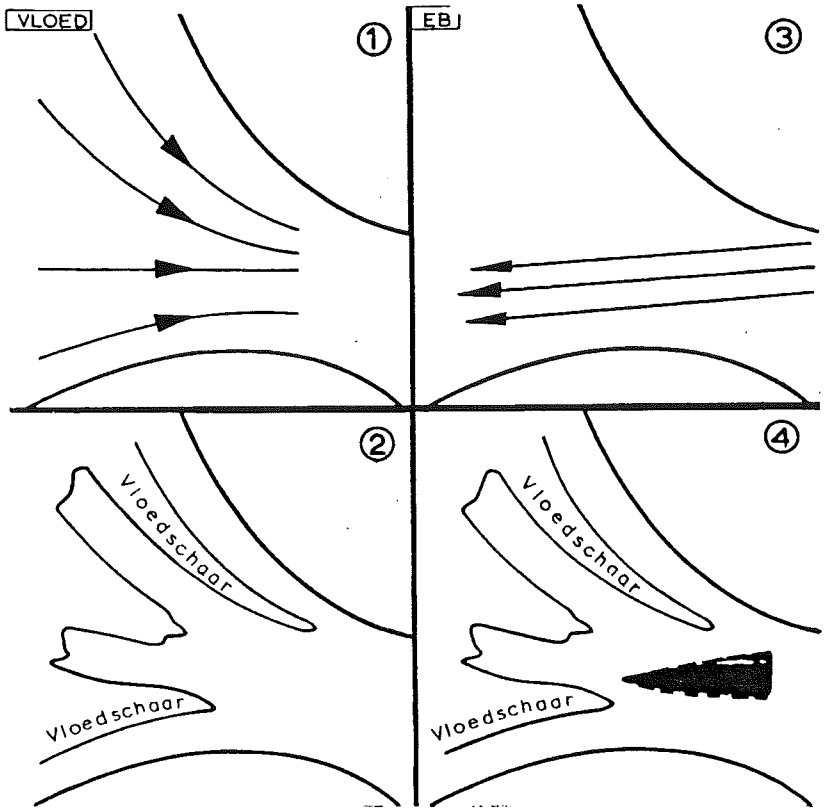

Figure 2-38: Flood- and ebb-channels in a tidal estuary

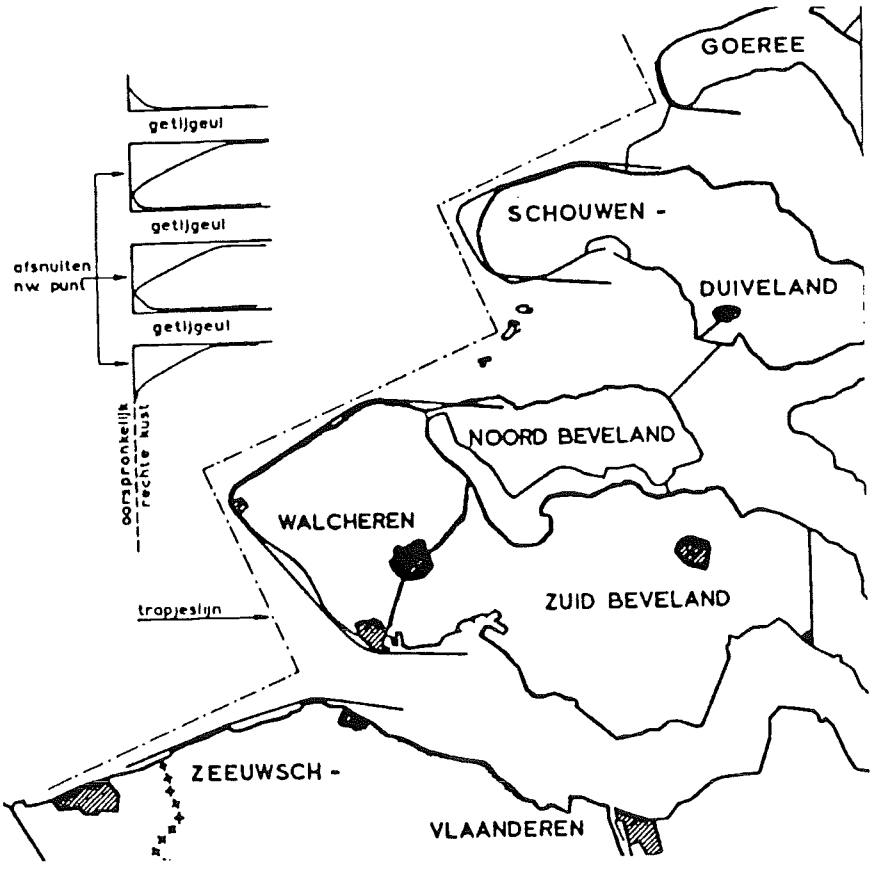

Figure 2-39: stepping stone shape af coastline near an inlet

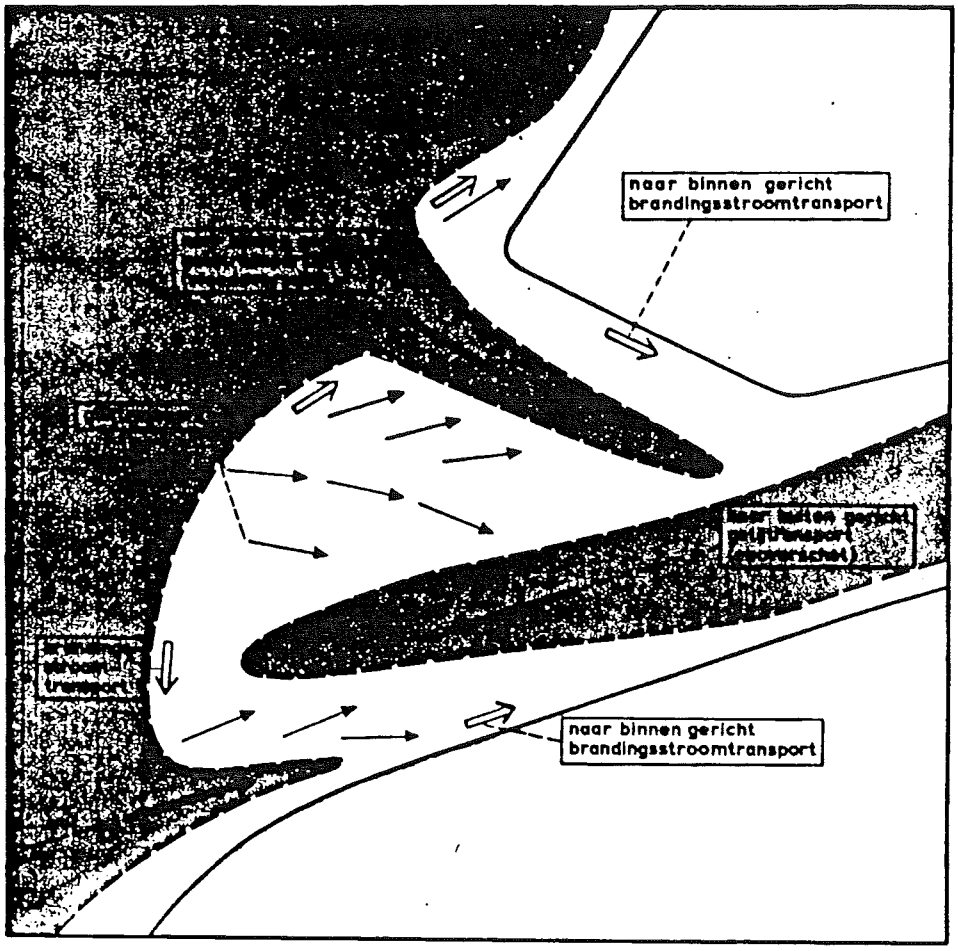

Figure 2-40: Schematic display sand transport near an inlet

2.6 The outher deltas of the wadden islands

The boundary conditions for the motion of the coast are given by the inlets. Therefore it is important to consider the motion of the tidal channels. Fig. 2-41, 2-42 and 2-43 depict the motion of the tidal channels in the inlets of Texel, Vlie and Eems respectively. The arrows indicate the motion of the channels since the last recording. What is known about these deltas?
The cross-sections of the tidal channels fit in reasonably with the theory Per Bruun and Gerritsen [8]. As a variation Haring [21] found that the quotient of the tidal volume (ebb + flood) and the total profile area of the tidal channel, was about 55 cm/sec, except for the inlet of Texel and the inlet of the Vlie, where it was 75 cm/sec (cf Dronkers [1]). This higher velocity might be influenced by the littoral drift because that will possibly narrow the tidal channels. Van Veen [22] states, that the largest tidal channels are mainly orientated in the direction of the greatest water gradient, averaged per tide. If the tidal amplitude is everywhere the same (which is often not the case), this direction is perpendicular to the cotidal lines (fig. 2-37; sect.2.5): the gradient between A and B is much larger than between A and C.
Two reasons can be given for erosion of the coast near these inlets.
As has been pointed out by van Bendegom [23], the submerging of the Wadden during flood-tide takes place with higher velocities than the retreating of the water over the shoals during ebb-tide. Thus, the water loses a part of its sediment here, which causes the Wadden shoals to reach an equilibrium at about the mean water level. Now the relative sea-level rise in the Netherlands during the last 20 centuries was about [1] 6 cm/century, which would result in a "sand hunger" of the Wadden shoals of about 1 mln m^3/year (distributed over all inlets). However, this will mostly be confined to finer sediments (D_m about 100-150 μ).
The second reason (sect. 2.5) is, that the water during the flood tide gets an acceleration, entering the inlet, but that during the ebb-tide it gets a retardation and this will give a jet-stream with vortexes on its side. Therefore in the tidal channels near the beaches, there is surplus of flood discharge and in the center tidal channel a surplus of ebb discharge. The flood erodes the beaches and the ebb gives an outer delta, which can reach up to mean sealevel (Noorderhaaks in Inlet of Texel). This delta gives a shelter against these waves, which would transport material away from the delta. As the waves come alternately from both sides, this process reinforces the erosion of the beaches near the inlets. Thus the erosion of Texel could be rather well explained [24]. After some time an equilibrium should be reached.
Two reasons can also be given for the motion of the tidal channels:
A meandering effect and longshore sand drift. It will be clear, that the resulting sand drift perpendicular to the tidal channel can not be derived from the velocity of the tidal channel, because of the meandering effect. The high amount of sand transport in the tidal channels can be attributed to the high current velocities and this meandering.
The motion of the tidal channels and the effects of their orientation has been investigated (fig. 2-44). The center line of each of the bars gives the orientation of the tidal channel in course of time. The width of the bar gives the development of the wet surface of the representative cross section. The time-integrated slopes of the water-surface as a function of the orientation have been displayed in fig. 2-44 [2]) as far as known. These give no evidence about the Van Veen theory (fig. 2-37; sect.2.5).

In fig. 2-45, derived from fig. 2-44, the rotation of the tidal channels in the Dutch Wadden delta is shown. Mainly these turn clockwise, although very slowly, and there is a slight indication (correlation coeff. 0,24), that the large tidal channels turn slower than the small ones.

In 1992 Huys [51] extended the investigation of Bakker & Joustra [29] concerning the rotation of tidal channels to the Friesche Zeegat.

---

[1] These estimates of Van Bendegom seem rather low, compared with later ones during the ISOS- and Coastal Management reports (ca.1990).
[2] These have been derived from Van Veen [21] and Ferguson [24]

As a challenge to future researchers Bakker [52] drafted tentatively the DC-formula [1]:, stating that the rotation velocity of a tidal channel is inversely proportional to its depth and to its radius of curvature, The background idea is, that the spiral current will probably be inversely proportional to the longitudinal curvature and the cross-transport in the channel roughly proportional to this current (convection more important than stirring). The assumption of inverse proportionality with channel depth implies a cross-transport of sand. independent of depth.

Fig.2-46 shows Huis' data, on which the equation is based upon.
The formula reads;

$$e_r = \frac{10}{R \cdot h} \tag{2.10}$$

in which: e_r is the transversal erosion velocity of the channel in km/yr; R is the radius of curvature in km and h is the channel depth in m.

[1] "DC" stands for: "Dutch Courage"

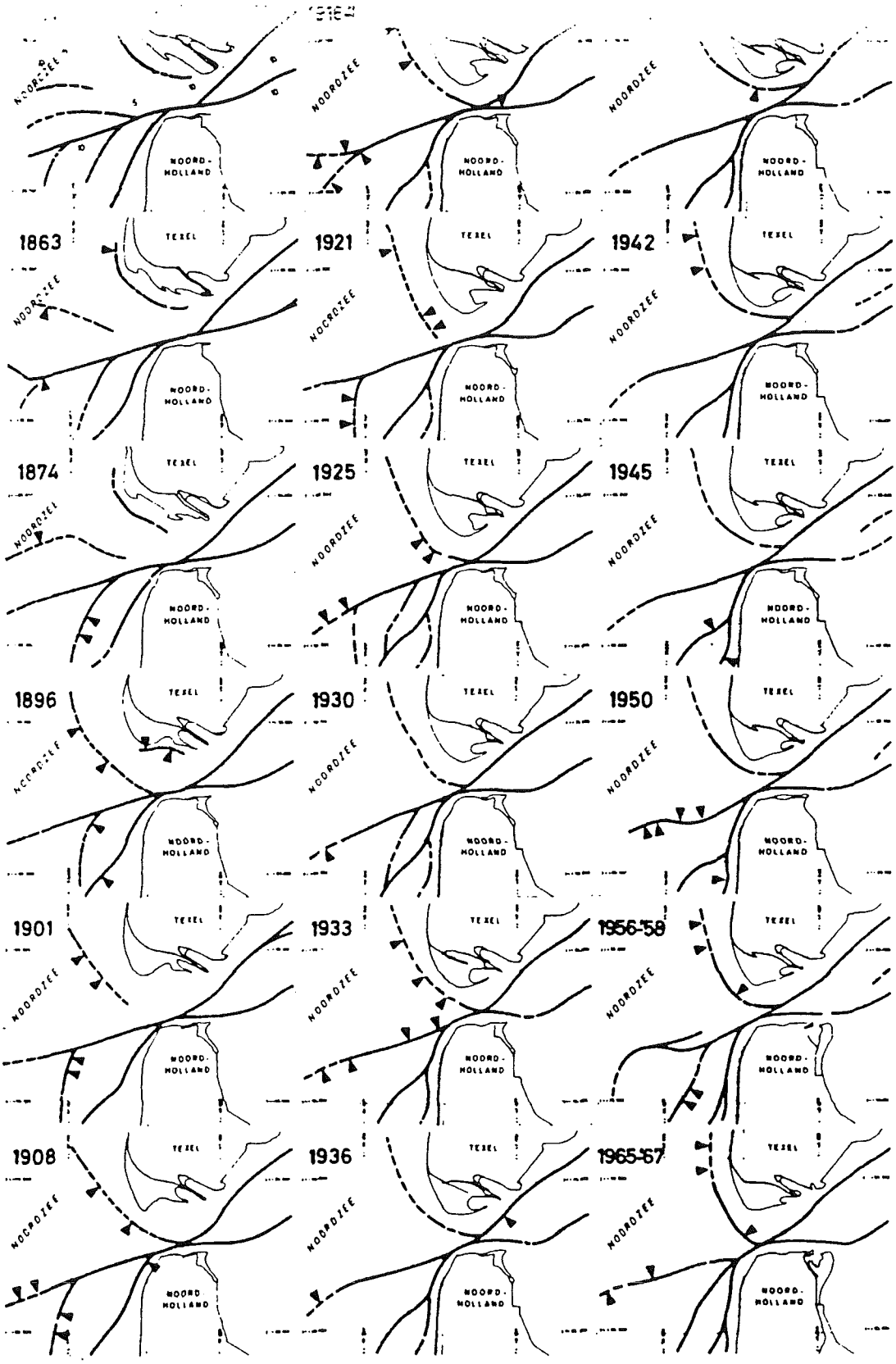

Figure 2-41: Marsdiep

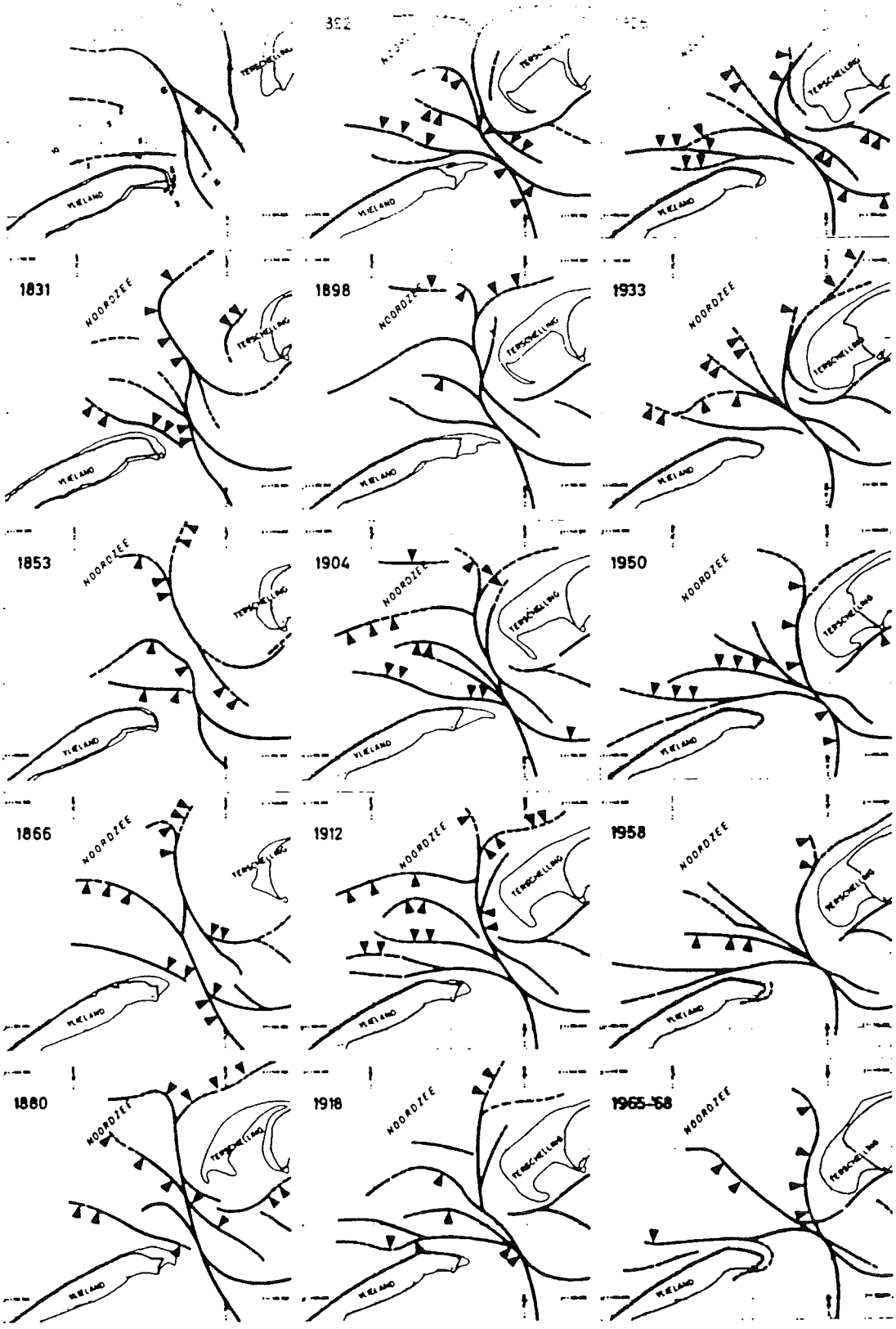

Figure 2-42: Vlie

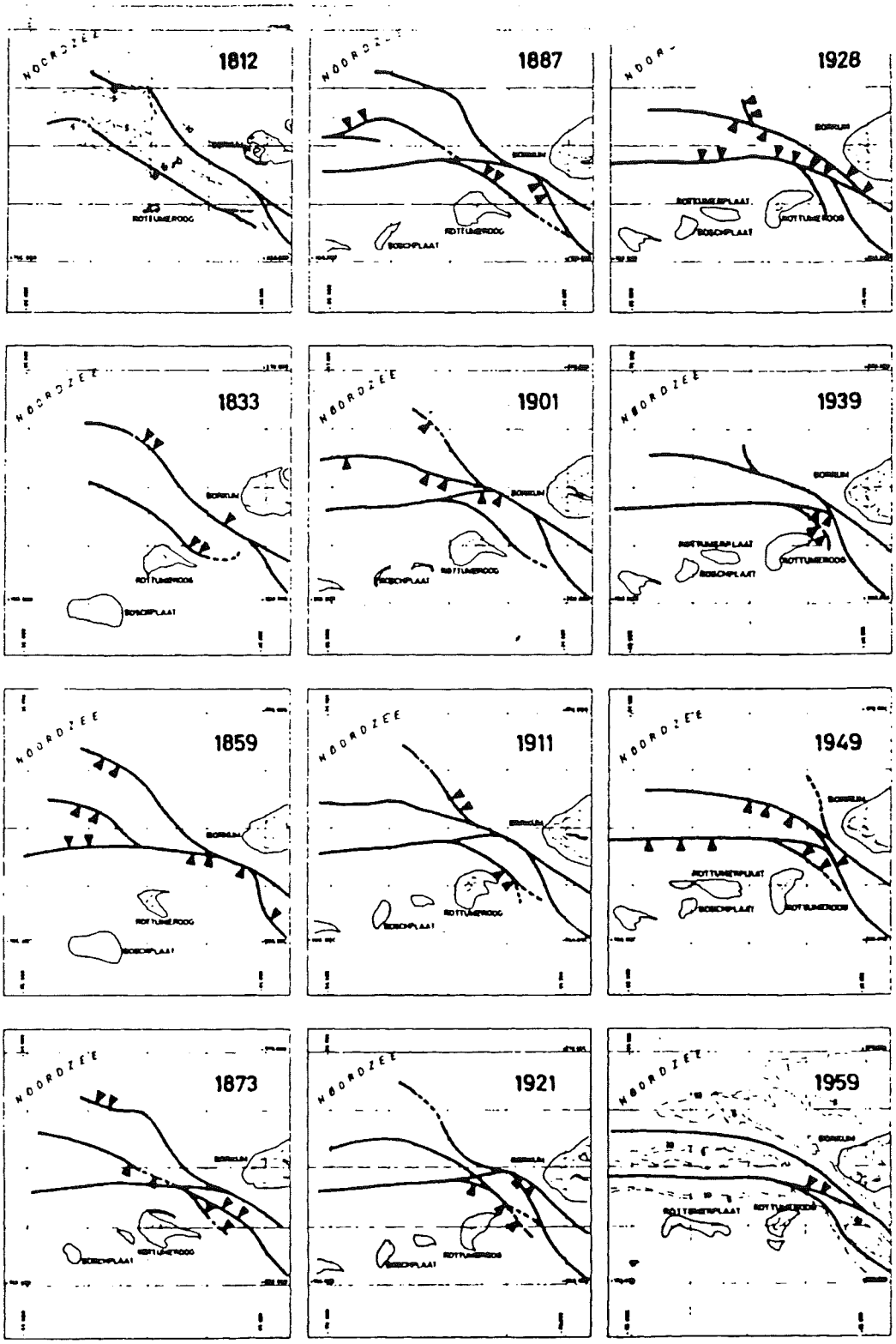

Figure 2-43: Eems

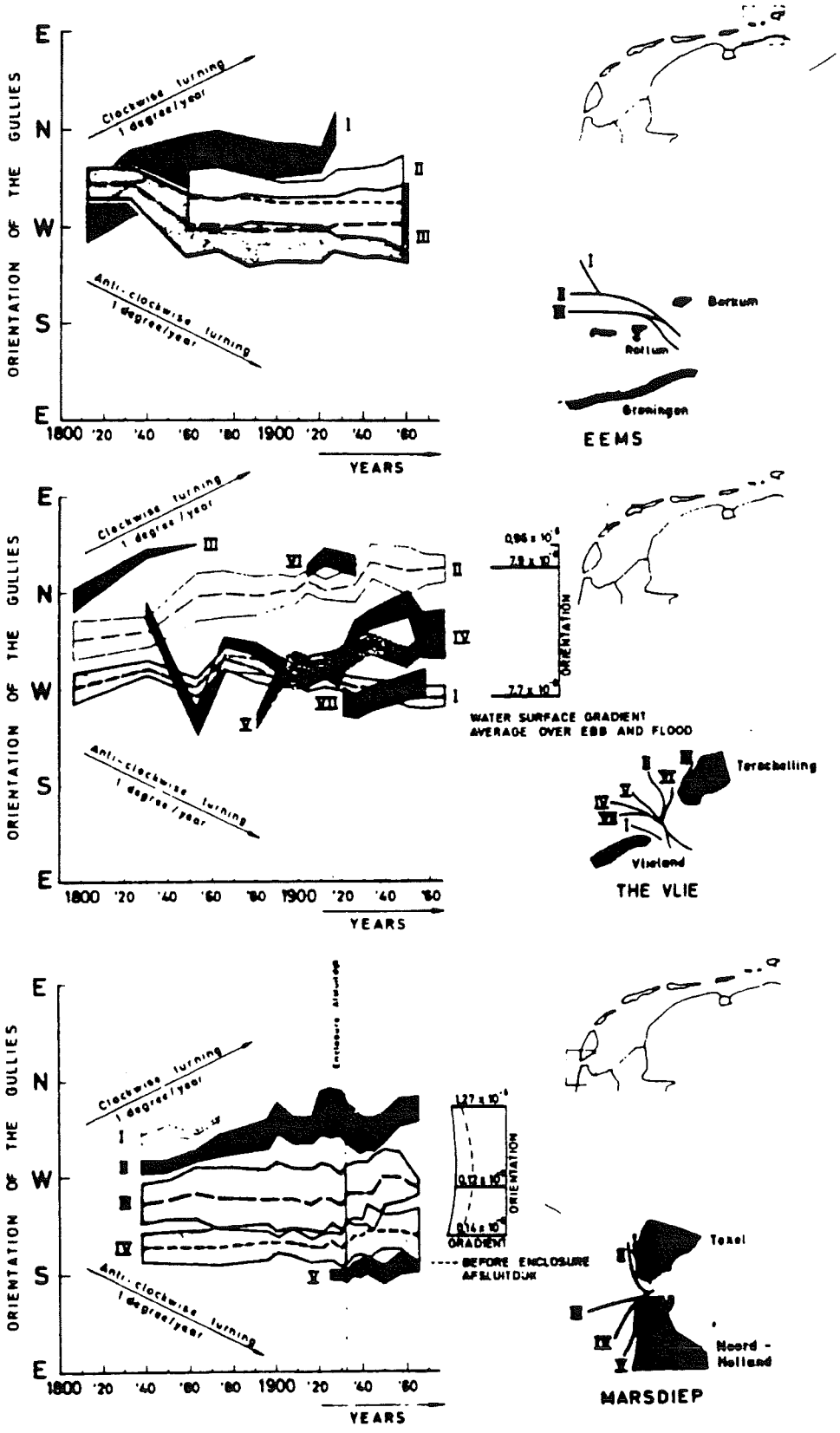

Figure 2-44: Direction and cross-section tidal channels.

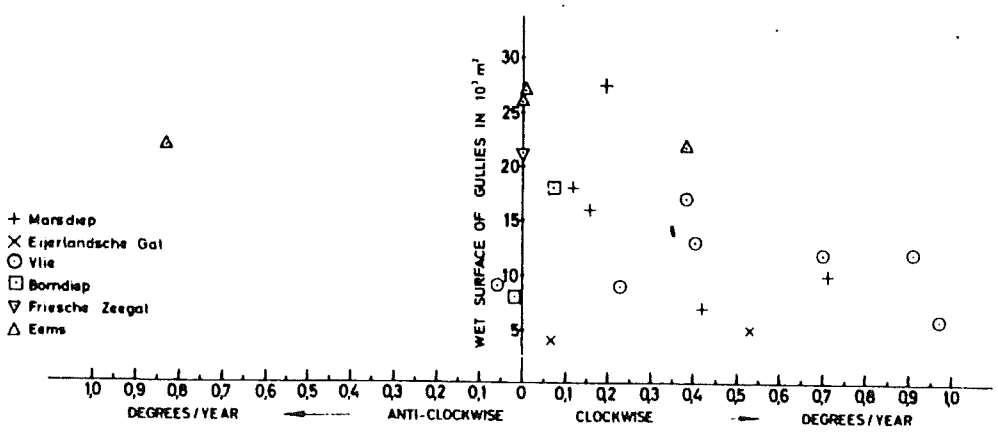

Figure 2-45: Correlation cross-sections and orientation tidal channels.

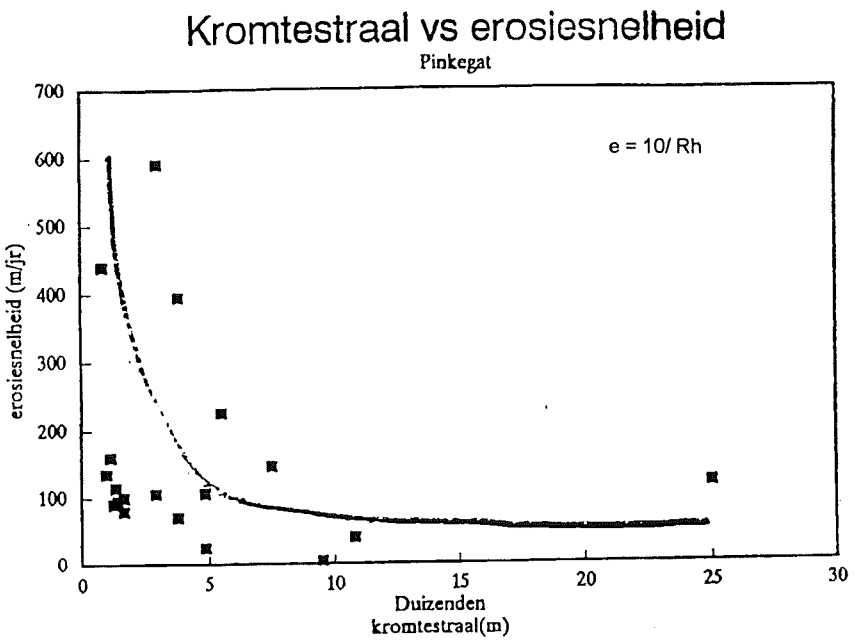

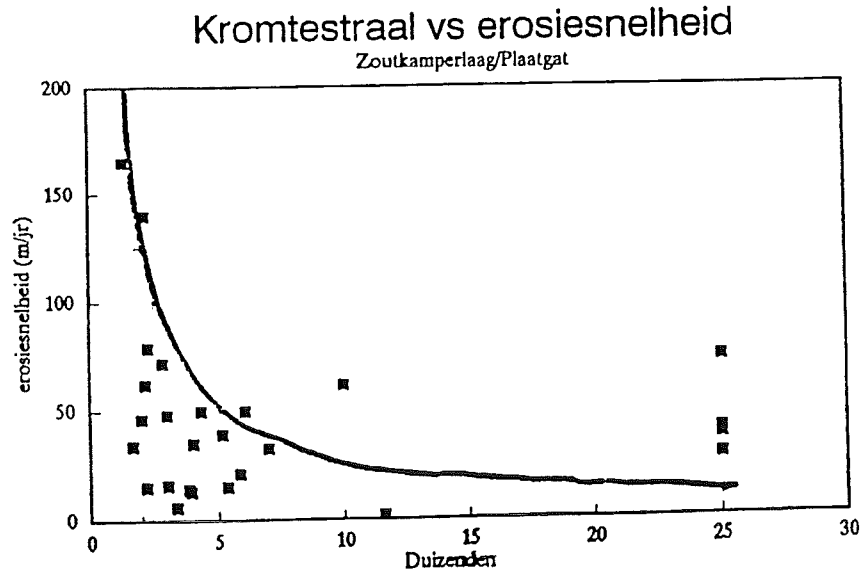

Figure 2-46: The DC formula

2.7 Changes of the Zealand coast by Man and Nature

In Zealand the mechanisms, treated in sect 2.5 cause three "turf's" of the various inlets, with specific influences:

- The one of the Brouwershavense Gat
- The one of the Eastern Scheldt
- That of the Western Scheldt

Referring to sect 2.4 and 2.5 concerning waves and tides, now those effects will be combined.

With this general theory on the background the different inlets will be investigated more into detail::

- What has happened with the Brouwershavense Gat after the enclosure?
- What affects the outer delta of the Eastern Scheldt, in the past and in the future?
- What happened in the mouth of the Western Scheldt and which will be the influence of the harbor works have near Zeebrugge?

Fig. 2-47 shows the mouth of the Brouwershavense Gat after the enclosure. The most important channel of the system is the Brouwershavense Gat itself, from which the name of the inlet is derived. Near Scharendijke the channel was "leaning" to the bank of Schouwen - ("(in)scharen" in Dutch means: "to erode because of a meandering channel") - and dug itself in; in this way a scour hole emerged with a depth of 47 m.

After closing the inlet the current was "paralyzed". Owing to this on the first hand the equilibrium of the sand balance between the outer delta and the estuary was disturbed, with the consequence that the shoreface of the outer delta is moving landward (fig. 2-48).
On the other hand because of this the old channels became potential areas of sedimentation. Figure 2-49 shows the accretion and erosion near the dam. The red numbers stand for erosion, the green ones for the shoals.
As far as the origin and the way of transport of the concerning sediment one has to remind a number of possibilities, which probably happen in combination:
Settling of flood transport, which isn't removed during ebb; think specially on fine material like silt.
Sand, which is removed from the shoals
As a consequence of the reduction of the current velocity these shoals are not supplied with sand; the balance between current supply and erosion by wave action will be outweighted in favor of the last one. Consequence is lowering of the shoals. In this way for example the Middelplaat in front of the Brouwersdam lowered its level after the enclosure;
Littoral drift (i.e., sand which originates from the heads of the islands and of the banks of the shoals) which sedimentates in the channel and is not carried away.
For the Northern side of Schouwen the development is probably mainly defined by the littoral current; this is not much different since 1971, as fig. 2-50 shows.
Only the immediate surroundings of the Brouwersdam showed a clearly stronger accretion. The accretion near the Zeepe dunes is probably a consequence of the permeable groins, constructed between 1960 and 1975

Can, on account of the present experience, a prognosis be made?

For the short term prognosis can be supposed that the changes are so slow, that it will last very long before the boundary conditions in the process change significantly, in other words, that for instance a beach will develop at the site of the Brouwershavense Gat. Likewise the shifting of the outer delta is so slow, that for long the wave boundary conditions will not be affected. There is no reason the presume, that the development the next years will be different from what is found so far.

On the long term -order of half a century- there will by a straightening of the coast, presuming, that man won't interfere once more.

If one directs his attention on the Eastern Scheldt (fig. 2-51), one finds, as a matter of speaking, a double system:
The Northern tidal basin stretching at the east side to Keeten-Mastgat-Zijpe and in the present situation reaching till the Volkerakdam and the Dam over the Hellegatplaten;
The Southern tidal basin: the proper Eastern Scheldt.

Although some things mix up in the embouchure and although there are transverse connections, one could see, partly schematized, the Hammen as tidal gorge for the Northern tidal basin and the Roompot as tidal gorge for the Southern part.
Now specially the Northern part is artificially expanded, particularly by the closing of Grevelingen in 1964 and the Volkerak in 1969, but also before, since 1900 by several clearings and normalizations.
Because the tidal capacity of the Eastern Scheldt increased, the current velocity increased as well with as consequence larger capacity of sand transportation. As profile expansion could not take place in horizontal sense, the basin deepened, linked with a seaward transportation of sand.

Fig. 2-52 shows the average deepening of the basin between 1872 and 1972. Parallel to the scouring an increasing growth of the outer delta can be seen.

Fig. 2-53 shows the shifting of the channels in horizontal sense in the past century.

1827 The first figure one shows in the mouth of the Eastern Scheldt the two main channels the Hammen-Westgat and the Roompot, and in between a shoal without a channel connecting the two main channels. In origin the Schaar van de Roggenplaat can be observed, while the Hondengat, the channel along the Kop van Schouwen, in that time was a passable deep channel.
1886 This channel has become smaller in 1886. The most striking in this figure is that there exists a connection channel -de Geul- between de Hammen an the Roompot , which about this time has it's largest capacity.
1953 After about 1900 the Geul is decreasing in capacity and a more inward laying connection between the both main channels the Westgat and the Roompot viz. the Schaar of the Roggeplaat appears. The Hondengat has disappeared. Also in this figure: the ebbchannel of the Vuilbaard and the floodchannel of the Roompot; here is clearly a difference between the ebb- and the floodchannel.
1970 In the situation of 1970 this system has almost become an indifferent channel. Also the short-cutting between the ebb channel by the ebb channel of the Roompot of the Westgat can be observed, to a certain extent. The Geul is almost disappeared while in 1971 it has been enclosed by the "damsection Geul".

The construction of the storm surge barrier will[1] create a situation in the outer delta, being between the complete blocking and opening of the Eastern Scheldt. The current velocities will decrease. At a distance of approx. 12 km seaward of the storm surge barrier the reduction of the current velocity will be negligible and, moving in the direction of the storm surge barrier, the reduction of the current velocity will increase till approx. 26%. The consequences can hardly be quantified at this moment. Before, the influence has been discussed of the enlargement of the tidal basin and the tidal volume; one could expect that the reducing of the tidal volume means: "the way back"; in this case the reducing of the outer delta and the accretion of the Eastern Scheldt. Doubtlessly the channels will move, as a consequence of the changes in the tide propagation, but presumable this will have no effect on the seaward sides of the islands. For the littoral drift will hardly change. Naturally it is recommendable to follow the changes as scrupulous as possible. Even if the expectations

[1] written in 1980

would be disqualified, it will be technically possible to take shore protecting measures, like beach nourishment to annihilate the unwanted consequences.

Moving the attention to the embouchure of the Western Scheldt, one sees the channel system (fig. 2-54) that fairly approaches the basic scheme, shown in fig.2-40.
at the North-side one finds the system Oostgat-Galgeput, of which the Oostgat surely has a resulting flood discharge. More Southward one finds the main channel the Wielingen, where theoretically a resulting ebb discharge may be expected. Indeed the fact that the water of the Wielingen has less salt content than in the Oostgat (as a consequence of the discharge of the Scheldt) points in that direction. The current and discharge measurements however give a very confused image. The Wielingen and the Oostgat enclose the Vlakte of the Raam, on which, as a secondary channel, the Deurlo is situated. South of the Wielingen one finds the Appelzak which, in the past, had a flood channel character.
Although the Oostgat has a fairly stable character, still, in the course of centuries a considerable erosion took place. This is due to the fact that the littoral drift along the coast gets little natural nourishment at the Northside, (Westkappelse Seawall) neither from the outer delta because of the tidal channel "Oostgat", closely located to the coast,. Because of this, near Westkapelle approx. 250 m dune disappeared into the sea since 1450 (fig. 2-55).
In front of the coast of Zeeuwsv-Vlaanderen it specially attracts the attention, that the Wielingen shifted somewhat between Cadzand and the Zwarte Polder to the South and West where it expanded in the deeper regions (fig. 2-56). The channel silted up from 25m to 12 m near Groede and eroded in the Western part. The shallow part between Wielingen and Appelzak largely disappeared: the intermediate bar the Binnen-Paardenmarkt eroded, where the Appelzak itself became shallower, just like the southern part of the Wielingen on the Belgian territory. Only the eastern outlet of the Appelzak got more or less the character of an outlet of the Wielingen and eroded and shifted, like the profiles of figure 2-57 show. Here also manmade changes are performed.

Fig. 2-58 shows the last plans[1], which the Belgian government has concerning the neighboring coastal area: expansion of the harbor till approx. 3250 m of the coast, beach nourishment of 9 mln m^3 on the beach (presently: performed) and the expansion of a long groin specially through the deeper parts of the Appelzak, which should hamper the tidal and littoral transport of the supplied sand (fig. 2-59)

Note:
It must be pointed out that because of thorough knowledge of coastal dynamics of the Belgian coastal engineers involved in this project consensus between the Dutch and Belgian coastal authorities could be reached on improvement of the plans with respect to the coast, to mutual benefit of as well Belgium as the Netherlands.
This remark will be elucidated during the lectures..

[1] again: written in 1980

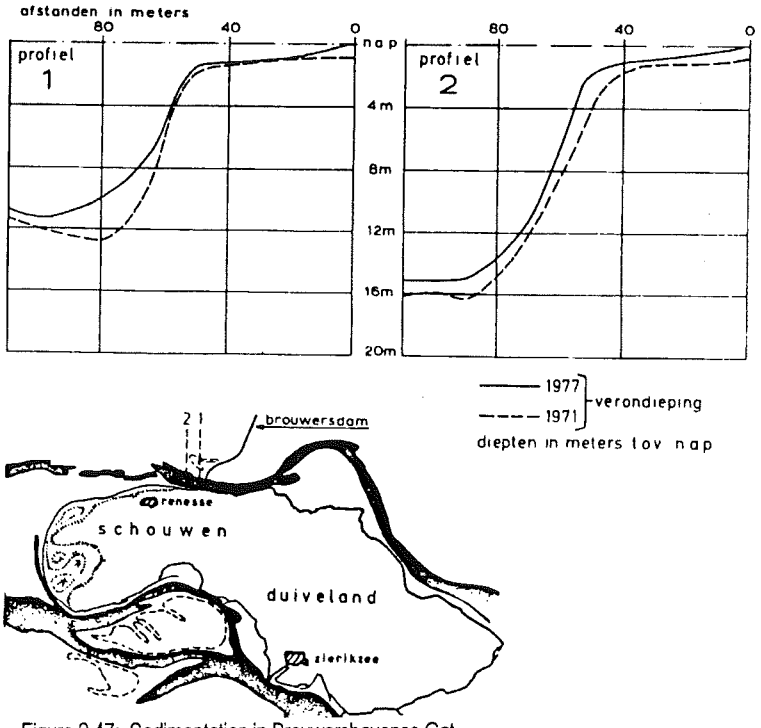

Figure 2-47: Sedimentation in Brouwershavense Gat.

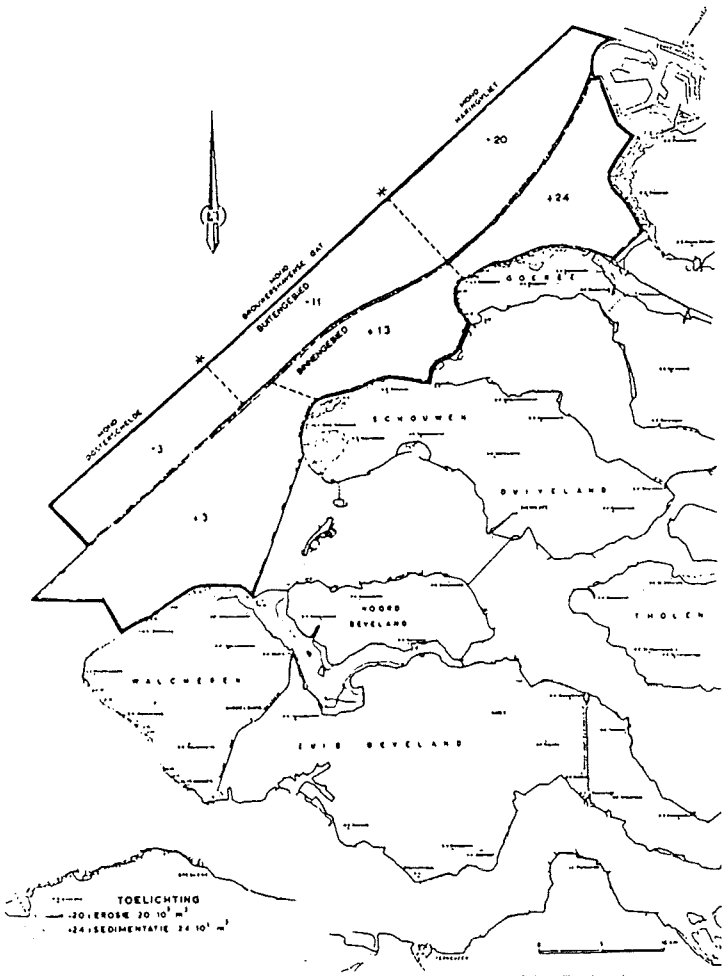

Figure 2-48: Erosion and sedimentation in the Northern part of the Zeeland area.

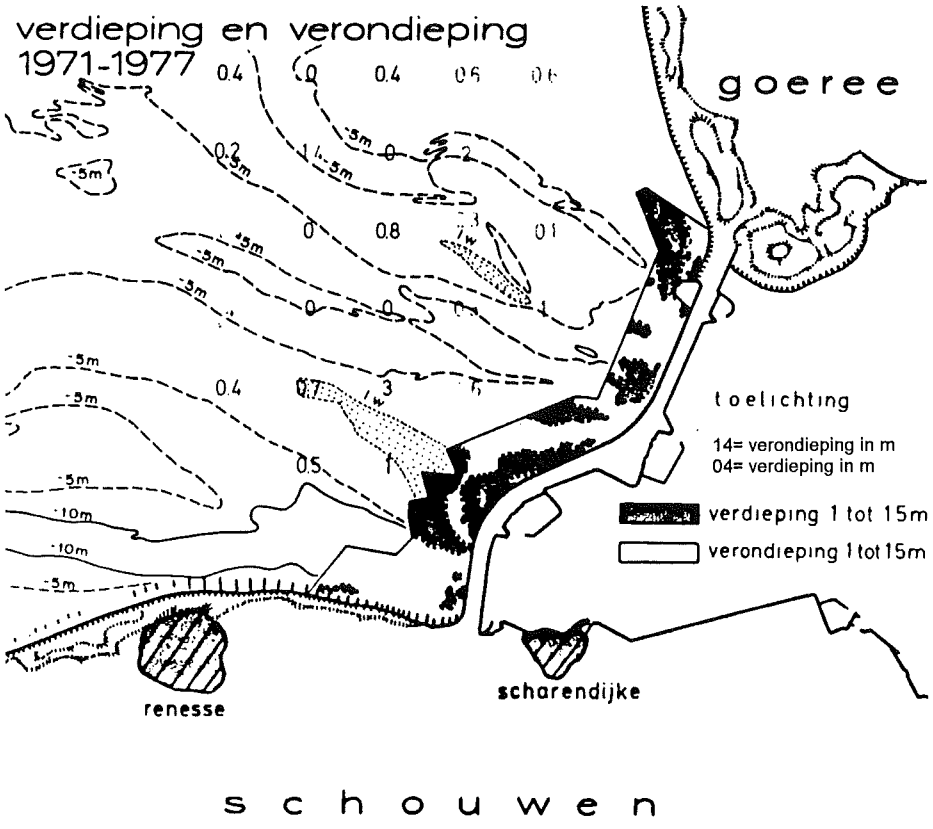

Figure 2-49: Erosion and sedimentation near the Brouwersdam.

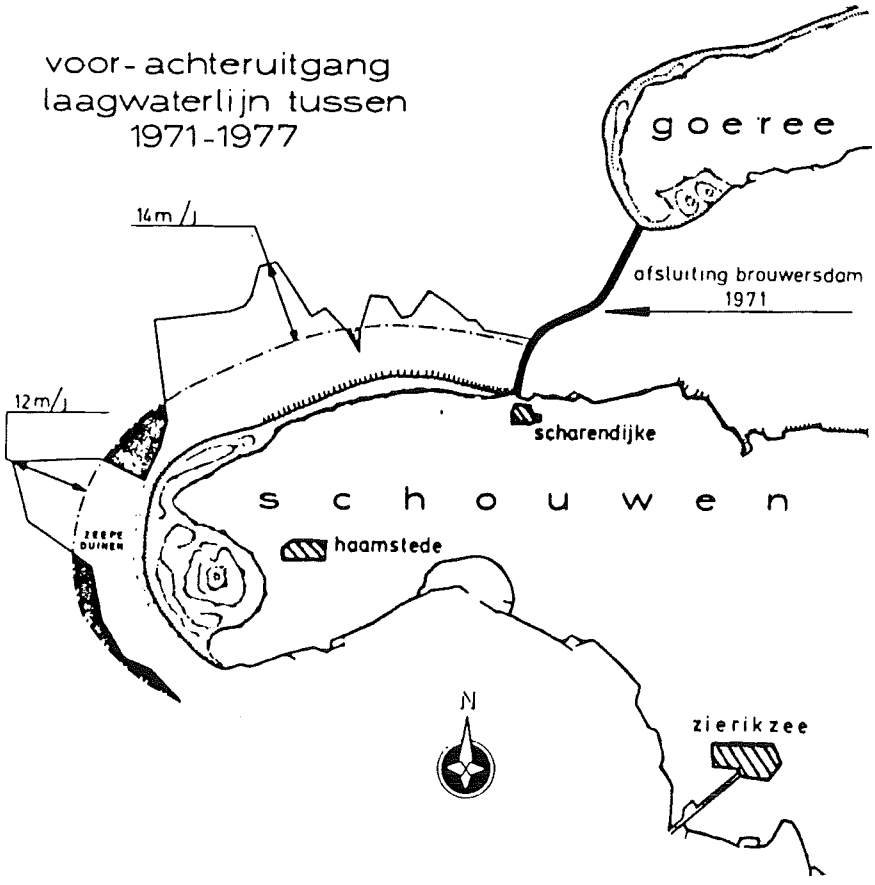

Figure 2-50: Erosion and sedimentation along the Schouwen coast.

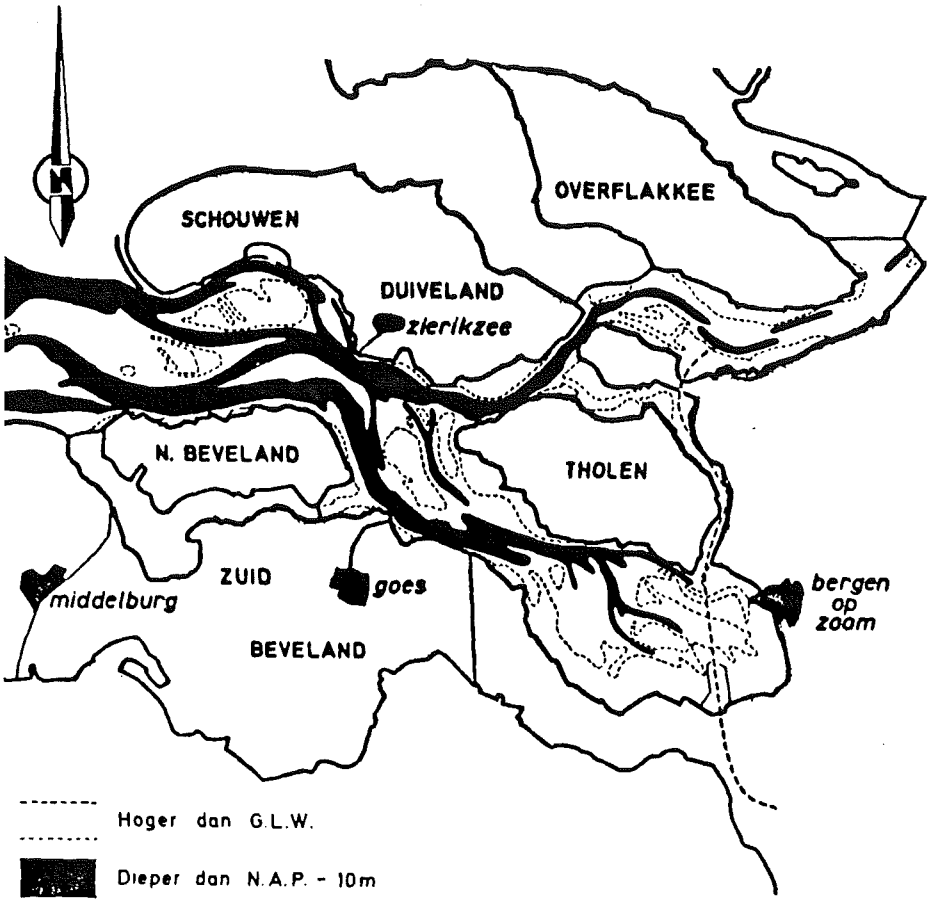

Figure 2-51: The channel system in the Eastern Scheldt.

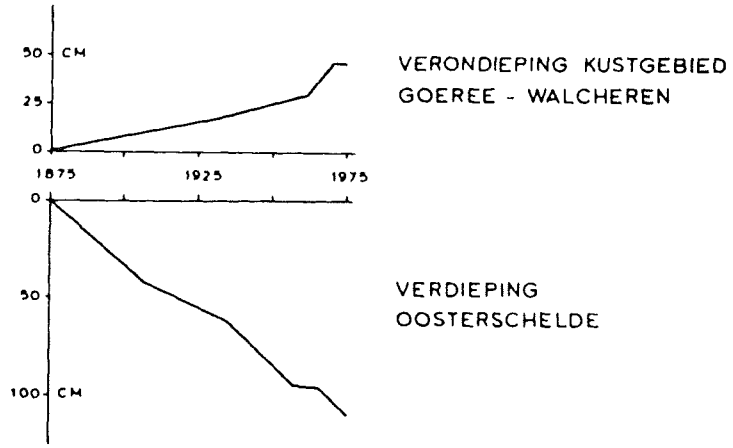

Figure 2-52: Erosion of the Eastern Scheldt and sedimentation in the outher delta.

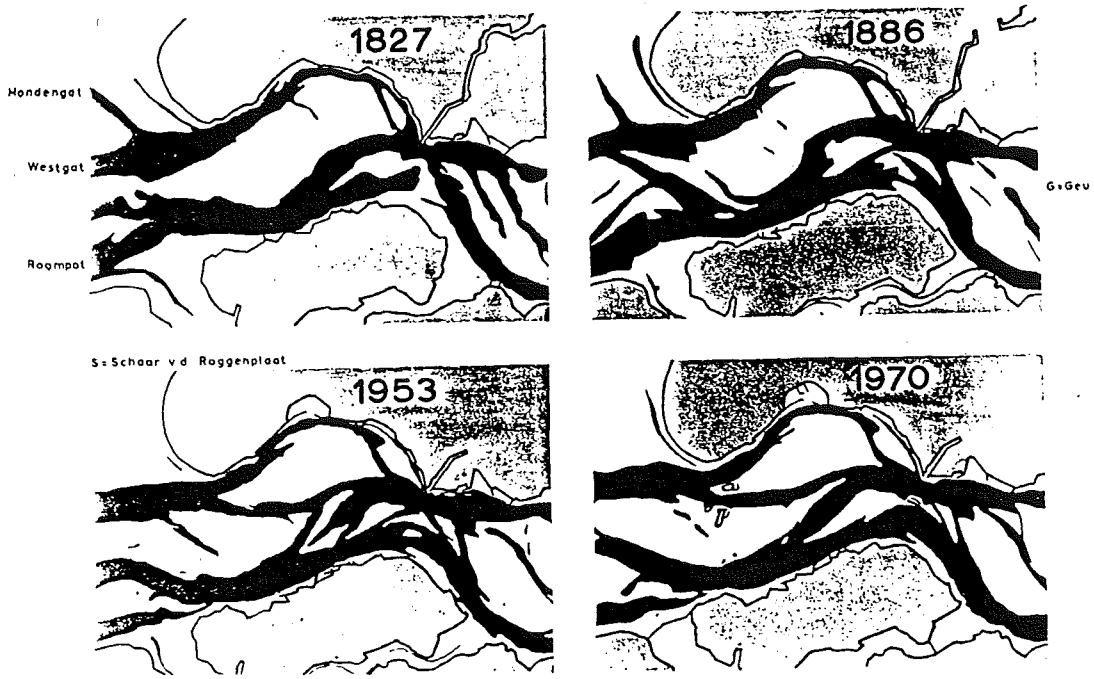

Figure 2-53: Development tidal channels in the outher delta of the Eastern Scheldt.

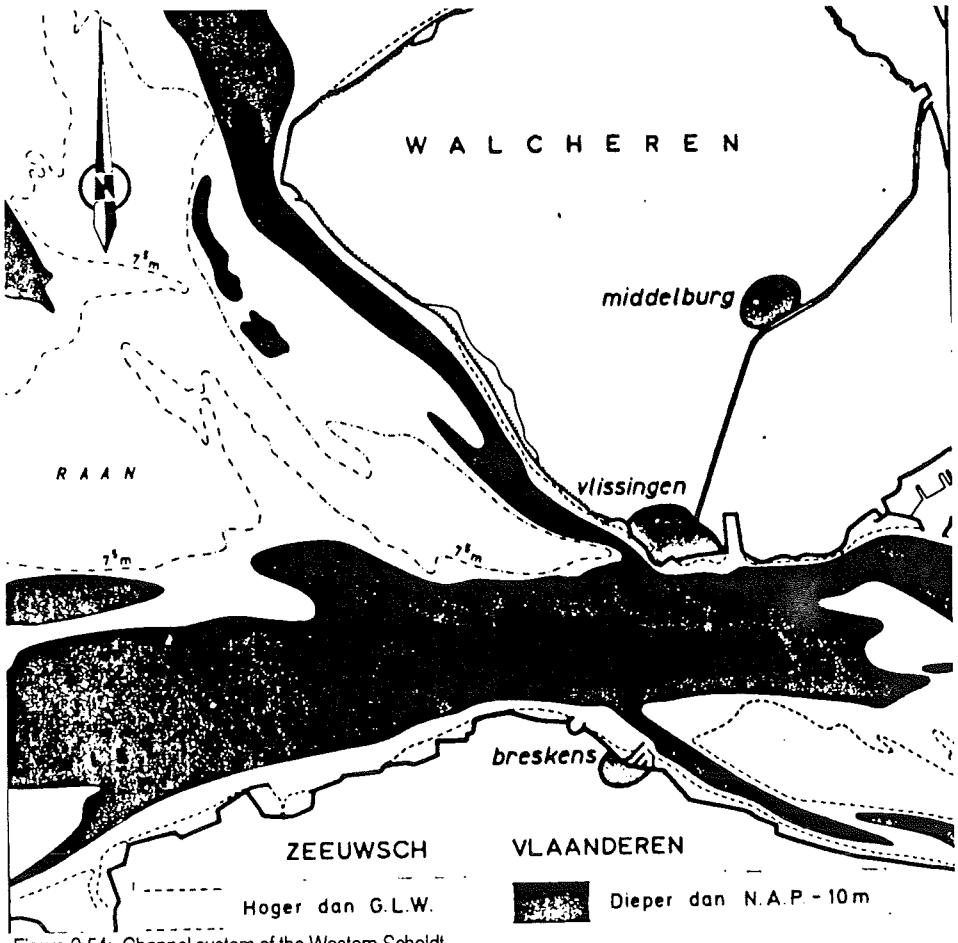

Figure 2-54: Channel system of the Western Scheldt.

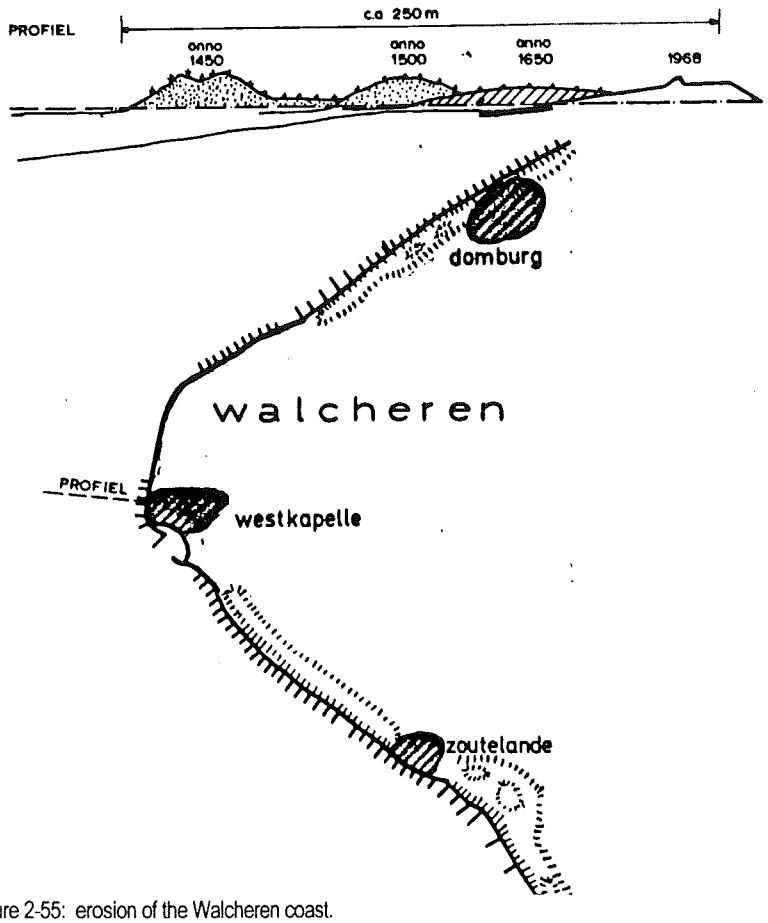

Figure 2-55: erosion of the Walcheren coast.

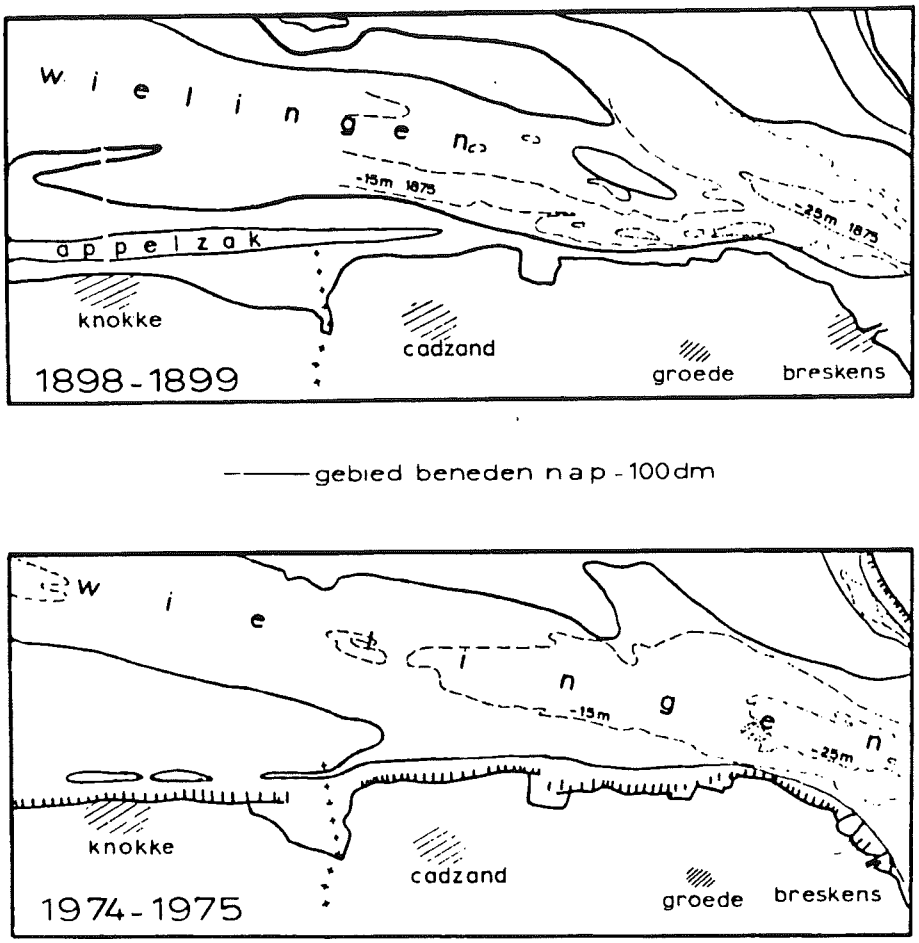

Figure 2-56: Development tidal channels in the outher delta of the Western Scheldt.

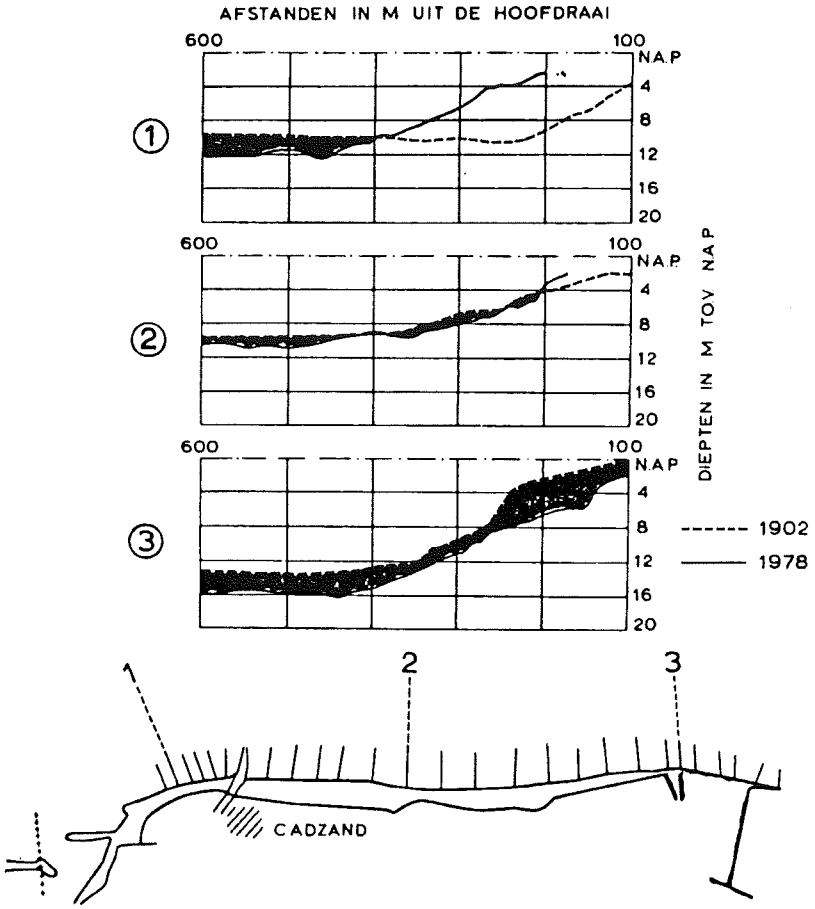

Figure 2-57: Erosion and sedimentation of the Dutch coast near the Belgian border.

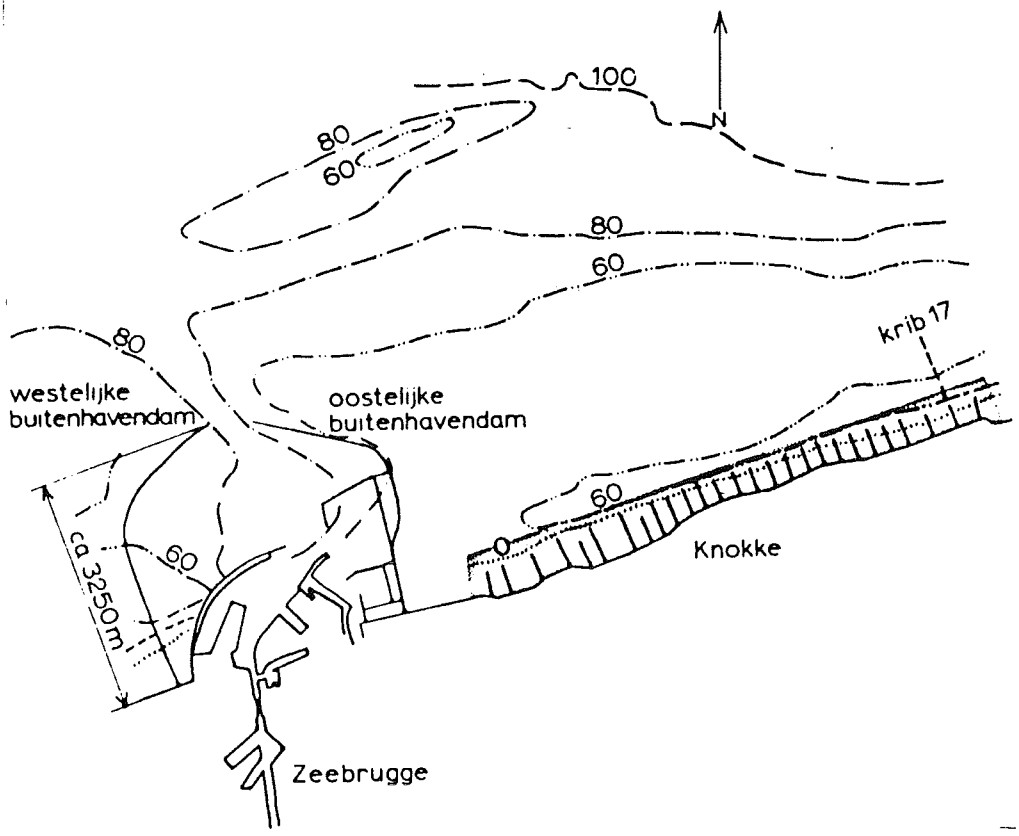

Figure 2-58: Enlargement harbor molesof Zeebrugge.

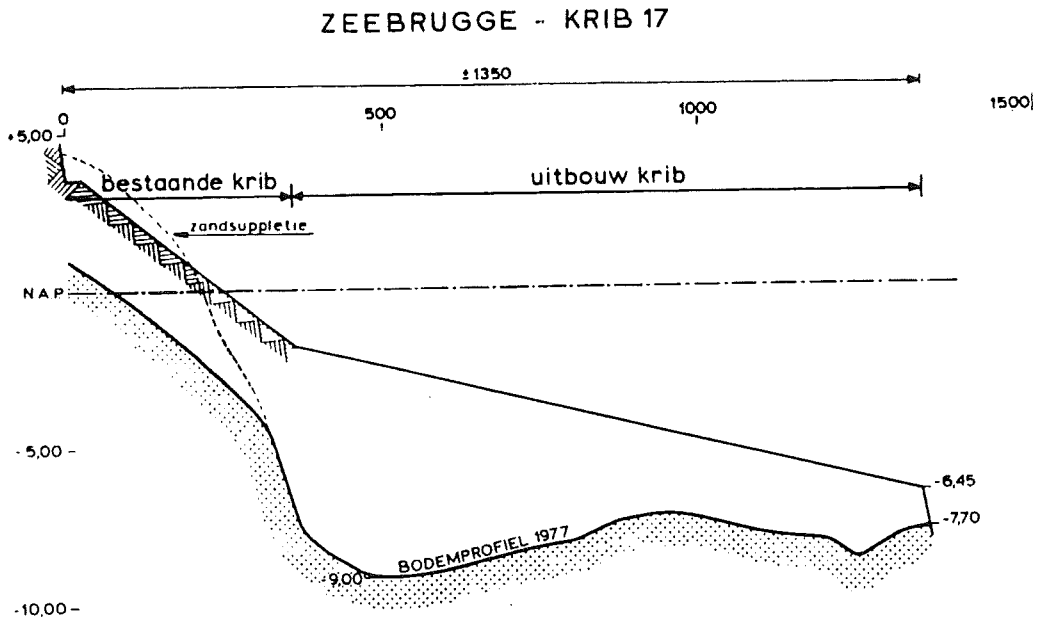

Figure 2-59: Design for a long groin, projected near the Belgian border.

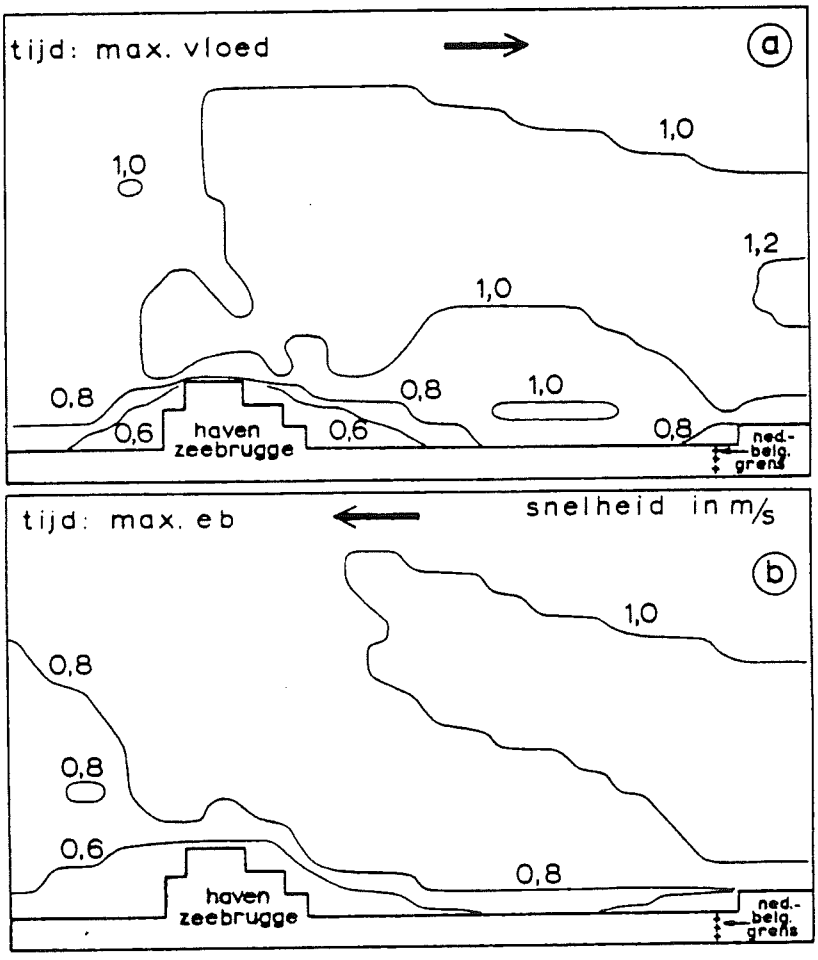

Figure 2-60: Maximum flood- and ebb-velocities near Zeebrugge harbor (result Belgian computations).

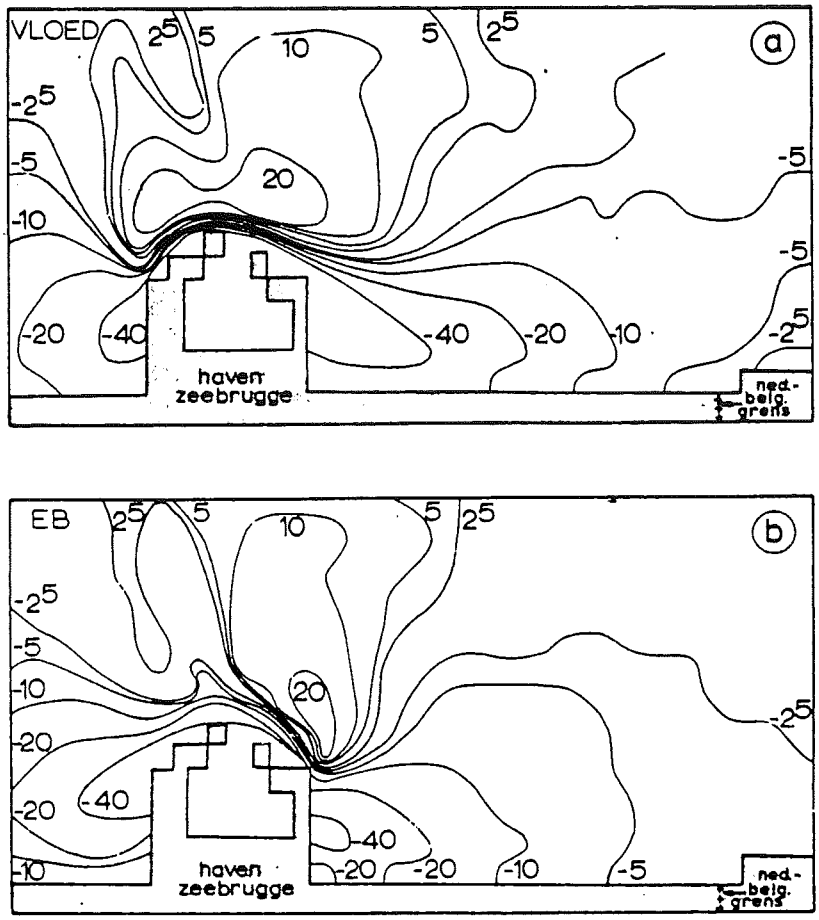

Figure 2-61: Change of maxima tidal velocities near Zeebrugge harbor (result Belgian computations).

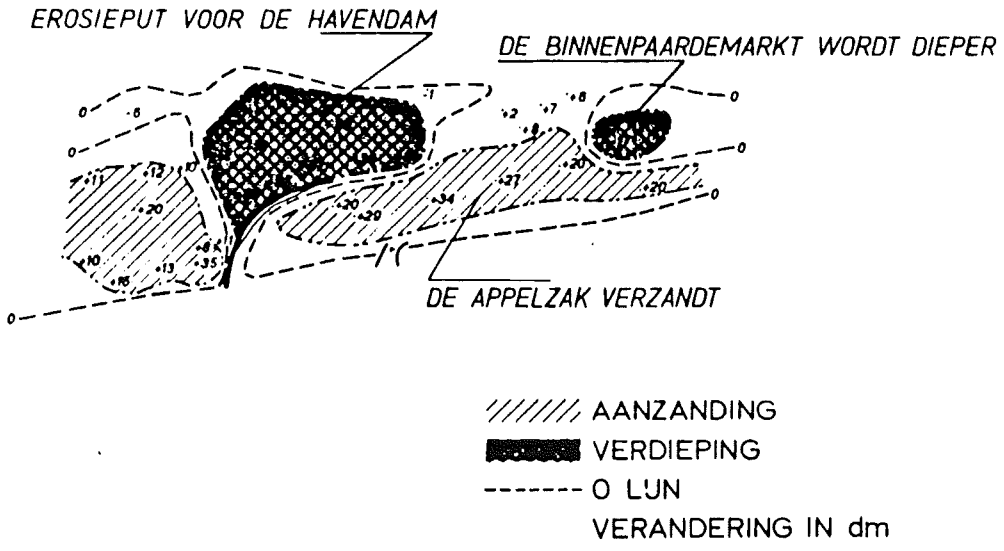

Figure 2-62: Erosion and sedimentation after construction harbor moles Zeebrugge. Situation 1908 referred to original situation (1901).

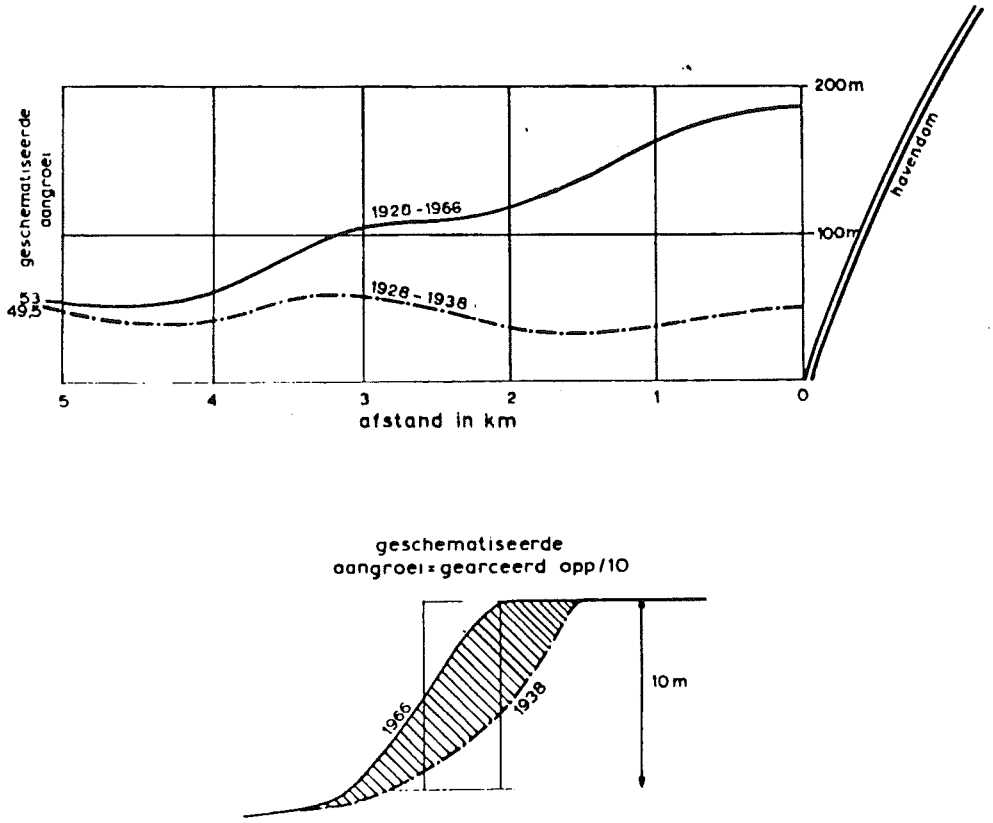

Figure 2-63: Accretion West of Zeebrugge (schematized); 1928-1966.

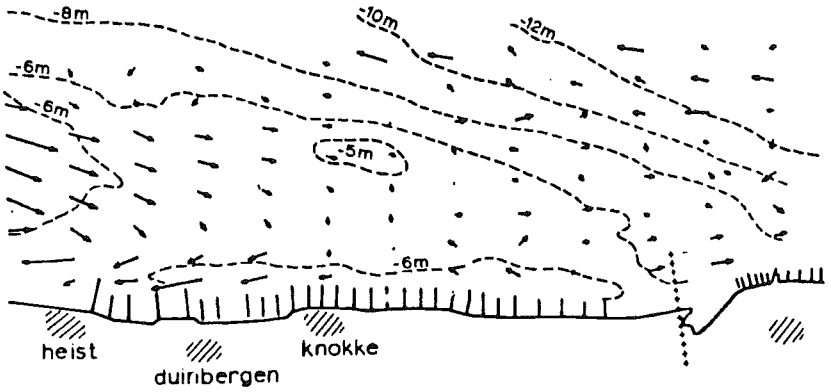

huidige toestand

b

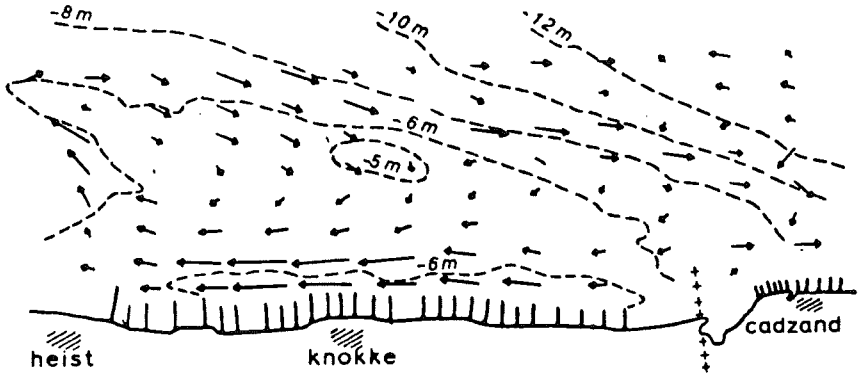

uitgebouwde havenhoofden

c

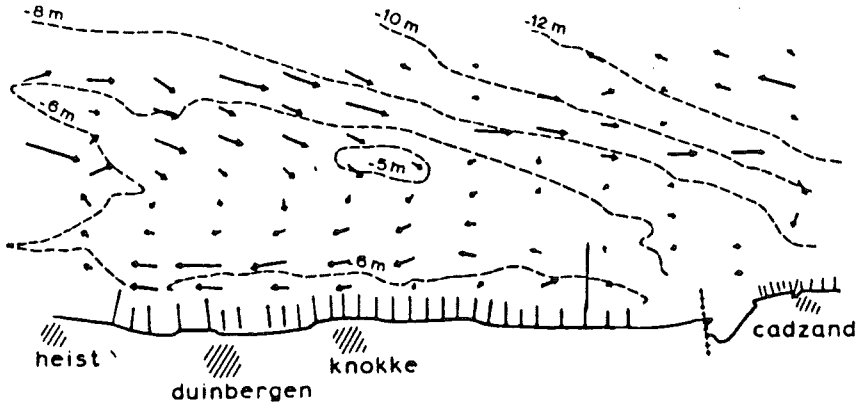

Figure 2-64: results Belgian computations of resulting sandtransport, caused by tidal motion.

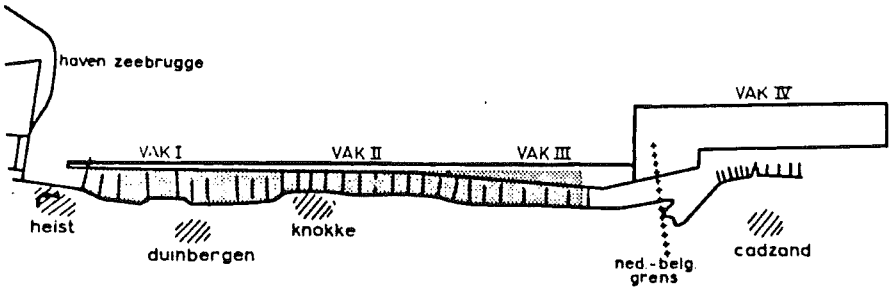

Figure 2-65: Areas in which coastal accretion and erosion has been computed.

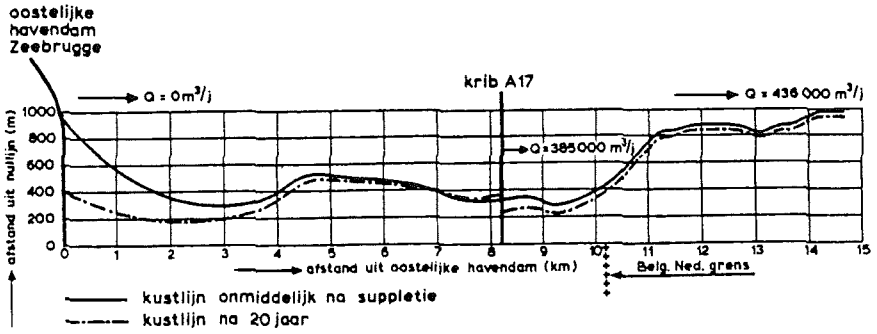

Figure 2-66: effect on the coastline of a long groin at the Belgian side of the Zwin.

jaarlijkse aanzanding in m/jaar t.g.v getijtransport (met uitsluiting invloed brandingsstroom transport)				
vak	I	II	III	IV
Huidige toestand	+4,8 ± 2,8	-0,69 ± 2,14	-2,71 ± 1,43	+0,22 ± 0,63
Wijziging t.o.v huidige toestand t.g.v. uitbouw:				
a. Zonder krib	-2,96	-0,48	+0,63	-0,24 ± 1,06
b. Met krib	-5,68	+0,55	+1,46	+0,18 ± 0,83
+ = aanzanding of : wijziging ten gunste			- = erosie of wijziging ten ongunste	(1e regel) (2e,3e ..)

Table 2-4 : Calculation accretion in m/yerar, by tidal transport.

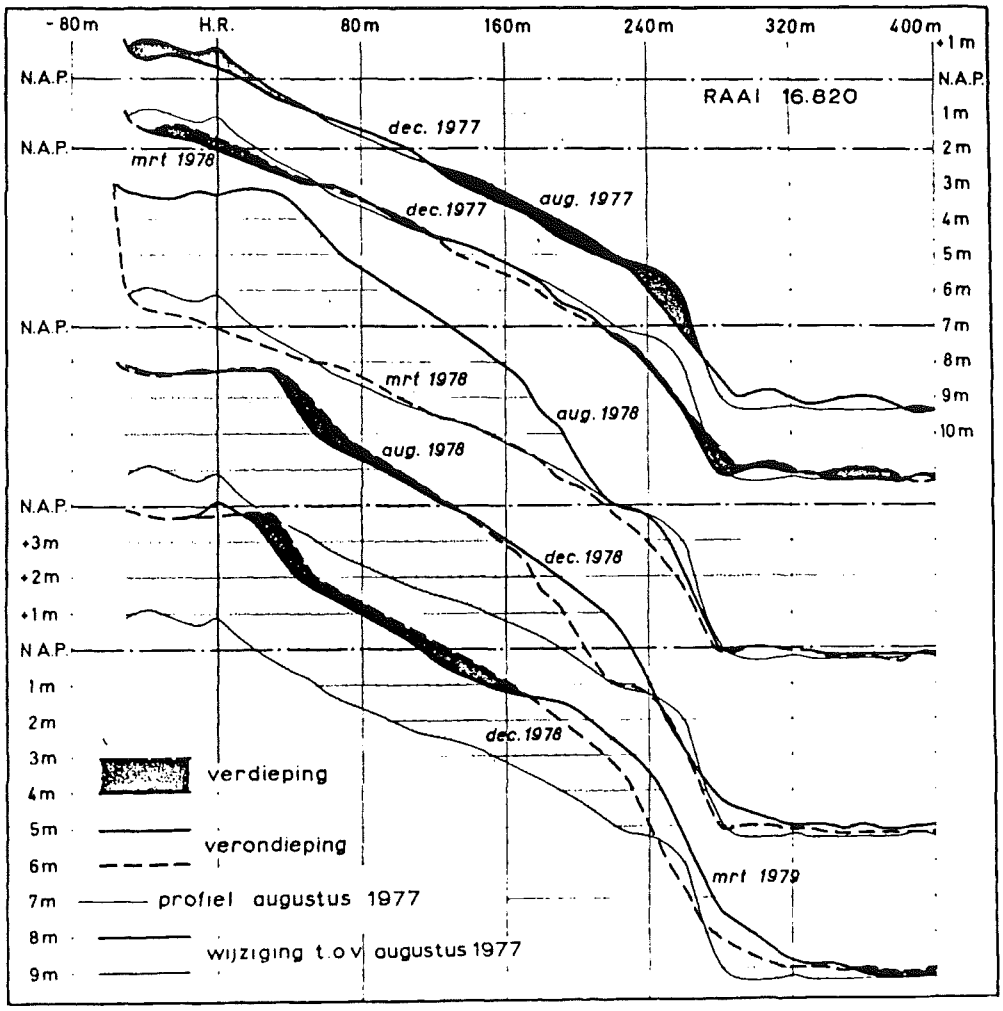

Figure 2-67a: Changes of the coastal profile in two ranges at the Eastern boundary of the sand supply near Zeebruge / Knokke in the period short before and after the supply

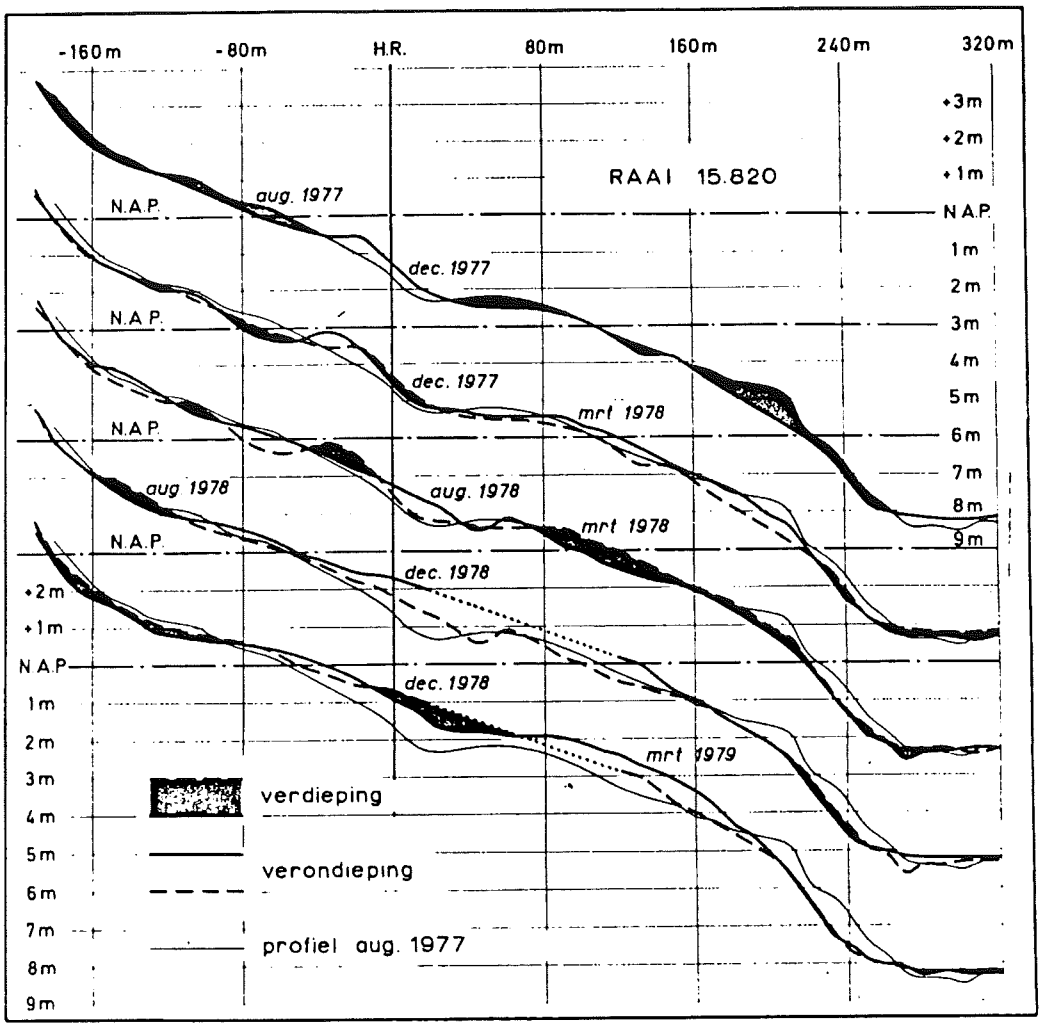

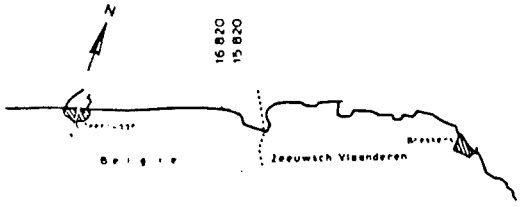

Figure 2-67b: Changes of the coastal profile in two ranges at the Eastern boundary of the sand supply near Zeebruge / Knokke in the period short before and after the supply

2.8 Literatuurlijst

1) J.J. Dronkers;
Research for the coastal area of the Delta region of the Netherlands;
ICCE Washington 1970.

2) L.R. Wentholt;
Stranden en strandverdediging (Beaches and beach protection), Delft.
Ph. D. Thesis 1912.

3) J. van Veen;
Onderzoekingen in de hoofden (Investigations In the Soutern Northsea), Delft.
Ph. D Thesis 1936.

4) J. van Veen;
Eb- en vloedschaarsysteem in de Nederlandse getijwateren (Ebb- and flood channel systems in the Dutch tidal waters).
Tijdschrift Kon. Ned. Aardr. Gen. 67 pp. 45-65 (1950).

5) L. van Bendegom;
Beschouwingen over riviermorphologie (Considerations about river morphology). De Ingenieur 59, 24 jan. 1947.

6) L.M.J.U. van Straaten;
Directional effects of winds, waves and currents. Geologie en Mijnbouw 23, 1961.

7) T. Edelman en D.N. Eggink;
Some characteristics of the Dutch coast; I.C.C.E. 1962.

8) Per Bruun and F. Gerritsen;
Stability of coastal inlets.

9) E.W. Bijker and J.N. Svasek;
Two methods for determination of morphological changes, induced by coastal structures.
Int. Nav. Congr. 1969.

10) W.T. Bakker;
A mathematical theory about sandwaves. Shore and Beach, Oct. 1968.

11) L. Knop;
Onderzoek Noordzeekust Petten-Huisduinen (Investigations Northsea coast Petten-Huisduinen).
Study Departement Rijkswaterstaat, nr. 584.

12) R. Dorrestein;
Wind and wave data of Netherlands lightvessels. Med. en Verh, K.N.M.I. no. 90.

13) K. van Harreveld;
Correlatie van golfgegevens Triton-1964/65 met overeenkomende gegevens van het lichtschip Goeree (Correlation of wave measurements Triton-1964/65 with corresponding data of the lightvessel Goere Rijkswaterstaat, Deltadienst, Waterloopkundige Afdeling, nota K 288.

14) J.A. Battjes;
Private communication to Ir. H.N. Svasek.

15)W.T. Bakker, E.H.J. Klein Breteler and A. Roos;
The dynamics of a coast with a groyne system.
ICCE 1990; Washington
16)W.T. Bakker;
Computation littoral drift with Svasek-method.
Rijkswaterstaat, Dept. for Coastal Res., Rep. W.W.K. 69-7.

17)W.T. Bakker and N.J. Opdam;
Influence of waves and tides on the littoral drift in the surf zone.
Rijkswaterstaat, Dep. for Coastal Res., Rep. W.W.K. 70-8.

18)H.J. Opdam;
A wave tide model for the Dutch coast.
M. Sc. Thesis., Delft 1970.

19)A.J. Bowen;
The generation of longshore current on a plane beach.
Journal of Marine Research 27, no. 2, May 1969.

20)E.H.J. Klein Breteler;
A tidal model for the coast of Hook or Holland - IJmuiden.
Rijkswaterstaat, Dept. for Coastal Res., Rep. W.W.K. 70-10.

21)J. Haring;
Oppervlakte van bet dwarsprofiel van de NederLandse zeegaten als functie van het getij-volume (Area of the cross-section of the Dutch inlets as a function of the tidal volume).
Rijkswaterstaat, Delta Works, Rep.K 251.

22)J. van Veen;
Zeegat van het Vlie (Inlet of the Vlie) (1934). Rijkswaterstaat, Dir. Benedenrivieren.

23)L. van Bendegom;
Grondslagen der Kustverdediging (Principles of coastal protection), Rijkswaterstaat.

24)Th.J.C. Wijnant;
Littoral drift near Texel.
Rijkswaterstaat, Dept. for Coactal Res.

25)Kustontwikkeling; verleden, heden, toekomst.
Samenvatting colloquium waterloopkundig Laboratorium en Rijkswaterstaat (mei 1985).
Ook verschenen in een artikelenreeks in het Polytechnisch Tijdschrift okt/nov 1985.

26)J. Wiersma;
De kust in vier dimensies.

27)L.M.J.U. van Straaten;
Directional Effects of winds, waves and currents. Geologie en Mijnbouw, 23, 1961

28)L.M.J.U. van Straaten;
Coastal barrier deposits in South and North Holland in particular in the areas around Scheveningen and IJmuiden. Meded. Geol. Stichting Serie 17, p.41-75

29)W.T.Bakker and D.Sj Joustra;
The History of the Dutch Coast in the last century
xIIth Int.Conf. on Coastal Engng., Washington 1970
Ook; Rijkswaterstaat, Afd. Kustonderzoek, Studierapport WWK 70-12

30)P.Vellinga;

Beach and dune erosion during Storm Surges. Techn. Universiteit Delft; Proefschrift; 1965

31)T. Edelman;
Erosie en aanwas van het kustvak Den Helder-hoek van Holland.
Rijkswaterstaat, Afd. Kustonderzoek, Studierapport WWK 61-1 (1961)

32)H. de Vroeg;
Schematisering brandingsruggen m.b.v. jaarlijkse kustmetingen
Technische Universiteit Delft, vakgroep waterbouwkunde, afstudeerverslag (1987)

33)W.T.Bakker;
Berekening van bet langstransport door golven met de methode van evenwijdige dieptelijnen.
Rijkswaterstaat Afd. Kustonderzoek, studierapport WWK 69-7 (1967)

34)W.T. Bakker en H.J. Opdarn;
Over de invloed van golven en getij op het zandtransport in de brandingszone.
Rijkswaterstaat, Afd. Kustonderzoek, Studierapport WWK 70-9 (1970)

35)M.A.M. de Ras;
Onderzoek naar de grootte van het langstranport langs de kust bij ijmuiden door de combinatie van getijstroom en golforbitaalbeweqing
Rijkswaterstaat, Afd. Kustonderzoek, Studierapport WWK 71-11 (1971)

36)M. Dyhr-Nielsen en T.Sorensen;
Some sand transport phenomena on coasts with bars.
XII th Int.Conf. on Coastal Engng., Washington 1970, p.855-866

37)F. Gerritsen and J. van Heteren;
Effect of low-frequency oscillations on coastal morphology.
XIX th Int.Conf. on Coastal Engng., Houston 1984

38)A.J. Bowen and D.L. Inman;
Edge waves and crescentic bars.
Geoph. Res., 14, p 5479-5490

39)G.Symonds, D.A.Huntley and A.J.Bowen;
Two-dimensional Surf-beat: Long-wave generation by a time-varying breakpoint.
Geoph. Res., 87,C1, Jan 20 1982, p.492-498

40)W.R.Dally;
Longshore bar formation- surf beat or undertow?
Coastal Sediments (87; New Orleans; p71 t/m 86

41)J. Groenenboom;
Onderzoek naar de kustontwikkeling bij de havendammen van IJmuiden.
Technische Hogeschool, vakgroep Kustwaterbouw, Afstudeerverslag.

42)W.T. Bakker;
De nauwkeurigheid, waarmee een trend kan worden bepaald.
Rijkswaterstaat, Dienst Getijdewateren, Notitie GWAO-87.

43)E.F.J. de Mulder;
Geologische geschiedenis van de Hondsbossche zeewering. Derde uitgave Kring van Vrienden van de Hondsbossche, 1983

44)H. Schoorl;

Diverse publicaties van 1973,1979,1982 en 1983 (compilatie van de Mulder)

45)S. Boer, H.J. de Vriend & H.G. Wind;
A system of mathematical models for the simulation of morphological processes in the coastal area.
XXX th Int.Conf. on Coastal Engng., Houston 1984

46)W.T. Bakker & H. de Vroeg;
De Hollandse kust bekeken: analyse van 20 jaar kustgedrag.
De Ingenieur, mei 1988.

47)W.T.Bakker en J.H.M. de Ruig;
Enige opmerkingen over de gewenste nauwkeurigheid en informatiedichtheid, benodigd voor het kustmeetsysteem.
Rijkswaterstaat, Dienst Getijdewateren, notitie GWAO-87.460 (nov.1987)

48)T. Edelman;
Verstoringen in de kustlijn tge de aanwezigheid van zeegaten.
R.W.S. afd kustonderzoek nota WWK-61-3 (1961)

49)van Rijn, de leeuw;
Zandtransportmodel Westerschelde, stochastisch onderzoek zandtransportformule.
Delft Hydraulics Laboratory, juni 1985.

50)J.F. Agema;
Verandering van de Zeeuwse kusten door mens en natuur.
R.W.S. , interne nota, WWKZ-80.v016

51)S. Huys;
Geulmigratie op de Buitendelta. Het Friese zeegat en het Amalander Gat
Rijksuniversiteit Utrecht (1992)

52)J.P.M. Mulder, H.J. de Vriend, A.W. Heemink;
Validation of large scale morphological models.
report on a workshop at Noordwijk (Netherlands) on 7 and 8 February 1994

3. Line theories in coastal dynamics

3.1 Introduction

The solving of coastal problems will remain for years rather an art than a knowledge, with the slogan: 'the art of engineering is to get sufficient conclusions from insufficient data". However also art needs skill, and a mathematical theory; which clarifies in an exact way the implications of several schematizations of reality, may provide a part of this skill. At the moment only several aspects of the processes, which occur in nature can be schematized and translated into a mathematical theory. In the transition of the real prototype to the mathematical model the danger is hidden, to concentrate on an insignificant feature, which gives pseudo exact results. This can be avoided by active knowledge of the prototype and carrying out measurements in prototype and hydraulic models , from which a "smoothing of data" can result. It is cheaper and faster to consider only one of the three aspects: prototype, theory and laboratory, however, often only a combination of all of these aspects reveals the truth. The theory indicates pertinent contradictions in the measurements, but measurements in prototype are necessary to keep the attention on invalid schematization.

This book deals on "Coastal Dynamics", which will be defined in a narrow sense as a mathematical theory, which starts from given equations of motion for the sediment, which leads with the continuity equation and given boundary conditions to a calculated (eventually schematized) coastal topography, which is generally a function of time. This is clearly analogous to aero- and hydrodynamics, thermo-dynamlcs, hydrology and other related fields. The subject of this book, however, covers only a specific part of the Coastal Dynamics. It is based upon the notion of old masters, that for a manager the back-side of a cigar-box should be large enough to evaluate all the information and anti-information which is poured over him. For instance: statements, based upon high-tech number-crunching can find a sad end when those do not match large-scale continuity. Think for instance of tidal computations, in which time-varying boundary conditions (shoals which emerge above water level during a part of the tide) are not reproduced accurately enough.

The positive role of refined numerical techniques on solving problems in coastal dynamics should be stressed. However, one will not find much about it in this book. Emphasis is on physics, rather than on mathematics. It is meant for coastal managers, to inspire them, to enable them to put sensible questions and, if necessary, to say: "Oh, no sir".
The theory would be sterile without a consideration about the validity of the equation of motion, so much the more, while these equations of motion are not as evident, straight-forward and single- valued as for instance the Euler - equations in hydrodynamics.
The Newtonian laws are not quite sufficient for the computation of the sediment motion, because the motion of grains is subject to stochastic processes as the shape of the grains, the shape of the granular bed surface, turbulence, irregular wave motion etc.
In modern sophisticated computermodels a physical approach going far into details is possible, this includes the consideration of water and sand apart from each other, investigation of turbulent and viscous forces on the grains, and calculation of the sediment motion.
This is a difficult and tiresome way, which has to be followed and will give finally the best results.
However, the building of constructions cannot wait for that, as it has not done in the past and therefore a short-cut from theory to practice has to be made, which involves the use of experimental data. This includes entirely the loss of the paradise of exactness. As the accuracy of the experimental data is very poor, this is a serious draw-back. Instead of the real equations of motion substitutes have- to be chosen and when it is not carefully examined, if and when these assumed equations of motion are valid, the mathematical theory is just an escape from reality.

In the mathematical theory, all constants and variables are indicated by symbols and it is suggested, that the numerical value of many of these constants can be found from prototype data. Without a discussion about at least the order of magnitude of these constants. the theory is no more than a start for future research.

Under coastal dynamics in a broader sense also these discussions about the validity of the equations of motion and the order of magnitude of the assumed constants will be included. In this book the sediment transport formulae which are used are not thoroughly discussed. The coastal dynamics, as presented in this course provides a far from complete theory.

The aim is threefold:

- It is a start for future research;
- it leads to qualitative conclusions about the effect of coastal constructions;
- some of the results are already available for practical computations.

Although based upon universal physics, applications treated are more or less tailor made for Dutch circumstances. The same holds for schematizations used.

Chapter 2 gives an overview of the Dutch coast. The papers, on which it is based upon, are written for a broad public and thus sometimes might give more basics than necessary for most of the present readers.
Chapter 3 gives (at this moment more or less classical) line theory. Ch.4 to 6 (determination coastal constants; experimental verification (laboratory and nature) and evaluation) try to expose, whether nature knows coastal dynamics.
In ch.7 theory is generalized, by taking line theory as a specific case of diffusitivity theory. Ch.8 deals with modern ways of data-assimilation in theory. In ch.9 the ideas on longshore and cross-shore diffusitivity are summarized.
Where the former chapters mainly deal with uninterrupted coasts (apart from single discontinuities like harbor moles or groins, in ch.10 some ideas are exposed concerning interaction of delta's and tidal basins: an important subject for the Netherlands, as a large part of the coast consists of tidal lagoons and estuaries (ch.2.1)..

As mentioned in the preface, in this book coastal dynamics is considered from one viewpoint. Thus the attention should be drawn on the appendix, in which a number of Dutch coastal specialists give additional information and thus can deliver the three-dimensional view.

3.2 One line theory, no diffraction[1)]

3.2.1 Assumptions

a) The coastal profile can be schematized with one part lying at a depth h which is deep enough that the littoral transport can be neglected and another part where an equilibrium profile is formed. This part shifts to seaward and landward, as accretion and erosion occur, but its shape doesn't change (Figure 3.1).

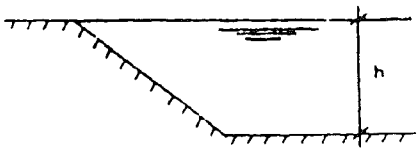

Figure 3.1: Schematized coastal profile

b) The dynamics of one "Coastline" will be considered using one of the depth contours (It is immaterial which one, as they are all considered to be parallel.). Assume all the transport equations apply, then the total transport S^* along the coast (only) is a function of the coastal direction; this function is linearized:

$$S^* = S_0^* - s\frac{\partial y}{\partial x} \qquad (3.1)$$

Denoting symbols:

x	= An axis lying in the mean coastal direction
y	= An axis perpendicular to x and positive in the seaward direction
S_0^*	= The net transport when the coast is parallel to the x direction
s	= A proportionality constant

From Figure 3.1 one can observe that the angle of wave incidence decreases when $\partial y/\partial x$ increases and as long as the angle is not too big (which has been assumed), a decrease in the amount of transported material results. Assuming transport equation applicable means therefore that the transport due to wave action is considered the most significant.

In chapter 4 the magnitude of S_0^* and s is investigated.

Initially we assume:

d) Small angle of wave incidence, equal to α_0, if the coastal direction is parallel to the x-axis:

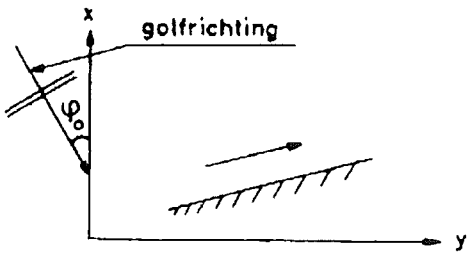

Figure 3.2: Definition wave direction α_0

$$S_0^* = s\,tg\alpha_0 \qquad (3.2)$$

$$S^* = s(tg\alpha_0 - \frac{\partial y}{\partial x}) \qquad (3.3)$$

[1)] This chapter (up to 3.3) is translated from Bakker (1971) by G. Mocke.

3.2.2 The Coastal Equation of Pelnard-Considére

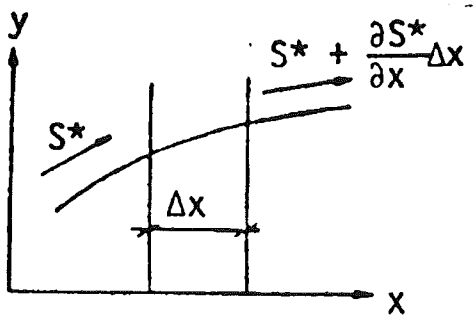

Figure 3.3a: Plan view of coast

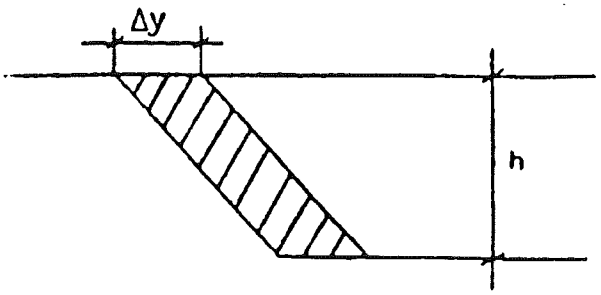

Figure 3.3b: Belonging cross-section

The continuity equation gives (fig 3.3a en b) :

$$\frac{\partial S^*}{\partial x}\Delta x\Delta t + h\Delta x\Delta y = 0 \qquad (3.4)$$

where:

$$\Delta y = \frac{\partial y}{\partial t}\Delta t$$

this gives:

$$\frac{\partial S^*}{\partial x} + h\frac{\partial y}{\partial t} = 0 \qquad (3.5)$$

Substitution of (3.1) in (3.5) yields:

$$\frac{\partial y}{\partial t} = \frac{s}{h}\frac{\partial^2 y}{\partial x^2} \qquad (3.6)$$

The equation (3.6) will be considered to be the "Coastal Equation of Pelnard-Considére." Pelnard-Considére (1956) was the first to publish a paper on this theory as well as to check it against experiment. The original idea however stems from Bossen.
Grijm (1960,1964) developed a similar theory with a more complicated transport formula. He assumed the transport to be proportional to *sin* 2α, in which α is the angle of wave incidence.

	Hydrologie	Thermodynamics	Electricity	Tidal theory Lorentz method	Coastal Dynamics
Current	v water	q heat flux	i electronics	v water	S* sand
Because of a gradient of;	z piezometric level	T temperature	v potential difference	z water level	y coastal direction
Dynamic equation	$v = -K \cdot \partial z/\partial s$ K= permeability	$q = -\lambda \cdot \partial T/\partial s$ λ= conductivity	$i = -1/R \cdot \partial v/\partial s$ R= resistance	$v+\frac{1}{K}\frac{\partial v}{\partial t} = -g\frac{\partial z}{\partial s}$ K= linear coefficient $= \frac{8g}{3C_h^2}\cdot\frac{V}{h}$ C_h= chezy coeff. h = depth	$S^* = S_0^* - s\,\partial y/\partial x$ S_0^*= stationary transport $s = [\partial S^*/\partial\alpha]_{\alpha=0}$ α= angle wave incidence
Continuity equation	$\frac{\partial z}{\partial t} = -\frac{KD}{\beta}\nabla^2 z$ β= porosity D= thickness soil layer	$\frac{\partial q}{\partial t} = \frac{\lambda}{c}\nabla^2 T$ c= heat capacity $\nabla^2 = \frac{\partial^2}{\partial x^2} + \frac{\partial^2}{\partial y^2}$	$\frac{\partial v}{\partial t} = \frac{D}{R_c}\nabla^2 v$ c= capacity per unit of surface D= thickness material	$\frac{\partial z}{\partial t}+\frac{1}{K}\frac{\partial^2 z}{\partial t^2} = -\frac{gD}{K}\frac{\partial^2 z}{\partial s^2}$ D= depth	$\frac{\partial y}{\partial x} = \frac{s}{h}\frac{\partial^2 y}{\partial x^2}$ h= depth s= coast constant h

Tabel 3-1: Analogies with Coastal Dynamics, after a similar table of De Josselin de Jong (1963)

3.2.3 Analogies

The equation (3.6) is the "diffusitivity equation" applicable to many disciplines, as depicted in table 3-1. In this table the analogy with tidal theory (Lorentz method) is somewhat dubious. An analogy only exists when the inertial term is small with respect to the friction term (shallow water). For this case an analogy exists between water surface and coastline and current with sand transport.

3.2.4 Law of Scale

N.B. The Coastal equation (3.6) is independent of S_0^*!

Theorem 1

If $y_1(x,t)$ and $y_2(x,t)$ both satisfy the coastal equation (3.6) then this equation is also satisfied by:

$$y_3 = Ay_1 + By_2$$

where A and B are arbitrary constants. The proof follows from the linearity of equation (3.6).

Theorem 2

If $y(x,t)$ satisfies the coastal equation (3.6), then also $y(A\,x, A^2\,t)$ satisfies this equation. The proof follows by substituting the latter expression in equation (3.6).

Example of theorem 2:

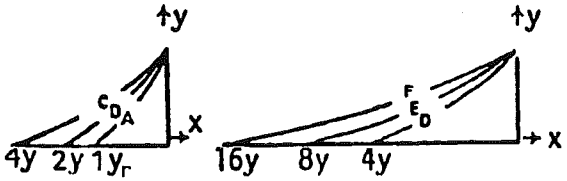

Figure 3.4a:
succesive coastlines
A, BC

Figure 3.4b:
succesive coastlines D,E,F
$y_D(2x,t) = y_A(x,t)$

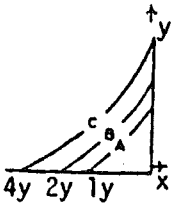

Figure 3.5a:
succesive coastlines
A, B, C

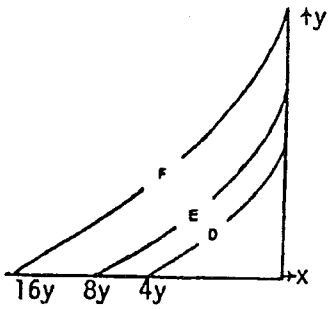

Figure 3.5b:
succesive coastlines
D,E,F $y_D(2x,t) = 2y_A(x,t)$

Let the coastline after 1, 2 and 4 years be given by the curves A, B and C respectively in fig. 4a and let a certain coastline after 4 years be such that it can be found from curve A by multiplying the x-scale by 2 and leaving the y scale constant (curve D). In that case the coastlines E and F originating from D and corresponding to 8 and 16 years may be found by multiplying the x-scales of the curves B and C by a factor of 2.

Example of theorems 1 and 2:

Let the coastline after 1, 2 and 4 years be depicted by the curves A, B and C in fig. 5a and assume a certain coastline after 4 years to be such that it can be found from curve A by multiplying the x and y scale by a factor of 2 (curve D). Then the coastlines E and F for 8 and 16 years respectively may be found from D by multiplying the x- and y-scale of curve B and C by 2.

This is the case because according to theorem 1 the y-scale may be multiplied by any factor. Here, A = 2, B = 0 in theorem 1.

Remark in connection with these examples:

If it would be possible to choose curve A such that curve C coincides with curve D, then the whole coastline would be predictable with time. For instance curves G and H for 32 and 64 years may be determined by multiplying curves E and H by a factor of 2 and so on. In this case the x scale is proportional to $\sqrt{t}$.
Indeed it shows to be possible to choose curve A in this way, as will be elaborated in the proof of the following theorem 3.

Theorem 3

There exists such curves y^*, only a function of x^*, such that from these solutions of the coastal equation can be derived by multiplying y^* by t^n and X^* by $\sqrt{t}$. In this n may be arbitrary.

Proof [1)]

Let $y = y^* \cdot t^n$ and $x = x^* \cdot t^m \rightarrow x^* = x \cdot t^{-m}$

$$\frac{\partial y}{\partial x} = t^n \frac{dy^*}{dx^*} \cdot \frac{\partial x^*}{\partial x} = t^{n-m} \frac{dy^*}{dx^*}$$

$$\frac{\partial^2 y}{\partial x^2} = t^{n-m} \frac{d^2 y^*}{dx^{*2}} \cdot \frac{\partial x^*}{\partial x} = t^{n-2m} \frac{d^2 y^*}{dx^{*2}}$$

$$\frac{\partial y}{\partial t} = \frac{d(y \cdot t^n)}{dt} = nt^{n-1} \cdot y^* + t^n \frac{dy^*}{dx^*} \cdot \frac{dx^*}{dt}$$

In which:

$$\frac{dx^*}{dt} = \frac{\partial (xt^{-m})}{\partial t} = -mxt^{-m-1} = -m\frac{x^*}{t}$$

[1] Similair reasonings given in literature by Edelman (1964).

By this:

$$\frac{dy}{dt} = t^{n-1}(ny^* - mx^* \frac{dy^*}{dx^*})$$

The coastal equation thus gives, see (3.6)

$$t^{n-1}(ny^* - mx^* \frac{dy^*}{dx^*}) = \frac{s}{h} t^{n-2m} \frac{d^2y^*}{dx^{*2}}$$

$$ny^* - mx^* \frac{dy^*}{dx^*} = \frac{s}{h} t^{1-2m} \frac{d^2y^*}{dx^{*2}}$$

On the left hand side is a function, independent of t. Also the right hand side must be independent of t.

This can only happen if:

$$m = \tfrac{1}{2}$$

Furthermore y^* must be a solution of the (ordinary) differential equation

$$\frac{s}{h}\frac{d^2y^*}{dx^{*2}} + \frac{1}{2}x \cdot \frac{dy^*}{dx^*} - ny^* = 0 \qquad (3.7)$$

As was shown to be reasonable from theorem 2, it appears that m should be ½ . It will be clear that n may take ony any arbitrary value; however, the shape of y^* is influences by n.

Theorem 4

Let $y(x,t)$ satisfy the coastal equation (3.6). Then the solution of the equation:

$$\frac{1}{A^2}\frac{s}{h}\frac{d^2y}{dx^2} = \frac{\partial y}{\partial t}$$

Is given by the following functions: 4[a]: $y(x/A, t)$

4[b]: $y(x, A^2t)$

This is found from substitution.

In fig. 3.6 these theorems are depicted.

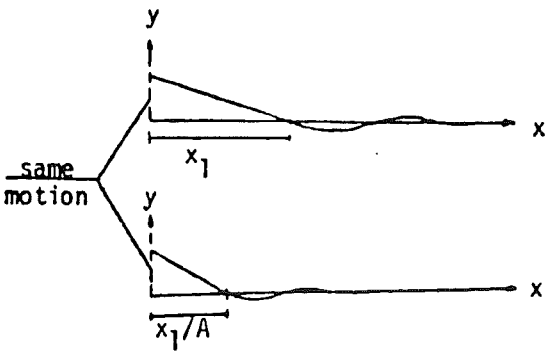

Figure 3.6a: Depicting theorem 4a

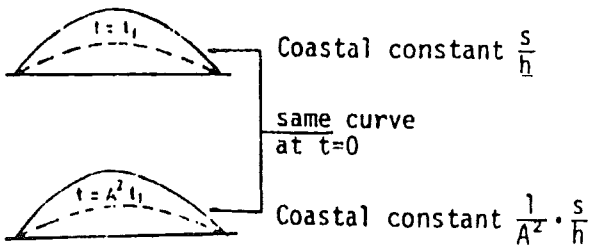

Figure 3.6b: Depicting theorem 4b

The theorems 2 and 4 may be summarized by reducing (3.6) to basic form:

$$\frac{d^2y}{dx'^2} = \frac{\partial y}{\partial t'} \qquad (3.8)$$

this can be done by introducing $x' = x / L_1$ and $t' = t / T_1$ in which should be valid:

$$\frac{L_1^2}{T_1} = \frac{s}{h} \tag{3.9}$$

3.2.5 Applications of the laws of scale in some simple cases.

The solution of the coastal equation depends largely on the boundary conditions. According to theorem 1, a case with difficult boundary conditions can be decomposed in a number of cases with simple boundary conditions, after which these solutions may be superimposed.
In the course of this section a number of these simple cases will be dealt with; the superposition is left to the reader. Formulas will be avoided in this section as much as possible.

3.2.5.1 Reflections by a harbor mole.

Given is the coastal shape y_0 as function of time for a coast, being bordered on one side by a changing delta and which remains at rest at the other side (Fig 3.7). At time $t = 0$ the coast is straight. The direction of wave incidence is parallel to the y-axis (wave crests parallel to the x-axis).

Question: how changes this coast, if at time $t = 0$ a harbor mole is constructed which hampers all transport.

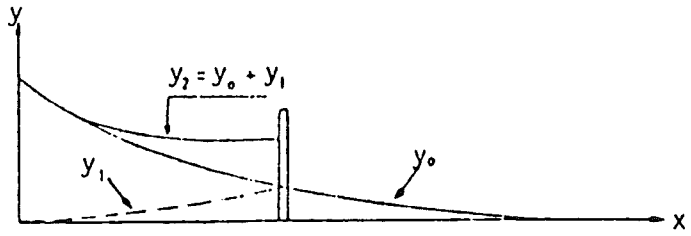

Figure 3.7: Reflection of the coastal shape by a harbor mole

Solution:
At the site of the mole the transport should be zero; this can only be the case of the angle of wave incidence at that site is zero, i.e., if the coast at that site is parallel to the x-axis. According to theorem 2 (with substitution $A = -1$) the reflected coastline y_1 is also a solution of the coastal equation; furthermore, as the coastal equation is linear also y_2, equal to $y_0 + y_1$ suffices with respect to this equation (theorem 1). The solution y_2 obeys as well the condition that the coast as the site of the harbor mole is parallel to the x-axis. Therefore, y_2 is the requested solution.

3.2.5.2 Partial reflection by a groin system

Instead of constructing a harbor mole, which stops all transport, now a series of groins is constructed at time $t = 0$.

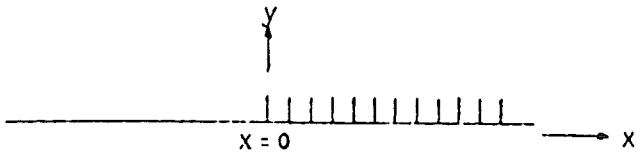

Figure 3.8: Coast with a groin system

Question:
How does the coastline change ?

Solution:
Groins hamper a part of the transport, occurring at a coast without groin [1]. This implies that the longshore transport changes less when the coastal direction changes, i.e. the coastal constant s/h in (3.6) decreases.
Assume, that $\bar{s}$ along the protected coast is a factor p smaller than along the unprotected coast $(p<1)$ [2] it looks obvious, that along the unprotected coast reflection will occur. Let the reflection coefficient be r_e.
Take the origin of the coordinate system at the site of the first groin, let y_u be the y-coordinate of the unprotected beach and y_p the y-coordinate of the protected beach. Then the coastline of the unprotected beach can be found from the original coastline y_0 by taking the reflection into account:

$$y_u(-x) = y_0(-x) + r_e y_0(x) \tag{3.10}$$

Thus the y-coordinate at the first groin ($x= 0$) becomes $(1 + r_e)\, y_0$. This boundary condition y_p for the protected part implies the same function of time as $y_0(0)$ only $y_p(0)$ is $(1+ r_e)$ times as large.
According to theorem 1 and 4a the solution of the protected part will be:

$$y_p = (1 + r_e)\{ y_0(x\sqrt{p})\} \tag{3.11}$$

This function suffices, as well with respect to the boundary conditions as with respect to the coastal equation for the protected part.
Thus the magnitude of the reflection coefficient r_e results from the continuity equation at $x=0$: the longshore transport left and right of the first groin should be equal.
Because the direction of wave incidence is parallel to the y-axis, S_0* will be equal to zero; thus is found from (3.1):

$$-s\left[\frac{\partial y_u}{\partial x}\right]_{x=0} = -ps\left[\frac{\partial y_p}{\partial x}\right]_{x=0}$$

Expressing y_p and y_u in y_0 with the aid of (3.10) and (3.11) results into:

$$(1 - r_e)\left[\frac{\partial y_0}{\partial x}\right]_{x=0} = -\frac{p(1 + r_e)}{\sqrt{p}}\left[\frac{\partial y_0}{\partial x}\right]_{x=0} \tag{3.12}$$

from which r_e is found:

$$r_e = \frac{1 - \sqrt{p}}{1 + \sqrt{p}} \tag{3.13}$$

Fig 3.9 shows the construction of the requested coastline from y_0.

[1] In section 3.3.4.5. this process will be considered in more detail.
[2] It will appear, that under peculair circumstances p can be larger than 1 (sec 3.3.4).

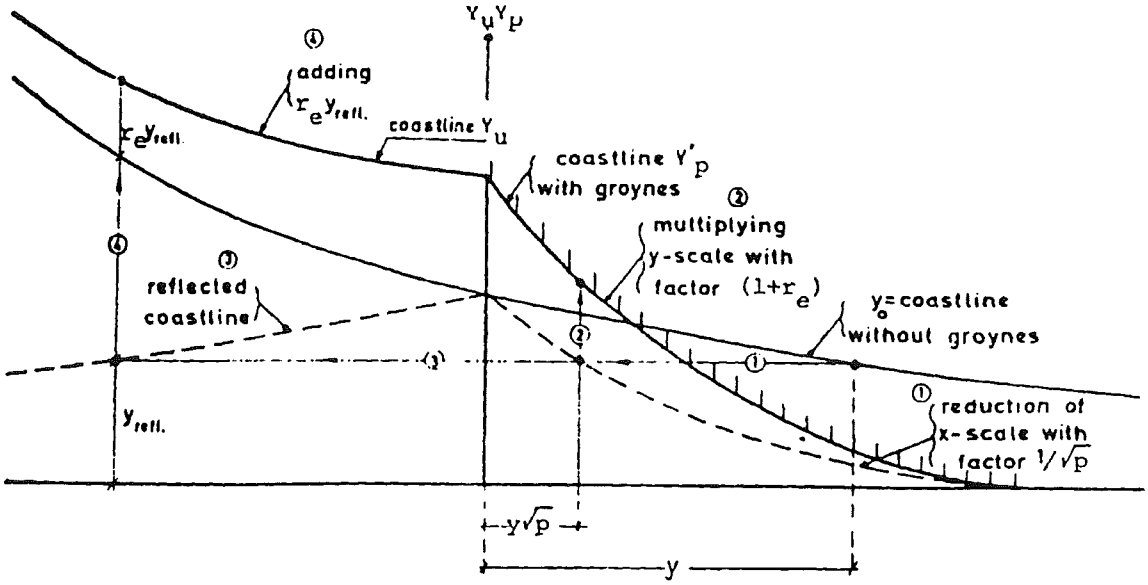

Figure 3.9: Construction of coastal shape of a partly protected beach from a given shape y_0 which would occur if the coast would not be protected

3.2.5.3 Accretion of a coast near a harbor mole

Consider a coast which is straight at time *t= 0* with a wave impinging obliquely on the coast (fig. 3.10). At a time *t= 0* a harbor mole is constructed which acts so as to stop all transport.

Required:
The Coastal shape

Solution:
On the site of the harbor mole the transport is zero at any time. Therefore at this site the coast can be shown to be parallel to the direction of the wave crests. At long distances from the harbor mole the coast is parallel to the x-axis. As the direction of the tangents to the curve may not change, this means that the scale of the coastal shape in the y-direction should increase in the same way as in the x-direction, therefore with $\sqrt{t}$.Therefore the total area increases with a factor of *t*. This can also be found using continuity per unit of time: the harbor mole captures an amount of sand S_0*.

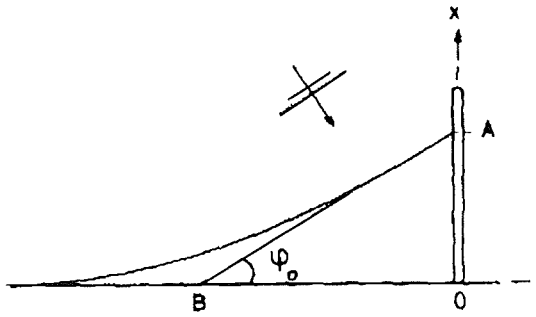

Figure 3.10: Coastal shape near a harbor mole. the tangents at x= 0 and x= ∞ are parallel to the wave direction and the x-axis respectively.

The area, enclosed by the x- and y-axis is approximately 1.5 times as large as area OAB (fig. 3.10) (or as per the computation in section 3.2.6.1., which follows, $\pi/2$ times as large).

The area is therefore: $$S_0 \cdot \frac{t}{h} = \frac{\pi}{2} \cdot \frac{1}{2} \frac{OA^2}{tg\alpha_0}$$

from which: $$OA = \frac{2}{\sqrt{\pi}} \cdot \sqrt{S_0 \cdot tg\alpha_0 / h} \cdot \sqrt{t} \qquad (3.14a)$$

By the use of (3.2) the following may be found:

$$OA = \frac{2}{\sqrt{\pi}} \cdot tg\alpha_0 \sqrt{(\frac{s}{h} \cdot t)} \qquad (3.14b)$$

Alternately: $$OA = \frac{2}{\sqrt{\pi}} \cdot S_0 \sqrt{\frac{t}{sh}} \qquad (3.14c)$$

Example: S_0*= 200.000 m^3/year, s= $5 \cdot 10^6$ m^3/year/rad, h= 5m;
it follows that OA= 45 √t meter

IN THE SECTIONS 3.2.5.4 TO 3.2.5.6 THE CASES ARE TREATED WHICH BELONG TO THE SAME "FAMILY" OF SOLUTIONS.

3.2.5.4 Erosion behind a harbor mole (Fig. 3.11 a).

The next figure speaks for itself:
Erosion behind a harbor mole (anti-symmetric with the accretion).

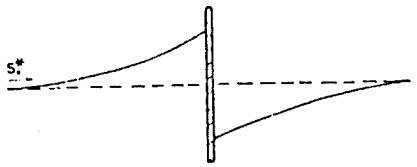

Figure 3.11a: Erosion behind a harbor mole

3.2.5.5 A river delta with constant sand supply S_d* per unit of time (fig. 3.11 b)

The accretion at the site of the river mouth given by: $$OA = \frac{1}{\sqrt{\pi}} \cdot S_d^* \sqrt{\frac{t}{sh}}$$

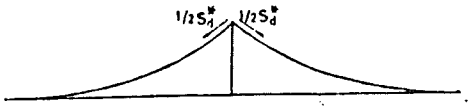

Figure 3.11b: the shape of a river delta

3.2.5.6 Erosion behind the last groin of a beach groin system (Fig 3.11c)

At the site of the last groin the erosion is $(1-\sqrt{p})$ times the erosion behind a harbor mole (p is defined in in (3.2.5.2). This is shown in the following:
The horizontal scale of the protected part is $\sqrt{p}$ times the scale of the unprotected part (theorem 4a) Assume that S^*_{unpr} per year erodes from the unprotected part. Therefore $\sqrt{p} \cdot S^*_{unpr}$ erodes from the protected part.

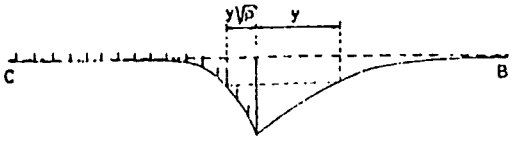

Figure 3.11c: Erosion behind the last groin

Furthermore the transport at point B in fig. 3.11c (at large distance from the first groin) is according to (3.1) equal to S_0*. At point C in Fig 3.11c (also a great distance from the first groin, but on the protected coast) the transport is equal to $p \cdot S_0$*. Per unit of time erosion is therefore:

$$(1 - p)S_0^* = (1 + \sqrt{p})\, S^*_{unpr}$$

Thus the eroded pit becomes:

$(1 - p) / (1 + \sqrt{p}) = (1 - \sqrt{p})$ times as deep as in the case of a long harbor mole.

3.2.5.7 Accretion of a coast, which has reached the head of a groin.

Assume that the length of the groin is l and the time (after the construction of the groin) for the coastline to reach the head of the groin is t_1. Thus by reference to (3.14b) t_1 may be found as follows.

$$t_1 = \frac{\pi l^2}{4tg^2\alpha_0} \cdot \frac{h}{s} \qquad (3.16)$$

The coast will accrete according to figure 3.12a. Note that at a point corresponding to $x = 0$ the coast remains at the same site. Thus the coast does not accrete in the y-direction. By application of the Law of scale it is logical to assume a coastal shape whereby the scale increases in the x-direction (in proportion with $\sqrt{t}$), but not in the y-direction.

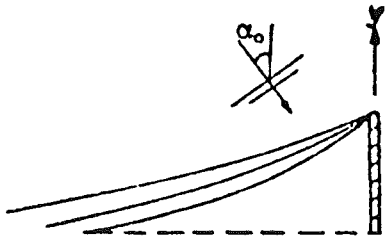

Figure 3.12a: Accretion of a coast, after it reached the head of the mole

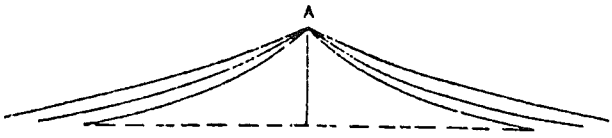

Figure 3.12b: Instantaneous dumping of sand at one place

The solution y^* of eqn. (3.7) for $n = 0$ could be shown to apply here. However, the coastal shape before $t = t_1$ was a solution of the equation (3.7) for $n = ½$ and both solutions (for $n=0$ and $n = ½$) do not coincide. After a short time past $t = t_1$ the shape $[y^*]_{n=1/2}$ will change gradually to the shape $[y^*]_{n=0}$.
Once the shape is adapted the gradient $\partial y/\partial x$ will decrease in proportion to $1/\sqrt{t}$. Therefore the transport along the groin will increase, following (3.3) and proportional to $\alpha_0 (1 - \sqrt{t_2 / t})$ where t_2 is a proportionality constant with dimension "time" ($t > t_2$).

Remark: Analogous to section 3.5.7 it may be demonstrated that the sand-supply needed to keep point A in figure 3.12b at its present position, decreases in proportion with $1/\sqrt{t}$.

3.2.5.8 Instantaneous dumping of sand at one place:

At a certain time a quantity of sand S^{**} is dumped on a beach in the shape of a Gauss curve as per figure 3.13. The Gauss curve is essentially a solution of equation (3.7) for $n = -½$.

In the course of time this quantity disperses over a larger part of the coast, i.e. the scale increases with $\sqrt{t}$, the y-scale should thus decrease with $1/\sqrt{t}$ in order to hold the dumped quantity constant. The coastal shape according to section 3.2.6 can be expressed in the following formula:

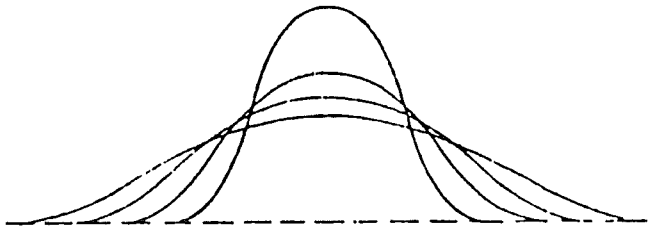

Figure 3.13: Instantaneous dumping of sand at one place

$$y = \frac{S^{**}}{2\sqrt{\pi s h t}} \cdot e^{\frac{-hx^2}{4st}} \qquad (3.17)$$

Example: $S^{**} = 200.000\ m^3$, $s = 5 \cdot 10^6\ m^3$/year, $h = 5m$;

$$y = \frac{11.25}{\sqrt{t}} \cdot e^{\left(\frac{-x}{2000t}\right)^2}$$ (x and y in m, t in years)

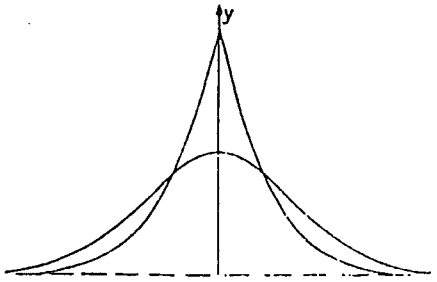

Figure 3.14: The shape of the coastline after an instaneous dumping and after continous dumping, both after one year (same amount per year).

Figure 3.14 shows in the same figure the delta according to section 3.2.5.3 and the dumped material as per (3.17). If the quantities S_d^* and S^* dumped in one year are equal, the accretion at the site $x = 0$ is for the delta twice as large as that for the dumped material. the most seaward point of the dump attenuates with $1/\sqrt{t}$.

The points of contraflexure on the Gauss curve are at distance $\pm x_b$ from $y = 0$, where:

$$x_b = \sqrt{2\frac{s}{h}t} \tag{3.18}$$

About 2/3 of the dumped material lies between $x = -x_b$ and $x = +x_b$. In the above mentioned example x_b equals $1.4\sqrt{t}$ km.

3.2.6 Analytical basic solutions

For a general solution of the coastal equation is referred to Bakker (1971). For practical use, however, the basic "tools" of two kinds of analytic solutions and a numerical method will be mostly sufficient. In this section 3.2.6 these two kinds of analytic solutions will be displayed, where in 3.2.7 a numerical solution will be given. This method can be used also in a graphical way.

3.2.6.1 The error function family

The kind of analytical solutions, which will be mentioned in this section belong to the same "family" because all are integrals of derivatives of each other.

Theorem 5
If y(x, t) suffices the coastal equation (3.6), then the following functions suffice this equation as well:

1 the partial derivatives of y to x and t;
2 the integrals of y to x and t, provided that the integration "constants" are indeed constant and are (generally) no functions of t or x respectively.

Proof:
If (3.6) is valid, then (3.6) remains valid, when the lefthand-side and righthand-side are differentiated (c.q. are integrated under the conditions, mentioned ad 2). Changing the succession of differentiation (c.q. integration) yields the proof of Theorem 5.

A simple way of getting solutions from (3.6) is solving equation (3.7). The simplest solution is found when $n = 0$; in this case the equation reads:

$$\frac{s}{h}\frac{d^2y^*}{dx^{*2}} + \frac{1}{2}x^* \cdot \frac{dy^*}{dx^*} = 0 \tag{3.19}$$

Assume $dy^*/dx^* = p_1$, then is found from (3.19):

$$\frac{s}{h}\frac{dp_1}{p_1} = -\frac{1}{2}x^* \cdot dx^* \quad \rightarrow \quad p_1 = Ae^{-\frac{x^{*2}h}{4s}}$$

$$y^* = A\int e^{-x^{*2}h/4s}dx^*$$

Substitution of $y^* = y\,t^n$ and $x^* = x\,t^m$ with $n = 0$ and $m = ½$ yields for y:

$$y = A'\int e^{-x^2h/4st}d\left(x\cdot\sqrt{\frac{h}{4st}}\right) \tag{3.20a}$$

If for A' is chosen: $A' = 2/\sqrt{\pi}$ and if the integration boundaries are chosen as shown below, then (3.20 a) becomes the "complementary error function":

$$y = \frac{2}{\sqrt{\pi}}\int_{x\sqrt{h/4st}}^{\infty} e^{-x^2h/4st}d\left(x\cdot\sqrt{\frac{h}{4st}}\right) \tag{3.20b}$$

$$y = erfc\left(x\cdot\sqrt{\frac{h}{4st}}\right) \tag{3.20c}$$

In order to explain the shape of the function at the right-hand side of (3.20 c), this function will be differentiated to x; according to Theorem 5, this again yields a solution of the differential equation:

$$y = \frac{A''}{\sqrt{t}}e^{-x^2h/4st} \tag{3.21}$$

[1] Here "y" simply denotes "a solution of the coastal equation". More formally the solutions of (3.20a) and (3.21) should be marked off from each other, by a subscript for instance. However no confusion is forseen.

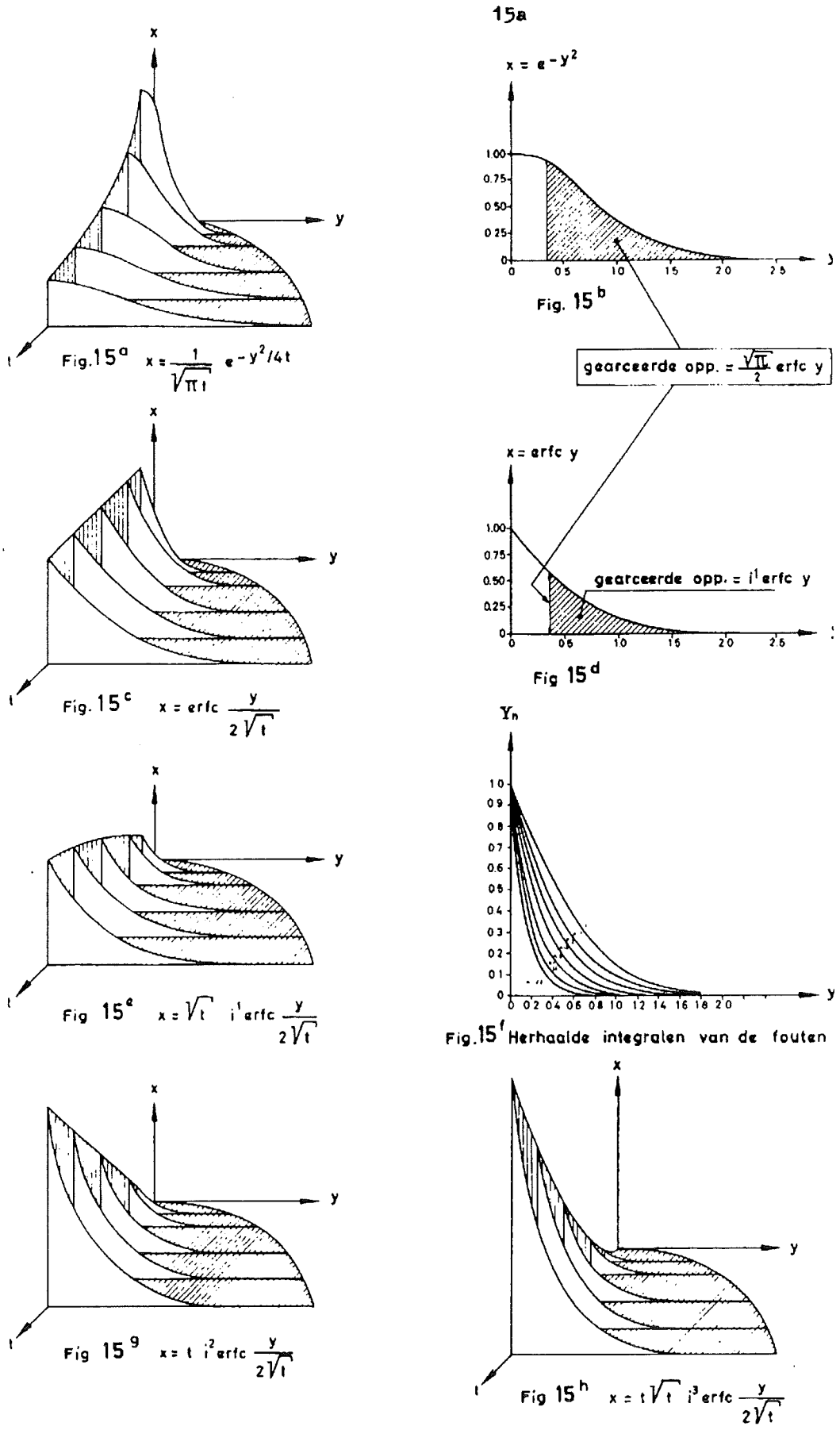

Figure 3.15: Basic solutions of the coastal equation

Fig 3.15a displays the solution (3.21). Fig 3.15 b gives the curve $y = e^{-x2}$. As (3.20b) shows, the hatched area in this figure equals $\sqrt{\pi}/2$ times the y-coordinate of *erfc x*; last mentioned function is given in fig. 3.15d. However, in the exponent of (3.21) one finds "x^2/t" instead of purely "x^2" and therefore, when integrating according to (3.20 b) the factor "$1/\sqrt{t}$" in (3.21) disappears in (3.20c).

The solution given by (3.20c) and shown in fig. 3.15 c therefore appears to be independent of time at $x = 0$.

Repeated integration of (3.20c) to x gives the solution:

$$y = \sqrt{t}\, i^1\, erfc\, x \cdot \sqrt{\frac{h}{4st}} \quad {}^{1)\,2)} \qquad (3.22)$$

$i^1\, erfc\, x$ is the first integral of the error function, the hatched area in fig. 3.15 d. According to the theory of the error functions, the total integrated area of *erfc x* between 0 and ∞ equals $\sqrt{\pi}/2$.

The integration can be continued, giving functions as:

$$y = t^{\frac{1}{2}n'}\, i^{n'} erfc\, x \cdot \sqrt{\frac{h}{4st}} \quad {}^{3)} \qquad (3.23)$$

With this function, at $x = 0$ the y-coordinate increases accordingly:

$$[y]_{x=0} = t^{\frac{1}{2}n'}$$

It thus shows, that the solutions of (3.7) for $n = \frac{1}{2} n'$ are found as:

$$y^* = i^{2n} erfc(x^* \sqrt{h/s}) \qquad (3.24)$$

For the mathematical properties of the error function and related functions is referred to Abramowitz and Stegun (1971), ch. 7, from which the following is derived. The error function is defined as:

$$erf\, u = \frac{2}{\sqrt{\pi}} \int_0^u e^{-u^2} du \qquad (3.25)$$

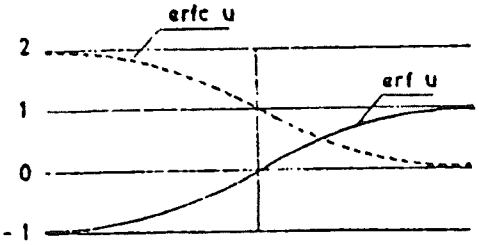

Figure 3.16: The error function and the complementary error function.

The error function can be developed in a series in the following way:

$$erf\, u = \frac{2}{\sqrt{\pi}} \int_0^u e^{-u^2} du = \frac{2}{\sqrt{\pi}} \sum_{n=0}^{\infty} \int_0^u \frac{(-u^2)^n}{n!} = \frac{2}{\sqrt{\pi}} \sum_{n=0}^{\infty} \frac{(-1)^n u^{2n+1}}{(2n+1)n!} \qquad (3.26)$$

The first approximation of *erf u* for small values of u is therefore $2u/\sqrt{\pi}$.

---

[1] The constant factor $2\sqrt{}$ (s/h) is omitted.

[2] i^1erfcx is a usual notation for this kind of functions; any coincidence with the "i" of complex numbers is purely accidental.

[3] The constant factor $(2\sqrt{(s/h)})^{n'}$ is omitted.

The function increases when u goes to infinity. It is strongly related to a function often used in error theory: the probability of exceedance of a value x by a normal distributed stochastic variable $\underline{x}$ with mean m and standard deviation σ equals:

$$P_r(\underline{x} > k) = \frac{1}{2} erfc(\frac{x-m}{\sigma\sqrt{2}}) \tag{3.27}$$

where: $erfc\ u = 1 - erf\ u$ (3.28)

Integration of erfc from u to ∞ gives $i^1 erfc\ u$. Direct integration of the error function, using partial integration gives:

$$\begin{aligned} i^1 erfc u &= \int_u^\infty erfc\ u\ du = u\ erfc\ u \Big|_u^\infty - \frac{2}{\sqrt{\pi}} \int_u^\infty u e^{-u^2} du \\ i^1 erfc\ u &= -u\ erfc\ u + \frac{1}{\sqrt{\pi}} e^{-u^2} \end{aligned} \tag{3.29}$$

The integrals of the error function are tabulated by Abramowitz and Stegun (1971), table 7.4. They are "normalized" to the functions Y_n (Fig 3.15f) [1)], i.e. multiplied by a constant in this way, that $Y_n(0)$ equals 1. The relation between $i^n\ erfc\ u$ and $Y_n(u)$ appears to be:

$$Y_n(u) = 2^n \Gamma(\frac{n}{2} + 1) i^n erfc\ u \tag{3.30}$$

Where: $\Gamma(n/2+1) = (n/2)!$ if n is even ($n \geq 2$)

And: $\Gamma(n/2 + 1) = n/2 \cdot (n/2 - 1)\ (n/2 - 2) \ldots 3/2\ \sqrt{\pi}$ if n is odd ($n \geq 3$)

From Abramowitz and Stegun (1971) the following recurrences can be derived:

$$Y_n(u) = Y_{n-2}(u) - 2\frac{u}{n} \frac{\Gamma(\frac{n}{2}+1)}{\Gamma(\frac{n}{2}+\frac{1}{2})} \cdot Y_{n-1}(u) \tag{3.31}$$

Instead of integrating (3.21), this function can be differentiated as well. Then one finds functions as displayed in fig. 3.17. However, the velocity of attenuation increases with the number of times, that (3.21) is differentiated: the y-coordinate is proportional to $f^{n/2}$ when one differentiates n times.

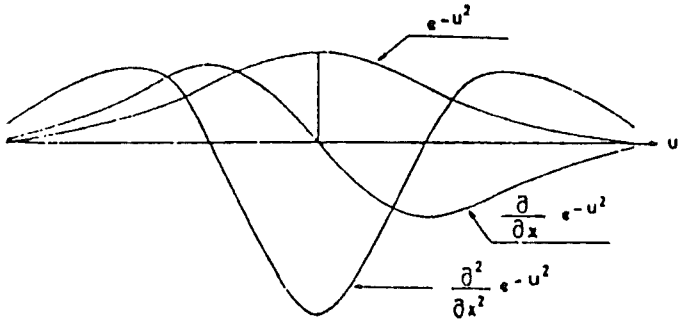

Figure 3.17: The derivatives of the Gauss Curve

Example:
Let a certain quantity of sand be dumped on the beach in an arbitrary shape. The coastal shape can be thought of to be composed of a Gauss curve plus a number of curves of the kind shown in fig. 3.17. In course of the time a kind of "survival of the fittest" takes place: the Gauss-curve attenuates the slowest and will be visible therefore during the longest time. In whatever shape the sand is dumped, after some time, a Gauss-curve will result.

3.2.6.2 Periodical solutions

Quite another way of solution of the coastal equation (3.6) is splitting the equation into variables.

Assume:

$$Y=X \cdot T$$

where X and T are only functions of x and t respectively. Substitution in (3.6) yields:

$$X\frac{dT}{dt}=\frac{s}{h}T\cdot\frac{d^2X}{dx^2}$$
$$\frac{h}{s}\cdot\frac{1}{T}\cdot\frac{dT}{dt}=\frac{1}{X}\frac{d^2X}{dx^2} \qquad (3.33)$$

The left-hand side of (3.33) is a function of t, the right-hand side a function of x; therefore, the equation only holds if left-hand side and right-hand side are a constant. Mention this constant: $-k^2$. Then one finds for X and T:

$$T=e^{-k^2\frac{s}{h}t};X=A_1e^{ikx}+B_1e^{-ikx}$$

or:
$$y=(A_1e^{ikx}+B_1e^{-ikx})e^{-k^2\frac{s}{h}t} \qquad (3.34)$$

The integration constants A, B, and k can be complex.

Consider first the case, that k is real; an appropiate choice for A_1 and B_1 gives:

$$y=e^{-t\ /\ T_0}(A\cos ky+B\sin ky) \qquad (3.35)$$

Let k be: $k = 2\pi/L$, then for T_0 is found:

$$T_0=\frac{L^2}{4\pi^2}\cdot\frac{h}{s} \qquad (3.36)$$

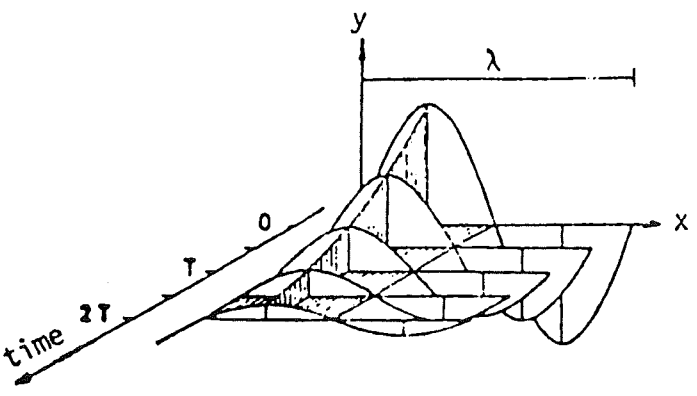

Figure 3.18; Attenuation of the wave shape of a simusoidally shaped coastline

This function is displayed by a standing, attenuating wave (fig. 3.18)

Example:
L = 200m; h = 5m, s = 5.10^6 m^3/year

The wave attenuates each 10^{-3} year = 8 hours a factor e. If λ= 2km this lasts for 10^{-1} year $\cong$ 1 month.

N.B.: If s is negative (large angle of wave incidence; transport increases when the angle of wave incidence decreases) then T_0 will be negative, i.e. y increases for increasing t, which means, that the coast is unstable!

Consider now the case, that k is complex. Let k^2 be $-2\,i\,k_1^2$, in which k_1 is real (i.e. k^2 is barely imaginary), then k will be:

$$k = \pm(1 - i)\,k_1 \tag{3.37}$$

Then (3.34) reads:

$$y = e^{2ik_1\frac{2s_1}{h}}\{A_1 e^{k_1 x(1+i)} + B_1 e^{-k_1 x(1+i)}\}$$

Retain the real part:

$$y = A_1 e^{k_1 x}\cos(k_1 x + \omega_1 t) + Be^{-k_1 x}\cos(-kx + \omega_1 t) \tag{3.38}$$

in which $\omega_1 = \dfrac{2\pi}{T_1} = 2k_1^2 \cdot \dfrac{s}{h}$

Or, after substitution of $L_1 = 2\pi/k_1$:

$$L_1 = \sqrt{4\pi\frac{s}{h}T_1} \tag{3.39}$$

The first term represents a sandwave, travelling and attenuating in negative x-direction, the second one a wave, travelling and attenuating in positive x-direction. Fig. 3.19 shows the behaviour of the second tern in the course of the time. After ca ½ L_1 the wave is attenuated. The propagation velocity L_1/T_1 is proportional to $1/\sqrt{T_1}$ according to (3.39). The wave propagates therefore slower, when the period is larger.

Example:
T_1 = 1 year, s = 5.10^6 m^3/year, h = 5m
Then L_1 equals: L_1 = 3.5 km.

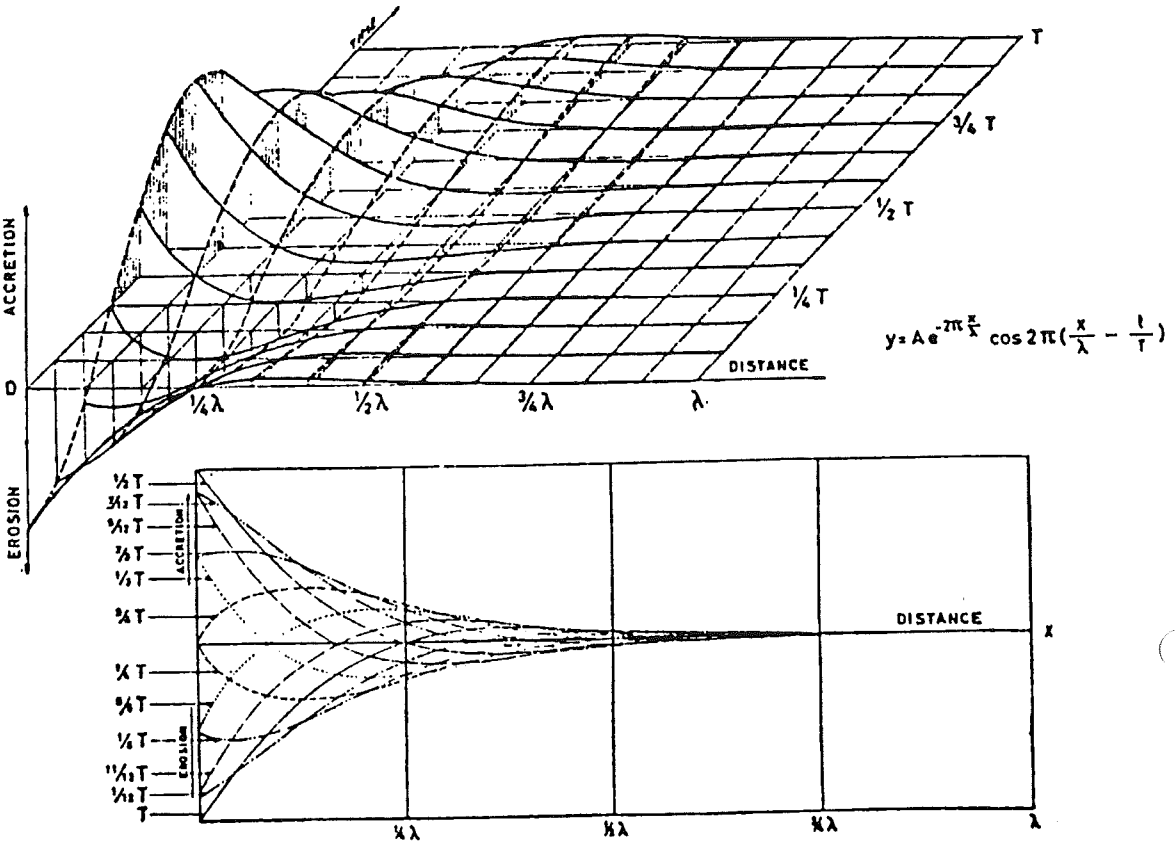

Figure 3.19: Shape of sandwave as function of time

3.2.7 Graphical solutions

The coastal equation (3.6) can be solved very simply numerically or even graphically. In these notes, only a simple graphical method will be explained. This method is mostly credited to Schmidt (1926); the first application is by BINDER (1910) [1) 2)].

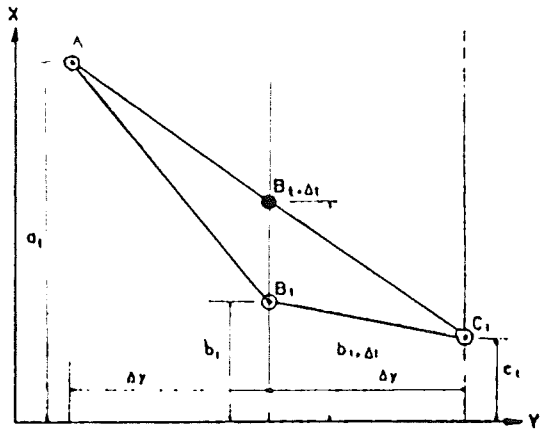

Figure 3.20; The graphical method of Schmidt

It is a forward differential method, where from 3 points of the coastline at a certain time the situation of one point at a successive time is calculated.

[1] Referred is also to Langejan and de Josselin de Jong (1963), dealing about ground water flow; much of the exposure given in sect. 3.2.7 originates from this paper.

[2] The method is treated here because it gives very much feeling for the feature of diffusion. Needless to say that in the number-chruncher's era there are more accurate ways. However, nature will not see the difference.

The coastal equation (3.6) is written as a differential equation:

$$\frac{b_{t+\Delta t}-b_t}{\Delta t}=\frac{s}{h}\frac{\dfrac{c_t-b_t}{\Delta x}-\dfrac{b_t-a_t}{\Delta x}}{\Delta x}$$

$$\frac{b_{t+\Delta t}-b_t}{\Delta t}=\frac{s}{h}\frac{a_t-2b_t+c_t}{(\Delta x)^2} \qquad (3.40)$$

$$b_{t+\Delta t}=\frac{s}{h}\frac{\Delta t}{(\Delta x)^2}(a_t+c_t)+(1-2\frac{s}{h}\frac{\Delta t}{(\Delta x)^2})b_t$$

Here Δx and Δt can be chosen rather arbitrarily; however, if Δt is chosen too large with respect to Δx, then the numerical process becomes unstable. The largest Δt, for which stability is guaranteed equals:

$$\frac{s}{h}\cdot\frac{\Delta t}{(\Delta x)^2}=\frac{1}{2}\rightarrow\Delta t=\frac{(\Delta x^2)}{2s/h} \qquad (3.41)$$

In this case the solution becomes very simply, as is shown by substituting (3.41) into (3.40):

$$b_{t+\Delta t}=\frac{1}{2}(a_t+c_t) \qquad (3.42)$$

Every point $B_{t+\Delta t}$ of the coastline at time $t+\Delta t$ now can be found from two neighbouring points A_t and C_t lying at the coastline at time t, at a distance Δx from the considered point. For this goal the line A_tC_t is drawn; where this line intersects the x-coordinate of B_t is the point wanted point $B_{t+\Delta t}$.

In the case that a coastline is given as initial condition, and furthermore the y-coordinate of the coast in the course of the time at both boundaries, the method does not lead to difficulties. However, more explanation is wanted when the transport, i.e. the coastal direction is given at a boundary.

Suppose, for instance, that the coast extends in positive x-direction from $x= 0$ and that the coastal direction is given in $x= 0$. Assuming the point "B" from fig. 3.19 lying on the y-axis (fig. 3.21), then the validity exists:

$$\left[\frac{\partial y}{\partial x}\right]_{x=0}=\frac{c_t-a_t}{2\Delta x} \qquad (3.43)$$

In this case, however, A is an unknown, non-existing point on the wrong side of the boundary, for the same reason $b_{t+\Delta t}$ from (3.42) cannot be determined. However, from equations (3.42) and (3.43) the unknown a_t can be eliminated from which a relation can be derived between the unknown $b_{t+\Delta t}$ and the known values C_t and $[\partial y/\partial x]_{x=0}$

$$b_{t+\Delta t}=c_t+\Delta x\left[\frac{\partial y}{\partial x}\right]_{x=0} \quad \text{for x =0} \qquad (3.44)$$

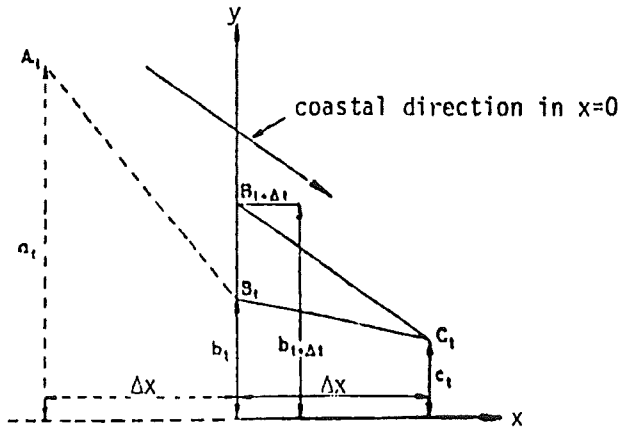

Figure 3.21; Graphical method of Schmidt for a given transport at one boundary

Therefore (fig. 3.21), a line drawn through C_t parallel to the tangent to the: coast in B_t does not intersect the y-axis in B_t (as one would expect) but $B_{t+\Delta t}$.

The method can be sophisticated in some ways:

1 Different values of the coastal constant s/h along the coast
2 Doubling the x-scale, after some time; according to (3.41) this gives a time-scale being 4 times as large (fig. 3.22)
3 local refining the x-scale. Fig. 3.23 gives an example. Only over the refined areas one calculates $y_{t+\Delta t}$, $y_{t+2\Delta t}$ and $y_{t+3\Delta t}$; for the rest only $y_{t+4\Delta t}$.

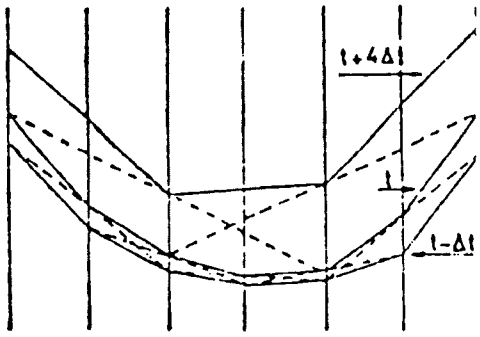

Figure 3.22; Doubling the x-scale gives a time-scale, being 4 times as large

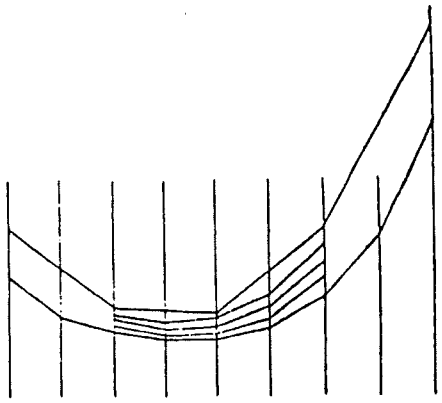

Figure3.23: Local refinement of the x-scale

3.3 2-Line Theory

3.3.1 Introduction

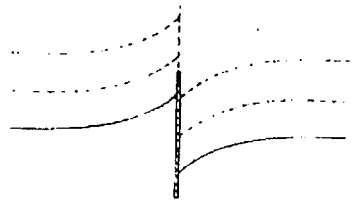

Figure 3.24a: Coastline with parallel depth contours

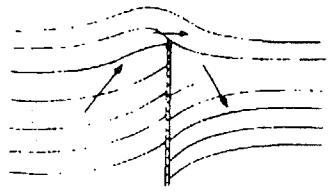

Figure 3.24b: A better approximation. The arrow denote the direction of the sand transport. From Bakker (1971).

The accretion of a coast all the way into the end of a groin is highly unlikely to occur. In particular, in the vicinity of the groin the assumption that all the contour lines remain parallel during the accretive process can lead to considerable deviations from reality. This is depicted in figure 3.24

In an investigation of the effect of construction, which interrupts a part of the littoral drift the capabilities of theory are limited. It is impossible to even qualitively predict anything about factor *p* from section 3.2.5.2, where *p* indicates how the transport diminishes when groins are constructed.
In this chapter we will treat a theory, in which beach and inshore are considered separate and
can move separate to each other. However there is a dependence on each other as offshore transport can occur from beach to inshore and inversely.

3.3.2 The mechanism of a groin

The theory of transport near a groin is based on basic concepts developed by Van Bendegom (1969). The concepts are as follows:

Shortly after the construction of a groin on a coast in equilibrium, the groin will stop the sand transport near the beach, but not along the inshore zone. The beach, therefore accretes; however the inshore zone does not accrete with result:
the profile on the windward side of the groin becoming steeper than the equilibrium profile. On the leeward side of the groin erosion takes place on the beach, causing on this side a profile flatter than the equilibrium profile. Therefore on the windward side sand rolls downward, while on the leeward side it is transported in an upward direction. This is caused by asymmetry of the incident waves, where, high swash velocities alternate with lower backwash velocities (fig 3.24b)

Another important mechanism which occurs at the groin is the so called rip-current. A groin does not only inhibit sandtransport, but also the longshore current. This current will be bent in a seaward direction, and hence a considerable amount of sand will be discharged from beach to inshore.

Both mechanisms will be considered separately. With reference to the rip-current it will only be investigated as regards to the consequences of a certain amount of sand S^*_{rip} being transported from beach to inshore. For the magnitude of S^*_{rip} reference should be made to chapter 3.5. However for both considered mechanisms, a mathematical model is required which treats beach and inshore separately.

3.3.3 Definitions and assumptions

a) A beach groin is defined as a vertical obstacle which stops sand transport along a beach, but not along the inshore zone (Fig 3.25)

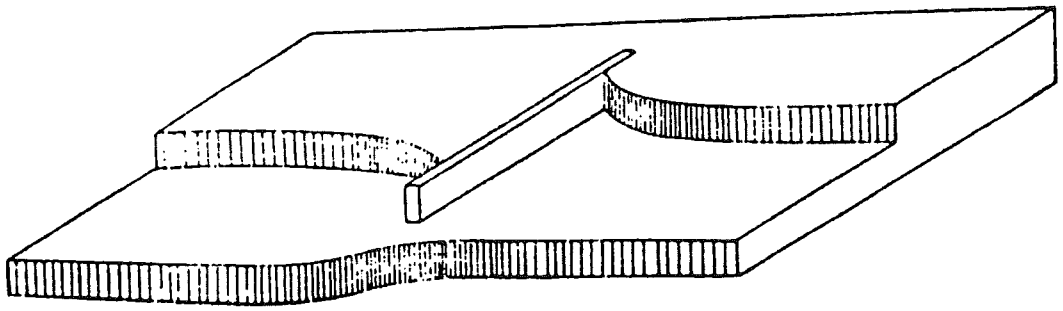

Figure 3.25: Schematized coastal topograghy near a groin according to the two line theory. From Bakker (1969)

b) The coastal profile is divided into three parts, a beach; an inshore zone and a horizontal part in between. By definition the boundary between beach and inshore lies at the construction depth h_1 of the beach groin. The inshore zone lies between h_1 and $h = h_1+h_2$.

c) The beach and inshore zone are furthermore schematized as a stepwise profile, according to figure 5.26. The areas PQSR and *RTUV* in figure 5.26a are the same as the corresponding areas in figure 5.26b. Figure 5.25 merely gives a three-dimensional view.

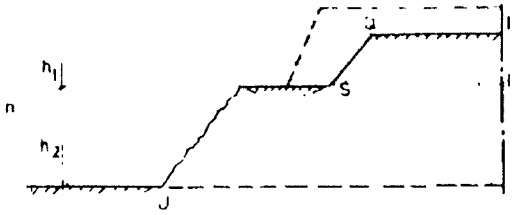

Figure 3.26a: Schematized profile

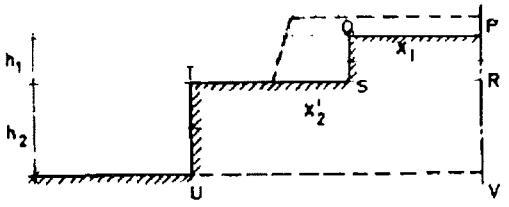

Figure 3.26b: Two-line theory

d) In a plan view one observes two lines at a distance y_1 and y_2' from the x-axis. These will be called respectively the "line of the beach" and the "line of inshore."

e) The "equilibrium distance" W is the distance $y_2' - y_1$ between beach and inshore, which exists when the profile is in equilibrium.

f) The following dynamic equations are assumed. If the distance $y_2' - y_1$ is equal to the equilibrium distance W no interference is assumed. If the distance is smaller than W, then the profile is too steep and an offshore transport will result. A transport in the direction of the coast (onshore) occurs in the inverse case. This relationship is linearized, the offshore transport per unit length is considered to be (fig. 3.27):

$$S_y = s_y (y_1 - \{y_2' - W\}) \qquad (3.45)$$

in which s_y is a proportionality constant. The dimension of s_y is (L/t), opposite to s_1, in which the dimension is (L/t^3). Use of a simple notation gives the following:

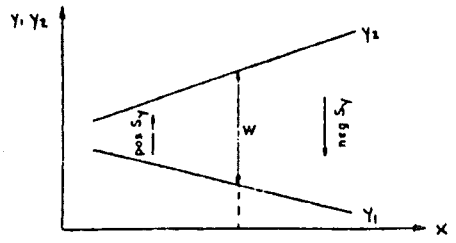

Figure 3.27: Schematized offshore/onshore transport

$$y_2 = y_2 - W \qquad (3.46)$$

$$S_y = s_y (y_1 - y_2) \qquad (3.47)$$

g) With reference to the longshore transport, the assumption of Pelnard-Considere, according to Sect. 3.2, will be applied for both the beach and inshore zones.

$$S_1^* = S_{01}^* - s_1 \frac{\partial y}{\partial x}$$
$$S_2^* = S_{02}^* - s_2 \frac{\partial y_2}{\partial x} \qquad (3.48)$$

Here S_{01}^* and S_{02}^* are the transport when $\partial y_1/\partial x$ and $\partial y_2/\partial x$ are zero.
s_1 and s_2 are proportionality constants, analogous to s in equation (3.1).

3.3.4 The Stationary Case

3.3.4.1 General Solution

In this section the stationary case will be tested. With reference to the continuity equation, the following is yielded for respectively the beach and inshore:

$$\frac{dS_1^*}{dx} + S_y = 0$$
$$\frac{dS_2^*}{dx} - S_y = 0 \qquad (3.49)$$

After substitution of the transport equations (3.47) and (3.53) one finds the coastal equations:

$$-s_1 \frac{d^2 y_1}{dx^2} + s_y (y_1 - y_2) = 0$$
$$-s_2 \frac{d^2 y_2}{dx^2} + s_y (y_2 - y_1) = 0 \qquad (3.50a,b)$$

The solution of these simultaneous differential equations should proceed by by substituting y_2 from (3.50a) in equation (3.50b) and hence solving this last mentioned equation.
One then finds:

$$y_1 = Ae^{x/L_0} + Be^{-x/L_0} + Cx + E$$
$$y_2 = -\frac{s_1}{s_2}(Ae^{x/L_0} + Be^{-x/L_0}) + Cx + E \qquad (3.51)$$

In which:

$$L_0 = \sqrt{\frac{1}{s_y(\frac{1}{s_1} + \frac{1}{s_2})}} \qquad (3.52)$$

The equation (3.52) can be solved for a number of boundary conditions. For elaboration refer to: Bakker (1967), (1968). Here only the boundary conditions will be mentioned and the results will be shown.

3.3.4.2 Rip Currents

Rip currents are situated a distance $2L$ apart, by which an amount of sand S^*_{rip} is transported from beach to inshore (fig.3.32a)

Boundary conditions:

$$\left[\frac{\partial y_1}{\partial x}\right]_{x=L} = -\frac{S^*_{rip}}{2s_1}$$

$$\left[\frac{\partial y_1}{\partial x}\right]_{x=-L} = \frac{S^*_{rip}}{2s_1}$$

$$\left[\frac{\partial y_2}{\partial x}\right]_{x=L} = \frac{S^*_{rip}}{2s_2}$$

$$\left[\frac{\partial y_2}{\partial x}\right]_{x=-L} = -\frac{S^*_{rip}}{2s_2}$$

Results:
see fig. 3.28b for $L = L_0$ and fig. 5.28c for $L >> L_0$

$$y_1 = \frac{S^*_{rip}}{2s_1 L_0}\frac{cosh(x/L_0)}{sinh(L/L_0)}$$

$$y_2 = \frac{S^*_{rip}}{2s_2 L_0}\frac{cosh(x/L_0)}{sinh(L/L_0)} \qquad (3.53)$$

The mean distance between the line of the beach and line of inshore will be

$$W + S_{rip}*/2s_y L.$$

Rip currents are thus shown to cause a flattening of the profile. The mean distance between beach and inshore can also be derived directly from the offshore transport equation.
In the stationary case as much sand should be transported shorewards as is transported seawards by the rip current.

$$S^*_{rip} = -\int_{-L}^{+L} S_y dx$$

$$S^*_{rip} = -s_y \int_{-L}^{+L} (y_1 - y_2) dy$$

Define O_1 and O_2 as the hatched areas in figure 3.28b, in other words, $O_1 = 2\,L\,y_{1\,mean}$ and $O_2 = 2\,L\,y_{2\,mean}$, in which $y_{1\,mean}$ and $y_{2\,mean}$ indicate the average value of y_1 and y_2 between $x = -L$ and $x = +L$.

Then validity exists for:

$$S^*_{rip} = -s_y(O_1 + O_2)$$

$$S^*_{rip} = -2Ls_y(-y_{1mean} + y_{2mean}) \qquad (3.54)$$

$$y_{1mean} - y_{2mean} = \frac{S^*_{rip}}{2Ls_y}$$

3.3.4.3 Groins [Bakker (1967, 1968)]

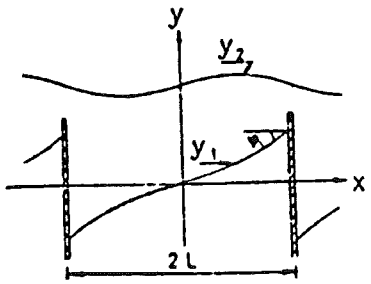

Figure 3.33: Coast with groins (no rip-currents)

Groins are situated at a mutual distance of $2L$ apart. Boundary conditions:

$$\left[\frac{\partial y_1}{\partial x}\right]_{x=L} = \frac{S_{01}^*}{s_1}; \qquad \left[\frac{\partial y_1}{\partial x}\right]_{x=-L} = \frac{S_{01}^*}{s_1}$$

$$[y_2]_{x=\pm L} = 0; \quad antisymmetry: y_2(x) = -y_2(-x)$$

Results (fig. 3.29):

$$y_1 = \frac{S_{01}^*}{s_1} \cdot \frac{x + \frac{s_2}{s_1} L \frac{sinhx/L_0}{sinhL/L_0}}{1 + \frac{s_2}{s_1}\frac{L/L_0}{tanhL/L_0}}$$

$$y_2 = \frac{S_{01}^*}{s_1} \cdot \frac{x - L\frac{sinhx/L_0}{sinhL/L_0}}{1 + \frac{s_2}{s_1}\frac{L/L_0}{tanhL/L_0}} \qquad (3.55)$$

For small distances between the groins ($L < L_0$) the beach turns in the direction of the wave crests while the inshore remains practically straight. From (3.2) this shows that S^*_{01}/s_1 equals the angle of wave incidence on the beach). The difference between the siting of the beach on the left and right hand side of the groin amounts to:

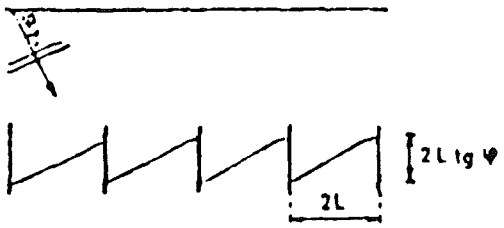

Figure 3.29: Beach and inshore when the groins are near to each other

$$[y_1]_{x=L} - [y_1]_{x=-L} \approx 2L \tan\alpha$$

In which $\tan\alpha = S^*_{01}/s_1$ $(L < L_0)$.

For large distances between the groins this distance tends to:

$$[y_1]_{x=L} - [y_1]_{x=-L} \approx 2\frac{s_1 + s_2}{s_2} \cdot L_0 \tan\alpha$$

If only one groin is constructed then the following coastal shape results: (eroding part)

$$y_1 = -\frac{S_{01}^*}{s_1} \cdot L_0\left(\frac{s_1}{s_2} + e^{-y/L_0}\right)$$

$$y_2 = -\frac{S_{01}^*}{s_2} \cdot L_0\left(1 - e^{-y/L_0}\right) \qquad (3.56)$$

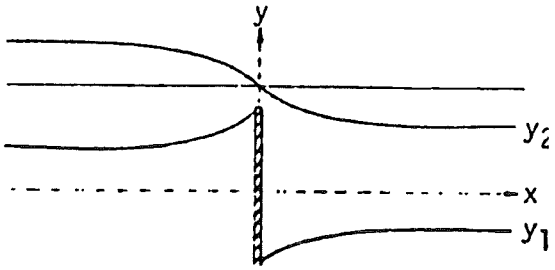

Figure 3.31: Beach and inshore at a coast with one groin

In figure 3.32 the coastal shape is sketched for the case that on the lee-side of every groin a rip current is situated. The coastal shape can be calculated by linear superposition of (3.53) and (3.55).

The coastal shape, as well as the amount of sand that passes through, depend to a great extent on the magnitude of the rip current.

As in this section only stationary cases are considered, the accumulated longshore transport is everywhere equal.
When no groins are constructed this equals:

$$S^*_0 = S^*_{01} + S^*_{02}$$

After construction it is changed into:

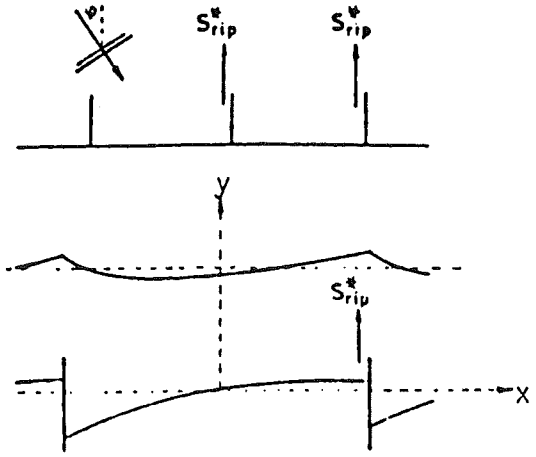

Figure 3.32: Beach and inshore at a coast with groins

$$S^* = S^*_0 - (S^*_{01} - \frac{1}{2}S^*_{rip})\frac{1+\frac{s_1}{s_2}}{\frac{L}{L_0}cot\,anh\frac{L}{L_0}+\frac{s_1}{s_2}} \qquad (3.57a)$$

Therefore as long as S^*_{rip} is smaller than 2 S^*_{01}, the transport will decrease after construction of the groins.
(3.57a) can also be written as:

$$S^* = S^*_{02} + S^*_{01}\frac{\frac{L}{L_0}cot\,anh\frac{L}{L_0}-1}{\frac{L}{L_0}cot\,anh\frac{L}{L_0}+\frac{s_1}{s_2}} + \frac{1}{2}S^*_{rip}\frac{1+\frac{s_1}{s_2}}{\frac{L}{L_0}cot\,anh\frac{L}{L_0}+\frac{s_1}{s_2}} \qquad (3.57b)$$

For small values of L/L_0, the value of *cotanh* (L/L_0) will be practically equal to 1; then the transport shows to be:

$$S^* = S_{02}^* + \tfrac{1}{2} S_{rip}^*$$

For large values of L the transport will approach S^*_o.

3.3.4.4 Transition of two-line theory to one-line theory

In section 3.2.5.2 we made the statement that: "Groins hamper a part of the transport which occurs at a coast without groins. This implies that the longshore transport changes less when the coastal direction changes, i.e. the coastal constant s/h in (3.6) changes. It is assumed that s along the protected coast is a factor p smaller than it is along the unprotected coast". Afterwards it was proved that p influenced the coastal shape considerably. If S^*_{rip} would be taken as zero, then p could be calculated as follows.

Compare fig. 3.33 with fig. 3.33b and fig. 3.33c with fig. 3.33d

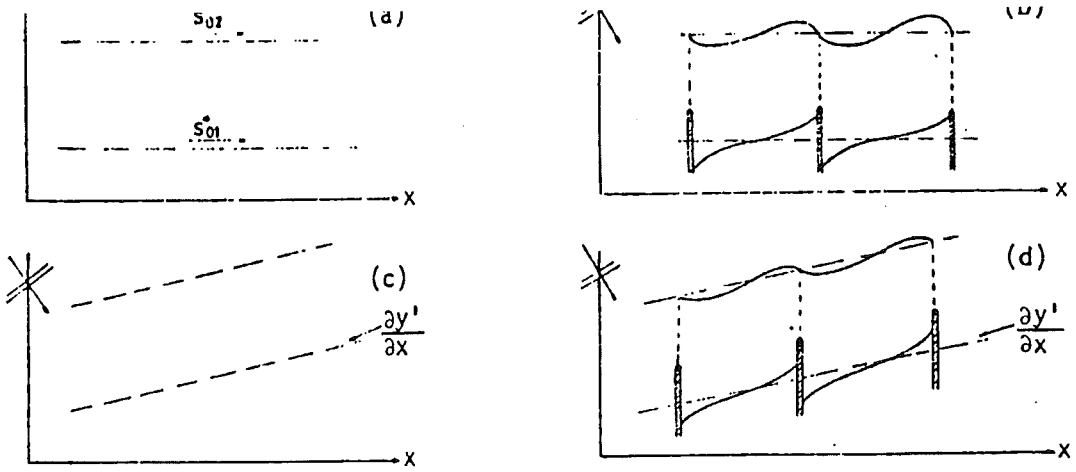

Figure 3.33: Fig.d can be derived from fig. b by turning the x-axis over an angle arctan $\partial y'/\partial x$, taking the transport along beach and inshore in fig. c as "stationary transport" (analogus to S^*_{01} and S^*_{02} in fig. a).

The transport in fig. 3.37a is $s^*_{01} + s^*_{02}$, the transport in fig. 3.33b is given by (3.63) (with $S^*_{rip} = 0$). In fig. 3.33c the transport along the beach is $S^*_{01} - s_1\,\partial y'/\partial x$ to compare with a transport S^*_{01} in fig. 3.33a. Similarly, the transport along the inshore is $S^*_{02} - s_2\,\partial y'/\partial x$ instead of S^*_{02} in fig; 3.33b. Therefore, the transport in fig. 3.33d can be found from (3.57b) (with $S_{rip} = 0$), by substituting "$S^*_{01} - s_1\partial y'/\partial x$" for S^*_{01}.and "$S^*_{02} - s_2\partial y'/\partial x$" for S^*_{02} One turns then virtually the x-axis over $tan^{-1}\,\partial y'/\partial x$.

Thus one finds, that in the case $S^*_{rip} = 0$, one can write the following for (3.57):

$$S^* = (S_0^*)' - s'\frac{\partial y'}{\partial x} \tag{3.58}$$

in which:

$$(S_0^*)' = S_{02}^* + S_{01}^*\frac{\frac{L}{L_0}\cot anh\frac{L}{L_0} - 1}{\frac{L}{L_0}\cot anh\frac{L}{L_0} + \frac{s_1}{s_2}} \tag{3.59}$$

and

$$s' = \frac{s_1 + s_2}{1 + \frac{s_1}{s_2}\cdot\frac{L_0}{L}\tanh\frac{L}{L_0}} \tag{3.60}$$

$s' = ps$ in which $s = s_1 + s_2$

$$p = (1 + \frac{s_1}{s_2}\cdot\frac{L_0}{L}\tanh\frac{L}{L_0})^{-1} \tag{3.61}$$

as $S^*_{rip} = 0$

This is therefore the desired result for p; however, this has been found with the assumption that $s^*_{rip} = 0$. This however is a considerable restriction. If one does take S^*_{rip} into consideration, the result will depend very much on the relationship assumed between S^*_{rip} and S^*_{01}. The most logical assumption seems to be that S^*_{rip} is proportional to S^*_{01}.

Hence:

$$S^*_{rip} = s_{rip}\cdot S^*_{01} \tag{3.62}$$

s_{rip} is therefore a dimensionless coefficient, of which the magnitude can be found by calculating the current velocity in the rip current first (sec. 3.8.2.) and then calculate the transport, for instance with the Byker formula [1]. Then in the way as given before one finds the following:

$$(S_0^*)' = S_{02}^* + S_{01}^* \frac{\frac{L}{L_0} cot\, anh \frac{L}{L_0} - 1 + \frac{1}{2} s_{rip}(1 + \frac{s_1}{s_2})}{\frac{L}{L_0} cot\, anh \frac{L}{L_0} + \frac{s_1}{s_2}} \tag{3.63}$$

and

$$s' = (s_1 + s_2) \frac{1 + \frac{s_{rip}}{2} \cdot \frac{s_1}{s_2} \cdot \frac{L_0}{L} tanh \frac{L}{L_0}}{1 + \frac{s_1}{s_2} \cdot \frac{L_0}{L} tanh \frac{L}{L_0}} \tag{3.64}$$

$$p = \frac{1 + \frac{s_{rip}}{2} \cdot \frac{s_1}{s_2} \cdot \frac{L_0}{L} tanh \frac{L}{L_0}}{1 + \frac{s_1}{s_2} \cdot \frac{L_0}{L} tanh \frac{L}{L_0}} \tag{3.65}$$

If $S^*_{rip} < 2\, S^*_{01}$, p will be smaller than 1 (the coastal processes are slowed down), otherwise p is greater than 1. In the last case the groins have a deleterious rather than constructive effect.

3.3.4.5 Permeable Groins

Assume, that only a part of the sand transport is inhibited by the groins, for instance because these groins are permeable or are low groins. Assume, that an amount S^*_{perm} is allowed to pass through, where S^*_{perm} is proportional to S^*_{01}:

$$S^*_{perm} = s_{perm}\, S^*_{01}$$

where s_{perm} is a permeability coefficient.

In case treated in 3.3.4.3 (no rip-currents) $\partial y_1/\partial x$ in $x = \pm L$ will be a factor $1 - s_{perm}$ smaller. One may consider S^*_{perm} as a part of S'^*_{02}; this means that the formulae keep their validity if read as follows:

$S^*_{02} + S^*_{perm}$	for S^*_{02}
$S^*_{01} - S^*_{perm}$	for S^*_{01}
$s_{np} / (1 - s_{perm})$	for s_{np}

[1] See also Byker's class notes (1976)

3.3.5 Non-stationary processes

3.3.5.1 The basic equations

The equations of motion for the unstationary case are:

$$s_1 \frac{\partial^2 y_1}{\partial x^2} - S_y(y_1 - y_2) = h_1 \frac{\partial y_1}{\partial t}$$
$$s_2 \frac{\partial^2 y_2}{\partial x^2} - S_y(y_2 - y_1) = h_2 \frac{\partial y_2}{\partial t} \qquad (3.66)$$

Adding of both equations gives:

$$\frac{\partial^2 (s_1 y_1 + s_2 y_2)}{\partial x^2} = \frac{\partial (h_1 y_1 + h_2 y_2)}{\partial t} \qquad (3.67)$$

which can be writen as:

$$\frac{s}{h}\frac{\partial^2 y}{\partial x^2} + \frac{h_1 h_2}{h^2}\left(\frac{s_1}{h_1} - \frac{s_2}{h_2}\right)\frac{\partial^2 (y_1 - y_2)}{\partial x^2} = \frac{\partial y}{\partial t} \qquad (3.68)$$

in which:

$$\frac{s}{h} = \frac{s_1 + s_2}{h_1 + h_2} \qquad (3.69)$$

$$y = \frac{1}{h}(h_1 y_1 + h_2 y_2) \qquad (3.70a)$$

$$h = h_1 + h_2 \qquad (3.71)$$

$$y_- = y_1 - y_2 \qquad (3.70b)$$

y represents the "average coastline", i.e. the weight average between the line of the beach and the line of the inshore. From (3.68) it shows, that the equation (3.6) of Pelnard-Considère is valid as well in the two line theory, if $s_1/h_1 = s_2/h_2$. The analytic elaboration of the equations (3.68) has only been carried out for the case, that $s_1/h_1 = s_2/h_2$. In that case one can write (3.68) as:

$$\frac{s}{h}\frac{\partial^2 y}{\partial x^2} = \frac{\partial y}{\partial t} \qquad (3.72)$$

and:

$$\frac{s}{h}\frac{\partial^2 y_-}{\partial x^2} - \frac{s_y h}{h_1 h_2} y_- = \frac{\partial y_-}{\partial t} \qquad (3.73)$$

The two-line problem has now been transferred -with the aid of (3.72)- to a one-line problem, where (3.73) gives an equation for the cross-shore transport.
Equation (3.73) is of the same kind as (3.72);
this shows to be the case by the substitution:

$$y_e = y_- \cdot e^{-t/T_0}; i.e.: y_- = y_e \cdot e^{-t/T_0} \qquad (3.74)$$

with:
$$T_0 = \frac{h_1 h_2}{s_y h} \qquad (3.75)$$

In this case the equation for y_e gets the same shape as (3.72).

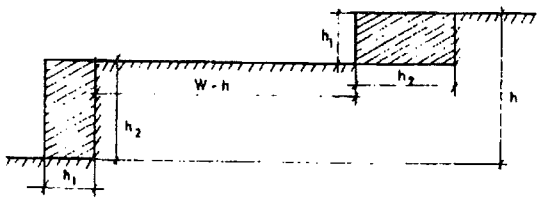

Figure 3.34: Meaning of T_0

T_0 is the time, necessary for cross-shore transport. S_y for transferring an amount of sand h_1h_2 from the beach to the inshore, when the distance between beach and inshore is kept continuously W-h (Fig 3.34). The equations (3.72) and (3.73) can only be solved simply in a small number of cases, as the boundary conditions give difficulties. Finally one then finds y_1 and y_2 from y and y_-:

$$y_1 = y + \frac{h_2}{h} y_- \qquad y_2 = y - \frac{h_1}{h} y_- \tag{3.76}$$

3.3.5.2 One single rip-current

A relatively simple problem is the morphodynamics of the development of a rip-current on a beach and inshore, which are originally straight. Let the development start at $t = 0$, at the site $x = 0$.
The mean coastline y keeps at its position: $y = 0$. However y_- changes; with the aid of Laplace-transform [18] can be found:

$$y_- = \frac{-S^*_{rip}}{4 s_y L_0}\left[e^{x/L_0} erfc\left(\frac{x/L_0}{2\sqrt{t/T_0}} + \sqrt{\frac{t}{T_0}}\right) + e^{-x/L_0} erfc\left(\frac{x/L_0}{2\sqrt{t/T_0}} - \sqrt{\frac{t}{T_0}}\right)\right] (x > 0) \tag{3.77}$$

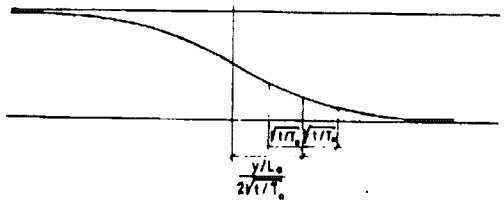

Figure 3.35:

From (3.76) one finds:

$$y_1 = h_2 y_- / h \quad and \quad y_2 = -h_1 y_- / h$$

For large t the solution tends to the stationary solution (fig. 3.36):

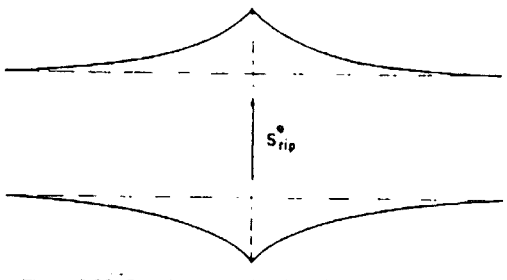

Figure 3.36: One rip-current (stationar)

$$y_1 = -\frac{S_{rip}}{2 s_1} L_0 e^{\mp x/L_0} \qquad y_2 = \frac{S_{rip}}{2 s_2} L_0 e^{\mp x/L_0} \tag{3.78}$$

The minus-sign holds on the righthand side of the rip-current, the plus-sign on the lefthand side.

Solutions like (3.77) can be used in all cases, where as well on the beach as on the inshore the transport in the point $x = 0$ is known and is constant in the time.

Case, In the above mentiones the coastline y (in the above mentioned) is kept at its place. By superposition of the "delta-solution" according to Pelnard-Considère one may find solutions for arbitrarily (but stationary) $\partial y1/\partial x$ and $\partial y_2/\partial x$ at $x = 0$ [18].

3.3.5.3 One single groin

Only for the case $s_1 = s_2$ and $h_1 = h_2$ it is possible to find an analytical solution for the sedimentation near a groin (in the case of oblique waves); the stationary final situation has already been given (eq (3.56)).

The boundary conditions are:

$$\frac{\partial y_1}{\partial x} = \frac{S_{01}^*}{s_1} \quad \text{at x=0} \qquad (3.79)$$

$$y_2 = 0 \quad ^{1)}$$

The problem has been solved using Laplace-transforms. The solution is given in [19] and [21]. The result is shown in fig. 3.41. The solution for the coastline y consists of a series of terms of the kind $t^{n-1/2}\, Y_{2n-1}$ where the Y-functions are ch 3.2.6.1..
The solution for y_- (i.e for the slope of the coast) consist of a series of terms $e^{-t\,To} \cdot t^{\,n-t} \cdot Y_{2n-1}$ and of the "rip-current"-solution (3.77):

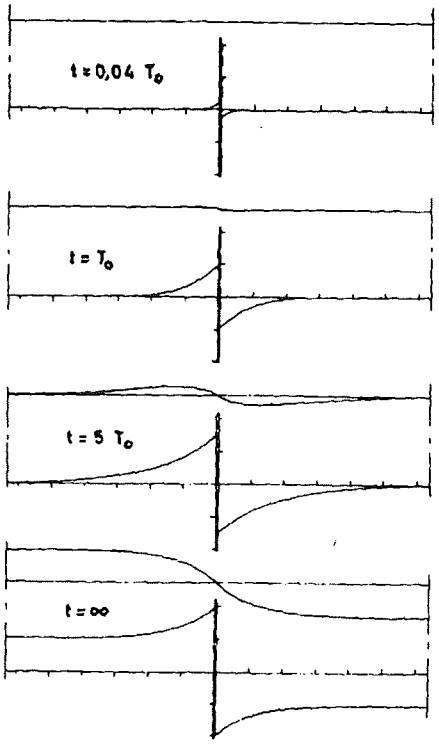

Figure 3.37a:

$$\frac{y_{1,2}}{L_0 \tan\alpha_0} = \frac{1}{2\sqrt{\pi t / T_0}}\left[\sum_{n=1}^{\infty}(-1)^n \frac{(t/T_0)^n}{(h-\frac{1}{2})n!} Y_{2n-1}\left(\frac{x/L_0}{2\sqrt{t/T_0}}\right)\right] \pm \frac{e^{-t/T_0}}{2\sqrt{\pi t/T_0}}\left[\sum_{n=1}^{\infty}\left(\frac{(t/T_0)^n}{n!} Y_{2n-1}\left(\frac{x/L_0}{2\sqrt{t/T_0}}\right)\right.\right.$$

$$\mp \frac{e^{-x\ L_0}}{2} erfc\left(\frac{x/L_0}{2\sqrt{t/T_0}} - \sqrt{\frac{t}{T_0}}\right) \pm \frac{e^{x\ L_0}}{2} erfc\left(\frac{x/L_0}{2\sqrt{t/T_0}} + \sqrt{\frac{t}{T_0}}\right) \qquad (3.80)$$

For large t the solution approaches the stationary solution (3.56), given in ch. 3.3.4.3.
The erosion, directly behind the groin can be computed for all cases in which $s_1/h_1 = s_2/h_2$ (The reason is, that although the Laplace-transformed $\bar{y}$ and $\bar{y}_-$ can be found for all cases, the inversion to y and y_- has up to now only been performed after the substitution of either $h_1 = h_2$ either $x = 0$).

The total erosion is found from the solution of the stationary problem (3.56). Substitution of $x = 0$ in eq (3.56) gives:

$$[y_1]_{x=0} = -L_0 \tan\alpha_0 \frac{s_1 + s_2}{s_2} \qquad (3.81)$$

From the non stationary solution can be derived , after which time ($1-\delta$) times the final erosion is observed ($\delta << 1$).
call this time t_δ; then for small δ the approximation is found:

$$t_\delta = \frac{1}{\pi\delta^2} \cdot \frac{s_1^2}{s_2 s^2} \cdot \frac{h}{s_y} \qquad (3.82)$$

[1] Symmetry!

It thus shows, that the time necessary to reach 0,99 times the final erosion is 100 times as long as the time to find 0,9 times the final value. The initial erosion is equal to the one of the one-line solution.
On the eroding side initially the coastline will develop itself in the way as given by (3.22) (one of the Pelnard-Considère solutions):

$$y_1 = -\tan\alpha_0 \sqrt{t}\ erfc(x \cdot \sqrt{h/4st}) \qquad (3.83)$$

with $\tan\alpha_0 = S_{01}/s_1$

Formally, in (3.83) "h/s" should be replaces by "h_1/s_1", but because of the condition $s/h = s_1/h_1 = s_2/h_2$ this makes no difference.

A special case of periodic solutions is the simulations of the influence of variable wave conditions on the boundary

When the wave direction changes periodically for instance according;

$$\varphi = \hat{\varphi} \sin\omega_\varphi t \qquad (3.84)$$

This generates a sandwave near a groyne.

$$y = \frac{\hat{\varphi}\lambda_\kappa}{2\pi\sqrt{2}} \cdot e^{-k_\varphi x} \cos(\omega_\varphi t - k_\varphi x) \qquad (3.85)$$

in which:

$$\lambda_\kappa = \frac{2\pi}{k_\varphi} = 2\sqrt{\pi \frac{s}{h} T_\varphi} \qquad (3.86)$$

T_φ being the period of the fluctuations of φ and λ_φ being the length of the sandwave.

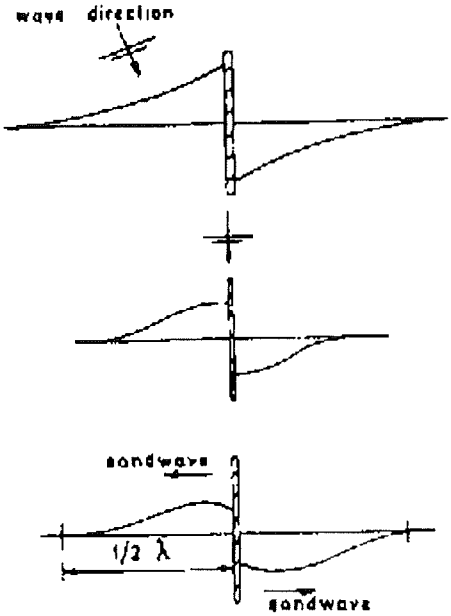

Figure 3.38: Generation of sandwaves by variable wave direction

The second influence of thle groyne is the wave-shelter. We shall assume first, that the sheltered area is large with respect to ½ $\lambda\ \varphi$. Q_0 and q_1 become functions of x, called Q_{01}* and q_1*. Consider fig. 3.39. The influence of diffraction will be neglected with respect to the influence of changing wave conditions.

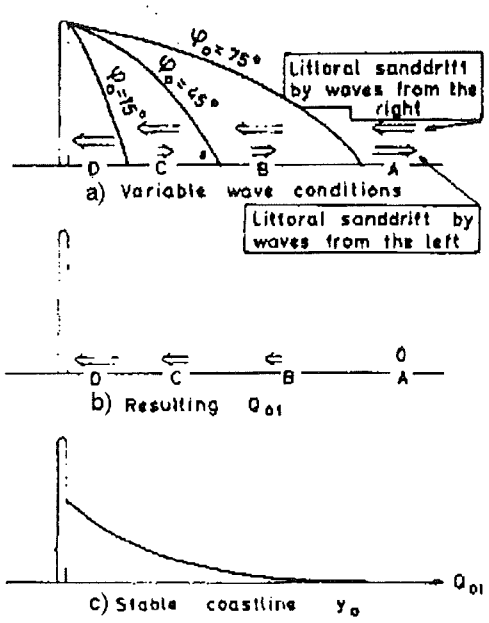

Figure 10.39:

The computation of Q_0 and q_1 in area A can be performed according to (29), (30) and fig. 3-14. But applying (3-44) to area B, all wave classes with $\varphi_0 \geq 75°$ must be excluded in the summation, in area C all wave classes with $\varphi_0 \geq 75°$, and so on.
When,for instance, the resulting transport in area A would be zero for a coastline parallel to the x-axis (fig. 10.39), the transport Q_{01}* ($\partial y_1/\partial x = 0$) (started because it changes in x-direction) will be larger and larger (in negative direction) in the areas B, C and D_1,and also q_1* will change.
Now we have returned to the normal computer program, only with other values for y_0 and y' then in the diffraction cases.
The stable coastline y_0 can be found from continuity: for y_0 the transport is everywhere the same:

$$\left[Q_{01}\right]_{x=\infty} = Q_1 \rightarrow \left[Q_{01}\right]_{x=\infty} = Q_{01}^* - q_1 \cdot \frac{dy_0}{dx} \rightarrow \frac{dy_0}{dx} = \frac{Q_{01}^* - \left[Q_{01}\right]_{x=\infty}}{q_1^*} \qquad (3.87)$$

From (3.87) the stable coastline y_0 can be found, which gives the initial value of the unstationary part y_1'.

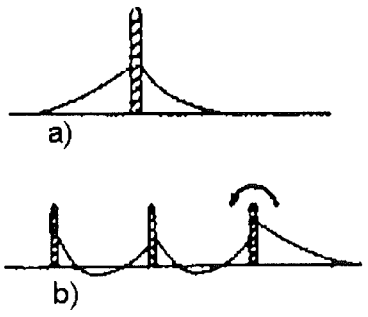

Figure 3.40:

In case of changing wave conditions, and no resultant drift, the final coastal shape near one single groyne will become just the stable shape y_0, because then everywhere the resultant drift is zero. This will give accretion on both sides of the groyne, which will be withdrawn from a very long stretch of coast (fig. 3.40a). in case of a row of groynes, the sand for the accretion near the groyne is withdrawn from the area in the sidst between the groynes, and only near the boundary of the groyne system some real accretion can be expected (fig. 3.40b). However, after some time this sand will move to the areas between the groynes, and so this shelter effect may give lose accretion (in case of no resultant drift), starting from the boundaries of the groyne system.

In case $\frac{1}{2}\lambda\varphi$ is not small with respect to the sheltered area, the best way of computation is a kind of 'hindcasting", using the one-line or two-line computer program described before, and changing the wave conditions during the program. This has been done at the Coastal Research Department of Rijkswaters taat.

3.4 More line theories

3.4.1 Equations for a more-line model

A logical extension moving from one-line to two-line modeling is more line modeling. The end of this chapter (3.4.3) will give some general considerations. Three-line modeling will be treated first. In the three-line model (used here) the coastal zone is schematized in zones (fig. 3.41), which will be called: "beach", "inshore" and "deeper part".

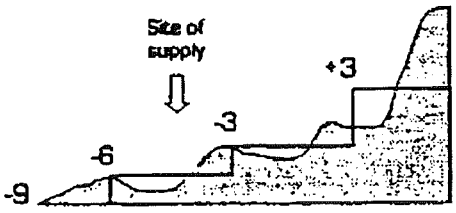

Figure 3.41: Schematization 3-line

In each zone it is assumed that all contour lines remain parallel and that the profile in this zone only moves horizontally. It is sufficient to compute only an average line in each zone, because it characterizes this zone. There is assumed to be a horizontal separation plane between the zones. The sediment transport between the lines is assumed to be proportional to the difference between the equilibrium distance and the actual distance between the characterizing lines.
In the present application an initial equilibrium position (before any supply takes place) is assumed, where the three lines are straight and parallel (fig. 3.42) Distances $y_{1.2.3}$, are the deviations of the lines of the beach, inshore and deeper part, compared with this initial position,. The y-value is computed by dividing the surplus volume in a zone (with respect to the initial Position) by its height. In case $y_1 = y_2 = y_3$, the profile again is an equilibrium slope. If longshore transport could be neglected (see 3.4.3) the coast would tend to this equilibrium, 'if for instance originally' sand on the inshore would have been supplied (fig.3.42).
The process, sketched above) results in cross-shore diffusion of sand. Adding longshore

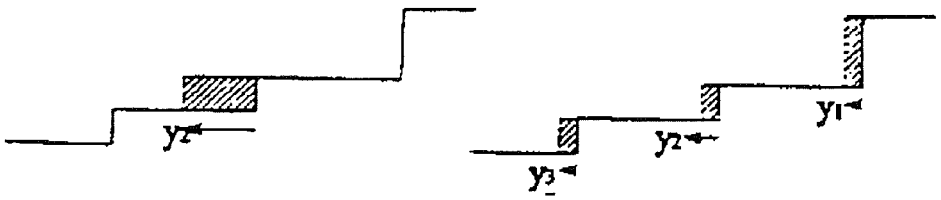

Figure 3.42: definition y_1, y_2, y_3

diffusion to the cross-shore diffusion, according to the approach of Pelnard-Considere (1954) and Bakker (1968a), the following dynamic equations can be derived:

$$\frac{dy_1}{dt} = \frac{s_1}{h_1} \cdot \frac{\partial^2 y_1}{\partial x_1^2} - \frac{s_{y1}}{h_1} \cdot (y_1 - y_2)$$

$$\frac{dy_2}{dt} = \frac{s_2}{h_2} \cdot \frac{\partial^2 y_2}{\partial x_1^2} - \frac{s_{y1}}{h_2} \cdot (y_1 - y_2) - \frac{s_{y2}}{h_2} \cdot (y_2 - y_3) \qquad (3.88)$$

$$\frac{dy_3}{dt} = \frac{s_3}{h_3} \cdot \frac{\partial^2 y_3}{\partial x_1^2} - \frac{s_{y2}}{h_3} \cdot (y_2 - y_3)$$

On the lefthand side is the accretion of line of beach, inshore and deeper part respectively. On the righthand side the gradient of the longshore transport is determined by the constants s_1, s_2 and s_3 respectively; the cross-shore transport ("beach to inshore" and "inshore to deeper part") by s_{y1} and s_{y2} respectively. $h_{1.2.3.}$ denotes the depth allotted to the three zones. Fig. 3.43 shows the diffusion of an (originally rectangular) supply shape in longshore and cross-shore direction in the course of time from Kersting (1995).

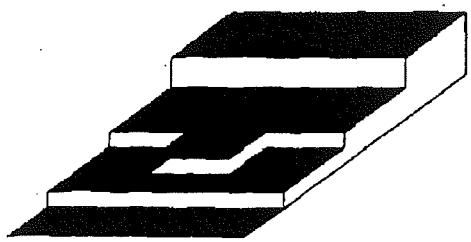

The situation at t=0.

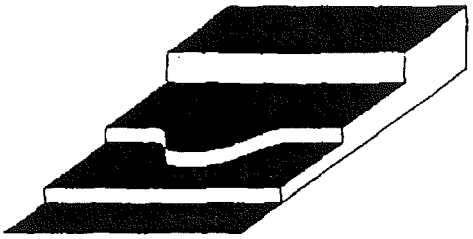

The situation after 1 year

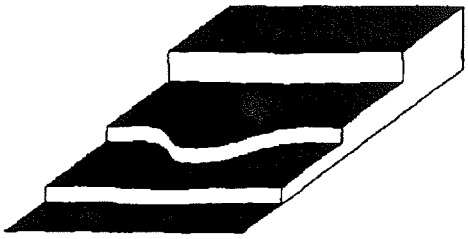

The situation after 2 years

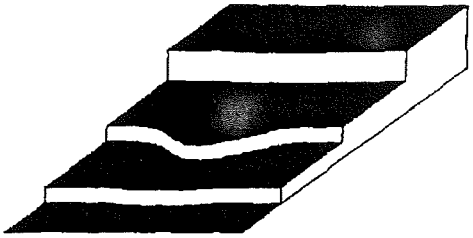

The situation after 3 years

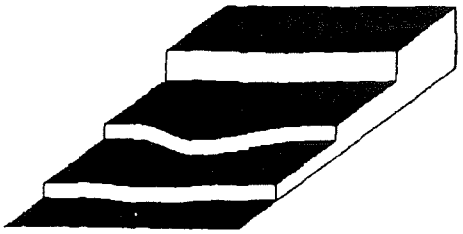

The situation after 4 years

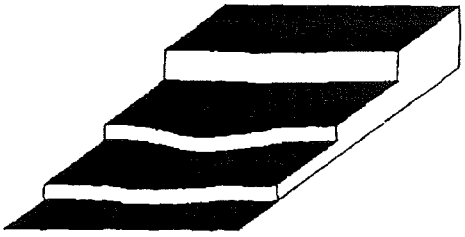

The situation after 6 years

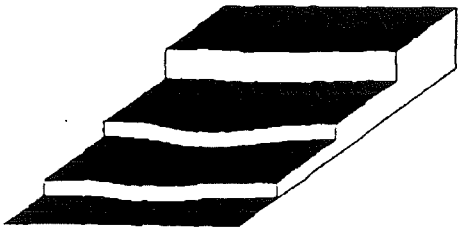

The situation after 8 years

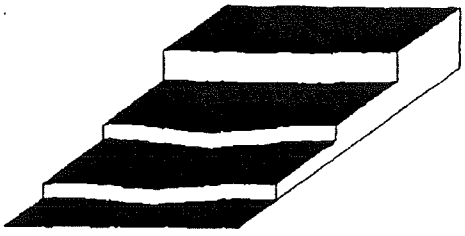

The situation after 10 years

Figure 3.43: Diffusion of supply

Fig 3.44 (from Groenenwoud et al. 1996) shows a plan view of such coast. Cases shown here are calculated numerically. Refer furthermore to sect 5.6.2.

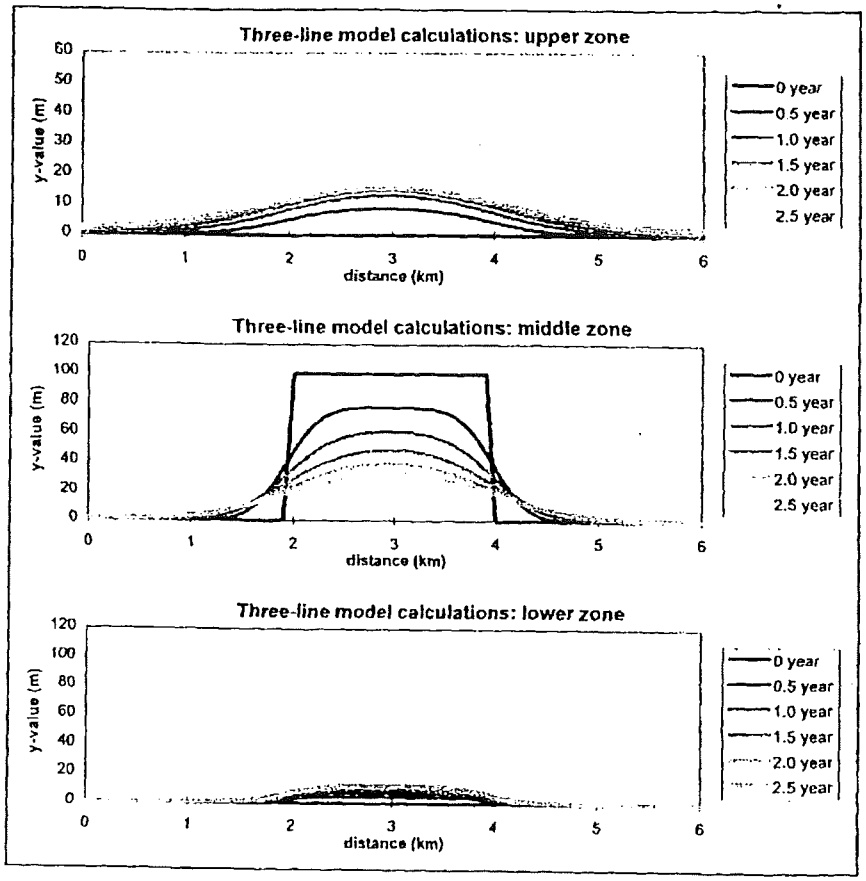

Figure 3.44: Development with time of a shoreface nourishment in middle layer

3.4.2. Smit's solution for the three-line model

The dynamic equations for the cross-shore transport S_{yi} between the layers (with i=1, 2) read:

$$S_{yi} = s_{yi}(y_i - y_{i+1}) \tag{3.89}$$

Continuity ($\Sigma(h_i, y_i)$ with i = 1..3 shows, that y_2 is implicitly determined by y_1 and y_3. Continuity also yields:

$$S_{y1} = -h_1 \frac{dy_1}{dt} \qquad S_{y2} = +h_3 \frac{dy_3}{dt} \tag{3.90 a,b}$$

Combination of (3.89) and (3.90a,b) leads to the vectorial equation:

$$\frac{d\vec{y}}{dt} = \overline{\overline{A}} \cdot \vec{y} \tag{3.91}$$

Where $\vec{y}$ is $y_{1,3}$ and the matrix $\overline{\overline{A}}$ is (a_{11}..a_{22}), where:

$$a_{11} = -\frac{s_{y1} \cdot (h_1 + h_2)}{h_1 h_2} \qquad a_{12} = -\frac{s_{y1} \cdot h_3}{h_1 h_2}$$
$$a_{21} = -\frac{s_{y2} \cdot h_1}{h_2 h_3} \qquad a_{22} = -\frac{s_{y2} \cdot (h_2 + h_3)}{h_2 h_3} \tag{3.92}$$

Displaying the solution gives a reason to define 5 timescales. Two of those are the timescales T_{01} and T_{02} of the two-line systems: "Beach and inshore" and "inshore + deeper part" (Bakker, 1968) equal to $-1/a_{11}$ and $-1/a_{22}$ respectively. The third one, T_* is related to the other diagonal of the matrix $\overline{\overline{A}}$:

$$T_*^2 = \frac{1}{a_{12} \cdot a_{21}} = \frac{h_2^2}{s_{y1} \cdot s_{y2}} \tag{3.93}$$

The last ones $1/\lambda_{1,2}$, as occur in the solution of (3.91):

$$\vec{y} = \vec{K} e^{\lambda_1 t} + \vec{M} e^{\lambda_2 t} \tag{3.94}$$

where $\vec{K}$ = (K_1, K_2) and $\vec{M}$ = (M_1, M_2), in which:

$$K_1 = \frac{a_{21}}{\lambda_2 - \lambda_1} y_{3b} + \frac{\lambda_2 + \frac{1}{T_{01}}}{\lambda_2 - \lambda_1} y_{1b} \qquad M_1 = +\frac{a_{21}}{\lambda_2 - \lambda_1} y_{3b} - \frac{\lambda_1 + \frac{1}{T_{01}}}{\lambda_2 - \lambda_1} y_{1b} \tag{3.95a,b}$$

$$K_2 = \frac{1}{a_{21}} \cdot \left(\lambda_1 + \frac{1}{T_{01}}\right) K_1 \qquad M_2 = \frac{1}{a_{12}} \cdot \left(\lambda_2 + \frac{1}{T_{01}}\right) M_1 \tag{3.95c,d}$$

where y_{1b} and y_{3b} are the initial values of y_1 and y_3.

3.4.3. More than 3 lines

3.5 Literature

1. R. Pelnard-Considère;
   Essai de théorie à l'evolution des formes de rivages en plages de sables et de galets.
   Quatrième Journées de l'Hydraulique, Paris 13-15 Juin 1954 Les Energies de la Mer,
   Question 3.

2. J. Larras;
   Plagea et cotes de sable.
   Collection du Laboratoire National d'Hydraulic, 1957.

3. W. Grijm;
   Theoretical forms of shorelines.
   Proc. of the 7th Cont. on Coastal Engineering, The Hague 1960.

4. W. Grijm.;
   Theoretical forms of shorelines;
   Proc. of the 9th Conf. on Coastal Engineering, Lisbon 1964.

5. W.T. Bakker en T. Edelman;
   The coastline of riverdeltas.
   Proc. of the 9th Conf. on Coastal Engineering, Lisbon 1964

6. T. Edelman;
   Vormverandering aan zandige kusten - deel I:
   Algemene inleiding en afleiding van de kustvergelijking.
   Afdeling Kustonderzoek, Studierapport W.W.K. 64-1.

7. C.R. Wylie Jr;
   Advanced engineering mathematics.
   McGraw-Hill Book Company, 1960

8. M. Abramowitz en I.A. Stegun;
   Handbook of mathematical Functions.
   Department of Commerce; National Bureau of standards, 1965.

9. T. Edelman;
   De basisoplossing voor een lineaire partiële djfferentiaalrergelijking. R.W.S.; Afdeling
   Kustonderzoek, Studierapport W.W.K. 71-17.

10. G. de Josselin de Jong;
    Consolidatie in drie dimensies, II.
    mededelingen, deel VIII no. 2, oktober 1963.

11. A. Langejan;
    Oplossing van consolidatieproblemen met behulp van de grafische methode van
    Schmidt.
    mededelingen, deel VII,no. 2, november 1962.

12. H. Bateman;
    Tables or Integral Transforms - Volume I.
    Cal. Inst. of Technology, Baternan Manuscript Project.
    McGraw-Hill, 1954.

13. R.I. Churchill;
    Operational Mathematics.
    McGraw-hill, 1958.

14. L. Binder;
Uber äussere Wärmeleistung und Erwarmung electrischen Maschinen.
Dissertatie Techn. Hochschule, München, 1910.

15. E. Schmidt;
Uber die Anwendung der Differenzenrechnung auf technische Anheiz- und Abkülungsprobleme.
Beitrage zur technischen Mechanik und technischen Physik, (August Töpp Festschrift) Berlin 1924, pag. 179-189.

16. W.T. Bakker;
A mathematical theory about sandwaves and its application on the Dutch Wadden isle of Vlieland.
Afdeling kustonderzoek, Memo 68-2.

17. L. van Bendegom;
Beschouwingen over de grondslagen van de kustverdediging. R.W S.; Directie Benedenrivieren - Noordelijke Afdeling Studiedienst, 1949.

18. W.T. Bakker;
One aspect of the dynamic of a coast, partly protected by a row of groynes.
Afdeling Kustonderzoek, Studierapport W.W.K. 67-5.

19. W.T. Bakker;
The dynamics of a coast with a groyne system.
Proc. of the 11th Conf. on Coastal Engineering, London 1968.

20. W.T. Bakker,
De invloed van rip-currents op een kustvorm.
Afdeling Kustonderzoek, Meno 68-3.

21. W.T. Bakker;
The influence of offshore transport on the dynamics of a coast with a harbour mole.
Afdeling Kustonderzoek, Studierapport W.W.K. 69-2.

22. W.T. Bakker,
The influence of diffraction near a harbour mole on the coastal shape.
Afdeling Kustonderzoek, Studierapport W.W.K. 70-2.

23. W.T. Bakker; E.H.J. Klein Breteler en A. Roos;
The dynamics of a coast with a groyne system.
Afdeling Kustonderzoek, Studierapport W.W.K. 70-13.

24. W.T. Bakker.
Berekening van het langstransport door golven met de methode van evenwijdige dieptelijnen.
Afdeling Kustonderzoek, Studierapport W.W.K. 69-7.

25. J. McCowan.
On the Highest wave of Permanent Type.
Phil. Mag. 55, Vol. 38, No. 233, Oct. 1894, par. 351-358.

26. E W. Bijker en J.N. Svasek;
Two methods for determination of morphologicti changes by coastal structures.
XXIInd Int. Nav. Congress, Sect. II, Subj. 4, pag. 18-202.

27. W.T. Bakker, H.G.H. ten Hoogen en G.H. Griev;
Berekening van het zandtransport volgens de methode Svasek bij een strand en een vooroever die een hoek met elkaar maken.
Afdeling Kustonderzoek, Studierapport W.W.K. 71-18.

28. J.A. Zaat;
Numerieke Analyse.
Deift; 1969.

29. D.L. Inmar, P.O. Komar and A.J. Bowen;
Longshore transport of sand.
Proc. of the 11the Conf. on Coastal Engineering, London 1968,

30. W.T. Bakker;
Littoral drift in the surf zone.
Afdeling Kustonderzoek, Studierapport W.W.K. 70-16.

31. E.H.J. Klein Breteler;
Getijberekening voor de kustzone tussen hoek van Holland en IJmuiden met behulp van het getijmodel van Booy.
R.W.S Kustonderzoek, studie rapport W.W.K. 70-10.

32. W.T. Bakker en H.J. Opdam;
Over de invloed van golven en getij op bet zandtransport in de brandingszone.
Afdeling Kustonderzoek, Studierapport W.W.K. 70-9.

33. H.J. Opdam;
Een mathematisch model van de kustzone, betreffende de invloed van golven, getij, wind en corioliskracht op de stroming. langs de kust.
Afdeling Kustonderzoek, Studierapport W.W.K. 70-11.

34. H.J. Opdam;
Experimentele fluorescëine metingen betreffende de invloed van golven en getij op de stroming langs de kust.
R W S.; Afdeling Kustonderzoek, Studierapport W.W.K. 71-5.

35. B. Voogt en A.J. Romein;
Afstudeerverslag, Afd. Weg- en Waterbouwkunde. T.H.- Deift; 1971.

36. W.T. Bakker;
37. The influence of longshore variation of the wave height on the littoral current.
Afdeling Kustonderzoek, Studierapport W.W.K. 71-19.

38. J.A. Battjes;
Radiation stress in short crested waves.
Journal of marine research, 30 (1), 1972.

39. W.T. Bakker
the influence of longshore variation of the wave height on the littoral drift.
Paper on the 13th Conf. On Coastal engieering, Vancouver 1972.

40. A.J. Bowen, B.L. Inman and V.P.Simmons;
Rip-currents.
Journal of geophysical research, 74 (23) 1968; p. 5469 - 5490.

41. A.J. Bowen
The generation of longshore currents on a plane beach.
Journal of Marine research, 72 (2), 1969.

42. G. van Bocheve en H.G.H. ten Hoopen;
Afstudeerverslag, afd weg- en waterbouwkunde.
-delft, 1971;

4. Determination of coastal constants

4.1 General considerations

4.1.1 Introduction

Apart from the mathematical formulation, the results of mathematical line modeling depend upon the magnitude of the "coastal constants", which serve as calibration constants in those models. Two ways to determine those constants pass the review. The first one is investigation of the former coastal behaviour. Here, Kalman filtering offers sophisticated means. The second one is calculation of the constants from the wave climate. For formulation of the constants, determined by longshore transport, use is made of the CERC-formula and (with respect to the two-line theory) of the Svasek variation of this approach. With respect to the constant determining the cross-shore transport (i.e. concerning the time scale of restoration to the equilibrium profile of a non-equilibrium profile) an effort is made to link with the Stive theory. Dimensionless equilibrium profiles of the offshore zone result in this way, however only of the part seaward of the outer breaker bar. On the time scale, according to which a non-equilibrium profile restores itself to an equilibrium profile, only global information is obtained, being restricted to the seaward part,

Mathematical line-models appear to be a useful tool in coastal engineering. Most significant categories are one-line models, which deal with the dynamics of "the" coastline and two-line models, in which beach and inshore each are represented by one line.
Constants, which appear in these models deal with the relation between the curvature of the line(s) and the accretion; furthermore, in the two-line theory, an additional constant determines the relation between the steepness of the profile (i.e., the distance between the lines) and the cross-shore transport. (ch.4.1.2).
There are two essentially different ways to find these constants. In ch.4.3, constants are found from coastal history; the coastal model is calibrated in this way.
A scientifically more satisfactory approach, and sometimes the only way, is to find the coastal constants from the wave climate and the grain characteristics (ch.4.2).
The second approach does not lead always to better results, as much depends on the accuracy of the used sand transport formula and the schematization. Anyway it gives a relation between more sophisticated theories and the simple line theories
In this paper, both ways for finding the coastal constants are enlightened. It will be assumed, that the reader is familiar with the use of these models as such; with respect to this is referred to, for instance
[1] to [6], [9], [16],[17],[26].

4.1.2 Considerations on coastal equations and coastal constants

The coastal equations for the two-line theory are [1],[2]:

$$h_1 \frac{\delta y_1}{\delta t} = s_1 \frac{\delta^2 y_1}{\delta x^2} - s_3 (y_1 - (y_2 - W))$$
$$h_2 \frac{\delta y_2}{\delta t} = s_2 \frac{\delta^2 y_2}{\delta x^2} - s_3 (y_1 - (y_2 - W)) \qquad (4.1a,b)$$

Generally, the indices "1" and "2" refer to beach and inshore respectively. The x-axis is in the main coastal direction and $y_{1,2}$ denotes the y-coordinate of beach and inshore; t is the time; h_1 and h_2 are the thickness of the sand layers, representing beach and inshore.
For the definition of beach and inshore and for the derivation of the equation (4.1a,b) is referred to [1] or [2].
The equations indicate, that accretion at beach and inshore are proportional to their curvature, with proportionality constant $s_{1,2}$ This apart from effects of cross-shore transport from beach to inshore, contained in the last term on the righthand side of (4.1a,b). This

transport S_y is linear with the distance between beach and inshore (proportionality constant s_y,) and constant zero when this distance is the equilibrium distance W.
The equations (4.1a,b) result from continuity and the dynamic equations for the transport S_1 along the beach:

$$S_1 = S_{01} - s_1 \frac{\partial y_1}{\partial x} \qquad (4.2)$$

and a similar equation for the transport S_2 along the inshore; in (4.2) S_{01} is the transport, when the beach is parallel to the x-axis.

The one- line theory (see for instance the initiating paper [26] and further [22]) only deals with a coastline y, governed by eq. (4.1) without indices and without the last term; as proportionality constant one just finds s.
The one-line theory starts from a similar equation as (4.2) for the transport S along the coast, which is found by omitting all indices "1" in (4.2).

In order to compare nature with theory (as well for hindcasting and calibration as for forecasting), it should be known, which constants should be substituted in the coastal equations and which boundary conditions should be applied.

Consider the two-line theory; most of the following can be translated easily to the one-line theory as well, which is left to the reader. The depths h_1 and h should be estimated from prototype data; on this subject shall be referred to.
Constants to be found are: the proportionality constants $s_{1,2},.s_y$ and the equilibrium distance W Generally (with proper boundary conditions) knowledge concerning S_{01} and S_{02} is not necessary for solving eqn. (4.1a,b); inversely, one may not expect, in general, to get information about those constants from the coastal behaviour.

Furthermore, for solving the equations, the boundary conditions should be known.
For hindcasting, one can start from known behaviour at the boundaries [3); generally however, after hindcasting and calibration one also wants to forecast.
The accuracy, with which the future boundary conditions can be determined can be decisive for the accuracy of the prediction (25). One should estimate those conditions with an eye on the physics of the process [2b], [5]. Possible boundary conditions to apply are:

- no changes at infinity ($y= 0$ for $x= inf$);
- extrapolation of existing trends at a certain site $x= x_1$
- all sand transport hampered at $x= x_1$.

Mathematically, the first two cases do not give difficulties, but in the last case (using the one-line theory as example) one should know as well s as the transport S_0 when the coast is in x-direction, in order to find S_0/s, being (according to (4.2)) the coastal direction at $x= x_1$.
While often the coastal constants are uniform along the coast, in the case of harbour moles the change of wave height and direction around the harbour results in variation of the coastal constants along the coast.
The line-theories in coastal dynamics are based upon a philosophy of wave induced transport in the surf zone. However, tidal-induced transport can be taken into account to a certain extent by introducing source- or sink-terms "p" in (4.1). Also p is a coastal constant, non-uniform in longshore direction. Introduction of those sources- and sinkterms will be subject of a next paper [25].

transport S_y is linear with the distance between beach and inshore (proportionality constant s_y,) and constant zero when this distance is the equilibrium distance W.
The equations (4.1a,b) result from continuity and the dynamic equations for the transport S_1 along the beach:

$$S_1 = S_{01} - s_1 \frac{\partial y_1}{\partial x} \tag{4.2}$$

and a similar equation for the transport S_2 along the inshore; in (4.2) S_{01} is the transport, when the beach is parallel to the x-axis.

The one- line theory (see for instance the initiating paper [26] and further [22]) only deals wi a coastline y, governed by eq. (4.1) without indices and without the last term; as proportionality constant one just finds s.
The one-line theory starts from a similar equation as (4.2) for the transport S along the coas which is found by omitting all indices "1" in (4.2).

In order to compare nature with theory (as well for hindcasting and calibration as for forecasting), it should be known, which constants should be substituted in the coastal equations and which boundary conditions should be applied.

Consider the two-line theory; most of the following can be translated easily to the one-line theory as well, which is left to the reader. The depths h_1 and h should be estimated from prototype data; on this subject shall be referred to.
Constants to be found are: the proportionality constants $s_{1,2_1}.s_y$ and the equilibrium distance W Generally (with proper boundary conditions) knowledge concerning S_{01} and S_{02} is not necessary for solving eqn. (4.1a,b); inversely, one may not expect, in general, to get information about those constants from the coastal behaviour.

Furthermore, for solving the equations, the boundary conditions should be known.
For hindcasting, one can start from known behaviour at the boundaries [3]; generally however, after hindcasting and calibration one also wants to forecast.
The accuracy, with which the future boundary conditions can be determined can be decisiv for the accuracy of the prediction (25). One should estimate those conditions with an eye or the physics of the process [2b], [5]. Possible boundary conditions to apply are:

- no changes at infinity ($y= 0$ for $x= inf$);
- extrapolation of existing trends at a certain site $x= x_1$
- all sand transport hampered at $x= x_1$.

Mathematically, the first two cases do not give difficulties, but in the last case (using the one line theory as example) one should know as well s as the transport S_0 when the coast is in direction, in order to find S_0/s, being (according to (4.2)) the coastal direction at $x= x_1$.
While often the coastal constants are uniform along the coast, in the case of harbour moles the change of wave height and direction around the harbour results in variation of the coast constants along the coast.
The line-theories in coastal dynamics are based upon a philosophy of wave induced transport in the surf zone. However, tidal-induced transport can be taken into account to a certain extent by introducing source- or sink-terms "p" in (4.1). Also p is a coastal constant, non-uniform in longshore direction. Introduction of those sources- and sinkterms will be subject of a next paper [25].

4. Determination of coastal constants

4.1 General considerations

4.1.1 Introduction

Apart from the mathematical formulation, the results of mathematical line modeling depend upon the magnitude of the "coastal constants", which serve as calibration constants in those models. Two ways to determine those constants pass the review. The first one is investigation of the former coastal behaviour. Here, Kalman filtering offers sophisticated means. The second one is calculation of the constants from the wave climate. For formulation of the constants, determined by longshore transport, use is made of the CERC-formula and (with respect to the two-line theory) of the Svasek variation of this approach. With respect to the constant determining the cross-shore transport (i.e. concerning the time scale of restoration to the equilibrium profile of a non-equilibrium profile) an effort is made to link with the Stive theory. Dimensionless equilibrium profiles of the offshore zone result in this way, however only of the part seaward of the outer breaker bar. On the time scale, according to which a non-equilibrium profile restores itself to an equilibrium profile, only global information is obtained, being restricted to the seaward part,

Mathematical line-models appear to be a useful tool in coastal engineering. Most significant categories are one-line models, which deal with the dynamics of "the" coastline and two-line models, in which beach and inshore each are represented by one line.
Constants, which appear in these models deal with the relation between the curvature of the line(s) and the accretion; furthermore, in the two-line theory, an additional constant determines the relation between the steepness of the profile (i.e., the distance between the lines) and the cross-shore transport. (ch.4.1.2).
There are two essentially different ways to find these constants. In ch.4.3, constants are found from coastal history; the coastal model is calibrated in this way.
A scientifically more satisfactory approach, and sometimes the only way, is to find the coastal constants from the wave climate and the grain characteristics (ch.4.2).
The second approach does not lead always to better results, as much depends on the accuracy of the used sand transport formula and the schematization. Anyway it gives a relation between more sophisticated theories and the simple line theories
In this paper, both ways for finding the coastal constants are enlightened. It will be assumed, that the reader is familiar with the use of these models as such; with respect to this is referred to, for instance
[1] to [6], [9], [16],[17],[26].

4.1.2 Considerations on coastal equations and coastal constants

The coastal equations for the two-line theory are [1],[2]:

$$h_1 \frac{\delta y_1}{\delta t} = s_1 \frac{\delta^2 y_1}{\delta x^2} - s_y (y_1 - (y_2 - W))$$
$$h_2 \frac{\delta y_2}{\delta t} = s_2 \frac{\delta^2 y_2}{\delta x^2} - s_y (y_1 - (y_2 - W)) \qquad (4.1a,b)$$

Generally, the indices "1" and "2" refer to beach and inshore respectively. The x-axis is in the main coastal direction and $y_{1,2}$ denotes the y-coordinate of beach and inshore; t is the time; h_1 and h_2 are the thickness of the sand layers, representing beach and inshore.
For the definition of beach and inshore and for the derivation of the equation (4.1a,b) is referred to [1] or [2].
The equations indicate, that accretion at beach and inshore are proportional to their curvature, with proportionality constant $s_{1,2}$ This apart from effects of cross-shore transport from beach to inshore, contained in the last term on the righthand side of (4.1a,b). This

4.2 CALCULATION OF COASTAL CONSTANTS FROM THE WAVE CLIMATE.

4.2.1 Introduction.

Naturally, the coastal constants should be related to the wave climate. Consider first the constants, determining the longshore transport.
However, trying to calculate these constants one has to cope with one of the nasty errors of nature: this shows often only a far and maybe accidental resemblance to mathematical feasible schematizations.
In the one- and two-line theories there exists a distinct level, above which all contour lines are unstationary; being all parallel to each other according to the one-line theory or parallel to either the "line of the beach" and "line of the inshore" respectively according to the two-line theory Below this level, there should be, theoretically, a (stable) horizontal plane [1], [26].
Along the dutch beaches, such a stable horizontal plane does not occur. In the mathematical model, one may mitigate the condition of such a plane, by assuming a stable sloping area below the dynamic area. Thus one finds two sloping areas (the lower one stable and the upper one dynamical) for the one-line theory (fig.4.1) and three (beach, inshore and a stable one, fig.4.2) for the two-line theory. In 4.3.3 it will be shown, that the choice of the level h between mobile and immobile coastal zone (or of h_{tot} - h_1+h_2 in the case of the two-line theory) is crucial for the result of the calculated "s".
In the following, first (sect.4.2.2), for the one-line theory the magnitude of the coastal constants S_0 and s as depending on deep water wave conditions is calculated, starting from the assumption of stationary and uniform wave conditions; the effect of the choice of the level h (the lower boundary of the movable zone) on the constant s will be investigated.
Furthermore, for the two-line theory, some remarks will be made on the effect of the direction of the inshore on the longshore transport between beach and inshore.
After this (sect.4.2.3), the way of calculation of the coastal constants in the case of variable wave conditions (i.e. in the case of a "wave climate") is elucidated. Next (sect.4.2.4), a program is described for calculation of the coastal constants, where the wave conditions near the beach do not need to be uniform along the beach, but may vary, for instance because of the vicinity of a harbour mole. Finally (sect.4.2.5) the constant s_y determining the cross-shore transport will be considered.

COASTAL CONSTANTS, DERIVED FROM FORMER COASTLINE BEHAVIOUR.
Investigating sand waves on the dutch Wadden island Vlieland [3], Bakker derives the coastal constant s/h of the one-line theory from nature by correlating the coastal curvature with the accretion and erosion of the coast.
In a more sophisticated way, de Vroeg et al.(4] calculate the coastal constants $(s/h)_{1,2}$ and S_y from the coastal data of beach and inshore by application of Kalman filtering. In ch. 4.3.2., more details are given. Kalman filtering combines the advantage of deterministic and statistical approaches. It is an algorithm which combines the measurements and physical knowledge of the system in order to achieve an optimal estimate of the behaviour of the system. The method has been applied between IJmuiden and Scheveningen.
Bakker, Bruning and Andringa [5] ,[6], [2] use a kind of CAD by displaying as well natural coastal behaviour in the shape of the lines of beach and inshore as coastal model results on the same screen and calibrating the results by changing the coastal constants, using the method of the least squares. Hindcasts concerning the coastal behaviour could be obtained in this way, accurate up to 10 m.
Table 4.1 gives values of the coastal constant s/h, found from various investigations. Also some results, found from wave climate calculations (ch.4.2) are mentioned.
Values of s_y of the order of 1 to 2 million m^3/ year seem usual, with Sylt and Cadzand at the low side and Scheveingen on the high side. This last value might be overestimated somewhat. Values found for s_y -taking the seperation plane between beach and inshore at the level at the vicinity of the low-water line- vary between 1.5 m/year (Sylt [2]) to 3 m/year (Cadzand [2]) for sand supplies. For long period features smaller values appear to be most probable (order of 0.5 m/year, fig. 4.7). Some none linearity of s_y is not unlikely. Janssen [19]

finds for Scheveningen, for a separation plane at about NAP -3m values of the order 0.1 to 0.2 m/yeart

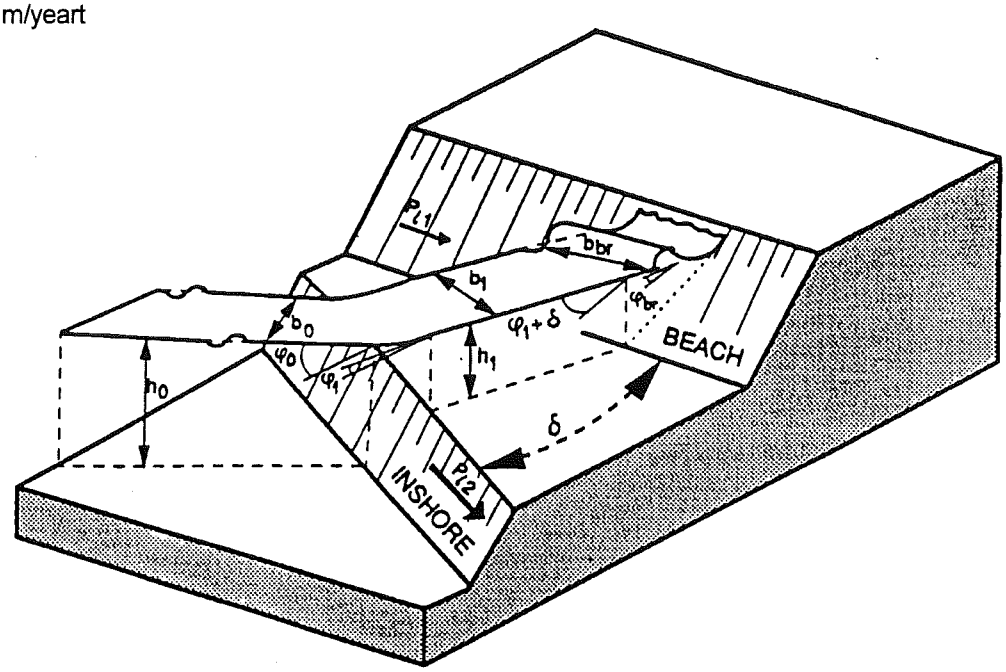

Figure 4.1a: Three dimensional view of beach profile with a wave ray approaching the beach. P_{l1}= longshore component of the wave energy along the beach. P_{l2}= longshore component of the wave energy along the inshore

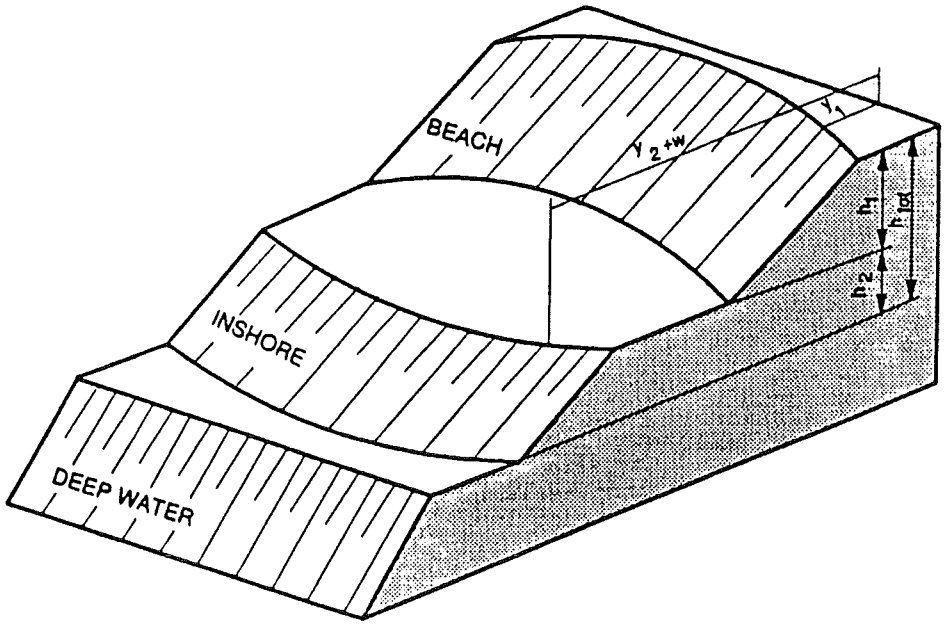

Figure 4.1b: Three-dimensional view of the bottom schematization, used for the calculation of the coastal constants according to the Svasek-formula

4.2.2 Waves stationary and uniform along the coast.

Ten Hoopen & Bakker [17] schematize [1] the coastal topography as shown in fig.4.1a, consisting of a beach and an inshore, having parallel depth contours, with a horizontal plane (at depth h_1) between. Beach and inshore make an angle δ with each other.
Starting from uniform and stationary wave conditions alongshore in deep water, this schematization allows for calculation of longshore transport along beach and inshore respectively. Use is made of a conception, originating from Svasek [8],[18] this leads to longshore transport, proportional to "the longshore component of the loss of energy flux between two depth contours" [2], which for beach (Pl_1) and inshore (Pl_2) can be specified by the following formutation ([17], taking the cosine of the breaker angle equal to 1):

$$Pl_1 = Kh_1^3 \frac{sin(\varphi_1 + \delta)}{c_1}$$

$$Pl_2 = K(h_{br}^3 - h_1^3)\frac{sin(\varphi_0)}{c_0} \qquad \text{when } h_{br} > h_1 \qquad (4.3a)$$

$$Pl_1 = Kh_{br}^3 \frac{sin(\varphi_1 + \delta)}{c_1} \qquad \text{when } h_{br} < b_1 \qquad (4.3b)$$

$$Pl_2 = 0$$

Here K is a proportionality constant, specified in (4.17b); c denotes the wave celerity and φ the angle of wave incidence; the indices "0","1" indicate the site: respectively at deep water and at the upper boundary of the inshore. The depth h_{br} denotes the breaker depth, specified in eqn (4.17a)..
Equations like (4.3a,b) form the basis of most computations, carried out ([15], [16],[21], [24]) on the coastal constants S_0 S_{01}, S_{02}, s, s_1, s_2. When (4.3b) is valid, one finds back the stable lower zone and the dynamical upper zone of the one-line theory. Computations concerning S_0 and s with respect to the one-line theory [3] are given into some detail in 4.3.3; calculations concerning the other mentioned parameters are carried out in a similar way [21], starting from a topography given in fig. 4.1b (three slopes) instead of the one given in fig.4.1a.[4] (two slopes).
Results (fig.4.2; ch. 4.3.3) give dimensionless expressions for the mentioned coastal constants, where $A_1 H_0^2 c_0$ is taken as reference; A_1 being a proportionality constant, (eqn.(4.20)) relating sediment transport to longshore component of energy flux; H is the wave height. Independent variables are wave direction, wave steepness and (for s) the location of the level h of the toe of the beach area.
Fig. 4.2 (one-tine theory) shows S_0 (dotted line) and s (drawn lines) as function of the deep water angle of wave incidence; curves are valid for various values of c_1/c_0. The indicated values are valid for such wave steepness S_0', that the ratio c_{br}/c_0 is equal to 0.5 in the case that the waves are normally incident to the inshore as well as to the beach . For other wave steepness (only) the vertical scale of fig. 4.2 has to be adapted (eqn.(4.20) (giving the relation between S_0' and c_{br}/c_0) and (4.22)).
For large values of as well angle of wave incidence as well c_1/c_0, negative s-values are found. Bakker & Edelman [22] point out, that coastlines can be unstable under those conditions. This may be one reason for the origin of beach cusps.
For a given wave steepness, the constant s increases when c_1 decreases (fig 4.2), i.e. when the depth h up to which the contour lines are parallel to the shoreline decreases.

---

[1] In [17], a more general case is treated than considered in the following, i.e. the "beach" Is bordering a shoal, which eventually may be submeerged.
[2] As Battjes points out, a flux is a scalar. Thus it cannot have a "longshore component". Here the meaning of the used term will be specified as a vector in longshore direction with length $\Delta \sin\varphi\cos\varphi$
[3] More accurate than mentioned before: putting $(\cos\varphi_{br}^2)^{1/5}$ to 1 instead of $\cos\varphi_{br}$
[4] Thus accounting for turning of depth contours of the inshore zone by dynamical shore processes, which is not involved in eqn. (4.3a)

Fig. 4.3 depicts a physical explanation. In fig. 4.3a, the contour lines up to very deep water are parallel to the shoreline. Before breaking, wave crests have the opportunity to refract, becoming more or less parallel to the plan-shape of the shoreline. Therefore breaker angles will be small and so will be the transport gradients. The opposite is the case when the wave crests do not have the opportunity to adapt itself to the beach planform (fig. 4.3b).
For small values of c_1/c_0 only positive values of s are found (fig.4.2), because also at large angles of deep water wave incidence, the angle of incidence at the shoal of depth h_1 does not become large.

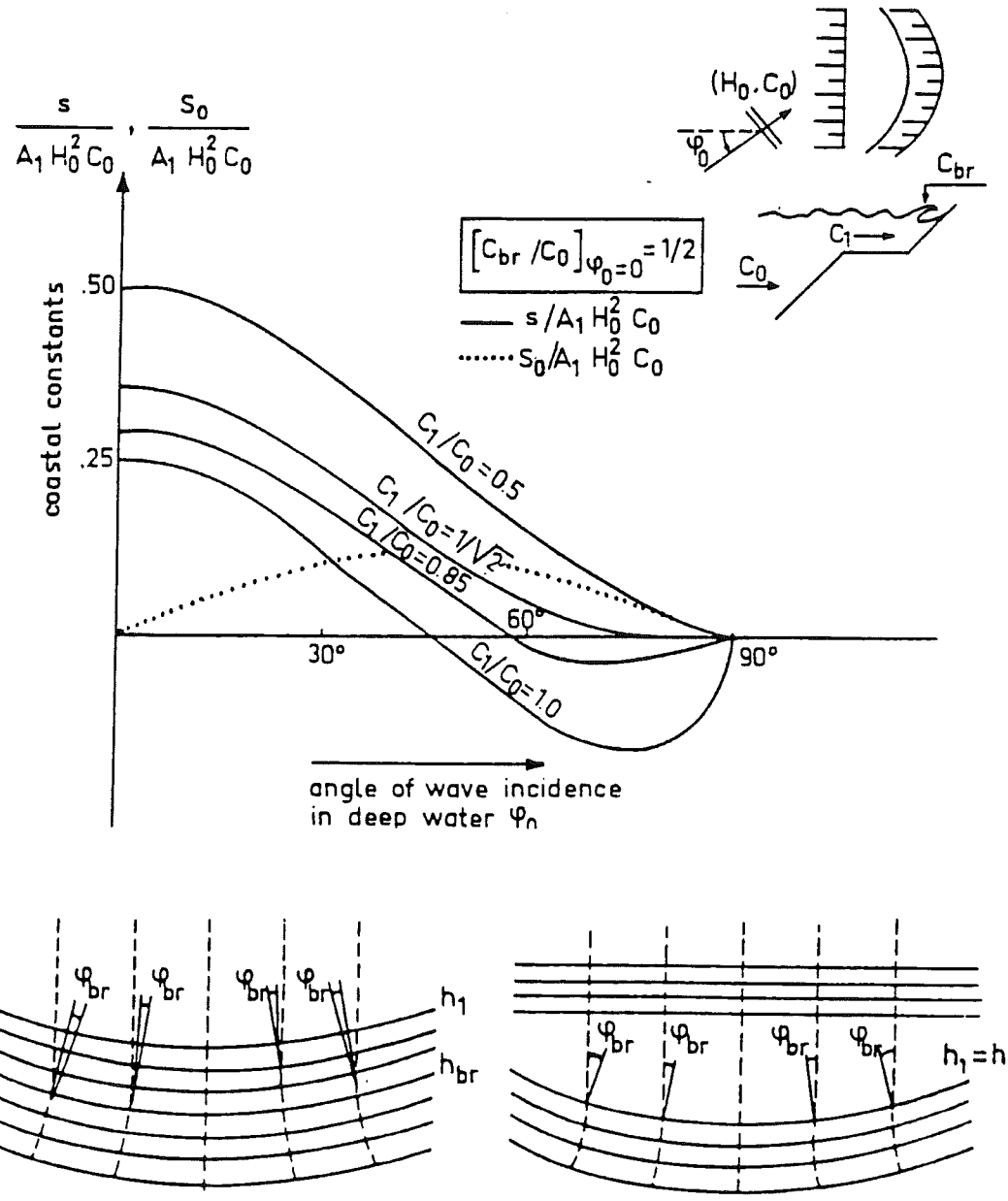

Figure 4.3a, b: The breaker angle decreases, when h_1 increases

4.2.3 Wave climate (uniform along the coast).

Bakker, ten Hoopen and Grieve [5], [7] calculate the constants s_1 and s_2 for the longshore transport from the wave climate, starting from eqn. (4.3 a,b), taking the probability of each wave class into account (ch. 4.2.4).

By giving the angle δ between beach and inshore respectively a positive value and a negative value of the same magnitude, one finds (by subtracting the values for the transport along the beach in both cases and dividing by 2δ) the rate of change of the transport s_1 along the beach, depending on the beach orientation.

4.2.4 The KC/KL programs.

A further extension, permitting variability of wave conditions alongshore, is given by the KC/KL-programs.
Constants can be calculated with the "KC"-program of Rijkswaterstaat and Delft University of Technology ("KC" stands for "Kustconstanten", dutch for "Coastal Constants"). Coastlines afterwards are calculated with the "KL"-program (-"kustlijn" - "coastline"). This gives the possibility to calculate the coastline near harbour moles.
The effect of eddies, occurring during the tidal cycle can be incorporated in introducing a sources-and sinksterm "p" in eqn. (4.1 a,b). An application for the coast of Holland will be treated in a future paper [25].

The KC/KL-program has been developed in cooperation between Rijkswaterstaat and Deift University of Technology. It is based upon investigations of Bakker [1], Bakker et al.[7], ten Hoopen & Bakker [16] and V. Bochove [13] , [14], [15]. Programming and documentation has been performed initially by A.Roos and H.W.M.Bots where the final version of the program has been made by A.Casteleyn, who also reported on this subject [16].
The programs KC and KL are built up in a modular way.
The program KC starts from a bottom topography, which can be described in the following way.
Assumed are parallel depth contours from deep water to a certain level (arbitrarily to choose), where the head of a harbourmole is situated (the existance of this harbourmole is optional); at this depth one finds a horizontal area, where diffraction takes place; from there landward, again one finds an upward slope with contour lines parallel to the contour lines in deep water; this up to a level h'_1 (with respect to mean sea level) where the waves are about to break. Here again one finds a flat area; from here upward, contour lines make an angle δ with the contour lines in deeper water (δ to be chosen arbitrarily) .(fig.4.1a).
For an arbitrary number of equidistant points along the x-axis (parallel to deep water) the wave height is calculated, taking as well as diffraction on the shoal at the level the contour lines in refraction into account, of the harbour mole (fig. 4.4).

As each computation at such is rather simple, the program allows for calculating in one run for:

- various values of δ;
- various places along the x-axis;
- various angles of deep-water wave direction;
- various water level elevations;
- various wave periods;
- three different fractions of the time, during which the tide level is one meter lower, c.q. higher than the mean level, c.q. is at the mean level;
- various values of the deep water wave height.

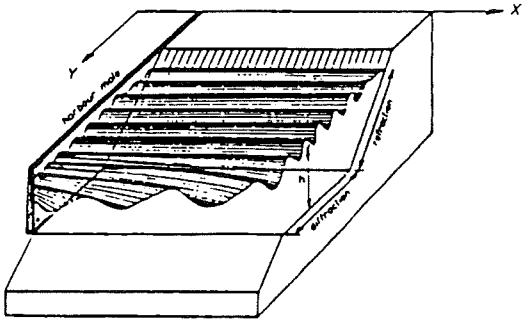

Figure 4.4

Each of the various topics, mentioned above means a loop in the program, where the loop of the first-mentioned topic embraces the loop of the of the later-mentioned topic.
The wave climate is characterized by considering various wave classes, each characterized by a certain deep-water wave height H, period T and direction φ and a certain probability of occurrence $P_r(H,T,\varphi)$.
Calculated is the expectation of the longshore component of the wave energy flux Pl_1 along the beach:

$$E(Pl_1) = \sum Pl_1 \cdot P_r(H,T,\varphi) \qquad (4.4)$$

where Pl_1 is given by (4.3a) or (4.3b), depending on the breaker depth. Here h_1 is the water depth, i.e. h'_1 plus the waterlevel elevation.
In the North-Sea, deep-water wave direction and wave height are determinec more or less by wind-direction and windforce. These in turn determine the set-up by storm surge of the North Sea level along the Dutch coast (overviewing for a moment the effect of tide). The relevant relations have been derived from data from Weenink from the Royal Dutch Meteorologica] Institute [12].
During the "water-level elevation"-loop the various possibilities that the water reaches the given level are considered, i.e. as well as (for instance) the possibility of small waves during flood tide as high waves (high North sea elevation) during ebb tide.
Assuming a linear relation between the littoral drift S and Pl_1 and calling $S(\delta_1)$ the value of S, when δ gets a certain value δ_1 one can find the value of the coastal constant S at a certain place as:

$$s = \frac{S(\delta_1) - S(-\delta_1)}{2\delta_1} \qquad (4.5)$$

The KL- program is a program, which calculates explicitely the y-coordinate of the coastline given the coastal constants (for instance found from the KC-program). Use is made of the equations (4.1a,b). There are various options, starting from various boundary conditions. One option is also to compare the calculations with given data concerning the behaviour of the coastline.

4.2.5 Final remarks.

The present paper gives the order of magnitude of coastal constants to be expected in nature and some ways of determination.
Still, some warning should be added. The equations (4.1) start from the assumption that beach and inshore form a self-contained system and that no interaction between the offshore zone and the inshore takes place. If this condition is not fulfilled in nature, also sophisticated mathematical methods (as for instance Kalman filtering) can give spurious results. Also calculation of coastal constants from the wave climate gives results, depending on the schematization. For instance, chapter 4.2.4 shows, that the choice of the level in the one-line theory, up to where the bed is assumed to be mobile does not influence only h but also s in the constant s/h.
Coastal engineering remains an art, apart from being a science.

4.3 Computating from hindcasting of field data

4.3.1 Direct comparisation coastline computations with field data

4.3.2 Kalman filtering

4.3.2.1 Kalman filtering in general.

The Kalman filter combines the advantages of the deterministic and the statistical approach, and has proven to be very suitable for recursively updating parameter estimates of time-varying model coefficients, based upon the latest data information. It is an algorithm which uses measurements, a physical model of the system and knowledge of the inaccuracy (noise) of both the measurements and the model, in order to achieve an optimal estimate of system behaviour (Kalman, 1969). The method has been explained in [4], concentrating on the application of the one-line theory. Here, the explanation will be briefly repeated; the complementary reading of [4] is recommended. Now, the application for the two-line theory of linear Kalman filtering will be highlighted.
The method is based on the concept of on the one hand the existence of a "system", not necessary stationary, but anyway systematically changing and on the other hand periodical measurements concerning some characteristics of the system, blurred by "noise". The noise has two reasons:

- reality is more complicated than the assumed system
- measurements show errors.

It is assumed, that prognostics of the characteristics to be measured can be found from a linear transformation of the system. This linear relationship implies on the other hand, that "backtransformation" of information on the characteristics involves information on the system.
The filtering procedure consists of cycles of linear transformations of respectively:

- the system (being transformed from the state at one time step to the state at the next time step)
- the anticipated result of the measurements at this "next timestep" (found from the state of the system);
- comparison between measurements at this "next timestep" and anticipated result; this gives a gain of information on the system, which is fed back by making a correction on the state of the system at the considered time. The "weight" assigned on the information derived from the measurements in relation to the weight assigned to the anticipated result depends on the given noise characteristics. It is derived in a mathematical way, starting from the least-square error standards.

All the information, as well concerning the backtransformation of measured characteristics to system as well concerning the relative importance of the measurements compared to "theory" is contained in the "Kalman gain matrix" $K(t)$, which (linearly) transforms the difference between measured and anticipated characteristics to a correction (valid for the present time step) of the system. This gain matrix forms the essence of the Kalman filtering. From it results the gain of information on the system, found from the last measurements. With the last-mentioned transformation the cycle is closed, apart from the fact, that also the gain matrix is corrected after each time step, depending on the ratio between the noise in the measurements and the noise in the latest estimate. (the larger the noise in the measurements, the less information the measurements give about the system).
Numerically, the use of Kalman filtering involves, that all measurements are elaborated in a sequential way, which means, that the computer may "forget" all previous measurements and all previous states of the system when elaborating "actual" measurements. This means, that only a confined amount of storage is required. All the relevant information about these former measurements is contained in the present state of the gain matrix, which is successively improved. For the general equations concerning the Kalman filtering is referred to [4].

4.3.2.2 Application on the two-line model.

Applying Kalman- filtering for the two-line theory, as "system" has been defined: the system of constants s_1, s_2, s_y having principally a "noise" $var(s_1)$, $var(s_2)$, $var\ (s_y)$. No covariance between s_1, s_2, s_y is assumed.
This definition of the system involves a simplified application of the Kalman filtering theory, for in the present case the system in principle is stationary, where, generally, the system is allowed to change in the course of the time. Still, estimates of the system may vary in course of time, because new information is delivered by the various measurements of the characteristics of the system.
These "characteristics" are defined as the y-coordinates of the lines of beach and inshore in the various measuring points.
Thus, defining a measuring equation as:

$$\underline{z}(t) = H(t-1)\cdot \underline{x}(t) + \underline{v}(t) \qquad (4.7)$$

where $\underline{z}(t)$ is the measured state, $\underline{x}(t)$ is the system state and $\underline{v}(t)$ denotes the inaccuracy of the measurements, the matrix H equals:

$$\begin{bmatrix} A_1(y1_1 - 2y1_2 + y1_3) & 0 & B_1(-y1_2 + y2_2 - W) & y1_2 \\ 0 & A_1(y2_1 - 2y2_2 + y2_3) & B_1(-y2_2 + y1_2 + W) & y2_2 \\ A_1(y1_{n-2} - 2y1_{n-1} + y1_n) & 0 & B_1(-y1_{n-1} + y2_{n-1} - W) & y1_{n-1} \\ 0 & A_2(y2_{n-2} - 2y2_{n-1} + y2_n) & B_1(-y2_{n-1} + y1_{n-1} + W) & y2_{n-2} \end{bmatrix}$$

where the column vectors $\underline{z}$ and $\underline{x}$ are respectively (written for typographical reason as row vectors):

$$\underline{z} = (y1_2, y2_2, \ldots\ldots y1_{n-1}, y2_{n-1}) \qquad (4.8a)$$

and $$\underline{x} = (s_1, s_2, s_y, 1) \qquad (4.8b)$$

In the matrix H, the constants $A_{1,2}$ and $B_{1,2}$ are equal to $\Delta t/(\Delta x^2 h_{1,2})$ and $\Delta t/h_{1,2}$ respectively.
In the system definition of x, the last unit "1" is added for numerical reasons.
The coefficient W, defining the equilibrium distance between beach and inshore, is not filtered at all. If as well s_y as W would have been filtered, a non-linear filtering technique should have been applied. The equilibrium distance is estimated from measurements.
The sensibility for the applied value of. W will be evaluated when considering the results of the Kalman filtering (sect. 4.3.2.3).
For the way of calculating the gain matrix is referred to [4], where one has to keep in mind, that F is the unit matrix.

4.3.2.3 Results.

Kalman filtering has been applied [36] for determining the coastal constants of the Rijnland coast. Later on the method has been applied on the total uninterrupted coast of Holland; this last investigation will be reported on in [25].
Fig. 4.5 (from [36]) shows some results for the two-line theory, applied on the Rijnland coast (range number RSP km 58.00 to 98.00); for results of application for the same area of Kalman-filtering starting from the one-line theory is referred to [4] and [36].
The "beach zone" included the dunes as well; and was schematized as the area between NAP (-about MSL) +15 m and the low-water line (NAP -.72 m); the inshore zone between NAP - .72 m and NAP - 5m.
Fig. 4.5 shows the values of the system (s_1, s_2, s_y) in course of time; the original estimate (1970) of (s_1, s_2, s_y) was $(0,0,0)$. Measuring noise has been estimated as 125 m^2 for the beach zone and 700 m^2 for the inshore zone. The result did not change considerably with assumptions of other values for this noise. The value of s_y showed sensibility for the magnitude, assumed for W (taken 280 m in fig. 4.5); the effect of this variation on s_1 and s_2 was much less.

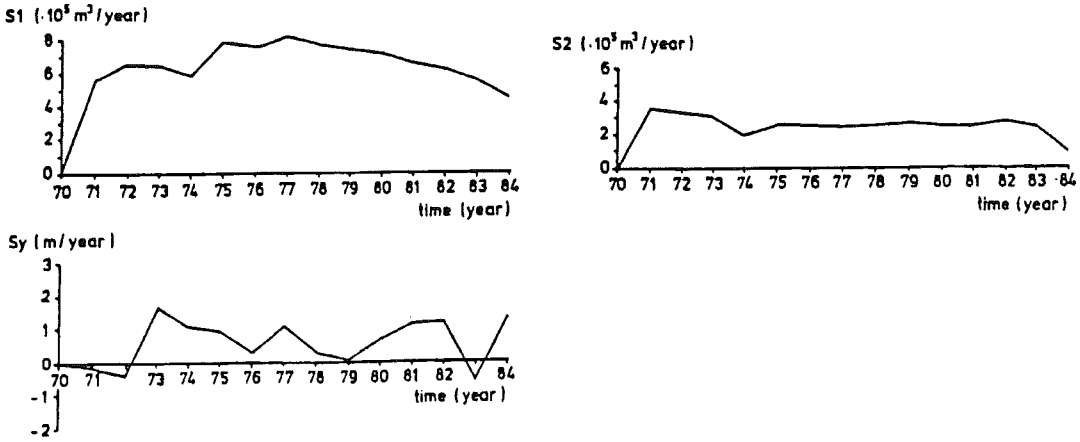

Figure 4.5: Calculated estimates for the coastal constants (s_1, s_2, s_y) as function of time, using Kalman filtering. Data Rijnland 1970-1980.

4.3.3 Effects of schematization

The effect of the determination of the depth h_1 and h_2 on the coastal constants

In this chapter, first dimensionless ratio's will be given, relating S_0 and s of the one-line theory to the deep-water wave conditions. Schematization is according fig.4.1a, where h_1 is assumed to be somewhat larger than h_{br}.
Later on, some results will be given concerning computations, in which part of the waves break on the inshore, starting from a schematization, given in fig.4.1b. Under those circumstances it is assumed, that the waves start to break on the inshore, where Svasek 's assumptions concerning the longshore transport are used.

The following calculation of the transport S along the beach starts from the schematization given in fig. 4.1a and from the assumptions, mentioned in [17]. These include for instance the use of the CERC-formula: the transport S is proportional to the longshore component of the energy flux Pl_1 :

$$S = A_1 * (8\, Pl_1 / \rho_w) \tag{4.9a}$$

with:

$$8\, Pl_1 / \rho_w = n_{br} H_{br}^2 c_{br} \sin \varphi_{br} \cos \varphi_{br} \tag{4.9b}$$

n being the ratio group velocity/phase velocity, H the wave height, c the phase velocity and φ the angle of wave incidence; The index "br" denotes breaking and $\rho_{w(s)}$ the specific density of water (sand).

Including in S also the volume of pores, when the material settles, one easily finds the constant A_2 in the equation $I_1 = A_2 \cdot Pl_1$, where I_1 is the immersed weight of transported material equal to:

$$A_2 = \frac{8(\rho_s - \rho_w) a_1}{\rho_w} A_1 \tag{4.10}$$

a_1 being the ratio of content of solid material (1-porosity ratio). Wave conditions are assumed uniform and stationary.

Furthermore, it is assumed, that the breaker depth is smaller than h_1. Then for the "longshore component of the wave energy flux" Pl_1 along the beach one finds (making use of conservation of energy flux between wave rays at a mutual distance b):

$$Pl_1 = \frac{b_0}{b_{br}} n_0 E_0 c_0 \sin\varphi_{br} \cos\varphi_{br} \tag{4.11a}$$

where $n_0 E_0 c_0$ is the wave energy flux in deep water; E denoting the wave energy per unit of area, c the phase- and nc the group-velocity. The index "0" refers to deep water and "br" to breaker conditions.

$$E = \rho_w g H^2 / 8 \tag{4.11b}$$

In (4.11b), g denotes the acceleration of gravity.

Using Snell's law, $\sin\varphi_{br}$ can be expressed as:

$$\sin\varphi_{br} = \frac{c_{br}}{c_1} \sin(\varphi_1 + \delta) \tag{4.12}$$

where the subscript "1" refers to the values at the level of the "toe" of the beach, and where φ_1 is the angle of wave incidence on the upper side of the inshore.
Applying Snell's law once again, one may replace c_1 in (4.12) by the deep water value c_0, finding:

$$\sin\varphi_{br} = \frac{c_{br}}{c_0} \frac{\sin\varphi_0}{\sin\varphi_1} \sin(\varphi_1 + \delta) \tag{4.13}$$

Make use of ([17]):

$$\frac{b_0}{b_{br}} = \frac{\cos\varphi_0}{\cos\varphi_1} \frac{\cos(\varphi_1 + \delta)}{\cos\varphi_{br}} \tag{4.14}$$

Substitution of (4.13) and (4.14) into (4.11) gives for Pl_1:

$$Pl_1 = n_0 E_0 c_{br} \frac{\sin 2(\varphi_1 + \delta)}{\sin 2\varphi_1} \sin\varphi_0 \cos\varphi_0 \tag{4.15}$$

Assume a ratio γ between the wave height H_{br} and the water depth h_{br} at the time of breaking and take the celerity of wave propagation of a nearly breaking wave equal to:

$$c_{br} = F_r \sqrt{g h_{br}} \tag{4.16}$$

where F_r is a kind, of Froude number, of the order 1. From the conservancy of wave energy between wave rays one finds (using (4.16):

$$h_{br} = \left[\frac{n_0 H_0^2 c_0 b_0}{\gamma^2 F_r \sqrt{g}\, b_{br}} \right]^{\frac{2}{5}} \tag{4.17a}$$

Here H_0 is "the" deep water wave height (in irregular waves: the wave height representative for the local wave energy [1)], i.e. $H_0^2 = H_{sign}^2/2$.

Firstly, using (4.9b), (4.12) and (4.16) it is easy to derive (4.11b), taking $\cos \varphi_{br}$ approximation equal to 1. One then finds for K:

$$K = n_{br} \gamma^2 F_r^2 g \tag{4.17b}$$

However, a more accurate expression for the transport S (expressed in deep water wave conditions) is possible as well, where on the other hand also the magnitude of s is investigated.
With the aid of the developed formulae it is possible to give the following kind of relations:

$$S_0 / A_1 H_0^2 c_0 = f(H_0/L_0, \varphi_0) \tag{4.18}$$

$$s / A_1 H_0^2 c_0 = f(H_0/L_0, c_1/c_0, \varphi_0) \tag{4.19}$$

where H_0/L_0 denotes the initial wave steepness and c_1 the wave celerity at the transition level between beach and inshore. However, a clear-cut relationship with the initial wave steepness requires assumptions concerning the magnitude of F_r and γ and thus loss of generality. Therefore, the independent variable H_0/L_0 will be replaced by the ratio between the deep water wave celerity c_0 and the wave celerity $[c_{br}]_{\varphi=0}$ when the wave breaks, under the condition, that all contour lines are parallel and that the waves are normally incident. With respect to this, the following relation can be found from (4.16) and (4.17a), taking $\delta = 0$:

$$\frac{c_{br}}{c_0} = \left[\left(\frac{F_r \sqrt{g}}{c_0} \right)^4 \frac{n_0 H_0^2}{\gamma^2} \frac{\cos \varphi_0}{\cos \varphi_{br}} \right]^{\frac{1}{5}} \tag{4.20}$$

When $\varphi_0 = 0$ (and thus $\varphi_{br} = 0$ one thus finds the following relation between c_{br}/c_0 and the wave steepness:

$$\left[\frac{c_{br}}{c_0} \right] = \left[\frac{4\pi^2 F_r^4 n_0}{\gamma^2} \right]^{\frac{1}{5}} \left(\frac{H_0}{L_0} \right)^{\frac{2}{5}} \tag{4.21}$$

For calculation of S_0 take the x-axis parallel to the depth contours of the inshore. Neglecting the difference between $(\cos \varphi_{br})^{1/5}$ and 1, from (4.9a,b), (4.14), (4.20) and the law of conservation of wave energy flux between wave rays follows directly for the transport S_0 when all contour lines are parallel ($\delta = 0$):

$$\frac{S_0}{A_1 n_0 H_0^2 c_0} = \left\{ \frac{c_{br}}{c_0} \right\}_{\varphi=0} \sin \varphi_0 (\cos \varphi_0)^{\frac{6}{5}} \tag{4.22}$$

The value of s can be found by differentiating (4.14) to δ and putting $\delta = 0$. With the aid of (4.9), (4.10) and (4.14) one finds:

$$s = A_1 n_0 F_r H_0^2 \sqrt{g h_{br}} \cos 2\varphi_1 \frac{\sin 2\varphi_0}{\sin 2\varphi_1} \tag{4.23}$$

[1] It is logical to take also γ in such a way, that the wave H_{br} is representative for the local wave energy. In [17], the formulas have been adopted in this way that they refer to H_{sign} (i.e., there also τ relates to the significant wave height in the breaker zone). Generally, only the relationship "H_0/γ" is important. When H_0 is replaced by a wave height with a certain probability of occurrence, γ should be adapted correspondingly.

which can be expressed in the wanted variables:

$$\frac{s}{A_1 c_0 H_0^2} = n_0 \frac{(\frac{c_{br}}{c_0})_{\varphi=0}}{\frac{c_1}{c_0}} \{1 - 2(\frac{c_1}{c_0})^2 \sin^2 \varphi_0\} \frac{(\cos \varphi_0)^{6/5}}{\cos \varphi_1} \qquad (4.24)$$

Fig. 4.2 shows $s/A_1H_0^2$ as function of φ_o (n_0 has been taken equal to ½);
the various curves are valid for values of c_1/c_0 equal to 1, 0.85, $1/\sqrt{2}$ and 0,5 respectively.
The value of $[c_{br}/c_0]$ has been chosen equal to 0.5; it shows from (4.24), that another value of $[c_{br}/c_0]_{\varphi=0}$ only influences the vertical scale of fig. 4.2.

Similar calculations [21] have been carried out concerning the two-line theory.
In that case, there has been started from a bottom topography, depicted in fig.4.1b and from the longshore transport equations, given by (4.3a) (i.e. $h_{br}>h_1$).
The result is:

$$\begin{aligned}
S_{01} &= A_1 \gamma^2 F_r g^{\frac{1}{2}} h_1^{2\frac{1}{2}} \sin \varphi_1' \cos \varphi_1' \\
S_{02} &= A_1 \gamma^2 F_r g^{\frac{1}{2}} (h_{br}^3 - h_1^3) h_{tot}^{\frac{1}{2}} \sin \varphi_2' \cos \varphi_2' \\
s_1 &= A_1 \gamma^2 F_r g^{\frac{1}{2}} h_1^{2\frac{1}{2}} \cos 2\varphi_1' \\
s_2 &= A_1 \gamma^2 F_r g^{\frac{1}{2}} (h_{br}^3 - h_1^3) h_{tot}^{\frac{1}{2}} \cos 2\varphi_2'
\end{aligned} \qquad (4.25a\text{-}d)$$

where φ_1' and φ_2' are the angles of wave incidence (when all contour lines are parallel) at depth h_1 and h_{tot} the last depth being h_1+h_2. However, eqns (4.25a-d) have a confined accuracy, as there is an effect of the refraction on the inshore on the transport along the beach, which is neglected in those equations. The rate of change of the transport along the beach as function of the direction of the inshore, divided by s_1 is depicted in fig. 4.6, being a function of h_1/h_{tot} (on the horizontal axis in fig. 4.6) and of the angle of wave incidence φ_2' at the depth h_{tot} (angles written near the various curves in fig. 4.6).
Fig.4.6 is derived from the following equation.

Call: δ_2 the angle of the inshore with respect to the depth contours in deeper water;
δ_1 the angle of the beach with respect to those contours;

Then for the transport S_1 along the beach is found:

$$S_1 - S_{01} = A_1 \gamma^2 F_r g^{\frac{1}{2}} h_1^{2\frac{1}{2}} \cos 2\varphi_1' [\{1 - \frac{\cos \varphi_2'}{\cos \varphi_1'} \sqrt{\frac{h_1}{h_{tot}}}\} \delta_2 - \delta_1] \qquad (4.26)$$

The term between accolades is depicted in fig. 4.6.

When the direction of the beach changes, the transport along the beach changes. However, when the direction of the inshore changes, the transport along the beach changes as well, because of different refraction on the inshore.
Indicated is the proportion between the rate of change of the transport along the beach, caused by the change of direction of the inshore, compared to the rate of change of the transport along the beach, caused by a change of direction of the beach.
Variables are the level of the separation plane between beach and inshore (i.e. h_1/h_{tot}) and the angle of wave incidence at the level h_{tot} (written by each line separately).

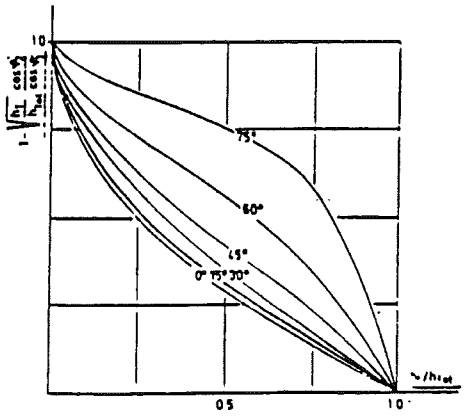

Figure 4.6: influence direction inshore/ influence beach versus h_1/h_{tot}. Indicated angles are angles of wave incidence at the level h_{tot}

Neglecting the term between accolades, from (4.26) one directly can derive(4.25c).
For assumptions made during the derivation is referred to [21].
Important is the assumption of uniform conditions along the coast, i.e. no effects of curvature of the inshore and of gradients in wave set-up [23].
Effects of curvature of the inshore on refraction are investigated by Jas [24].
Another effect of the curvature of beach and inshore, being conciously overlooked, is the following feature .
The used equation of sand motion is developed for a straight beach. As water entrains the sand, one has to take into account the continuity of water when applying straight-beach formula for curved beaches. Apart from cross-shore transport because of deviations of the equilibrium profile, cross-shore transport because of rip-currents, initiated by discharge of surplus of water to the inshore may occur. The order of magnitude of this feature is estimated by V.Overeem [27].

4.4 Focussing on cross-shore interaction.

Also an attempt has been made to express the constant s_y in the wave conditions. Firstly, there may be referred to Swart's Ph.D.-thesis [9]. Prototype data (ch.4.2) yield smaller values of s_y than resulting from his method.
A second line of thought is the following. Using the Baillard [10] transport formula and following a simplified Stive concept [11], the dimensionless equilibrium profile outside the surfzone can be expressed in wave steepness S_0' and dimensionless fall velocity of the sediment (fig 4.7a,b). With respect to the length scales, the deep water wave length is the reference. With respect to the fall velocity w, the reference is H_0/T, where H_0 is the rms-deep water wave height and T the wave period.
However, inside the surf zone this method does not succeed: the applied mathematical method predicts breaker bars and on the other hand is not sophisyticated enough to deal with slopes, rising in seaward direction. The same method has been used to calculate the dimensionless transport, caused by a slight deviation from the equilibrium profile. This yields a dimensionless time scale T_0/T for recuperation of the profile to the equilibrium profile. It is a function of wave steepness and dimensionless fall velocity.

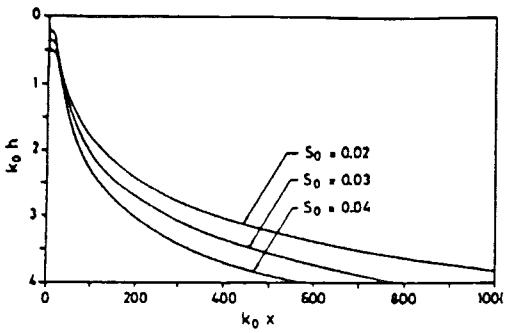

Figure 4.7a: Influence of steepness S_0' on the equilibrium profile H_{rms} / wT= 30/ π

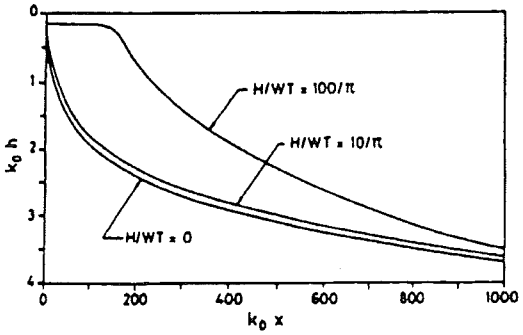

Figure 4.7b: Influence of the dimensionless fall velocity H_{rms}/wT on the equilibrium profile S_0'= 0,02

However, as the interaction between beach and inshore is a process, dominating mainly in the surf zone, up to now the developed method has practical limitations: it yields astronomical time scales, only of importance when dealing with problems as predicting the effect of sea level rise on coastal
behaviour. Maybe the method can be extended to the surf zone in the future.

COMPUTATIONS CONCERNING THE CONSTANT DETERMINING THE CROSS-SHORE TRANSPORT

Starting from the conception of an equilibrium profile, it is logical to assume, that a deviation from this equilibrium profile leads to a restoration to this profile at a certain time scale. This is the line of thought, leading to the two-line theory, where the distance between the line of the beach and the line of the inshore determines the cross-shore transport, being larger when the deviation from the equilibrium distance is larger. For uniform longshore conditions, this yields a negative- exponential decay of the deviation of the equilibrium profile. Independent of any assumptions on the mechanism which causes the equilibrium, the method essentially is right, if:

- the restoring mechanism indeed may be linearized over the range of deviations to be expected;
- beach and inshore itself show some restoring capacity of the equilibrium profile over that part of the equilibrium profile (i.e over the beach and inshore itself) with a time scale small compared to the time scale, determining the restoration of the overall profile. In other words: the theory assumes, that the volume of sand, contained in the beach area determines the cross-shore transport from beach to inshore (assuming fixed position of the inshore), not depending on the fact whether the sand is stored on the upper side or the lower side of the beach Unsaid, the theory implies more or less the assumption, that beach an inshore itself have an equilibrium profile.

If this is not the case, a more-line theory should be used [4]. In this chapter, one possible mechanism for restoration of the equilibrium profile is considered more into detail, i.e. the one, on which Stive's Crostran-model [11] is based.
The method is described into more detail by V.d Kerk [20].
Using the conception of Bailard [10], the local equilibrium slope β_e can be expressed as:

$$tan\,\beta_e = \frac{< q_{as} > + < q_{un} >}{< q_{s1} > / tan\,\beta_e} \tag{4.27}$$

in words: the equilibrium slope is found as the sum of the transports q_{as} (caused by the asymmetry of the waves) and q_{un} (caused by the undertow), divided by the rate of change of the gravity transport q_{s1} as function of the slope. The indication "<>" deals on expectations.
Stive [11] gives expressions for the various kinds of transport (relating those to the Bagnold/Bailard conception), for instance:

$$\frac{< q_{s1} >}{tan\,\beta_e} = \frac{F_b}{tan\,\phi(u3^*)} + F_s \frac{u_{rms}}{w} \varepsilon_s (u5^*) \tag{4.28}$$

where F_b and F_s refer to the effect of bottom- and suspended load; (un^*) denotes:

$$(un^*) = \frac{< |u|^n >}{u_m^n} \tag{4.29}$$

where u_m denotes the amplitude of the first harmonic of the orbital velocity. The angle ϕ is the angle of response of the material. The variables F_b and F_s depend on the bottom friction, exerted by the wave motion, Bagnold's [28] efficiency factor $\varepsilon_{b\,(s)}$ for bottom transport and suspended transport
respectively, the specific density of the sediment and the rms-orbital velocity u_{rms} furthermore, F_b depends on ϕ and F_s on the ratio u_{rms}/w, where w is the fall velocity of the material. Mind,

that the expression mentioned in (4.28), i.e. the denominator on the righthand side of (4.27) is no function of β_e, as $<q_{s1}>$ is proportional to $\tan \beta_e$.
Because the phase shifts between first- and second harmonic of the orbital velocity can amount in the breaker zone up to 90 degrees [1)], in which case $<q_{as}>$ has a value zero, Stive [11] schematizes, that $<q_{as}>$ is proportional to the percentage non-breaking waves. On the other hand, $<q_{un}>$ is direct proportional to $<u>$, the mean velocity of the undertow. For non-breaking waves, this (onshore) undertow can be approximated by Longuet-Higgins' "conduction solution"; for breaking waves, a first approximation of the (offshore) velocity has been given by Stive & Wind [29], later improved and extended by de Vriend & Stive [30] and by Battjes & Stive [31].
Making some short-cuts, V.d.Kerk [20] succeeded in writing (4.27) in the shape:

$$\frac{dh}{dy} = f(k_0 h, \frac{H_0}{wT}, S_0') \tag{4.30}$$

S_0' is the deep-water steepness and wT/H_0 a dimensionless fall velocity of the sediment; T being the wave period belonging to the largest wave energy density in the spectrum and H_0 the rms- deep water wave height. The wave number k_0 equals:

$$k_0 = \frac{4\pi^2}{gT^2} \tag{4.31}$$

Clearly, y being the offshore direction, the lefthand sides of (4.27) and (4.31) denote the same variable; furthermore the attractiveness of the presentation according to (4.31) is evident, inviting to solve the differential equation, thus yielding the dimensionless equilibrium profile:

$$k_0 h = f(k_0 h, \frac{H_0}{wT}, S_0') \tag{4.32}$$

Unfortunately, shortcuts are necessary. Sophisticated present wave height formulae as used in Crostran [32] take into account, that also at horizontal shoals waves decay. Therefore, formula of the kind (4.35) [33] are outdated:

$$\frac{H_{rms}}{h} = f(kh, S_0') \tag{4.33}$$

where k is the local wave number. In fact, the ratio H_{rms}/h can have various values for the same values of kh and S_0' However, for a gentle downward slope in seaward direction an approximation like the one, given in [33] is reasonable; it has been used here because an approximation like (4.33) is essential for the derivation of an equation like (4.29).
Then it is possible to write all the equations of the Stive model [11] in a dimensionless way [20], thus resulting in equilibrium profiles, depending on H_0/wT and S_0' (fig 4.7a,b) [2)].
As $<q_{as}>$ and $<q_{un}>$ counterbalance each other when the fraction of breaking waves increase ($<q_{un}>$ will then be seaward and increases), from (4.27) it shows that moving from the seaward side into the breaker zone, the bottom slope will decrease and become zero at a certain level. Landward of this point, the approximation has no sense any more, as (4.33) looses its validity. Thus anyway the existence of (an outer) breakerbar(s) can be explained, in a way resembling to the qualitative description of Dyhr Nielsen & Sorensen [33].
Also Bailard [10] calculates equilibrium slopes as function of similar parameters as given here. However, as Bailard does not take seaward undertow by breaking waves into account (as done by Stive) he finds very steep equilibrium slopes for small values of $k_0 h$. For further comparison is referred to V.d.Kerk [20].

---

[1] When the harmonics are given as cosine-functions of time
[2] For the undertow the formulation of [29] has been used as [30] was not yet published at the time of the investigation

A global comparison with Dutch coastal slopes in the offshore zone, of which data is presented by Postma & Kroon [35] shows a reasonable correspondence, when waves of small steepness are presumed.

Unfortunately, one cannot find cross-shore interactions between beach and inshore, starting from the above calculated equilibrium profiles, as the equilibrium profiles found are only valid outside the breaker zone, i.e.seaward of the inshore. However, one can investigate the behaviour of the offshore zone, following the ideas of the two-line theory. This in order to get an impression of the time-scales involved in the cross-shore processes in this zone.

Consider the dimensionless profiles of fig.4.7 somewhat closer. These will be schematized as shown in fig. 4.8.

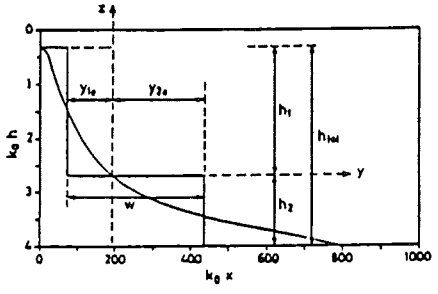

Figure 4.8: Schematization of the offshore zone in a "beach"" and an inshore""

The upper boundary is taken at the site of the outer. breaker bar, (depth: k_0h_{bar}); the lower at the boundary of initiation of motion, which has been tentatively taken as:k_0h= 4. The origin of the y-axis will be chosen at the mean position of the depth contours, i.e in the "hinge point" at a level k_0h_1 in such a way, that the content of the water landward of the vertical plane through the origin equals the volume of the (wet) sand seaward of that plane.

Call in the terms of the two-line theory the area above the level k_0h_1 the "beach" and the area below (up to the level k_0h= 4) the "inshore" (although these terms are here not totally appropriate). Let k_0h_{tot} be the height of the total considered area. Schematize beach and inshore as a stepwise profile, thus creating vertical planes, having the mean position of the depth contours of beach and inshore respectively (fig.4.8); these planes have a distance to the vertical xz- plane of respectively y_{1e} (in landward direction) and y_{2e} (in seaward direction) [1]. The equilibrium distance W in the considered case thus is $y_{1e}+ y_{e2}$. From continuity ($h_1y_{1e} = h_2y_{2e}$, where h_2 is defined as $h_{tot}-h_1$) one finds:

$$y_{1e} = \frac{h_2}{h_{tot}} W \tag{4.34}$$

Consider now a profile, having at every height a slope, being a factor α larger than the equilibrium slope β_e, where α is a fraction, somewhat larger than 1. If such slopes would have been integrated to give a profile, one would have found a distance between beach and inshore being W/α.
The distance y_1-y_2 between beach and inshore thus becomes (in linear approximation) $(\alpha-1)W$ smaller than the equilibrium distance, thus giving an offshore transport S_y (eqn. 4.1) of:

$$S_y = s_y(\alpha - 1)W \tag{4.35}$$

Generalizing (4.34), one finds for y_1:

$$y_1 = \frac{h_2}{h_{tot}} \frac{W}{\alpha} \tag{4.36}$$

The continuity equation reads:

[1] returning to nature and omitting the reference "k_0"

$$h_1 = \frac{dy_1}{dt} = -S_y \tag{4.37}$$

Differentiating (4,34) to *t* and substituting respectively (4.37) and (4.35) into (4.34) gives a differential equation in α-*1*, showing (for small values of α-*1*, compared to 4.1 a negative-exponential decay of α-*1*:

$$(\alpha - 1)_t = (\alpha - 1)_0 \exp(-t/T_0) \tag{4.38}$$

with: $$T_0 = h_1 h_2 / (S_y h_{tot}) \tag{4.39}$$

From (4.35) can be derived:

$$\frac{dS_y}{d\alpha} = s_y W \tag{4.40}$$

On the other hand, the gradient of S_y with respect to α is given by (4.28). By dividing this transport gradient by g^2T^3, (T being the wave period), (4.28) can be written in a dimensionless way. Let the dimensionless $<q_{s1}>$ be: $<q_{s1}>_{dim}$. Then eq. (4.28) can be written as a known function f_1 of the following dimensionless variables:

$$\frac{<q_{s1}>_{dim}}{\tan\beta_e} = f_1(S_0', \frac{H_{rms}}{wT}, k_0 h) \tag{4.41}$$

For the comparison with (4.40) the value of k_0h at the hinge point (i.e. $h = h_1 + h_{bar}$) will be relevant. Equalizing the righthand sides of (4.40) and (4.41)gives:

$$f_1(S_0', \frac{H_{rms}}{wT}) = \frac{s_y W}{g^2 T^3} \tag{4.42}$$

Substituting S_y, as given in (4.42), into (4.39) yields:

$$\frac{T_0}{T} = \frac{(\frac{W h_1 h_2}{h_{tot}})_{dim}}{16\pi^4 \cdot f_1(S_0', H_{rdms} / wT)} \tag{4.43}$$

where '[ ]$_{dim}$" indicates dimensionless variables (all the variables between the brackets, having the dimension "length", should be multiplied by k_0).
Thus the procedure for calculating the dimensionless time of decay of a disturbance is the following. Start from one of the dimensionless profiles, given in fig.4.7, valid for a certain value of S_0' and H_{rms}/wT. Calculate the area of "sand" in this profile and divide this by $4\text{-}k_0h_{bar}$ where k_0h_{bar} denotes the dimensionless height of the outer breaker bar. Let the division result in a distance k_0y'. Draw a vertical line at a distance k_0y' from the righthand side of the figure; on the lefthand side of the line is the "beach", on the righthand side the "inshore". Determine the height k_0h_1 (with respect to k_0h_{bar}) of the intersectionpoint of the vertical line with the profile.
Determine the area of sand above the level k_0h_1 and divide this by k_0h_1. this gives k_0y_{1e}' (y-coordinate of the line of the beach with respect to the lefthand side of the figure). Determine the coordinate k_0y_{2e}' of the inshore in a similar way; the distance between the line of the beach and the line of the inshore gives k_0W. In this way the numerator of eqn.(4.43) is determined; for the calculation of the denominator is referred to [20].
Very large time scales result from (4.43).

The following concluding remarks should be added.

- During the explanation, given above, the effect of the change of the undertow (and thus of the offshore transport) by a change of the coastal slope has not been considered. Not only the rate of change of the gravity transport (4.28) determines the equilibrium slope. In [20], this effect has been included in the computations by an iteration procedure.
- Only the sand balance between beach and inshore has been considered during the derivation of (4.43). It has not (yet) been investigated, whether it is allowed to assume a common time scale of a over the whole profile.
- It would be interesting to combine the results of the present study with the investigations on more-line theories, given in [4]; however, it is still more relevant to investigate the interaction in the surf zone with the breaker bars.

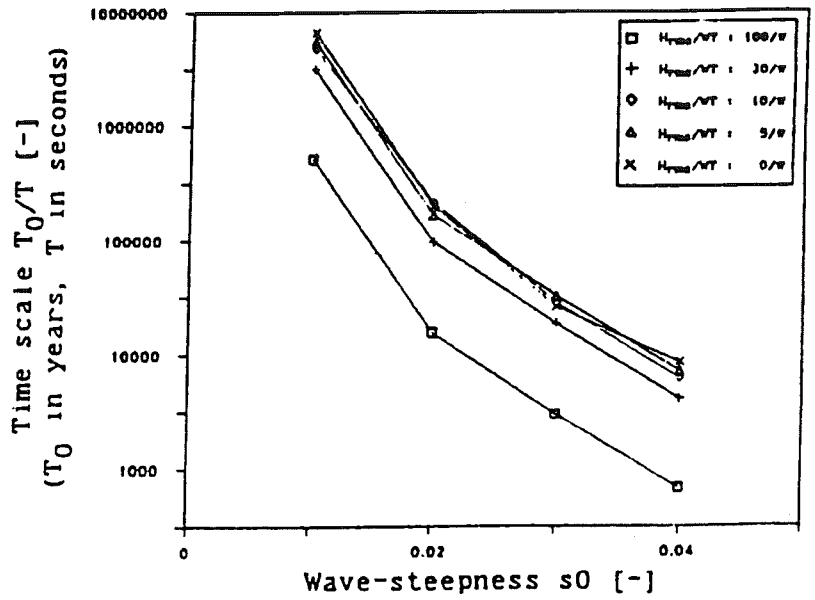

Figure 4.9: Dimensionless time scales T_0/T of restoration to the equilibrium profile

4.5 Literature

1. Bakker W.T;
   The dynamics of a coast with a groyne system

2. R.W.S. CUR en Delft Hydraulics;;
   Manual on artificial beach Nourishment

3. W.T. Bakker;
   Sand waves on the Vliehors
   Shore and beach, 1968

4. J.H. de vroeg, E.S.P. Smit and W.T. Bakker;
   Coastal Genesis
   Proc. 21th Int. Conf. On Coastal Engng. Malaga, 1988

5. E.T.F.M. Bruning;
   The accurancy of two-line models, tested on the German Wadden island Sylt
   Delft University of Technology, Coastal Engng. Group. M. Sc. Thesis (1988)

6. A.J. Andringa;
   Sand Nourishment at Zeebrugge
   Delft University of Technology, Coastal Engng. Group. M. Sc. Thesis

7. W.T. Bakker, H.G.H. ten Hoopen, G.R.M. Grieve;
   Computation of sandtransport according to the method of Svasek for a beach and inshore. Making an angle with each other.
   R.W.S. Dept for Coastal Res. Rep. WWK 71-18

8. J.N. Svasek;
   The influence of breaking waves on the stability of sandy coasts.
   Deltadienst, Waterloopkundige afdeling, Nota W 68.083 (1968)

9. D.M. Swart;
   offshore sediment transport and equibrium profiles.
   Delft Hydraulics laboratory, Publ. 131 (1974)

10. J.A. Bailnard;
    An energetics total load sediment transport model for a sloping beach.
    Journal of Geoph. Res. Vol 86. No. C11, pp. 10938-10934 (1981)

11. M.J.F. Stive;
    A model for cross-shore sediment transport
    Proc. 20th Int Conf. On Coastal Engng. Taipei 1986.

12. W.T. Bakker;
    Computation of the wave induced littoral drift according to the Svasek -method, adapted to parallel depth contours.
    Dept for Coastal Res. Rep. WWK 71-2

13. G. van Beschove;
    The GB2 diffraction program
    RWS, Dept. For Coastal Res. Memo 72-18

14. G. van Beschove;
    The GB4 refraction program
    RWS, Dept. For Coastal Res. Memo 71-19

15. G. van Beschove;
The GB6 refraction program
RWS, Dept. For Coastal Res. Memo 73-6

16. J.A. Castelyn;
numerical computations of the changes of coastal shapes under the influence of wave attack
Delft University of technology, Coastal Engng, group, techn. Rep, 75-1 (part I, II and III); M.SC.Thesis

17. H.G.H. ten Hoopen, W.T. Bakker;
Erosion problems of the Dutch island of Goeree.
Proc. 14th Conf. On Coastal Engng., Copenhagen, 1974 pp. 1213-1231

18. E.W. Bijker, J.N. Svasek;
Two methods for determination of morphological changes induced by coastal structures.
XXIInd Int. Nav. Congress 1969, Paris, section II, item 4.

19. J. Janssen;
Investigation of the coastal development and the sand transport at Scheveningen.
Delft University of technology, Coastal Engng, group, M.Sc.Thesis (1974)

20. C.P.T. vd Kerk
Theoretical calculations concerning the coastal constant s_y , starting from the Crostan conception.
Delft University of technology, Coastal Engng, group, M.Sc.Thesis (1987)

21. W.T. Bakker;
Coastal Constant computations
Tidal waters division, notitie GWAO 89.309

22. W.T. Bakker, T. Edelman;
The coastline of river delta's
Proc. 9th Conf. On Coastal Engng. Tokyo, 1963 pp. 199-218

23. W.T. Bakker;
The influence of longshore variation of the wave height on the littoral current.
Rijkswatertaat, Dep. for Coastal Res. Study rep. WWK 71-19 (1971)

24. D. Jas;
Detailed research concerning a new harbour entrance
Delft University of technology, Coastal Engng, group, M.Sc.Thesis

25. M.J. Dijkman, J.H. de Vroeg, W.T. Bakker;
Hundred-year prediction for the Holland coast
Paper submitted for the 22nd Int. Conf. on Coastal Engng. Delft 1990

26. R. Pelnard-Considère;
Essai de théorie à l'evolution des formes de rivages en plages de sables et de galets.
Quatrième Journées de l'Hydraulique, Paris 13-15 Juin 1954 Les Energies de la Mer, Question 3.

27. J.v. Overeem
Numerical model for the computation of coastal changes, caused by waves and tides
Delft University of technology, Coastal Engng, group, M.Sc.Thesis

28. R.A. Bagnold;
The flow of cohesionless grains in fluids
Phil. Trans. Roy. Soc. Series A, no 966,249 (1956)

29. M.J.F. Stive, H.G. wind;
Cross shore mena flow in the surf zone
Coastal Engineering, no4, p. 325-340

30. H.J. de Vriend, M.J.F. Stive;
Callibration and verification of a dissipation model for random breaking waves
of Geoph. Res. Vol. 90, no C5, 1985, pp. 9159-9167

31. J.A. Battjes, M.J.F. Stive;
Calibration and verification of a dissipation model for random breaking waves.
J. of Geoph. Res. Vol 90, no C5, 1985, pp. 569-578

32. J.A. Battjes, M.P.F.M. Janssen;
Energy loss and set-up due to breaking of random waves
Proc. 16th Int. Conf. on Coastal Engng. 1987, pp. 569-578

33. J.A. Battjes;
Computation of set-up, longshore currents, run-up and overtopping due to wind-generated waves.
Delft University of technology, Ph. D.Thesis (1974)

34. M. Dyhr-Nielsen, t. Sorensen;
Some sand transport phenomena on coasts with bars.
Proc. 12th Int. Conf. on Coastal Engng., 1970, pp. 855-866

35. W.T. Bakker, E.S.P. Smit,
Possible truth about coastal behaviour.
Tidal Waters Division, Rep. GWAO 87.004

36. J.H. de Vroeg;
The use of Kalman filtering for investigation of coastal behaviour.
Delft University of technology, Coastal Engng, group, M.Sc.Thesis (1987)

37. W.T. Bakker, C. vd Klerk & J.H.de Vroeg;
Determination of coastal constants in mathematical line models.
Second European workshop on Coastal Zones, Loutraki 1988

5. Experimental verification

5.1 Laboratory

5.1.1 Experiments in Delft Hydraulics Laboratory

5.1.1.1 Model facility and test procedure

The lay-out of the model basin is given in Fig. 5.5. A large amount of various conditions were installed, details of which are extensively discussed in [3] As bed material dune sand was used with ρ = 2650 kg m^{-3} and D_m = 0.220 mm. Either 0, 1 or 3 impermeable groynes were present, with their crests well above the water level, with rough 1:1 slopes and aligned perpendicularly to the coast. The spacing was 6 m and their length so that they obstructed the longshore current partly or completely. The regular waves had a period of 1.55 s or 1.15 s, and a height between 0.07 m and 0.14 m. Depending on the wave steepness and the local beach slope, either spilling or plunging breakers occurred, under an angle of appr. 5° with the shore line. Water and sand were fed upstream and caught downstream in order to represent an inifinitely long, straight beach.

In short, the procedure was to try and establish a dynamic equilibrium along a straight beach without groynes, and to assess meanwhile the development of the wave heights, the current velocity, the morphology and the trapped sand distribution. Then, after adding a groyne system, the new hydraulic and bathymetric development were recorded and subsequently compared with the theory. Here only a limited, though typical, selection of the numerous test results is presented, while in Ch. 5.1.3 a discussion is given, making use of some selected measuring data which are deemed useful for a good interpretation of the results.

5.1.1.2 Tests with a single groyne.

Representative as a "good" test isT22, where the main conditions were: wave height 0.075 m, wave period 1.55 s, water depth 0.38 m in front of the wave generators. The average rate of sand nourishment was 71 dm^3hr^{-1}, while 55 dm^3hr^{-1} was caught in the traps. The rate of water supply was constant at 30 dm^3hr^{-1} in order to feed the longshore current. The groyne extended seaward to 4.2 m, whereas the waves broke at appr. 3.5 m. Fig. 5.6 and 5.6a depict the beach, looking upstream, after 0.5 hr and 50 hrs. They show a quite regular accretion upstream, and erosion downstream of the groyne. This is also represented by Fig. 5.6b, a difference chart displaying the extent and the locations of erosion and accretion during the 50 hrs of the test. In an attempt to monitor the actual longshore sand transport by local measurements, the wave height and the longshore current distribution were frequently measured in sections perpendicular to the shore. These data, together with the local depth and the bed material characteristics, are enough to compute the longshore sand transport according to Bijker. Examples are given in Figs. 5.7a and 5.7b for a section 8 m upstream of the groyne, and at the groyne itsel respectively. The obvious decrease of the longshore sand transport capacity is in good accordance with the observed accretion of the beach. Fig. 5.7c shows both rates of longshore sand transport in the course of time. Typical accreting and eroding coastal profiles are given in Figs. 5.7d and 5.7e, respectively, the latter together with the distribution of the longshore sand transport as caught in the sand traps.

From Bijker's and Swart 's theories, together with the appropriate data from the experiment, the following quantities were derived for application of the theory:

upper level of beach : 0.51 m
elevation of interface : 0.24 m with respect to the level of the wave generator floor.
lower level of foreshore: : 0.18m

s_{01} = 87 dm^3hr^{-1}; s_1 = 994 dm^3hr^{-1}; s_{02} = 29 dm^3hr^{-1}; s_2 = 332 dm^3hr^{-1}; W= 7.62m; s_y= 0.0338 dm hr^{-1}

The resulting schematized beach- and foreshore-lines for 0.10 and 50 hrs are given in Fig. 5.7f, together with the comparable theoretical lines. The fit is quite good, especially for the

beach-lines. It is thought that this favourable result was reached under the influence of an extraordinarily regular breaker type (plunging), which was accompanied by a very regular longshore current. More over the groyne interrupted the longshore current almost entirely, thus obstructing the longshore transport of sand to a great extent.

Another test with a single groyne, T18, contrasted sharply with the above resullts main conditions were: wave height 0.10 m, wave period 1.55 s, water depth 0.38 m in front of the wavegenerators, average rate of sand nourishment 88 dm^3hr^{-1}, while 106 dm^3hr^{-1} was caught in the traps. The water discharge was constant at 55 dm^3s^{-1} In Fig. 5.8a the contours after 60 hrs are shown, where the attention is drawn to the clear accretion, but this time downstream of the groyne. Locally even a new beach line appeared seaward of the original one. The development can be followed on Figs. 5.8b and 5.8c, where difference charts of 0-20 hrs and 20-60 hr are showing how the bulk of the longshore sand transport moved around the groyne in two stages. In the intermediate stage the maximum accretion amounted to 20 cm at some distance downstream and seaward of the head of the groyne. After 20 hrs the bulk of this sand deposit was removed and shifted in shoreward direction, and somewhat more downstream. Fig. 5.9a shows that neither the upstream nor the downstream overall profile was subject to large changes. It also points towards a possible reason for the remarkable developments encountered here: the trapped sand distribution, averaged over 60 hrs, indicates that the groyne could hardly be expected to stop the longshore transport. However, the average trapped sand distribution in the preceeding test T17 (without groyne), was used to design this groyne length such that it would stop approximately 50% of the existing longshore sand transport.
After the above explanation it is not surprising that the experimental results are not well covered by the theoretical beach- and foreshore-lines (Fig. 5.9b), which are based on the following data:

upper level of beach : 0.46 m
elevation of interface : 0.235 m with respect to the level of the wave generator floor.
lower level of foreshore : 0.06 m

s_{01} = 73.5 dm^3hr^{-1}; s_1 = 840 dm^3hr^{-1}; s_{02} = 65 dm^3hr^{-1}; s_2 = 742 dm^3hr^{-1}; W= 10.08m; s_y= 0.029 dm hr^{-1}

The impression exists from various observations (see also Chapter 5) that secondary wave formation, caused by the bar at a distance of 11 m (Fig. 5.9a), may have played an important part in reestablishing the original coastal profile after 20 hrs. It is felt that this type of secondary waves has an important influence on coastal profile dynamics.

5.1.1.3 Tests with a row of three groynes.

In Fig. 5.10a the contours after 50 hrs of test T23 with three groynes are presente The conditions were: wave height 0.075 m, wave period 1.55 s, water depth 0.38 m in front of the wave generators. he average rate of sand nourishment was 44 dm^3hr^{-1} while 27dm^3hr^{-1} was caught in the traps. The average rate of water supply was 25 dm^3hr^{-1}. The groynes extended to 3.7 m. Until 20 hrs a plunging breaker occurre at appr. 3.7 m, whereas later on the spilling type dominated, with variations in breaker location. In Fig. 5.10b a clear rhythmic behaviour is revealed by the difference chart, both in longshore direction (as caused by the groynes) and in perpendicular direction (as caused by an overall coastal profile development). The various quantities with respect to the theoretical computations are:

upper level of beach : 0.51 m
elevation of interface : 0.255 m with respect to the level of the wave generator floor.
lower level of foreshore : 0.160 m

s_{01} = 87 dm^3hr^{-1}; s_1 = 995 dm^3hr^{-1}; s_{02} = 29 dm^3hr^{-1}; s_2 = 331 dm^3hr^{-1}; W= 8.10m; s_y= 0.032 dm hr^{-1}

Fig. 5.10c, displaying the experimental and theoretical lines representing the bead and the foreshore, reveals a reasonable equality as far as the beach is concerned. However, large deviations occur in the foreshore, where the typical rhythmic varations are not found back in the theory.

Test T34 had unusual conditions in so far that the water level fluctuated in a one-hour cycle 0.025 m plus and minus the average of 0.38 m above the wave generator floor. This was

done in order to shift also the type and the location of the breaking waves, in an attempt to avoid rip-current formation at fixed locations. The other conditions were: wave height 0.115 m, wave period 1.15 s, average rate of caught sand 74 dm^3hr^{-1}. The rate of sand nourishment was constant at 70 dm^3hr^{-1}, and the rate of flow was constant at 50 dm^3hr^{-1}. The groynes extended to 3.27 m, whereas the breaker location varied widely during the test. The quantities for the theoretical analysis were:

upper level of beach : 0.49 m
elevation of interface : 0.275 m with respect to the level of the wave generator floor.
lower level of foreshore : -0.01 m

s_{01} = 32.4 dm^3hr^{-1}; s_1 = 370 dm^3hr^{-1}; s_{02} = 35.6 dm^3hr^{-1}; s_2 = 407 dm^3hr^{-1}; W= 8.11m; s_y= 0.108 dm hr^{-1}

The result was not much better than that of test T23, as can be seen on Figs. 5.11a, 5.11b and 5.11c. Fig. 5.11b is a special chart, displaying the difference between test T34 and test T33 (without groynes but further with exactly the same conditions as-T34) after 30 hrs. The pattern of alternating erosion and accretion between the groynes is opposite to what should be expected from the theory. This is most probably caused by an intricate and unstable pattern of currents, stagnation areas, rip currents and regions of lower and higher waves.

5.1.2 Experiments in Laboratori Nacional de Engenharia Civil.

5.1.2.1 Model facility and test conditions.

Reference is made to [4] for details. Fig. 5.12 shows the lay-out of the model. A convex beach profile of pumice-stone (ρ= *1670 kgm^{-3}*, D_m = *1.25 mm*) was molded between two rockfill groynes E1 and E3. These groynes had 2 : 1 absorbent slopes and acted as training walls for the beach. A smaller groyne E2 in between with steep 1:5 slopes completely obstructed the littoral drift. The waves were 0.02 m high, had a period of 1s and were generated under an angle of 20° in a water depth of 0.40 m.

5.1.2.2 Test results and theoretical beach lines.

Various beach line positions were recorded during the 35 hr test, as presented in Fig. 5.13. These are compared to theoretical lines, which were determined as follows [8]. The active profile was schematized to a single beach line, because perpendicular transport across the 0.063 m depth contour was assumed negligible. This depth is twice the breaker depth as calculated for straight, parallel depth contours. Diffraction calculations were performed in the deeper, horizontal part of the basin, where after refraction was calculated up to the 0.063 m contour line, again assuming straight and parallel depth contour lines, remaining so during the whole test. The resulting values for the wave height H_1 and the angle of wave attack ϕ_1 at the 0.063 m depth contour are given in Fig. 5.14.

The final position of the beach is now assumed to be defined by ϕ_1 and H_1 in a first approximation. By ϕ_1 alone, the final beach line is determined by being parallel to the local wave crest as defined by ϕ_1 because only then the net transport along any part of the beach is equal to zero. By H_1 alone on the other hand, differences in wave set-up will develop, causing a varying longshore current velocity V_1 along the beach, where V_1 is a function of various parameters among which the beach line orientation [9]. By putting V_1 equal to zero, the final beach alignment is found. After adding the partial solutions for H_1 and ϕ_1 the final coastline is found as Y_0 in Fig. 5.15. By comparing this line to the experimental 35 hrs-line in Fig. 5.13, some differences can be found:

- In the experiment a certain amount of material does disappear into deeper water. Because Barcelo reports a rip-current near groyne E2, the theoretical line is adapted by taking a sand transporting rip-current into account near E2 with an adequate transport capacity. This will at the same time increase the theoretical beach line angle near groyne E2, bringing it closer to the measured position.
- Differences near groyne E1 are likely to be caused by a very low transport capacity in the model, whereas in the calculation no critical velocity for beginning of movement is used.

For the calculation of the coastline after 1, 4, 7, 15 and 35 hrs the dynamic equation is used (with $s_y = 0$), together with equation (1). Relevant quantitative parameters are: $S_{ripcurrent} = 3.4$ dm^3hr^{-1}, $S_{ol} = 27.8$ dm^3hr^{-1} acc. to Barcelo, $s_1 = 150$ dm^3hr^{-1}.
The resulting theoretical lines are given in Fig. 5.15; they fit quite well with the experimental lines of Fig. 5.13.

5.1.3 Discussion of the results.

The above examples are typical in so far that they indicate the rather large variation in the ability of the theory to fit with the experimental results. One should not be too surprised, in view of the wide deviations which were often present in the actual experimental conditions, as compared to the ideal conditions which were (tacitly) assumed in the theory. The main causes of deviation are discussed below.

- Variations in wave height as measured in cross-sections very close to each other, were frequently noted and were judged to have a strong negative effect on the homogeneous conditions sought. Fig. 5.16 shows a rather dramatic example, in which the wave height variations are at least partly due to the varying bed profiles. Of course there exists a strong mutual interaction between wave behaviour and coastal profile development.
- An example of the progressively deteriorating homogeneity in longshore direction of the coastal profiles is given in Fig. 5.17a. It shows the envelopes of all cross-sections after 10, 30 and 50 hrs in test T19 (without groyne).
- An effect, and simultaneously a cause, of the above mentioned non-homogeneity is present in the chaotic current pattern in the same test, as presented in Fig. 5.32. This test, too, began with a nice homogeneous and steady longshore current.
- Apart from being non-homogeneous, the current pattern was unsteady, as is shown in Fig. 5.18. It gives values of the longshore current in test T25, measured in two points I m apart perpendicular to the coast. The measurements were performed by timing floats over a distance of 1 m.
- Secondary waves were present under certain conditions. Apart from those, generated by the sinusoidally moving wave board [10], also secondary waves were generated while the regular waves passed over a large bar without breaking. In this respect it is interesting to note that Byrne [11] reports the same wave behaviour (long regular swell conditions) in the prototype (Fig. 19). Fig. 20a presents a coastal profile of test T19, with a bar and with the wave height over it; the wave breaks only at a distance of appr. 5 m. The respective wave forms as shown in Fig. 5.20b clearly show the presence of secondary waves (with period T/2) which are overtaken gradually by the faster main waves. Their presence has undoubtedly a large influence on the perpendicular sand transport [10], and further on the type of breaking and the kinematic results thereof. It is felt that the presence of those secondary waves can have a dominating effect on the formation and the stability of coastal profiles.
- The pair of Fig. 5.21a and 5.21b illustrates the strong relationship between secondary waves, bar formation, type of breaker, and subsequently the rate and distribution of the longshore transport. The conversion of the breaker type from spilling to plunging was in very good agreement with Galvin's results as far as the influence of the seaward slope of the breaker bar is concerned [12]. After this conversion the rate of longshore transport was appr. three times as large as before, and much more concentrated.
- The most obvious visible result of the increasingly non-homogeneous conditions in many tests was the formation of beach cusps. Both small (Fig. 5.22) and large (Fig. 5.23) examples have been recorded. It goes without saying that this is most unwelcome in tests which are ment to verify the effect of groynes on a sandy beach. Fortunately, the presence of a groyne appeared to induce a more stable condition, in which the cusp formation was partly suppressed.

5.1.4 Conclusions.

The conclusions which follow from these tests and their comparison with the theory can be summarized as follows.

- The theory is good in cases with a stable, neat, and well defined longshore current system, and if the groyne(s) intercept a substantial part of the long shore sand transport.
- In other, more complex systems, the theory in its present form is not adequate on a forecast basis. However, if the current pattern is well enough defined and specified, the theoretical result may be improved by taking into consideration the effects of stream refraction, diffraction, and rip-currents.
- The coastal current system should be studied in more detail in order to improve the theory of Bakker.

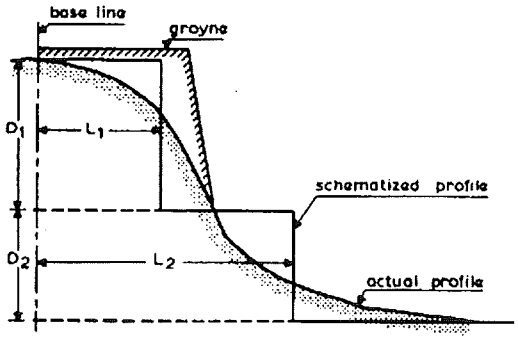

Figure 5-1: Schematization of coastal profile

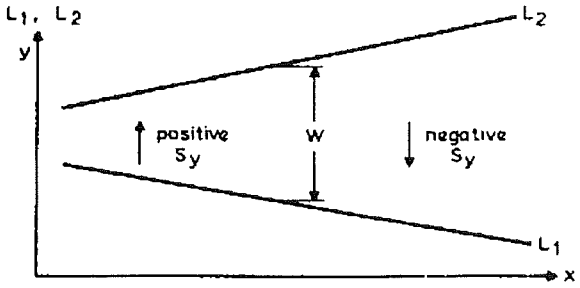

Figure 5-2: Top view of schematized coast lines

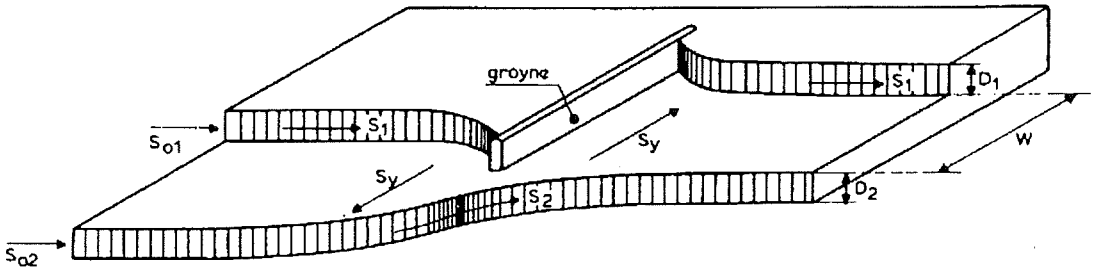

Figure 5-3: Visualization of theoretical coast

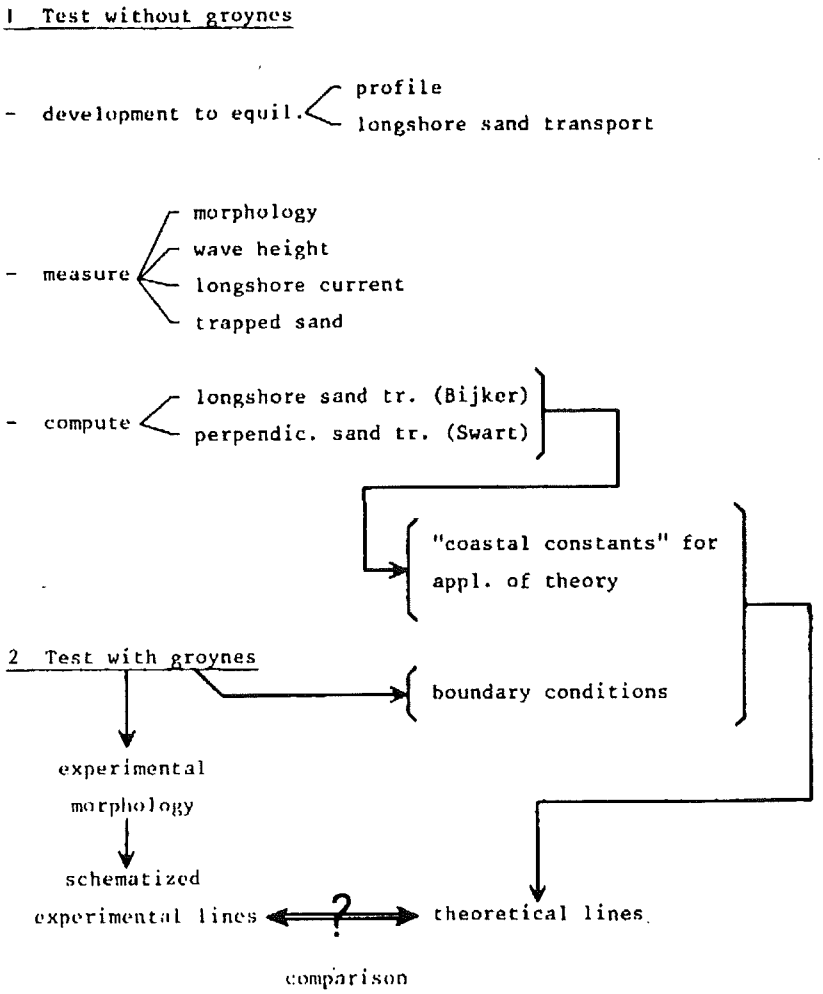

Figure 5-4: Procedure of verification

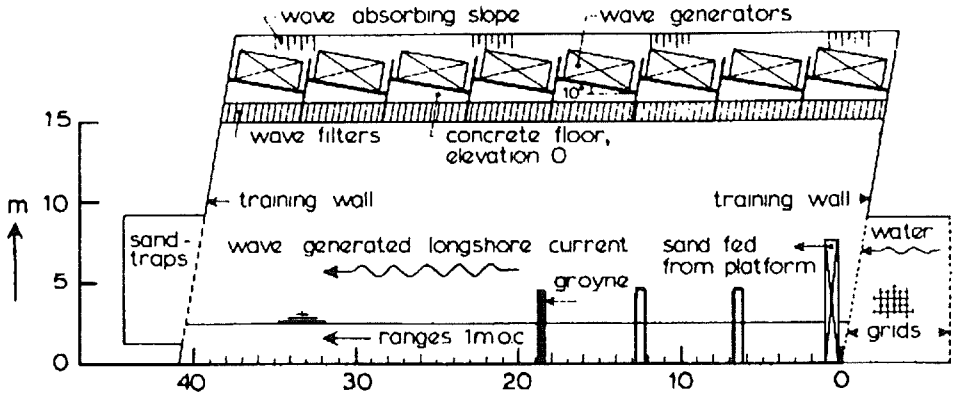

Figure 5-5: Lay-out of model facility

Figure 5.6: Test T22 after 0.30 hrs

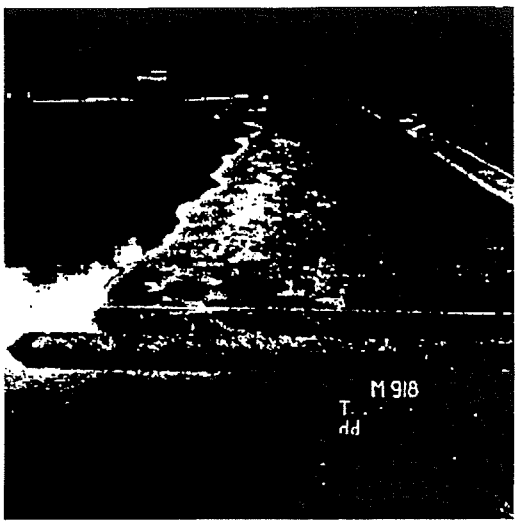

Figure 5.6a: Test T22 after 50 hrs

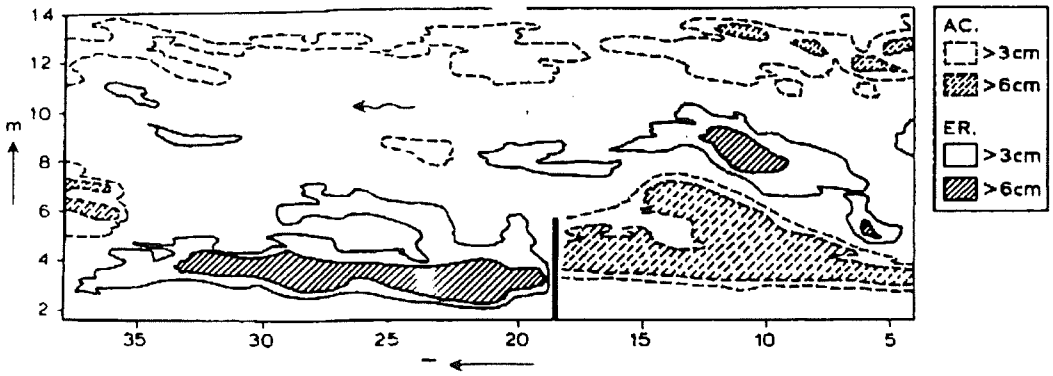

Figure 5.6b: Test t22, difference chart 0-50 hrs

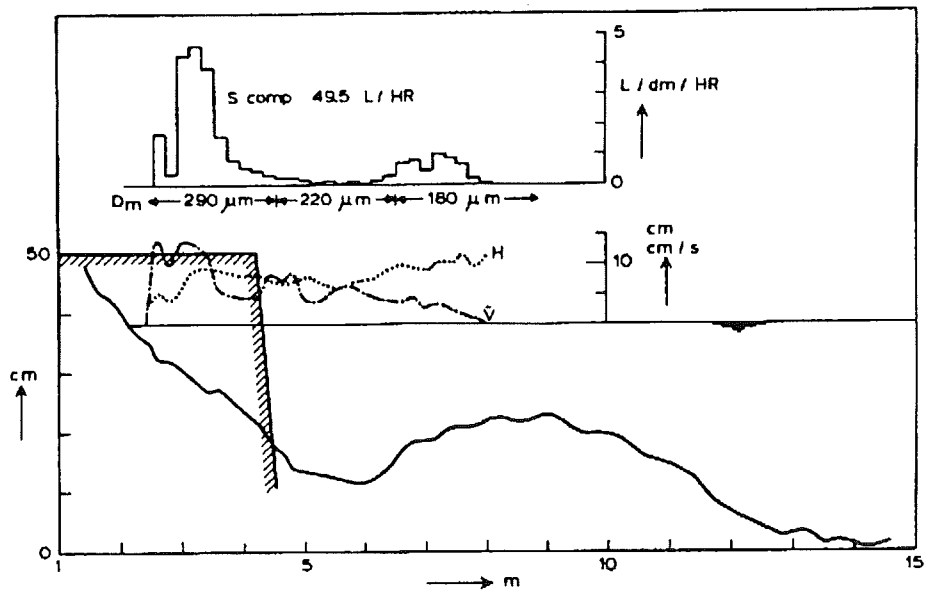

Figure 5.7a: Test T22, 8m upstream of groyne after 3 hrs

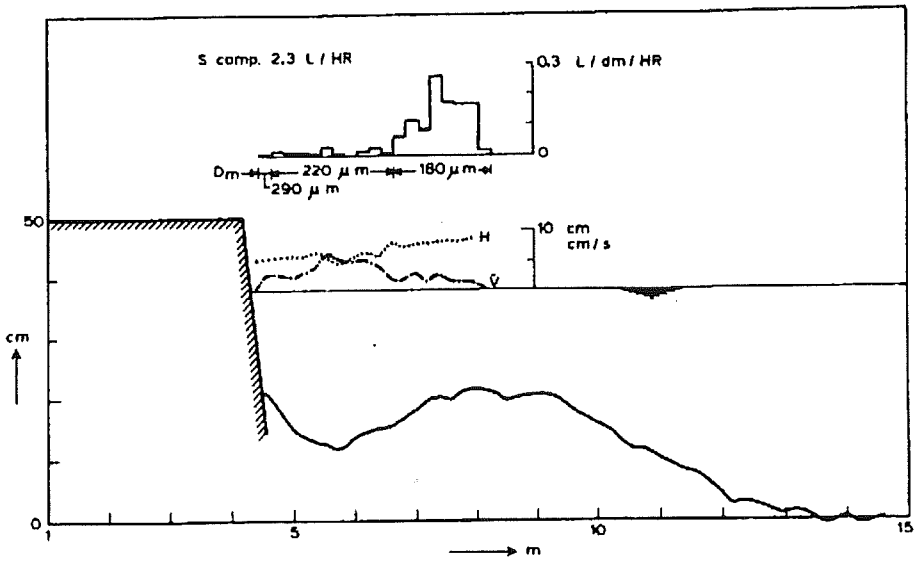

Figure 5.7b: Test T22, at groyne after 4 hrs

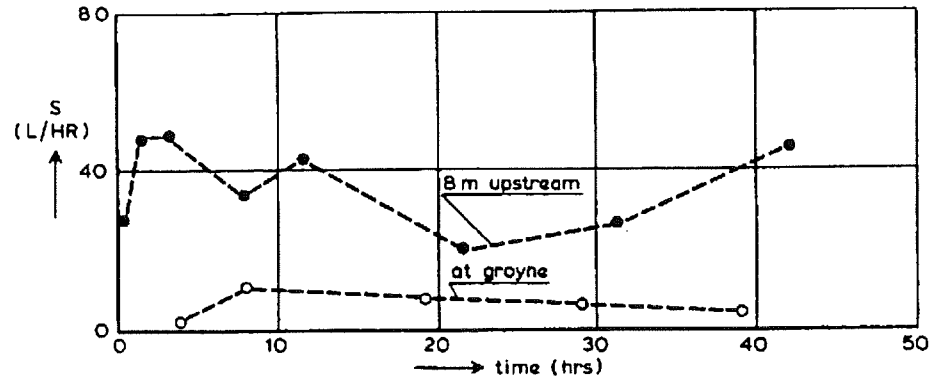

Figure 5.7c: Test T22, longshore transport according to Bijker

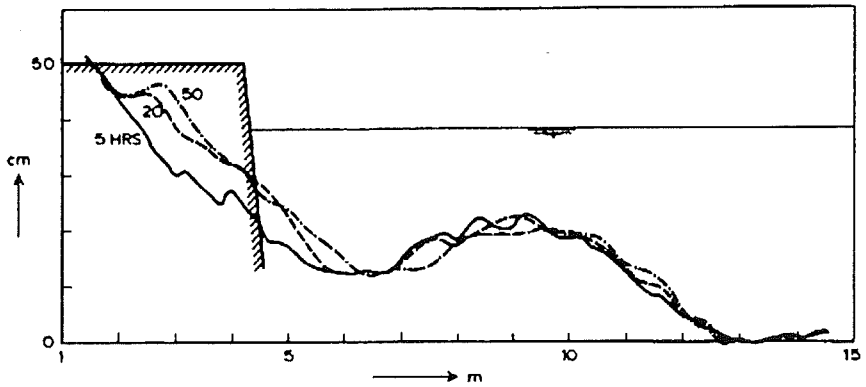

Figure 5.7d: Test T22, 3.5m upstream of groyne

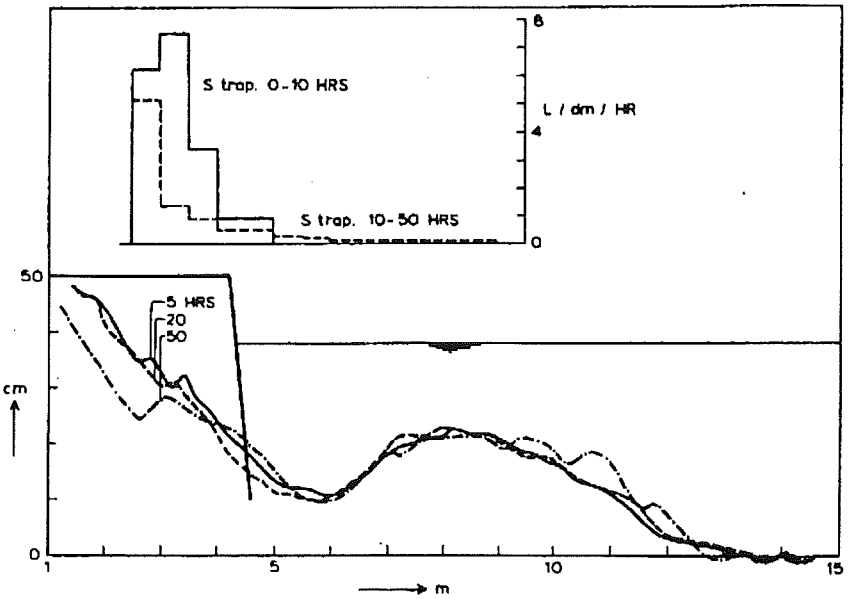

Figure 5.7e: Test T22, 3.5 m downstream of groyne

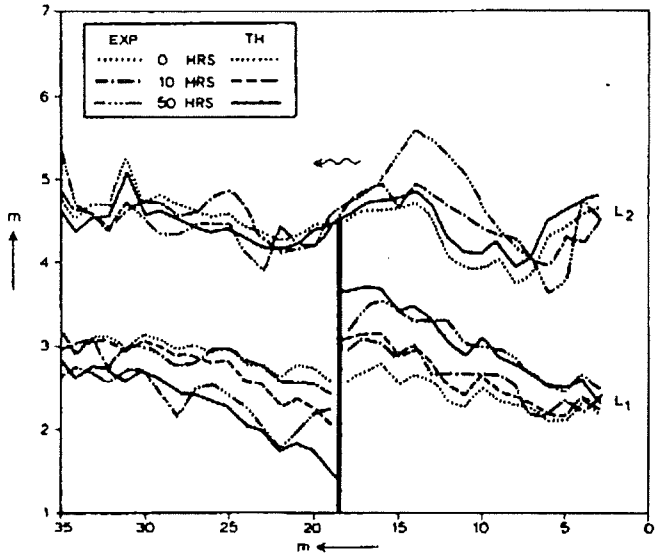

Figure 5.7f: Test T22, comparison of beach- and foreshore-lines

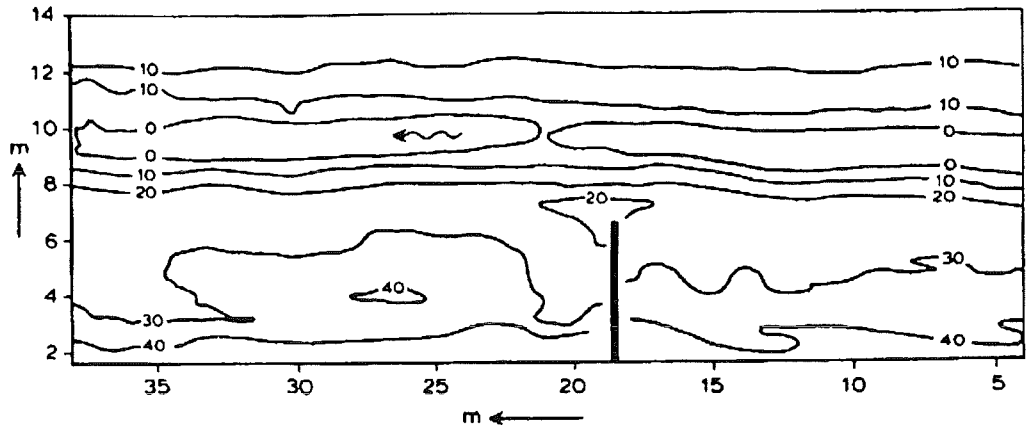

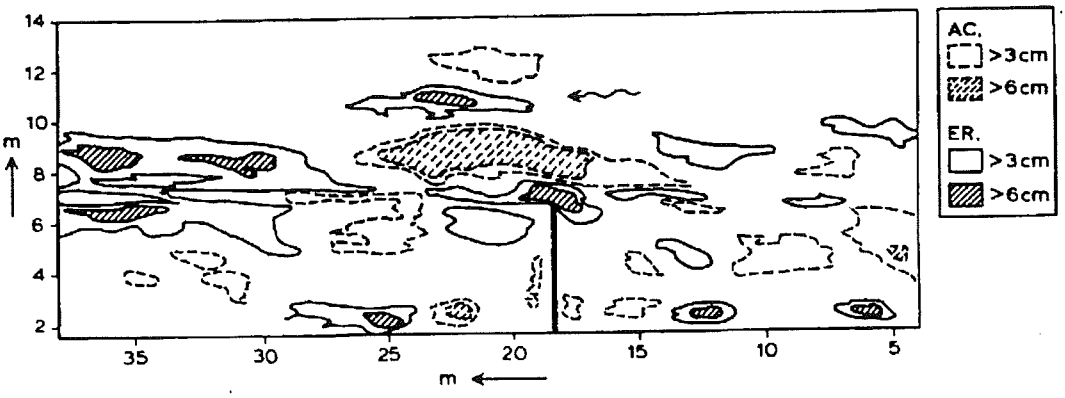

Figure 5.8a: Test T18, 60 hrs, contours in cm above model datum

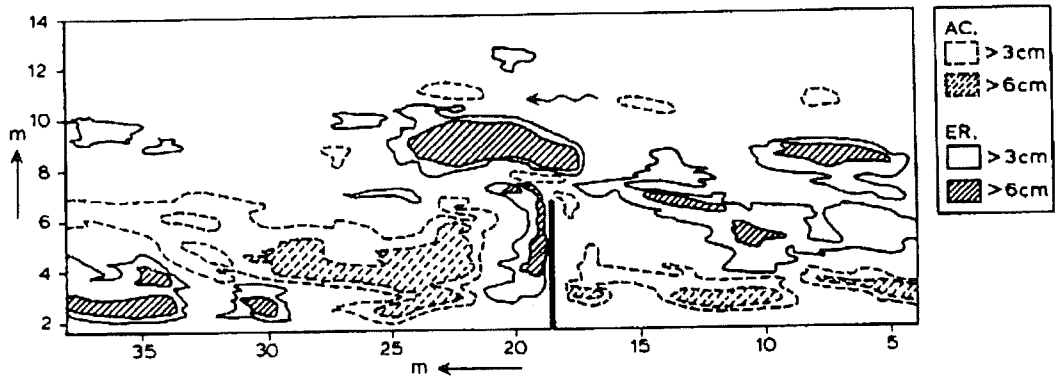

Figure 5.8b: Test T18, difference chart 0-20 hrs

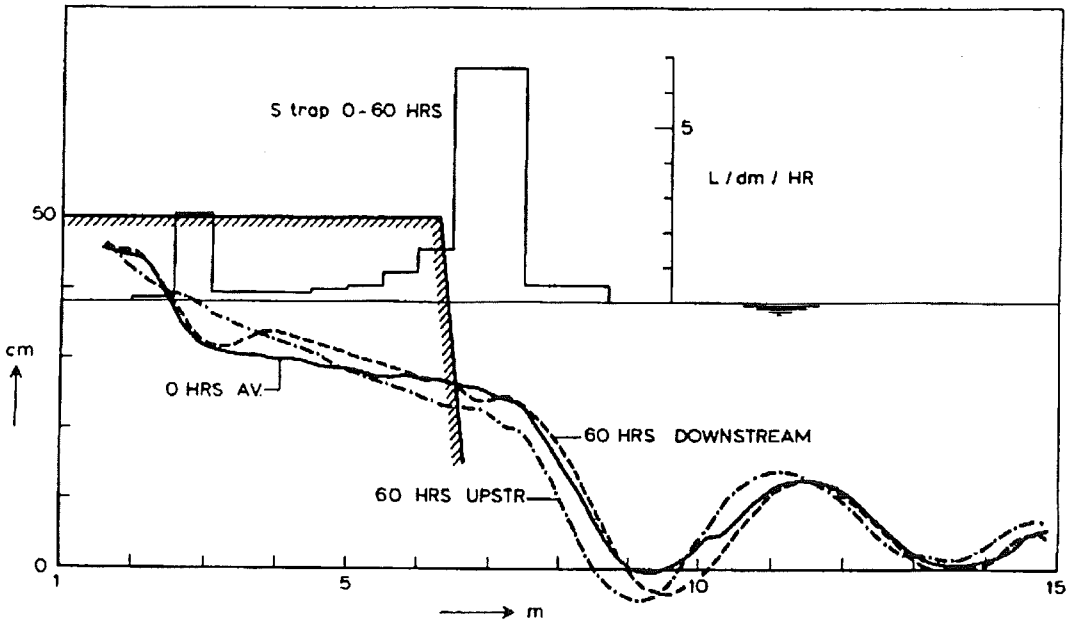

Figure 5.8c: Test T18, difference chart 20-60 hrs

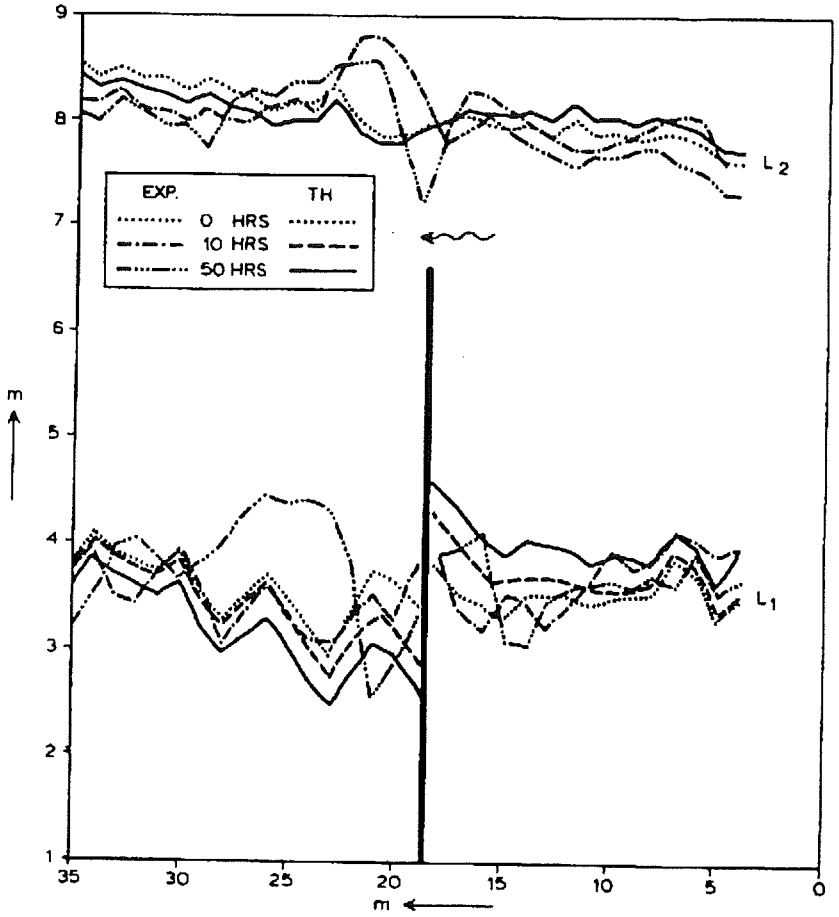

Figure 5.9a: Test T18, average upstream and downstream profiles

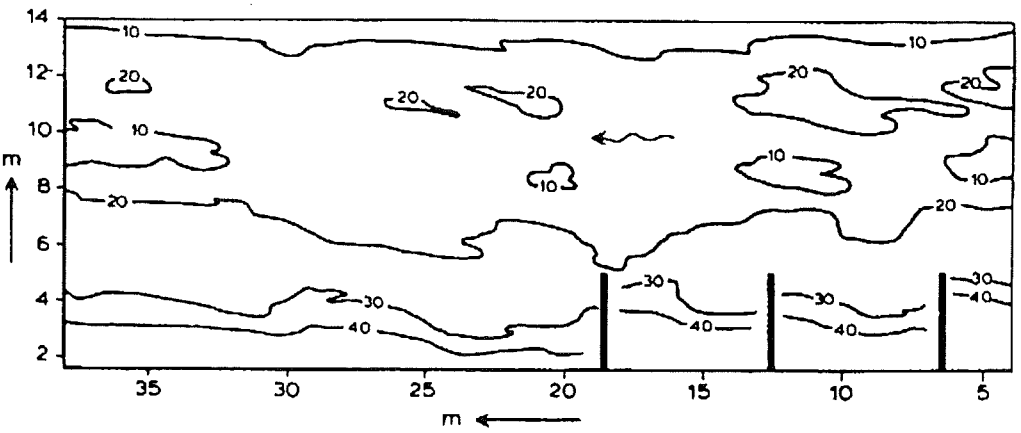

Figure 5.10a: Test T23, 50 hrs, contours in cm above model datum

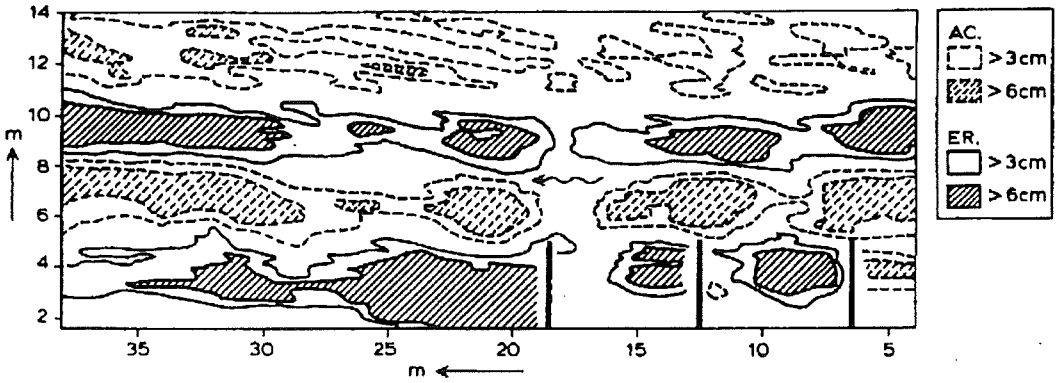

Figure 5.10b: Test T23, difference chart 0-50 hrs

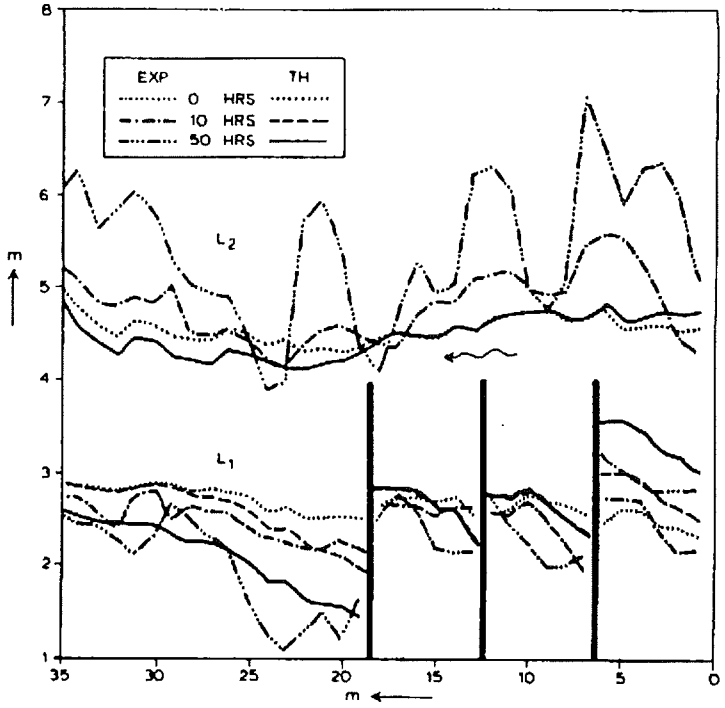

Figure 5.10c: Test T23, comparison of beach- and foreshore-lines

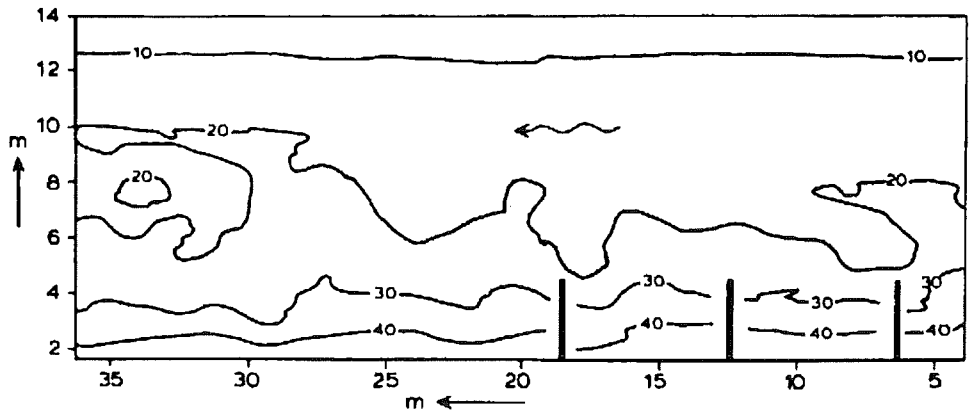

Figure 5.11a: Test T34, 45 hrs, contours in cm above model datum

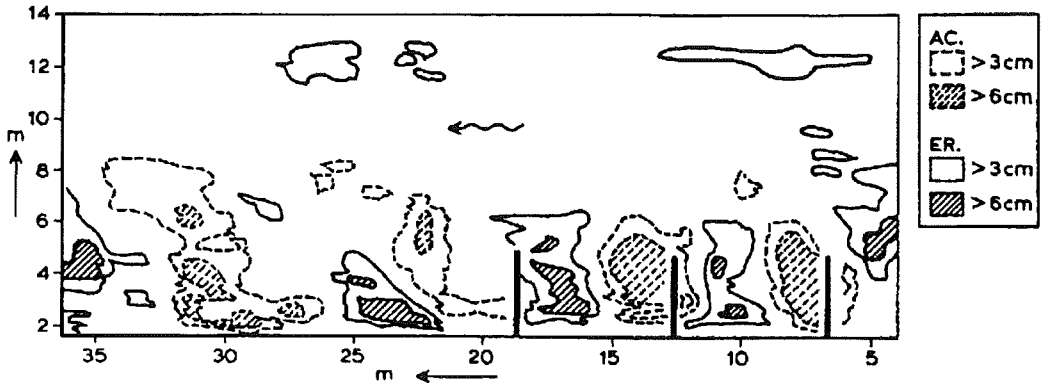

Figure 5.11b: Test T33/34, groyne effect 30 hrs

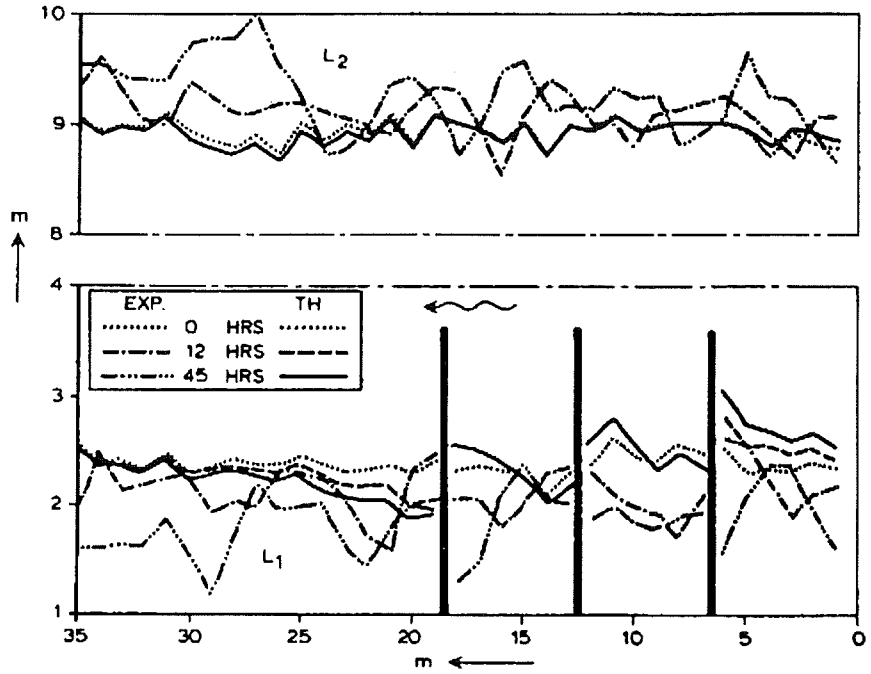

Figure 5.11c: T34, comparison of beach- and foreshore-lines

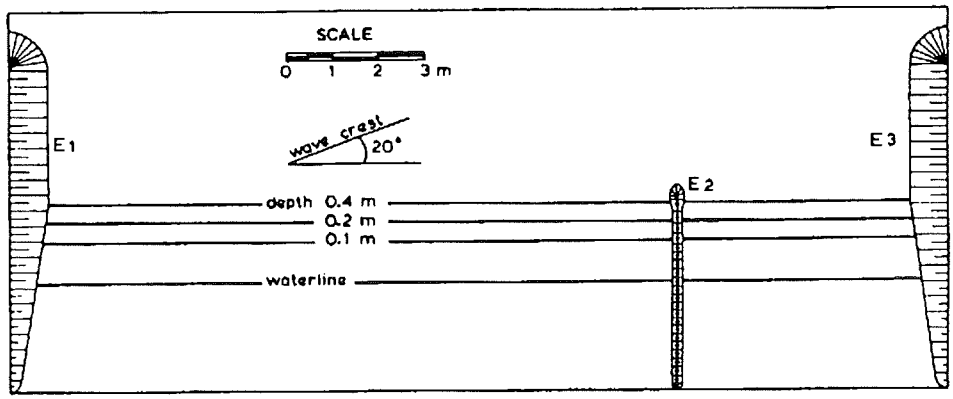

Figure 5.12: LNEC test, lay-out of model basin

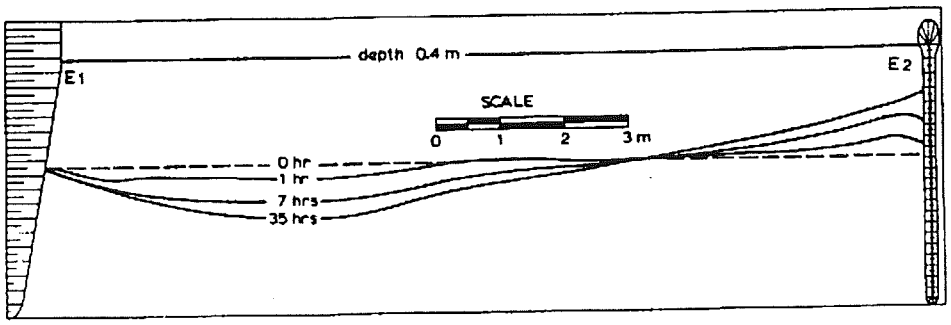

Figure 5.13: LNEC test, experimental beach lines

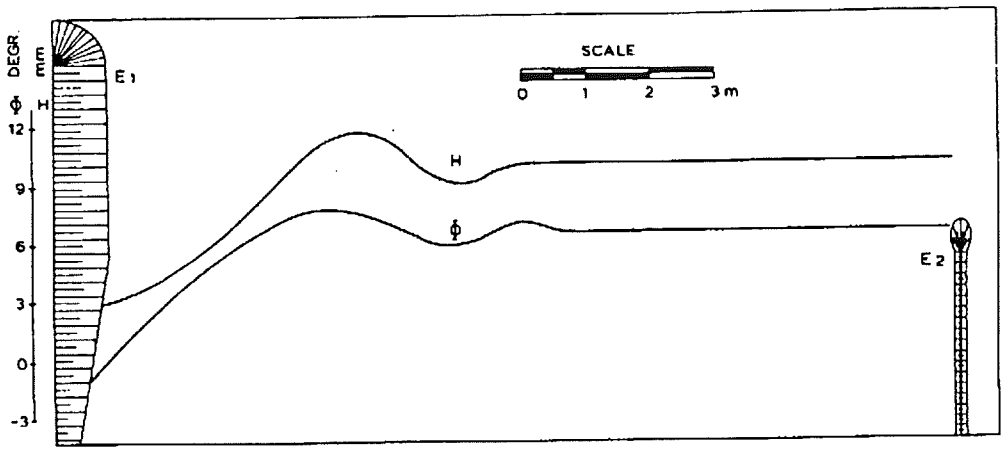

Figure 5.14: LNEC test, wave height and angle of wave incidence

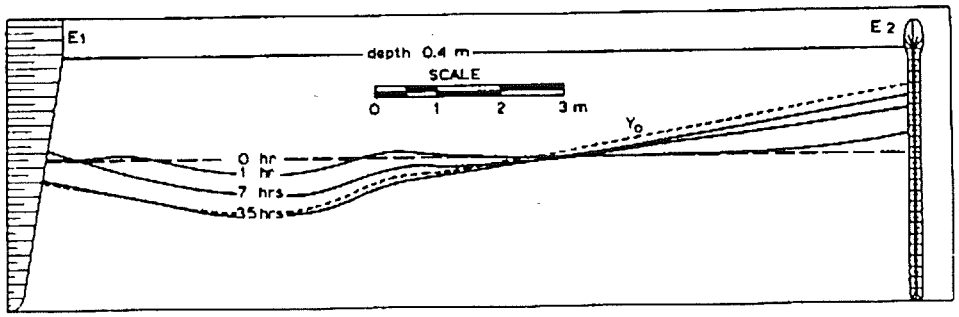

Figure 5.15: LNEC test, theoretical beach-lines

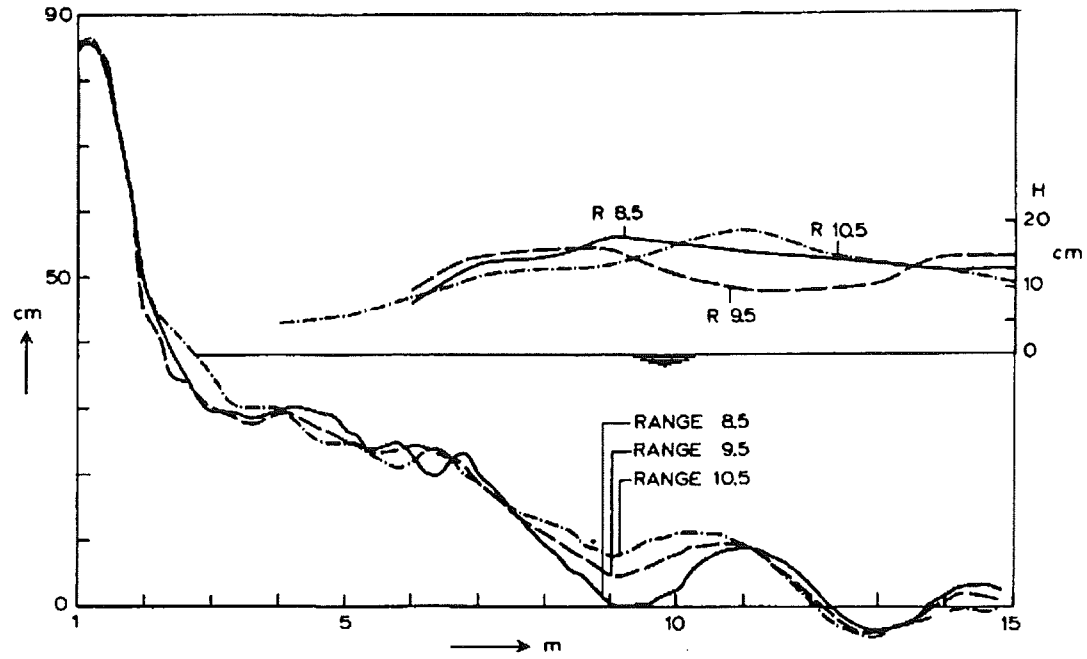

Figure 5.16: Test T2, variety in beach profiles and wave heights

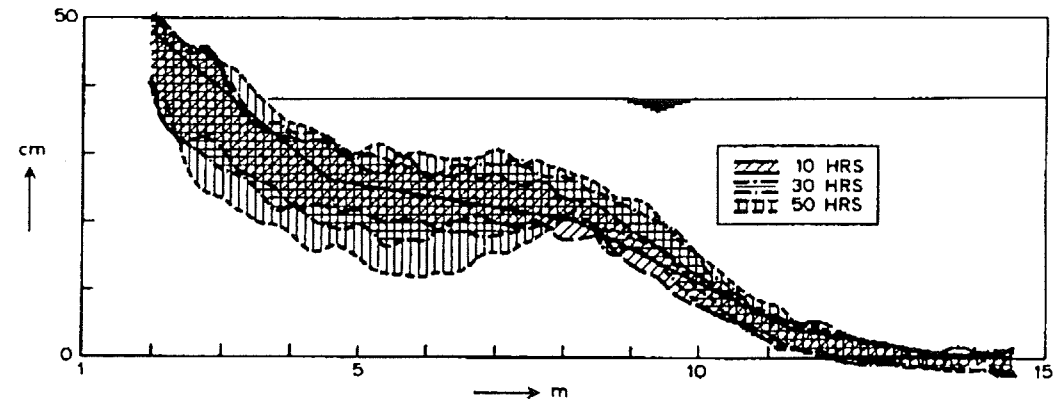

Figure 5.17a: Test T19, envelopes of beach profiles

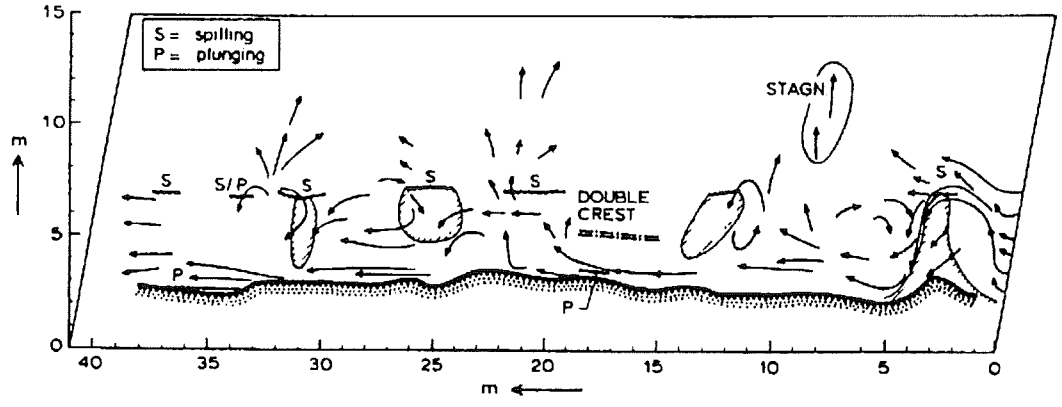

Figure 5.17b: Test T19, current pattern 77 hrs

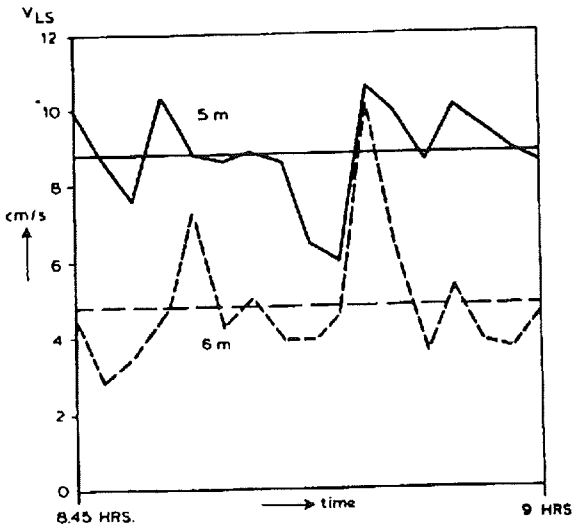

Figure 5.18: Test T25, unsteadiness in longshore current velocity

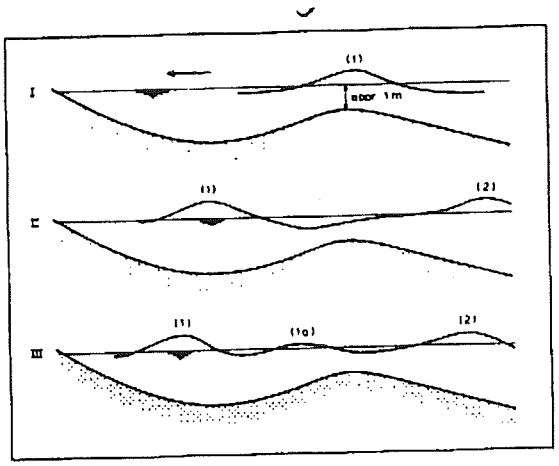

Figure 5.19: Prototype observation of induced multiple gravity waves (after Byrne)

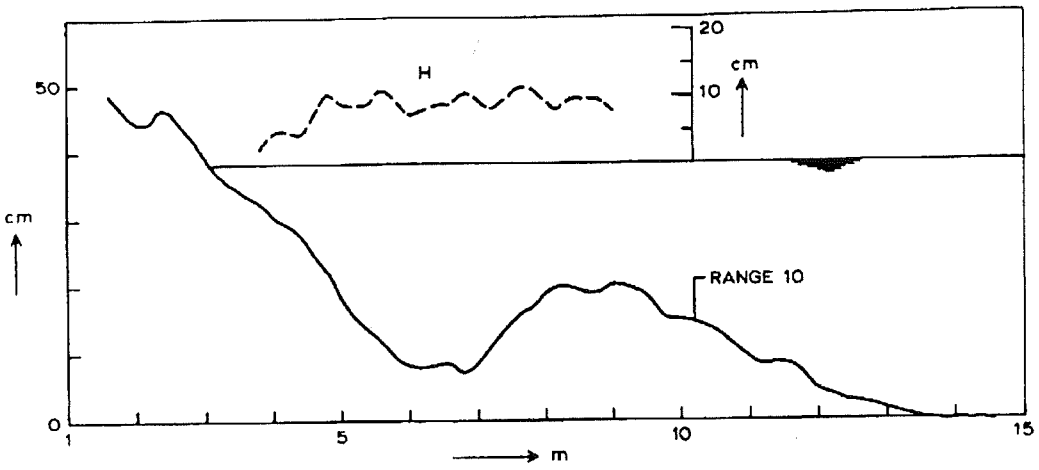

Figure 5.20a: Test T19, 105 hrs, bar profile and wave height

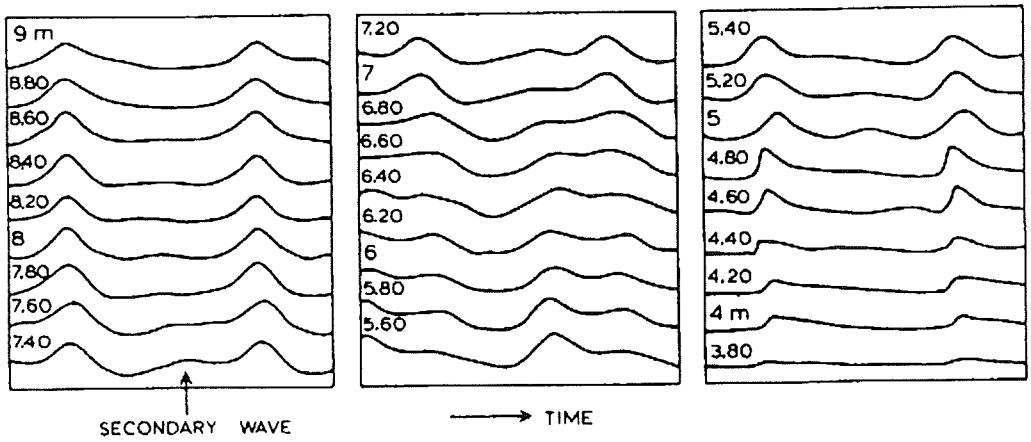

Figure 5.20b: Test T19, wave forms over bar profile from fig. 20a

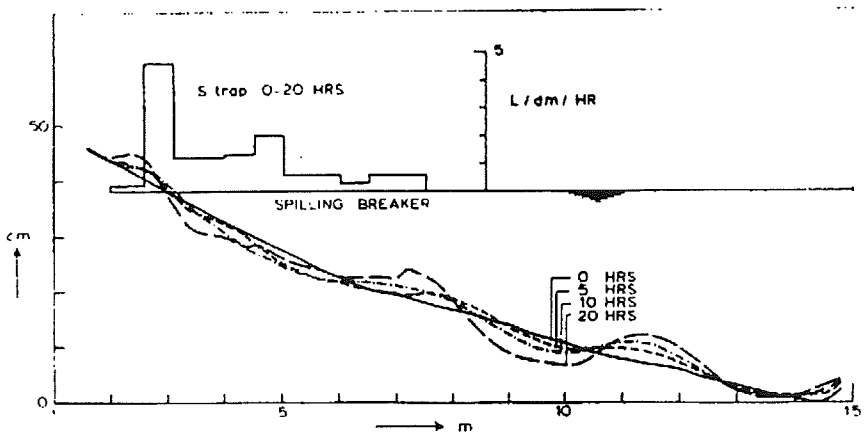

Figure 5.21a: Test T17, spilling breaker conditions 0-20 hrs

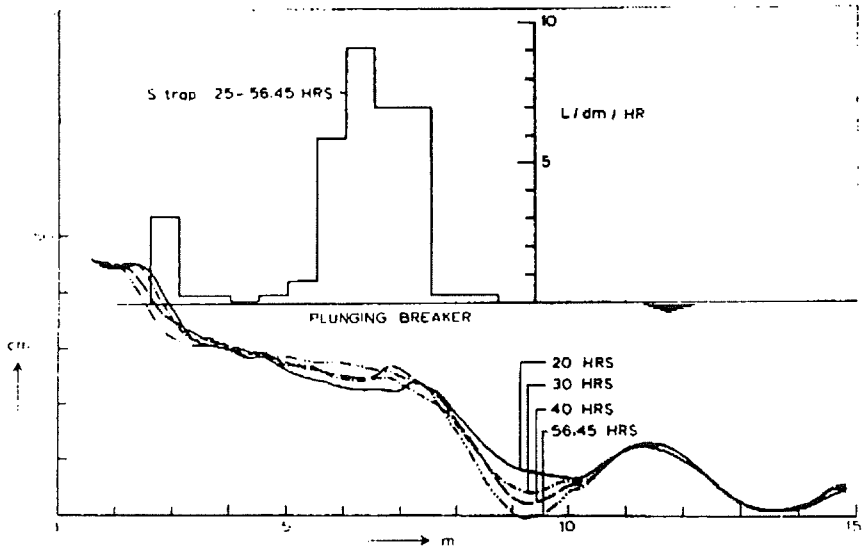

Figure 5.21b: Test T17, plunging breaker conditions 20-56. 45 hrs

Figure 5.22: Test T19, small scale beach cusps

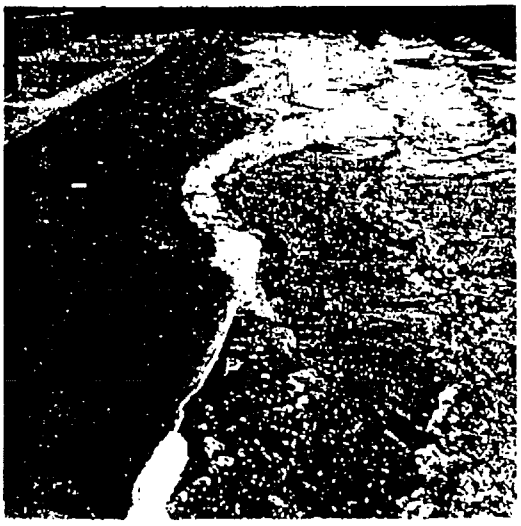

Figure 5.23: Test T27, Large scale beach cusps

5.2 Nature

5.2.1 introduction

5.2.2 Vliehors

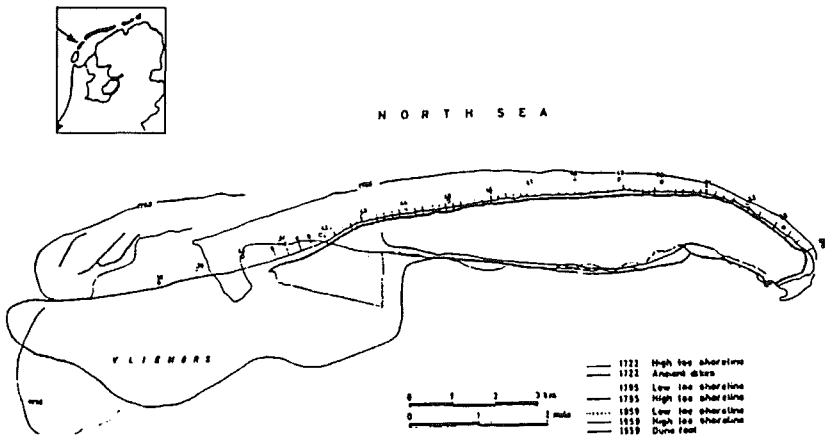

Figure 5.24: Vlieland. Former and present situation.

in this section, the previous theory will be applied to the Dutch Wadden Island of Vlieland. For more details is referred to Bakker (1968). In this section a practical application of the previous theory will be mentioned, on the North side, the Netherlands are bordered by a chain of "Wadden Islands". Between the islands and the continent is a region of tidal flats connected with the North Sea by tidal channels with a depth up to 60 ft. (fig. 5.24). This section deals with the second island from the West, called Vlieland. In the 17th century a dune ridge on the North side all along the island protected the two villages, West-Vlieland and East-Vlieland, against North Sea. However, since then, a very strong erosion occurred, especially on the West-side (about 1 mile in 250 years!); the village West-Vlieland had to be abandoned and the dune ridge all along the ,Western part of the island disappeared (fiq. 5.24). Only a sandbank, called Vliehors, a little bit southward of the original island reminds of the past. Nowadays, only seals and soldiers play their games there.

On the Eastern part, Rijkswaterstaat (the Governmental Board for Ways, Waterways and Harbors) constructed 53 groins during the years 1854 up to 1885, 6 groins from 1916 till 1923 (near the Eastend) and finally the five groins C, D, E, F, G on the extreme West (1957-1959).

One hundred years ago, Rijkswaterstaat made a fixed range system all along the Dutch coast and measured yearly the distance from the measuring poles to the High Water line and the Low Water line. The distance between two neighboring poles is 1 kilometer.
This section will give an analysis of the results of these measurements on the sandbank called Vliehors, the Western part of the island.

Measurements and visual analysis
Fig. 5.25 gives the range system and the measurements in the respective ranges 37 to 42, as a function of time. The upper line always represents the line of MLW [1)], the lower line the line of MHW and therefore the grey fields represent the tidal area. The tidal difference is about 1.50 metre (5 feet). A rising of the lines means accretion and descending of the lines means erosion.
Clearly, one observes the general erosion of this part of the coast, about 5 metres/year (interrupted lines in fig 5.25). But superponed, one also notices a kind of "sandwave" with a period of about 60 years.
Twice, in 1870 and 1930 a shoal of the outer delta of the inlet between Vlieland and the neighboring island, Texel, grew together with the Vliehors. Afterwards, this shoal seemed to move along the coast with a velocity of about 1/6 to 1/3 km/year.

[1] Mean Low Water

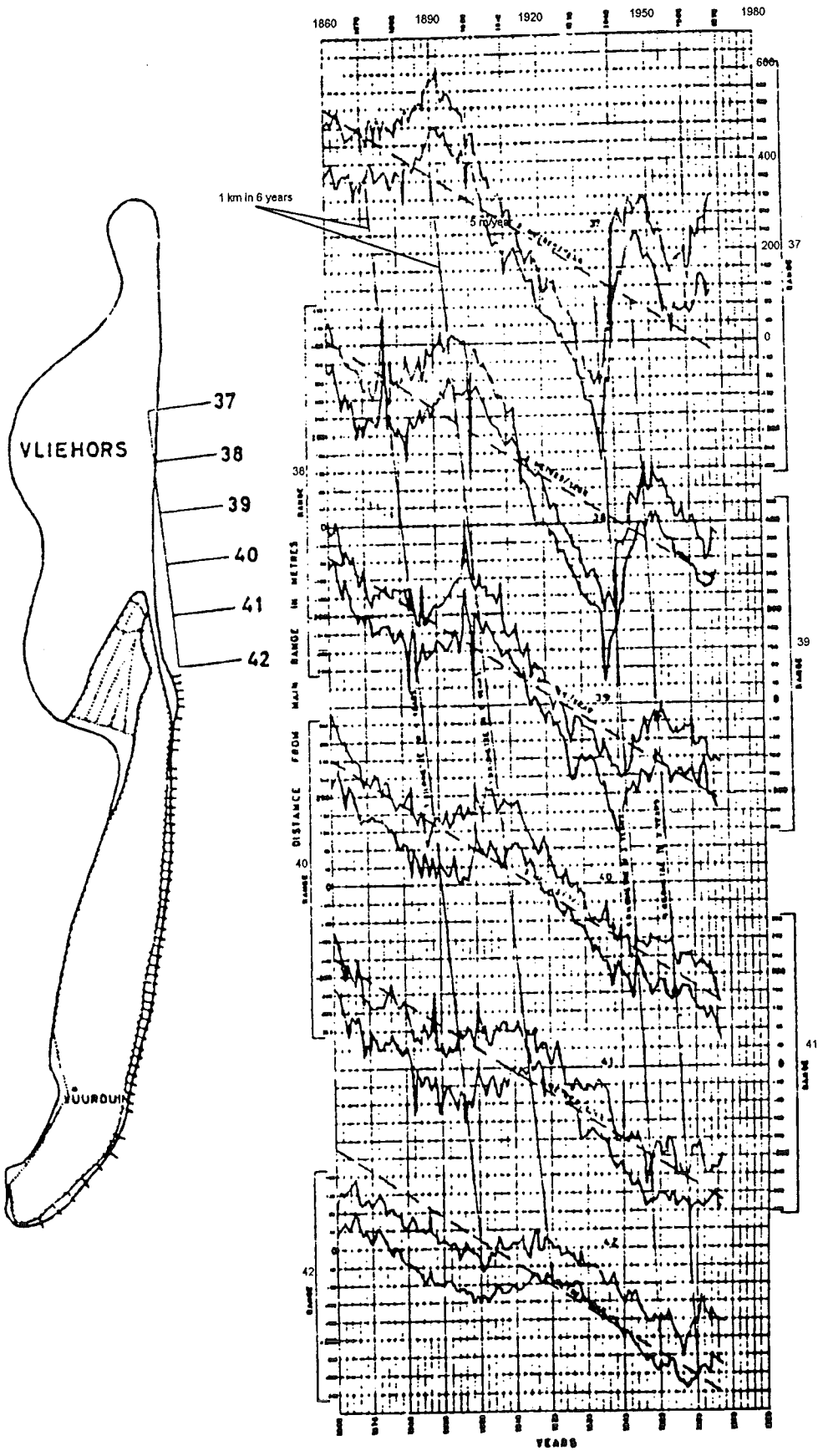

Figure 5.25: erosion and accretion on the vliehors

The coastline will be defined as the shoreline at mean water level, for which the mean value between the y-coordinate of the line of MLW and MHW will be taken.

In every year the littoral drift Q_L through range 37½ is, according to (5.1):

$$S_L^* = S_0^* - s\frac{y_{38} - y_{37}}{1000} \qquad (5.1)$$

in which $y_{37(38)}$ denotes the y-coordinate of the coastline in range 37(38) in metres, at time t. The factor "1000" in the denominator is the distance in metres between range 37 and range 38.
Likewise, one finds for the littoral drift through range 41½:

$$S_R^* = S_0^* - s\frac{y_{42} - y_{41}}{1000}$$

Therefore, the supply of sand in one year should be:

$$S_L^* - S_R^* = \frac{s}{1000}(y_{37} - y_{38} - y_{41} + y_{42})$$

If one assumes a cross-section of the coast, according fig. 5.1, then the mean accretion of the area should be:

$$\frac{S_L^* - S_R^*}{4000h} = \frac{1}{4}\frac{s}{h}x10^{-6}(y_{37} - y_{38} - y_{41} + y_{42}) \qquad (5.2)$$

in which h is the depth up to where accretion occurs, and "4000" is the length of the area.

In fact, the mean accretion of the area is:

$$mean\ accretion = \frac{1}{4}\{(y_{38} + y_{39} + y_{40} + y_{41})_{t+1} - (y_{38} + y_{39} + y_{40} + y_{41})_t \qquad (5.3)$$

Equalising (5.2) and (5.3) gives:

$$\frac{s}{h}x10^{-6}(y_{37} - y_{38} - y_{41} + y_{42})_{t+1/2} = (y_{38} + y_{39} + y_{40} + y_{41})_{t+1} - (y_{38} + y_{39} + y_{40} + y_{41})t \qquad (5.4)$$

This relation must be valid at every time t.
By correlating the right-hand side with the last factor on the left-hand side of (5.4), the author found for the proportionality constant of MLW and MHW will be taken at s/h the Vliehors:

s/h = 0.4 x 10^6 m^3/m depth/year/rad.

In fig. 5.26 the left-hand side (black line) and the right-hand side (grey line of equation (5.4) are plotted separately as a function of time. The correspondence between the black line and the greyline is rather good. However, the lines are shifted vertically with respect to each other. Even if S_L^* equals ;S_R^* (straight coastline), still an erosion occurs of 14.5 metre/year. We will call this "the offshore transport", because one of the causes for it can be transportation of material to deeper regions, where it is beyond the reach of the waves and not available for accreting of the coast.

Other reasons may be:
1. transportation of material over the shoal in case of storn surges; (this is the most probable reason, given the set-up at the seaside during storm conditions).
2. transportation of sand by wind;
3. influence of currents. These currents are not very large (about 1 knot).

In the case of the Vliehors, the sand wave solution gives for the wavelength L, and the propagation velocity respectively (T = 60 years, s/h = 0.4 km^2 /year):

$$L_1 = \sqrt{4\pi \cdot 0.4 \cdot 60} \approx 17.3\ km \qquad c=17,3/60= 0,29\ km/year$$

In reality, the velocity was 1/6 to 1/3 km/year.Over a distance of 4 km, the rate of attenuation is: $e^{-kx} = e^{-\frac{2\pi \cdot 4}{17.3}} = e^{-1.44} = 24\%$

In reality, the wave attenuated from 300 meters in range 37 (1936) to 76 metres in range 41 (1947). In fact, 25% remains.
Essentially, the wave form corresponds with the sandwaves we observed at the Vliehors, but there are some differences:

1. Evidently an offshore transport exists;
2. The sandwave does not propagate until infinity, but finds the groins of the protected part on its way;
3. The erosion and accretion is not exactly harmonically.

The first and last point will be considered more in detail.

Offshore transport

Without offshore transport, the coastal equation (3.6) was found. With offshore transport, this equation becomes:

$$\frac{s}{h}\frac{\partial^2 y}{\partial x^2} - p = \frac{\partial y}{\partial t} \qquad (5.5)$$

in which p is the erosion in meters/year, caused by the offshore transport, if the coastline is straight.

A solution of (5.5) is:

$$y = -At + (\frac{p-A}{2} \cdot \frac{h}{s})x^2 + Bx + C \qquad (5.6)$$

in which A, B and C are auxiliary constants. If $A = p$, then the coastline is straight and erodes with a velocity of p metres/year. If A = 0, then the coastline is a stable parabola. If $A < p$, then the coastline is a slightly eroding parabola. With the proper choice of constants and boundary conditions, for which is referred to Bakker (1968) the method of Schmidt results in the predicted erosion and accretion in the course of time as given in fig. 5.27.

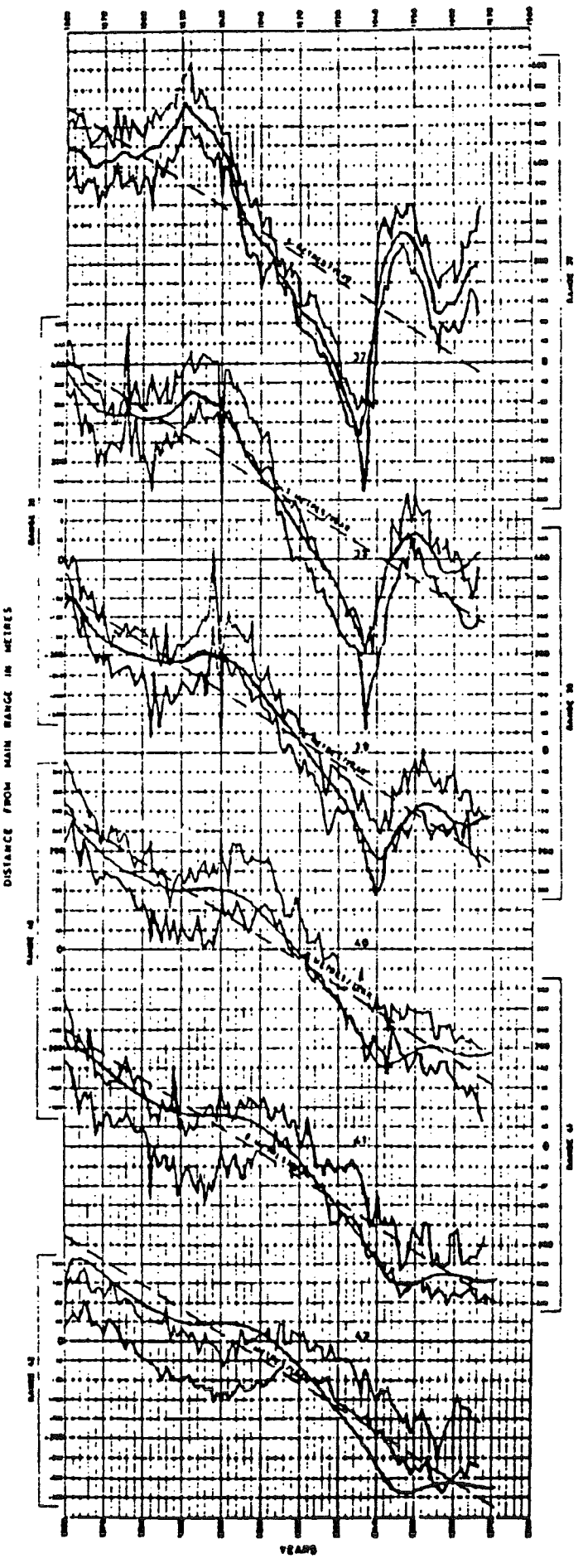
DISTANCE FROM MAIN RANGE IN METRES
YEARS

5.2.3 Sylt

This chapter deals with the results of hindcast computations for artificial beach nourishment projects at Sylt, Flushing, Ameland and zeebrugge, using both the one-line and two-line theories. The location of these project sites is given in Figure 5.28.

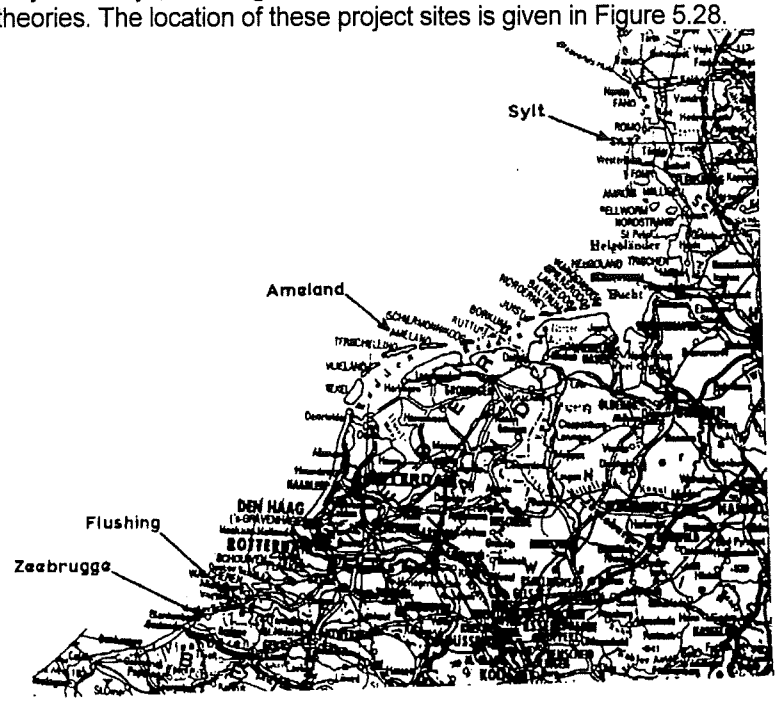

Figure 5.28: Location of project sites

On the Island of Sylt artificial beach nourishment projects have been under-taken in 1972 and 1978, in which the fills were placed as a stockpile groyne. In the following the performance of these sand groynes is analyzed by applying an analytical solution of the diffusion equation $\partial y/\partial t - (s/h)\, \partial^2 y/\partial x^2 = 0$ using both the one-line theory (Section 3.2) and the two-line theory (Section 3.3). The solution can be described by a Gauss-curve: $y(x,t) = A \exp(-Bx^2)$ where both A and B are a function of the time. The two-line theory, which is a more refined theory, is only applied for the 1978-nourishment, since the available data for this nourishment were more extensive than for the 1972-nourishment. The one-line evaluations of Section 3.2 gives insight in the quality of the above Gauss-solution for stockpile-type beach fills, as in the case of Sylt, and in the predictive power of transport computations to determine the coastal constant s. Refined analysis of the 1978-nourishment

5.2.3.1 General

Two-line models

Sylt

In order to examine the predictive value of the two-line theory compared to the one-line theory, computations for five options of schematization and applied theory have been carried out for the 1978-nourishment on the Isle of Sylt. The five options are shown schematically in Figure 5.29.

In all cases the original coastline before the nourishment is defined as a parabola that is retreating, such that the predicted erosion corresponds with the observed erosion in nature. Furthermore, it has been assumed that the initial shape of the nourishment can be described by one or two Gauss-curves for the one-line or two-line theory respectively. More specifically, the five options have been defined as follows:

Option 1: one-line theory for total profile between M.S.L. + 4m and M.S.L.

Option 2: one-line theory for the beach between M.S.L. + 4m and M.S.L. - 2m
Option 3: one-line theory for the beach and inshore with parallel lines
Option 4: two-line theory for the beach and inshore, analytical solution
Option 5: two-line theory for the beach and inshore, numerical solution

With respect to the accuracy the following standards have been applied for the comparison of the computational results:

- the theory should reproduce the overall development of beach and inshore as closely as possible;
- the close simulation of the evolution of the beach is of more importance than the close reproduction of the evolution of the inshore.

From a comparison of the standard deviation between the measured and computed coastlines, both for the initial shape and for the shape after one month and one year, it is concluded that for the case of Sylt the two-line theory gives the best results. The analytical solution (Option 4) gives the most accurate prediction of the evolution of the beach, while the overall picture is best predicted by the numerical solution (Option 5). A standard deviation of 10 m with respect to the line of beach and of 20 m with respect to the line of the inshore, resulting in an overall accuracy of 15 m, could be obtained.
A fast prediction of the evolution of the beach, which is not much worse than the two-line

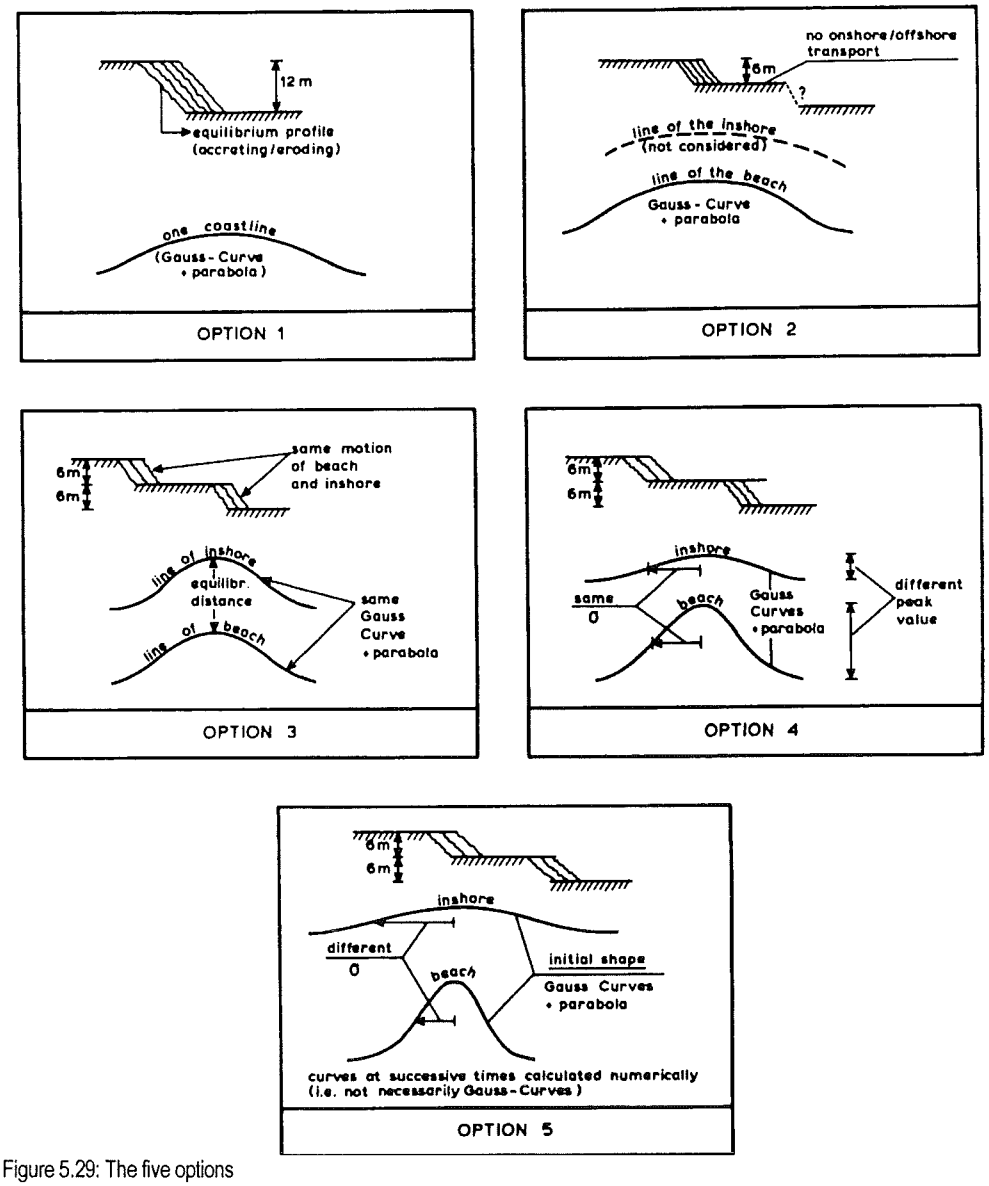

Figure 5.29: The five options

options, can be given by Option 2, where the one-line theory has been applied to the beach only. This shows that in the case of the 1978-nourishment on the Isle of Sylt, the dynamics of the beach are determined more by longshore transport than by cross-shore transport. The use of Option 3 with parallel lines for beach and inshore should not be recommended for this case, as it shows a rather large inaccuracy. In fact, the latter option starts from the conception that any deviation from the equilibrium profile is immediately corrected by cross-shore transport, which implies that this type of transport has a large effect on the evolution of the beach and inshore.

The deformation of two stock-pile type artificial fills on the island of Sylt, which were placed as a kind of sand groyne, has been analyzed. The first nourishment took place in 1972 and the second in 1978.

The analytical solution representing a Gauss-curve, $y = A\ exp\ (-Bx^2)$, of the diffusion equation, $\frac{\partial y}{\partial t} - \frac{s}{h}\frac{\partial^2 y}{\partial x^2} = 0$ was applied to analyze the deformation of the sand groyne.

The constants *A* and *B* are functions of time. The major conclusion of the computational efforts is that the considered coastlines agree reasonably well with a Gauss-curve and that the actual deformation speed of the sand groyne, represented by the increasing width at the points of contraflexure, corresponds with the theoretical widening, which is proportional to the square root of the time.

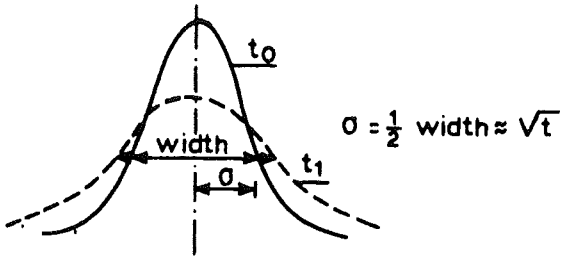

Figure 5.30: Principle of Gauss-curve

The hindcast computations resulted in a coastal constant $s = 0.7 \cdot 10^6\ m^3/yr/rad$ for the 1972-nourishment and $s = 0.9 \cdot 10^6\ m^3/yr/rad$ for the nourishment. The predicted value of *s*, based upon wave data is between $0.4 \cdot 10^6$ and $0.8 \cdot 10^6\ m^3/yr/rad$. The conclusion is that the difference between hindcasted and predicted values is rather small. Further it was observed that both fills behaved more or less similarly, apart from heavy losses during the first month after placement of the 1978-fill.

The above analysis of the deformation speed $\sigma \sim \sqrt{t}$ is independent of the actual volume of the fill. The behaviour of the fills differs if the analysis is based upon the position of the peak of the Gauss-curve. In that case the actual volume plays a role and the resulting values of s are non-consistent. For the 1978-fill, s is about half of the value for the 1972-fill. Therefore and because of the above correspondence between hindcasted and predicted values of s, it is recommended to determine the coastal constant from the observed growth of the width of the beach fill. Intermediate losses due to onshore-offshore transport are only of minor significance to the value of the coastal constant.

In this Section a refined analysis of the second beach nourishment on Sylt will be given. In this sub-section 5.2.3.1, the background of the analysis will be explained, leading to 5 "options" (mathematical theories / schematizations; Figure 5.29) which will be investigated in the following sub-sections:

5.2.3.2 one-line theory applied for total profile (between MSL+4 m and MSL-8 m).

5.2.3.3 one-line theory applied for beach (between MSL+4 and MSL-2 m).

5.2.3.4 parallel lines of beach and inshore.

5.2.3.5 analytical two-line theory.

5.2.3.6 numerical two-line theory.

The results of these investigations are summarized in Table 5.5 and are discussed at the end of the present sub-section, which in this way gives an overall picture of the whole Section 5.2.3.

For the study on morphological processes the coastal engineer has different mathematical models at his disposal. The question is what are the advantages and disadvantages of those various models. To try to give an answer to this question in the following a comparitive evaluation of mathematical theories, i.e. the one- and two-line theory will be given, using the accuracy as a measure, and starting from the data of the 1978-beach nourishment at Sylt.

For the evaluation, it is necessary to have a clear picture in mind concerning the requirements of such a theory. One has to distinguish:

- the accuracy of the theory; and
- the relevance of the theory.

For example, a theory may be perfectly accurate with respect to its mathematical predictive value, but when the assumed initial shape does not match the actual initial shape of the coast, the theory is not relevant. Therefore, it is necessary to define the standards with respect to relevance first, before considering the accuracy. The following standards are proposed:

a) The mathematical formulation of the initial shape should be able to cover the initial shape of the coastline, as usually found in practical cases, as close as possible.
b) For the prediction of future developments no information should be required other than that available at the time of the prediction.
c) The known behaviour of the coast before nourishment (for instance gradual erosion, sandwaves) should be incorporated in the mathematical formulation.

With respect to the accuracy (and also more or less in connection with the relevance) the following standards seem to apply:

d) The theory should reproduce the overall development of beach and inshore as close as possible.
e) The close simulation of the behaviour of the beach is of more importance than the close reproduction of the behaviour of the inshore.

Considering these standards in relation to the one-line and two-line theory, it has to be kept in mind, that within the scope of one theory various possibilities exist, namely:
- with respect to numerical or analytical application;
- with respect to the schematization.

With respect to numerical or analytical application, the first standard (a) would lead to a preference for numerical methods, which allow the exact covering of the initial conditions. However, these methods require generally a known behaviour of the boundary conditions in the course of time, which is in contradiction with standard (b).

Therefore, for all applied schematizations, the initial condition has been schematized in such a way, that a general analytical conception of the anticipated approximate behaviour of the coast was assumed; this includes assumptions concerning the boundary conditions for the future situations, which have to be calculated. The boundary conditions, following from this conception might be rather intricate. For instance, in the considered case of Sylt this involves a uniform erosion at the boundaries only up to the moment, that the widening and flattening Gauss-curve (see next specification) influences those boundaries perceivably.

To be more specific:
- It has been assumed, that the coast of Sylt before nourishment consisted of a retreating parabola (i.e. parallel depth contours of parabolic shape). The curvature of the parabola

has been assumed in such a way, that the predicted erosion corresponds with the erosion occurring in nature before the beach nourishment, thus covering standard (c).
- Furthermore it has been assumed, that the initial shape of the nourishment consisted of one or two Gauss- curves for the one- or two- line theory respectively (see 5.29).

From these assumptions and the assumed coastline theory the boundary conditions as a function of-time are determined.
Especially the accuracy of this last assumption gives only information on the usefulness (relevance) of the theory and tells nothing on its predictive value. Therefore, the accuracy of this initial condition, called S_{di} ("standard deviation-initial") will be kept separate from the calculated accuracy of the predicted curves at later times, symbolized by S_d The values of S_{di} and of S_d should be considered in relation to each other. If S_d is smaller than S_{di} then in the course of time the coastline tends to fulfil more and more the assumptions of the theory. Theoretically for the one-line theory it can be shown, that a coast being straight and at rest at infinity, will resemble more and more a Gauss-curve, independent on the initial condition.

After the foregoing rather general considerations, it is useful to concentrate somewhat more on Sylt, by considering the standards with respect to the accuracy and its consequences for the schematization.

As the theory should reproduce the overall development of beach and inshore as close as possible (standard d), a logical schematization appears to be: a one-line approximation where the "coast" covers the total profile between MSL + 4 m and MSL - 8 m. This will be the first option to be considered in the following.
As to be described later on, for this case the initial accuracy S_{di} and the overall accuracy S_d of the predicted coastlines after one month and one year will be calculated.

It is not clear, whether the above schematization covers also standard (e), i.e. a close simulation of the behaviour of the beach, to be defined as the area between MSL + 4 m and MSL - 2 m. One approach to fulfil this condition is to "forget" about the inshore (the area between MSL - 2 m and MSL - 8 m) and forget standard (d): apply the one-line theory only to the beach area. This will be the second option. When the same values should be found for S_{di} and S_d in the case of the first option and the second one, it is clear that the second one should be preferred, since a good reproduction of the beach behaviour is more important for a coastal manager than a good reproduction of the rest of the profile. However, it is not likely that the same values are found, since the offshore losses, to be expected in the second option, are not taken into account.

On the other hand, one also could check the assumption of the one-line theory, that all depth contours are parallel: this gives a third option. It involves, that the "line of the beach" (the mean of the contour lines between MSL + 4 m and MSL - 2 m) and "the line of the inshore" (the mean of the contour lines between MSL - 2 m and MSL - 8 m) have the same shape as the coastline found from the first option. These two lines can be found by moving this coastline in landward or seaward direction.

The results of the first and third options are somewhat difficult to compare. When S_d (or S_{di}) in the first and third option has the same value, this implies, that the line of the beach and the line of the inshore in the third option have the same accuracy as the coastline in the first option, i.e., "the profile fits at two places" instead of "in the middle"; under those circumstances the third option naturally should be preferred.
One might compare the accuracy, with which the line of the beach can be predicted according to the second and third option; this gives a validation of the schematizations concerned.

The two-line theory gives the opportunity to take the variation in coastal slope into account. The lines of beach and inshore are ruled by the same dynamic equations as in the one-line theory, however, sand loss from beach to inshore (offshore transport) is simulated when the profile is steeper than the equilibrium profile, and onshore transport when the profile is more gentle than the equilibrium profile. The relation between onshore/offshore transport and the mean slope of the coastal profile is linearized.

Two options will be considered. In both options, the mean coastline, i.e. the mean between the line of the beach and the line of the inshore will be the same as in the one-line theory (first option). In the fourth option the analytical two-line theory is used. This implies, that due to the limitations of the analytical approach, the values σ (half distance between the points of contra-flexure) for beach and inshore should be equal. However, contrary to option 3, the peak values of the Gauss-curve, representing beach or inshore, are not necessarily the same.
The fifth option, the numerical one, does not imply the restriction, that σ for beach and inshore are the same. Therefore, the initial inaccuracy S_{di} will be less for option 5 than for option 4, which means that the relevance of option 5 will be greater. The initial shape of the nourishment for option 5 is schematized by two Gauss-curves, one for the beach and one for the inshore.

Apart from the initial situation and the boundary conditions, the solution of a mathematical theory depends on calibration constants. The following analysis is confined to hindcasting. This means that the optimal values of the calibration constants are derived from the same data, as for which the theory is applied. Consequently, the accuracy will be flattered compared to forecasting.

It would be worthwhile to use the constants, obtained in this way, for nourishments at the same site in order to find the accuracy for forecasting. Some care is needed, since the calibration only covers a period of one year. It is possible that heavy storms might alter the interaction between beach and inshore considerably.

The used calibration constants are treated when considering the various options. The values are optimized by minimizing the value of S_d, i.e., the overall accuracy is as large as possible in this way. For the options involving two lines, the inaccuracy is calculated both for beach and inshore separately, and for beach and inshore together. As mentioned before, the values of S_{di} and S_d found for one-line theories are difficult to compare with those, found for two-line theories. Comparable are the values of the inaccuracy of the beach for option 2 to option 5, and the values
of S_{di} and S_d for the one-line options (1 and 2) or two-line options (4 and 5) separately. The final results are summarized in Table 5.5.

Anticipating Sections 5.2.3.2 to 5.2.3.6 and Table 5.5, it can be concluded that the accuracy of the results of a mathematical method depends on:
- the accuracy of the physical conception;
- the accuracy of the physical constants, used in the theory;
- the accuracy of the assumed initial condition and the boundary conditions;
- the accuracy of the numerical computation.
- the accuracy of the measured data.

In the analysis of the 1978-beach nourishment, the accuracy concerning items (d) and (e) is neglected. The accuracy concerning item (c) depends on the assumed schematization.

Figure 5.31 shows the one-line and two-line schematizations of the coastal profile for Sylt. The coordinate y of the coastline has been taken with respect to a straight reference line, following the general longshore direction.

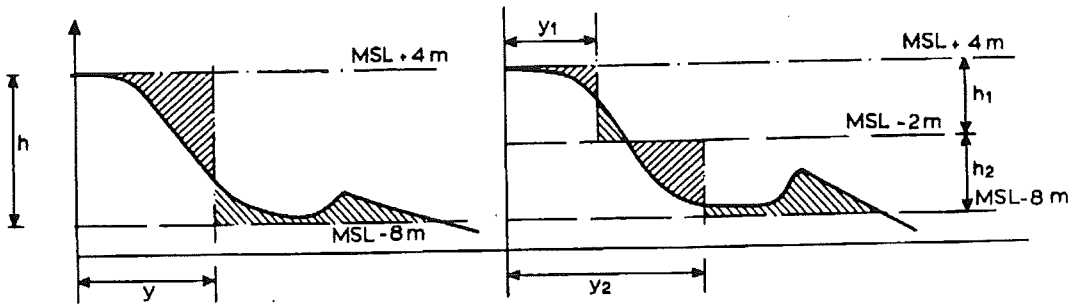

Figure 5.31: One- and two-line schematization for Sylt

Figure 5.33 (next section) shows the coastline according to measurements at 4 successive time steps, the first and second time step just before and after the nourishment. The third and fourth timestep are a month, resp. a year after the nourishment. Figure 5.37 shows the line of the beach and the line of the inshore at the same moments as mentioned in Figure 5.33 The calculated curves according to the various options, compared to the measurements, are displayed in Figure 5.36 and Figure 5.38 to Figure 5.41 (see Table 5.5).

In Sections 5.2.3.2. and 5.2.3.6 the 5 different options are treated in detail. In all those schematizations, it has been assumed that:

- the coast before the nourishment had the shape of a retreating parabola;
- the nourishment is subject to an initial loss L_l of 25%; and
- the gradient of the longshore transport with respect to the coastal direction equals 660,000 m^3/year/rad.

The curvature of the parabola and the magnitude of l_L and s has been determined by curve-fitting (Section 5.2.3.2).

The assumption (option 1), that the mean between all depth-contours between MSL + 4 m and MSL - 8 m just after the nourishment can be schematized according to a Gauss-curve, superposed on the initial parabola, is rather accurate (inaccuracy S_{di} = 15.6 m., Table 5.5, column 1).
With the optimal calibrated value of the before-mentioned gradients, it is found that the coastline at two successive times, a month and a year after the nourishment, can be predicted with an inaccuracy S_d = 11.3 m (column 1). It thus shows, that in the course of time the assumption "the coastline is a Gauss-curve" , tends to improve, as it should do theoretically.

The assumption (option 2, column 2), that the initial line of the beach is a Gauss-curve, where the line of the beach is defined as the mean of the contour lines between MSL + 4 m and MSL - 2 m, is worse than the assumption, that the coastline is a Gauss-curve (column 1). S_{di} = 21.2 m instead of 15.6 m.
However, the prediction of the line of the beach (assuming no loss from beach to inshore) after a month or a year is not significantly worse than the prediction of the coastline, S_d = 11.8 m instead of S = 11.3 m.

Considering line of beach and inshore together, the assumption (option 3, column 3) that during the nourishment the coast keeps its equilibrium profile is definitely not according to reality. The included assumption, that the line of beach and inshore have the same shape as the coastline, has an initial inaccuracy S_{di} = 39.5 m, and an overall inaccuracy S_d = 23.7 m after a month/year.

Taking the coastal profile into account, the analytical two-line theory (option 4, column 4) gives a-much better approximation. Initially, for the line of the beach and the inshore an inaccuracy S_{di} = 22.5 m and S_{di} = 23.2 m is found and an "overall" inaccuracy S_{di} = 22.1 m. After a month/year the overall inaccuracy diminishes to 16.5 m and the inaccuracy of the line of the beach to 9.6 m. Of all options, the analytical two-line theory predicts the beach shape best (standard e).

The numerical two-line solution (option 5, column 5) is a " taylormade" solution for the behaviour of the coast. Now both the different alongshore shape of beach and inshore, and the offshore transport is taken into account. Of course, the initial inaccuracy of the beach in column 5 and the initial value of "y_b" and "σ_b" are equal to those in column 2 (the optimal shape of the Gauss-curve through the beach). Both the initial overall inaccuracy S_{di} and the overall inaccuracy S_d after a month/year are the lowest for the numerical two-line option (option 5), when compared with the other two-line options (3 and 4). Standard (d) is fulfilled the best in this way. The accuracy of the prediction of the beach is somewhat less than the one found in option 4 (inaccuracy is 10.2 m instead of 9.6 m). The prediction of the inshore is better.

Summarizing, it is shown, that for the case of Sylt the best options are the analytical and numerical two-line theory (option 4 and 5); the analytical option is a little better with respect to the prediction of beach behaviour, the numerical one with respect to the overall picture.
A fast prediction of the behaviour of the beach, which is not much worse than the two-line option, can be given by using option 2 (considering the beach according to the one-line theory). This shows, that in the case of Sylt the dynamics of the beach is determined more by longshore transport than by offshore transport [2)].
For this reason the use of option 3 (parallel depth contours) should not be recommended for this case: it shows a rather high inaccuracy [3)]

- In should be noted, that this conclusion may not be valid, when another initial shape than the one of 1978 is used. Relative effect of longshore and onshore/offshore transport can be calculated with the two-line theory.
- In fact, this option starts from the conception, that any deviation of the equilibrium profile is "immediately" corrected by onshore or offshore transport, i.e. large effect of onshore/offshore transport.

5.2.3.2 One line theory applied for total profile

From the plan views given by Patzold (1980) the cross-section was determined between the levels MSL + 4.0 m and MSL - 8.0 m. The level of MSL - 8.0 m has been chosen in order to take all available data into account.
On the landward side, the boundary consists of a vertical reference plane, parallel to the mean coastal direction (Fig. 5.31).
By using a straight reference plane, instead of starting from differences between successive soundings, the original curvature of the coast can be taken into account.
From each cross-section, the average y-coordinate y of the depth averaged coastal profile can be found by division of the area by h = 12 m. Figure 5.33 shows a plot of y for the successive sections, thus yielding the "coast-line" at different times.

First, the natural coastal development has to be re produced, on which the development of the beach nourishment has to be superposed. The natural development is simulated by a parabola retreating linearly in the course of time (Fig. 5.32).

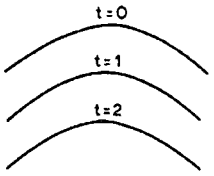

Figure 5.32: Coastline before nourishment: a gradual retreating parabola

$$y = \frac{1}{2} p^1 \cdot x^2 + p^1 \cdot \frac{s}{h} \cdot t \qquad (5.9)$$

where p^1 is a negative constant, to be found.

[2] In should be noted, that this conclusion may not be valid, when another initial shape than the one of 1978 is used. Relative effect of longshore and onshore/offshore transport can be calculated with the two-line theory
[3] In fact the option starts from the conception, that any deviation of the equilibrium profile is "immediately" corrected by onshore of offshore transport, i.e. large effect of onshore/ offshore transport.

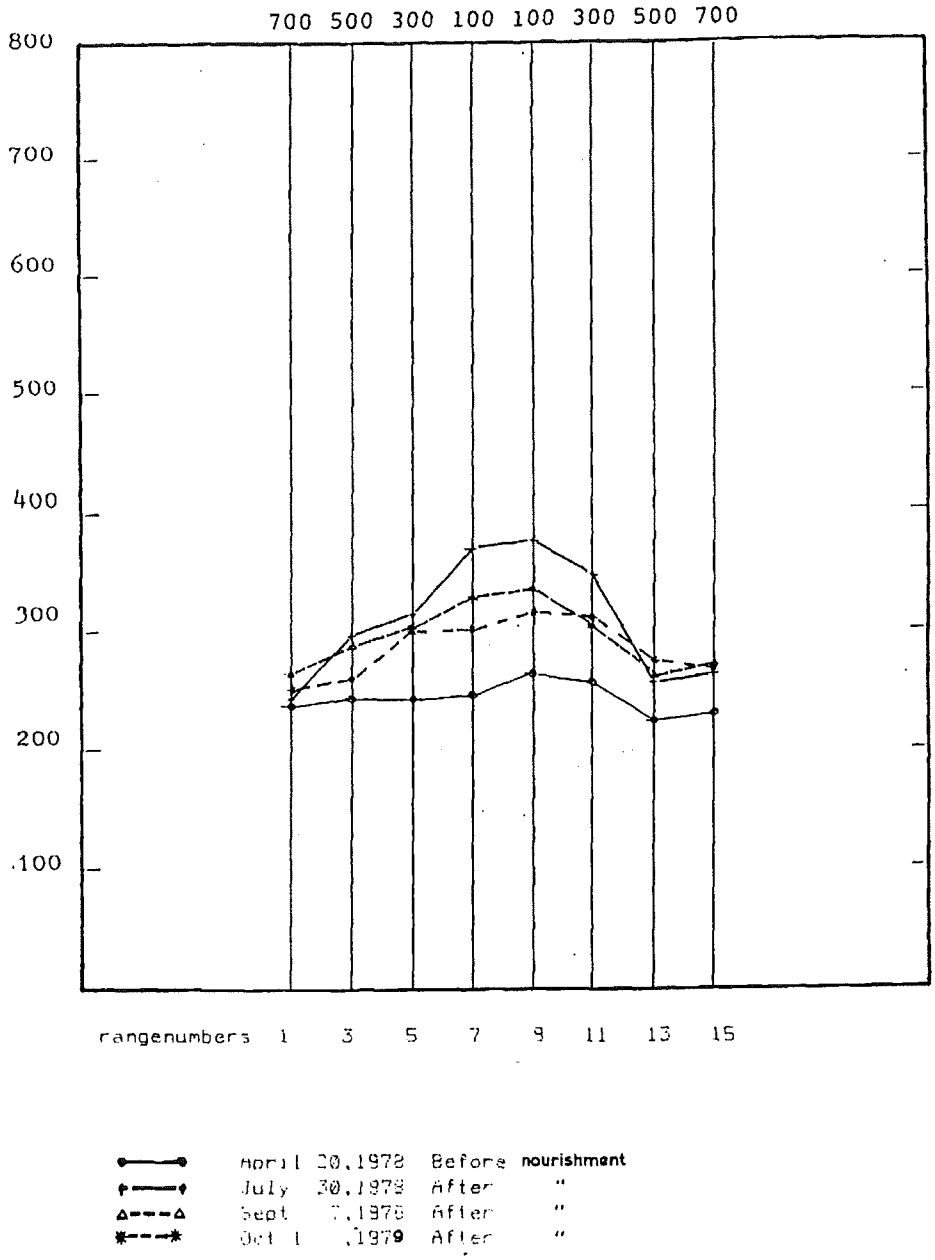

Figure 5.33: Coastline at succesive time steps (one-line)

According to (5.9), y is a solution of the coastal equation (3.6), as one readily finds. This coastal equation is based on continuity. However, the data show volumetric changes in the area considered, which can be caused by initial losses due to settling of material and washing out of fine sediment, offshore losses by heavy storms, etc.

Although the present investigation gives a hindcast instead of a forecast, the purpose is to provide information on the predictive value of the theory. Offshore losses by heavy storms are not predicted, and therefore, it was decided to consider the initial loss as a variable in the curve-fitting procedure.
The optimization was carried out starting from 3 degrees of freedom:

- p^1: the curvature of the parabola
- l_L: the initial loss (percentage)
- s: the rate of change of the transport S as a function of the coastal direction.

The data has been elaborated in the following way.

a) A certain value of p^1 is assumed. The area confined between the coastline before nourishment (April 20, 1978) and the reference line is known, which determines the location of the top of the parabola at *t= -0* (minus denotes before nourishment). The area contained between the coastline and the reference line is assumed equal to the area contained between parabola and reference line.

b) Using a curve-fitting procedure, the value of σ_i is determined, being the standard-deviation of the Causs-curve of the first coastline y(x) after the nourishment. Thus this coastline is approximated by (Fig. 5.34):

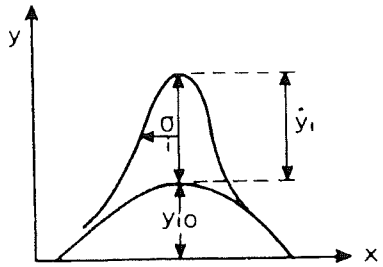

Figure 5.34: Initial shape of nourishment; Gauss-curve superposed on parabola

$$y_i = y_{i0} + \frac{1}{2} p^1 x^2 + \hat{y}_i e^{\frac{-x^2}{2\sigma_i^2}} \qquad (5.10)$$

where $y_{i0} + \frac{1}{2} p^1 x^2$ denotes the original parabola at time *t= -0*.

Given the value of σ_i, the value of $\hat{y}_i$ is determined by the area enclosed between the coastline at *t = + 0* (July 30, 1978) and the reference line.

The optimization of σ_i is accomplished in the following way. Determined is the value of the initial inaccuracy S_{di} being:

$$s_{di} = \sqrt{\frac{\{\sum_{n=1}^{m} (y_{meas}^{(n)} - y_{calc}^{(n)})^2\}}{(m-1)}} \qquad (5.11)$$

where m is the number of sections (m=8)

c) A value of the initial loss I_L and s is assumed.
From the relationship $\sigma_i = \sqrt{(2(s/h)T_1)}$ (see Section 2.2) the value of T_1 results directly from the assumed value of s and the value of σ_i found under b.
The coastline at tine t is calculated as:

$$y_{cal} = y_{i0} + \frac{1}{2} p^1 x^2 + p^1 \frac{s}{h} t + (1 - I_L)\hat{y}_i \sqrt{\frac{T_1}{(T_1 + t)}} e^{\frac{-x^2}{2\sigma^2 \frac{T_1 + t}{T_1}}} \qquad (5.12)$$

After this, the deviation between measured and calculated profile can be determined from:

$$s_d = \sqrt{\frac{\sum_{k=1}^{2} \sum_{n=1}^{m} (y_{meas}^{(k,n)} - y_{calc}^{(k,n)})^2}{(2m-1)}} \qquad (5.13)$$

where *k* denotes the first, respectively second measured coastline after nourishment. (i.e. the values of September 7, 1978 and October 1, 1979, the coastline at the "second" and "third time

d) From the foregoing, it appears that S_d is a function of 3 variables:

$$S_d = f(p^1, s, I_L) \tag{5.14}$$

Therefore the whole procedure is repeated for other values of p^1, I_L and s.

It must be kept in mind, that S_{di} has a different meaning than S_d. The value of S_{di} indicates, how the initial coastal profile corresponds with the assumption according to the theory. This value does not give any information on the value of the theory as such. The value of S_d gives the standard deviation between the theoretical, predicted coastline and the measured coastline, assuming sufficient calibration of the relevant constants. The relation between S_{di} and S_d gives insight in the relevance and usefulness of the theory for forecasting.

The results of the above described procedure are summarized in Figure 5.35. The variable on the horizontal axis is $-p^1 \cdot s/h$, which denotes the assumed rate of erosion of the coast in m/year before the nourishment took place (see Eq. 5.9). On the vertical axis the value of the inaccuracy, S_d according to Eq. (5.13) is plotted.
Curves are given for various values of I_L

Analyzing these results, one has to return to the physics. As Patzold states, the general retreat of the coast is in the order of 1 m/year.

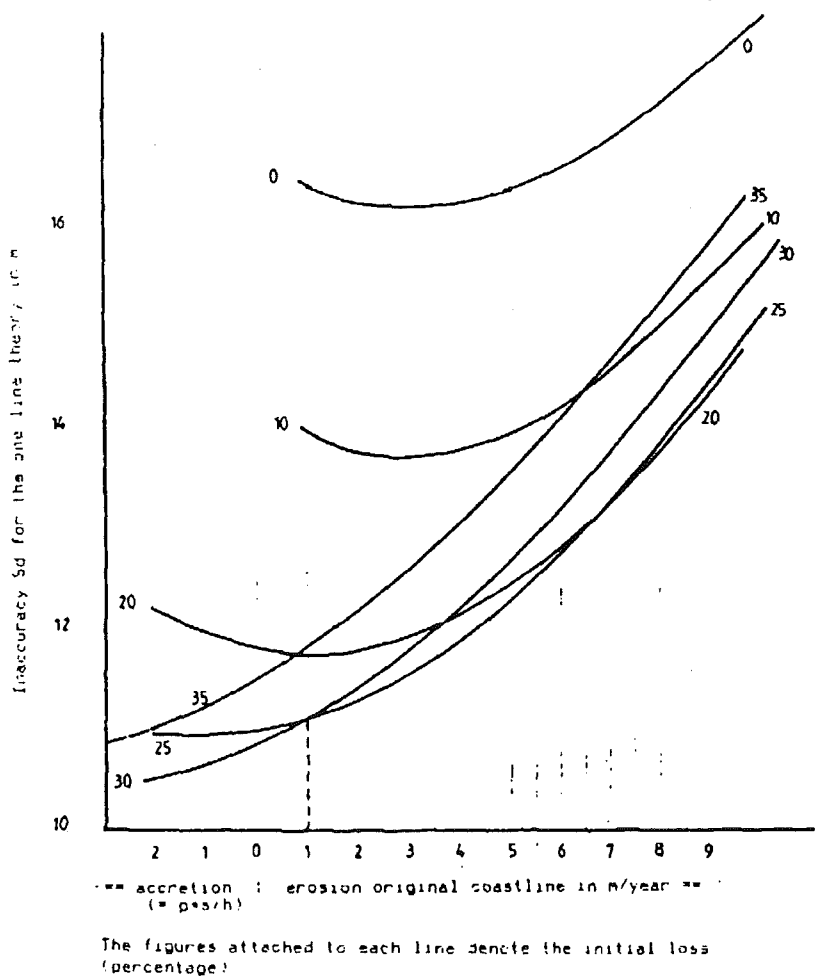

Figuur 5.35: Accuracy of one-line approximation as function of assumed rate of erosion of original coastline and of assumed initial loss (I_L)

From Figure 5.35, the most logical combination appears to be:

l_L = 25 %
s/h = 55,000 m^2/yr/rad s = 660,000 m^3/yr/rad
σ_i = 294 m
p^I = $-2 \cdot 10^{-5}$m
S_d = 11.3 m
S_{di} = 15.6 m

Figure 5.36 shows the results for the various times of the analysis ($t = -0$; $t = +0$, $t = t_1$ and $t = t_2$).

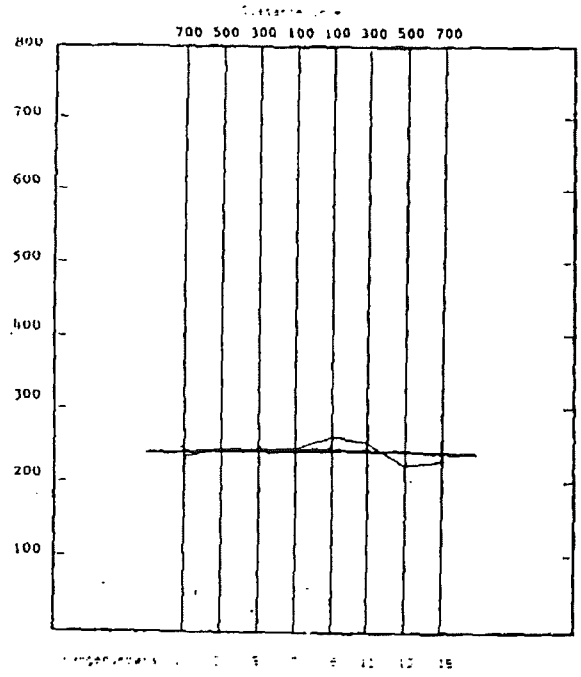

April 20, 1978 before nourishment

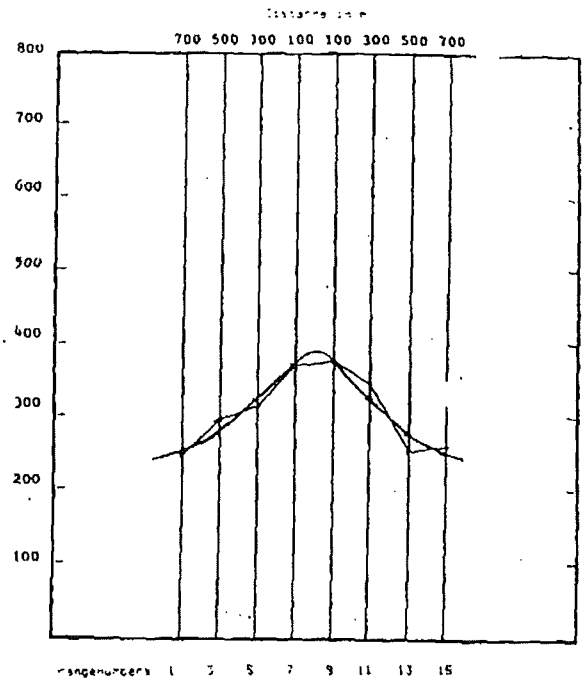

July 30, 1978 after nourishment

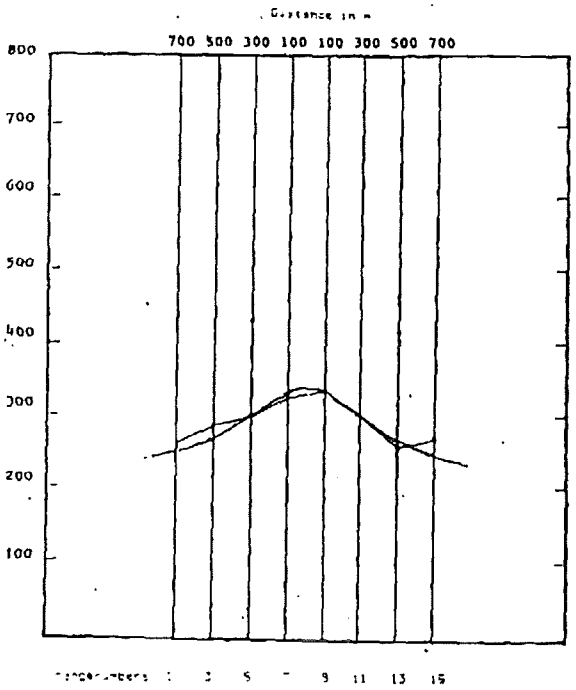

Sept. 7, 1978 after nourishment

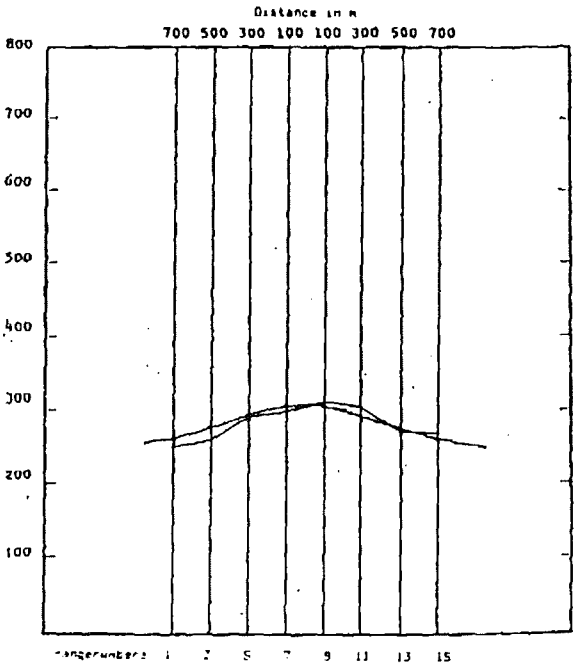

Oct. 1, 1979 after nourishment

Figure 5.36: Comparison of measured coastline and theoretical coastline (optimal hindcast)

5.2.3.3 One-line theory applied for the beach

This section deals with the second option (Fig. 5.29), where the attention is focussed on the beach. It is investigated, to which accuracy the behaviour of the beach can be predicted by applying the one-line theory only to the beach area (between the levels MSL + 4 m and MSL - 2 m, and neglecting the offshore transport between beach and inshore. Therefore the same procedure, as given in Section 5.2.3.3 has been applied for the line of the beach instead of the coastline, assuming that the curvature of the parabola as found in Section 5.2.3.3. (see Fig. 5.35) is correct, which means that no further tuning of shape of the parabola took place. Thus when applying Eq. (2.5) as the basic equation for the initial line of the beach, it was assumed that $p' = -2 \cdot 10^{-5}$ m

The value of y_{i0} differs from the one, used in Section 2.5.2. Assuming an equilibrium profile before the nourishment took place, the equilibrium distance W between the line of the beach and the line of the inshore can be found from the lines of beach and inshore at April 20, 1978 (see Fig. 5.37). A mean distance of 336.6 m is found.

The coastline is situated halfway between the line of the beach and the line of the inshore, since the representative "beach- layer" h_1, equals the inshore layer " h_2, i.e. $h_1 = h_2 = 6$ m. The parabola representing the beach should be shifted a distance w/2 = 168.3 m in landward direction with respect to the parabola representing the coastline. Thus, when applying Eq. (5.10) to the line of the beach, the value of $\hat{y}_i$ should be reduced with 168.3 m with respect to the value, used in Section 5.2.3.3.

The values of $\hat{y}_i$ and a σ_i are related in such a way, that the area under the Gauss-curve should be equal to the area, enclosed by the parabola and the line of the beach just after nourishment (July 30, 1978, Fig. 5.37). This gives one degree of freedom in determining σ_i by minimizing S_{di} according to Eq.(5.11).
In figure 5.38 the calculates and measured beach-lines are given at various time steps.

The calculations result in a value s_1/h_1= 55,000 m^2/yr/rad and a standard deviation S_d= 11.8 m. The value of s_1/h_1 is equal to s/h, found in Section 5.2.3.3. beach and inshore are equally sensitive to changes in longshore direction.

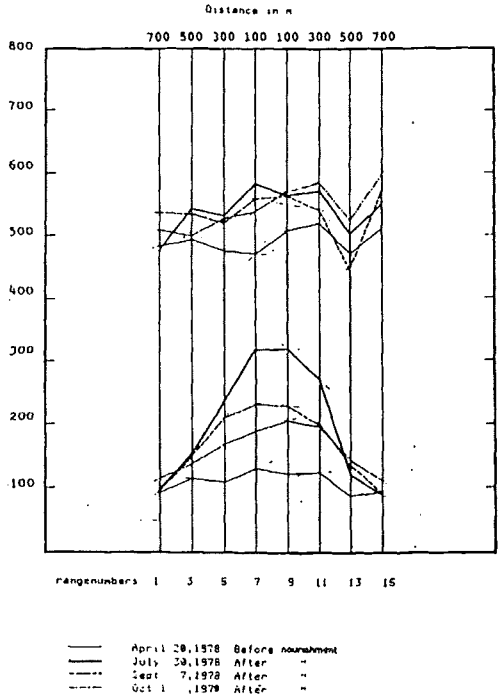

Figure 5.37: line of beach and inshore at successive time steps

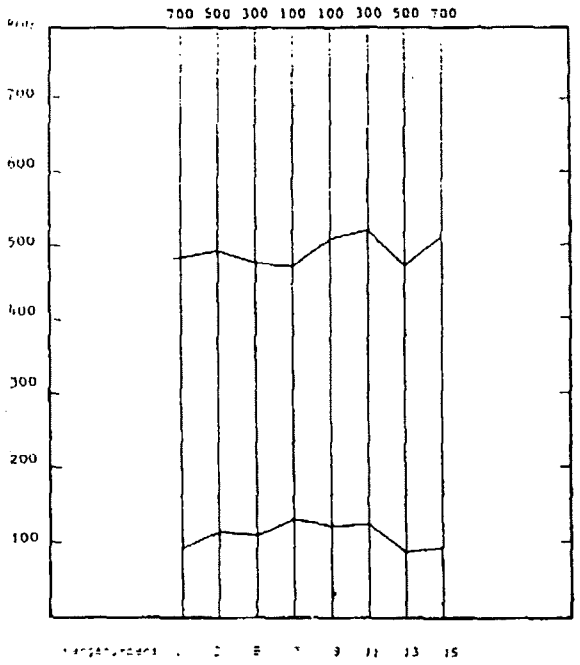

April 20, 1978 before nourishment

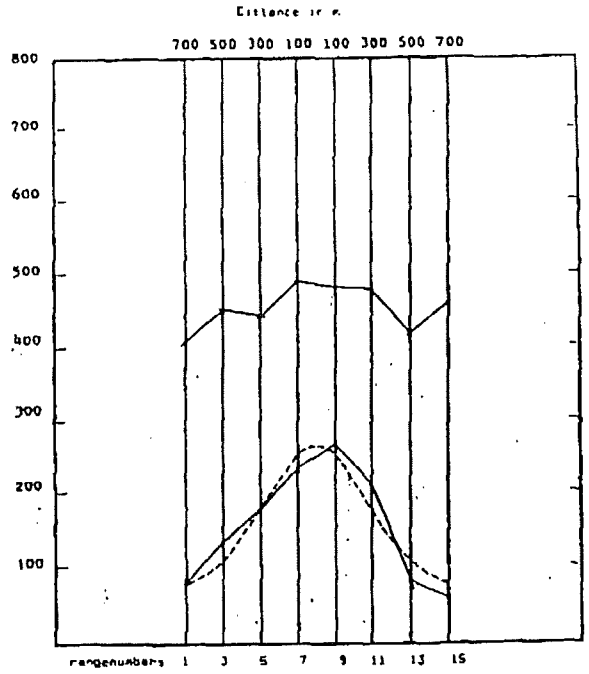

July 30, 1978 after nourishment

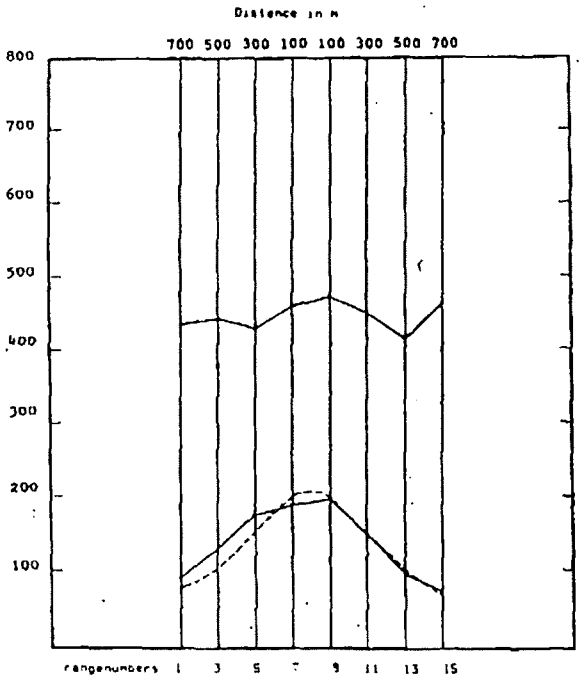

Sept. 7, 1978 after nourishment

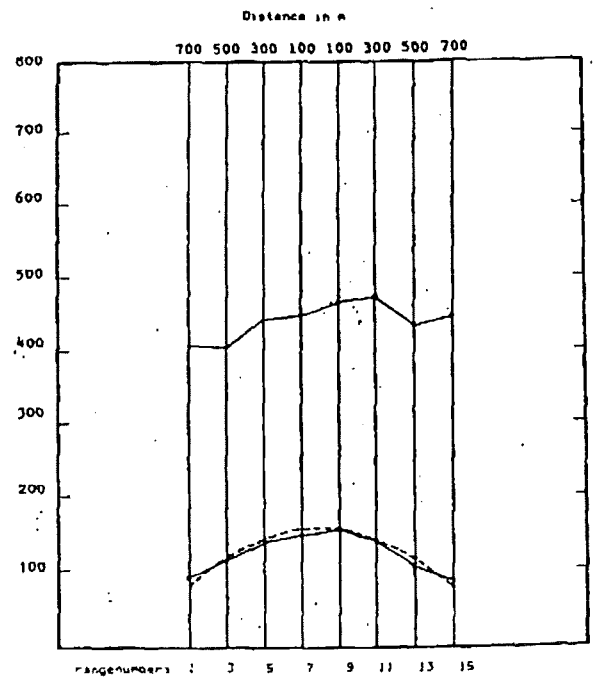

Oct. 1, 1979 after nourishment

Figure 5.38: Comparison of measured and calculated line of beach using one-line theory for beach only

5.2.3.4 Parallel lines of beach and inshore

This section deals with the third option (Fig. 5.29). It will be considered, whether better results can be obtained, when the coast is schematized according to two lines instead of one. According to one of the assumptions of the one-line theory, all depth contours should be parallel. Consequently, the line of the beach and the line of the inshore should have the same shape as the coastline and are only shifted with respect to each other.

In Figure 5.39 the final results of these one-line calculations have been plotted, together with the measured lines of the beach and the inshore at the corresponding time steps. It is assumed, that the distance between the lines of beach and inshore before the nourishment (i.e. at April 20, 1978) is an equilibrium distance. Therefore, the theoretical line of the beach at successive time steps is found by shifting the coastline, obtained in Section 5.2.3.3, over a distance of 168.3 m in a landward direction. The theoretical line of the inshore is found by shifting the coastline over the same distance in seaward direction.

Table 5-1 below shows the standard deviation (calculated according to (5.11)) for each of the successive time steps and for beach and inshore respectively.

	Beach	inshore
July 30, 1978	41.95	39.83
Sept. 7, 1978	27.22	34.35
Oct. 1, 1979	11.67	20.52

Table 5-1 Standard deviation (in m) of the beach and inshore using third option (parallel lines of beach and inshore).

The values on the first line of Table 5-11 (July 30, 1978, just after the nourishment) are combined to give the "overall initial standard deviation" S_{di}. This value S_{di} informs on the relevance of the theory (Section 5.2.3.1). The values on the second and third line (Sept 7, 1978 and Oct 1, 1979) are combined to give the "overall standard deviation" S_{di}, which informs on the accuracy of the theory (Section 5.2.3.1). The initial accuracy S_{di} is calculated for beach and inshore simultaneously:

$$s_{di} = \sqrt{\frac{\sum_{j=1}^{2}\sum_{n=1}^{m}(y_{meas}^{(n)}(j) - y_{calc}^{n)})^2}{(2m-1)}} \qquad (5.15)$$

where j= 1 (2) indicates the beach (inshore) respectively.

The inaccuracy S_d for the predicted lines of beach and inshore is calculated analogous to (5.13) and (5.15):

$$s_d = \sqrt{\frac{\sum_{j=1}^{2}\sum_{k=1}^{2}\sum_{n=1}^{m}(y_{meas}^{(k,n)}(j) - y_{calc}(j))^2}{(4m-1)}} \qquad (5.16)$$

where k and n have the same meaning as in (5.14).

This results in S_{di} = 39.51 m and S_d = 23.65 m.
Furthermore, the inaccuracy for beach and inshore separately are calculated,using Eq. (5.11) and (5.13).

The results are shown in Table 5.5.

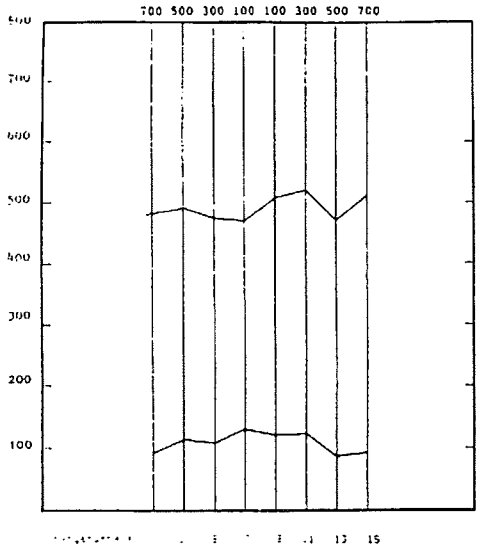

April 20, 1978 before nourishment

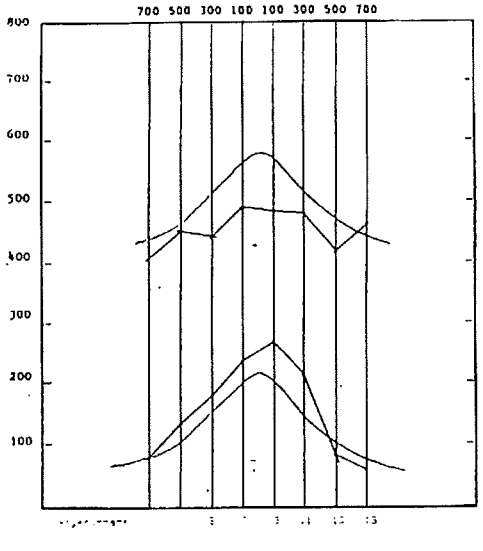

July 30, 1978 after nourishment

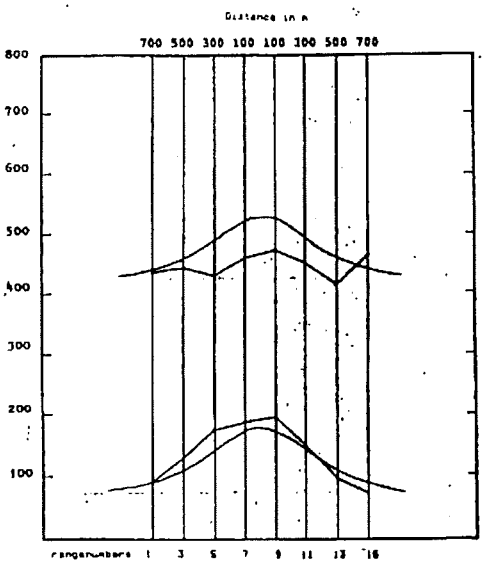

Sept. 7, 1978 after nourishment

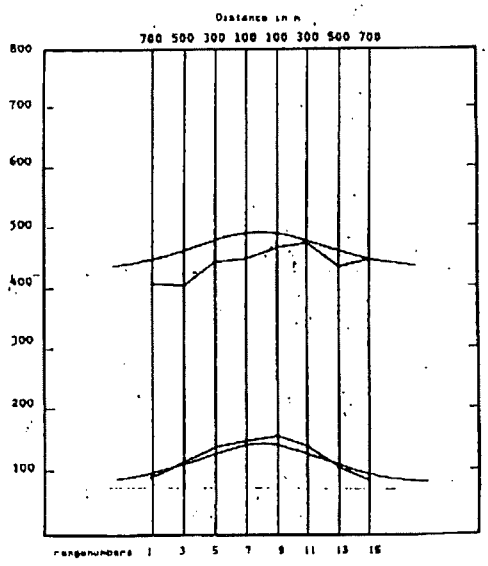

Oct. 1, 1979 after nourishment

Figure 5.39: Comparison of measured and calculated line of beach and inshore from the one-line theory assuming parallel depth contours.

5.2.3.5 Analytical two-line theory

Now it will be investigated, whether the result can be improved by taking the coastal slope and offshore transport into account. For this purpose, the two-line theory will be used.

Two approaches will be treated successively. According to the first approach, (option 4) analytical curves will be assumed for beach and inshore. The analytical solutions are, however, only available when $s_1 / h_1 = s_2 / h_2$ and therefore equal to s/h. As will be shown below, in this context the two-line-theory gives no extra degree of freedom. Namely starting from the constants found in the one-line concept and from the mean position of beach and inshore with respect to the reference line, one just finds the accuracy (standard deviation of line of beach and inshore) as a result.

According to the second approach (option 5, Section 5.2.3.6) no conditions concerning the ratio between s_1/h_1 and s_2/h_2 are given. In this case, a numerical method is used for calculation of the lines of beach and inshore. The ratio between s_1 and s_2 gives a new degree of freedom. Always, the value of s_2 is taken equal to the value of s, found in Section 5.2.3.2.

Concerning the offshore transport, the value of s_y can be obtained in the following way. The equation for the offshore transport S_y reads:

$$s_y = s_y\{y_1 - (y_2^1 - W)\} \tag{5.17}$$

in which
y_1, y_2^1 = coordinates of beach and inshore with respect to the reference line
W = the equilibrium distance
s_y = a proportionality constant

If the length of the coastal stretch to be considered equals l , integration of Eq. (5.17) over l yields:

$$\int_l s_y dl = s_y\{\int_l y_2^1 dl - \int_l y_2^1 dl + W \cdot l \tag{5.18}$$

Assume, that the coast before nourishment is in equilibrium:

$$w \cdot l = \int_l [y_2^1]_{t=0} dl - \int_l [y_1]_{t=-0} dl \tag{5.19}$$

Therefore, if O_1 equals the area contained between the line of the beach before nourishment and the same line after nourishment and if O_2 is defined in an analogous way with respect to the inshore, then substitution of Eq. (5.19) into Eq. (5.18) gives for the total transport per unit of time along the whole stretch:

$$\int_l S_y dl = s_y(O_1 - O_2) \tag{5.20}$$

where O_1 and O_2 are functions of time.

For small Δt, the left-hand side of the equation may be written as:

$$\int_l S_y dl = ([0_1]_t - [0_1]_{t+\Delta t}) h_1 / \Delta t \tag{5.21}$$

as follows from continuity. In (5.21) h_1 denotes the height of the beach.

From (2.11) and (5.17) it is found that:

$$s_y = \frac{-\Delta O_1 \cdot h_1}{\Delta t\,(O_1 - O_2)} \tag{5.22}$$

where
$\Delta 0_1 = [0_1]_{t+\Delta t} - [0_1]_t$

From the data, the following quantities of sand supply at the beach and the inshore over the considered stretch of the coast can be calculated (Table 5-2)

	30 Aug. '78	7 sept. '78	1 oct. '79
Beach Inshore	791.802 373.198	603.368 281.139	431.880 277.920
Total	1.165.000	884.507	709.800

Tabel 5-2: Quantities in m³ of sand supply beach and inshore, between sections 1-15

Because of the initial loss, the first period between August 30, 1978 and Sept. 7, 1978 is not useful for computation of s_y. On the other hand, the second period between Sept. 7, 1978 and Oct. 1, 1979 is too long for the application of (5.22). A better calculation can be made by first extending the computation from the length t of the coastal stretch to an infinite length, thus compensating for losses alongshore.

From the curve-fitting computations, given in Section 5.2.3.4, the percentage of material, disappearing alongshore can be calculated. The values mentioned in Table 5.2. have been corrected for this effect. The results are given in Table 5.3.

	30 Aug. '78	7 sept. '78	1 oct. '79
Beach Inshore	798.602 376.403	615.751 286.910	549.227 353.434
Total	1.175.005	902.661	902.661

Tabel 5-3: Quantities of sand supply at beach and inshore compensated for alongshore losses

Application of (5.22) yields for s_y ,when O_1 and O_2 are taken at Sept. 7, 1978:
s_y = - (549,227 - 615,751) x 61(1.026 (615,751 - 286,910)) = 1.14 m/year.

If O_1 and O_2 are considered on Oct. 1, 1979 one finds s_y= 1.92 m/yr.
Therefore an average value of s_y= 1.53 m/yr will be assumed.

Now the accuracy of the computation of beach and inshore will be calculated, using the before-mentioned "analytical approach" (option 4).

For the two-line model the following relations apply:

$$y_1 = y_{1,par} + y_{1,gaus}$$
$$y_2 = y_{2,par} + y_{2,gaus}$$

in which y_1 and y_2 denote the line of the beach and the inshore respectively, and where in:

$$y_{i,par} = \frac{1}{2} p^1 x^2 + p^1 \cdot \frac{s}{h} \cdot t + y_{i,0} \qquad (5.23)$$

$$y_{1,gauss} = \{1 + \frac{h_2}{h_1} \cdot e^{-\frac{t+T_2}{T_0}}\} \frac{S^{**}/h}{\sigma\sqrt{2\pi}} e^{-\frac{x^2}{2\sigma^2}} \qquad (5.24)$$

$$y_{2,gauss} = \{1 - e^{-\frac{t+T_2}{T_0}}\} \frac{S^{**}/h}{\sigma\sqrt{2\pi}} e^{-\frac{x^2}{2\sigma^2}} \qquad (5.25)$$

Here, the following symbols are used:
S^{**}= the total amount of sand supply
T_1 = constant with dimension "time", referring to a hypothetical moment (before t= 0) when the nourishment consisted of an infinite long dam

with zero width

T_2 idem, referring to a hypothetical moment, (before $t=0$), when the inshore was straight.

$Y_{i,0}$ = y-coordinate of the top of the parabola at time $t= 0$.

$$T_0 = \frac{h_1 h_2}{s_y h} \tag{5.26}$$

$$\sigma = \sqrt{2\frac{s}{h}(t + T_1)} \tag{5.27}$$

Integration of (5.24) and (5.25) over x yields:

$$O_1 = \int_{-\infty}^{+\infty} y_{1,gauss}\, dx$$

$$O_1 = \{1 + \frac{h_2}{h_1} e^{-\frac{t+T_2}{T_0}}\} \frac{S^{**}}{h} \tag{5.28}$$

and in the same way:

$$O_2 = \{1 - e^{-\frac{t+T_2}{T_0}}\} \frac{S^{**}}{h} \tag{5.29}$$

The value T_0 is found from (5.26):

$$T_0 = 6 \cdot 6 / (1{,}53 \cdot 12) = 1{,}96\ year$$

As $h_1 = h_2$,one finds from subtraction:

$$O_1 - O_2 = 2e^{-\frac{t+T_2}{T_0}} \frac{S^{**}}{h} \tag{5.30}$$

from which:

$$T_2 = T_0\, ln \frac{2S^{**}}{h[O_1 - O_2]_{t=t_2}} - t_2 \tag{5.31}$$

For the derivation of T_2 the "second time" t is used in order to avoid complications with the initial loss (which would have occurred if $t_1 = 0$ had been used).

Thus one finds from Table 5.2:

$$T_2 = 1.96 \cdot ln \frac{2 \cdot 902661}{12 \cdot (651{,}751 - 286{,}910)/6} - 0{,}10411 = 1{,}875\ year$$

From (2.24) can also be derived:

$$\frac{[O_1 - O_2]_{t=0}}{[O_1 - O_2]_{t=t_2}} = e^{t_2 / T_0} \tag{5.32}$$

Therefore, this ratio should be: *exp (0.10411 / 1.96) = 1.054.* According to Table 5.3 this ratio equals:

$$\frac{[O_1 - O_2]_{t=0}}{[O_1 - O_2]_{t=t_2}} = \frac{798{,}602 - 376{,}405}{615{,}751 - 286{,}910} = 1{,}284$$

Assuming the sand loss between $t = 0$ and $t = t_2$ evenly distributed between beach and inshore, this ratio reduces to (902,661 /1,175,005) x 1.824= 0.986, where the first two numbers refer to the total quantities of sand at $t = t_2$ and $t = +0$ respectively (Table 5.3).

This shows, that the ratio is of the same order of magnitude, as found from (5.32), and that the assumption of proportional initial sand loss on beach and inshore cannot be directly rejected. Therefore the same straightforward procedure as used for the one-line theory is applied also in this case:

a) "tune" the constants with the available degrees of freedom;
b) consider the best fit for the initial situation (inaccuracy S_{di});
c) take the initial loss into account;
d) calculate the line of the beach and inshore at time $t = t_2$ and $t = t_3$ and find the inaccuracy S_d

The tuning has been treated before. The best fit for the initial situation is found by superposition of Gauss-curves and parabolae. The curvature of the parabola is found from the one-line theory (Section 5.2.3.4.). The y-coordinate of the parabola for beach and inshore are found from the mean y-coordinate of beach and inshore at $t = 0$:

$$\begin{aligned} y_{1,par} &= y_{par} - 168.3\ m \\ y_{2,par} &= y_{par} + 168.3\ m \end{aligned} \qquad (5.38)$$

where y_{par} denotes the y-coordinate of parabola for the coastline, which is the mean between the line of the beach and inshore.

From (5.23) to (5.27), the y-values of the lines of beach and inshore at $t = 0$, $t = t_2$ and $t = t_3$ are calculated; no curve-fitting takes place. Figure 5.40 shows the lines of beach and inshore at time $t = -0$, $t = +0$, $t = t_2$ and $t = t_3$.

Using Eq. (5.15) and (5.16) for the overall initial inaccuracy S_{di} and for the overall inaccuracy S_d, the values S_{di} = 22.05 m and S_d = 16.51 m are found respectively. Furthermore, the inaccuracy for beach and inshore separately are calculated using Eq. (5.11) and (5.13). The results are shown in Table 5.5. For the beach an inaccuracy of 9.62 m is found.

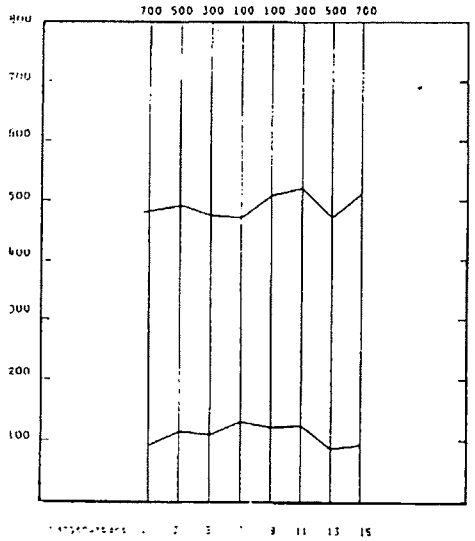

April 20, 1978 before nourishment

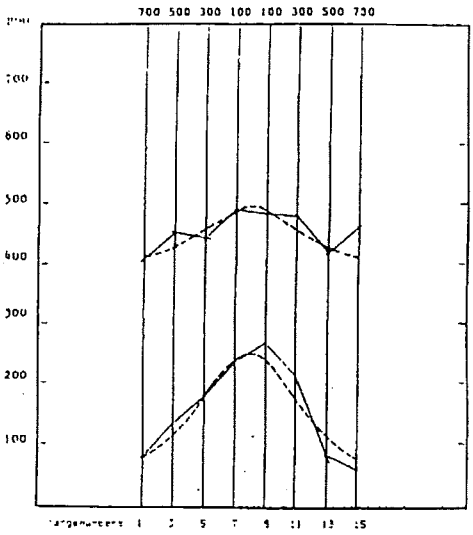

July 30, 1978 after nourishment

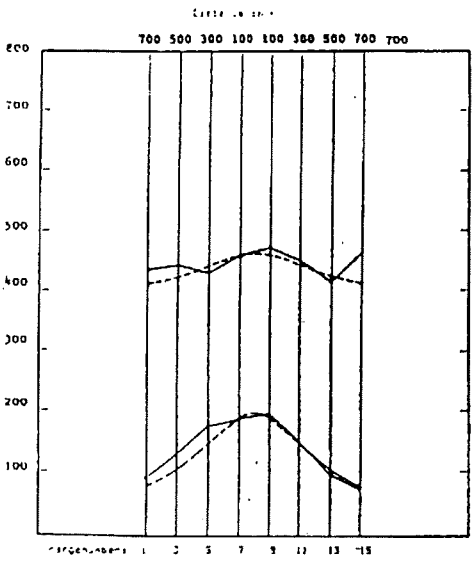

Sept. 7, 1978 after nourishment

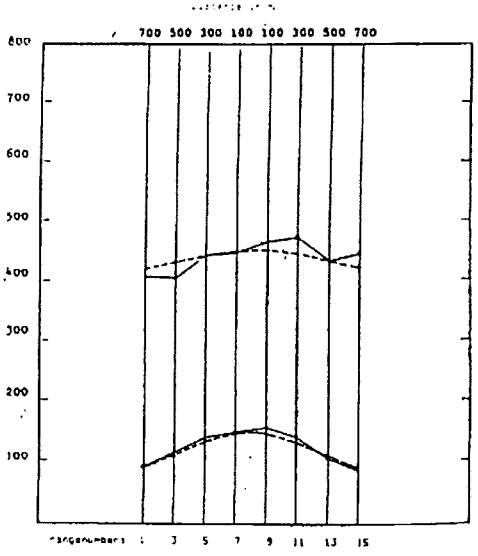

Oct. 1, 1979 after nourishment

Figure 5.40: Comparison of measured and calculated line of beach and inshore using the analytical two-line theory

5.2.3.6 Numerical two-line theory

The results may still improve, when in the initial condition the standard deviation of the Gauss-curves, representing beach and inshore respectively, are allowed to deviate from each other. However, under those circumstances an analytical solution is not known and a numerical approach is necessary.

As in the analytical case, the results of the one-line theory will be the starting-point for the two-line approach. The value of the gradient of the longshore transport 5 will be derived from the one-line approximation, but the subdivision in s_1 and s_2 will be optimized. This provides an extra degree of freedom.

The theory itself and the way of numerical elaboration is treated in Annex VI. The time step Δt and the distance between the gridpoints Δx are chosen as:

$$\Delta t = 0.05\ year \text{ and } \Delta x = 200\ m.$$

The positions of the initial parabolae for beach and inshore are taken equal to the ones, used for the analytical two-line approach. Thus, the area A confined between the measured line of the beach in its initial position (t= +0) and the beach-parabola is known. The Gauss-curve representing the initial beach position is optimized by varying its standard deviation, keeping the area between this Gauss-curve and the parabola equal to A.
In the same way the Gauss- curve, representing the inshore is determined. Starting from the equation for the superposition of parabola and Gauss-curve, for the initial curves is found:

$$y\ (1,par) = \tfrac{1}{2}\ (-2 \cdot 10^{-5})\ x^2 - 2 \cdot 10^{-5} \cdot (55 \cdot 10^{3})t + 77.1$$
$$y\ (2,par) = y\ (1,par) + 336.6$$

and for the initial Gauss curves:

$$y\ (1,gauss) = 195.0\ exp\ \{-x^2/(2 \cdot 276^2)\}$$
$$y\ (2,gauss) = 60.7\ exp\{-x^2/(2 \cdot 398^2)\}$$

For the initial inaccuracy s_{di} defined according to (5.15) is found:

$$S_{di} = 20.22\ m$$

Now the initial loss is taken into account by reducing the y-coordinates of the initial Gauss-curves for beach and inshore with 25%. Next, the lines for beach and inshore are numerically calculated at time $t = t_2$ and $t = t_3$. Here, the offshore transport is determined by the constant s_y, which is taken equal to 1.53 m/year, as treated in Section 5.2.3.5. curve-fitting takes place by optimization of the ratio between s_1 and s_2. A minimum value of the inaccuracy is found when $s_1 = s_2 = 330{,}000\ m^3/yr/rad$.

The inaccuracy S_d, defined according to (5.16) appears to be:

$$S_d = 15.10\ m$$

Furthermore, the inaccuracy of beach and inshore are calculated separately, using Eq. (5.11) and (5.13) for the initial situation and for the combination of second and third moment respectively. The results are given in Table 5-4.

	Beach	inshore
initial situation (S_{di})	21.25	21.06
second/third moment (S_d)	10.20	19.16

Table 5-4 Inaccuracy of numerical two-line computation for beach and inshore respectively

The lines of beach and inshore for t= +0 , t_2 and t_3 are given in Figure 5.41.

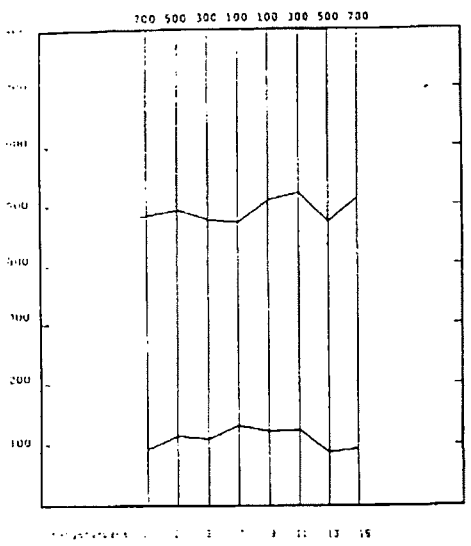

April 20, 1978 before nourishment

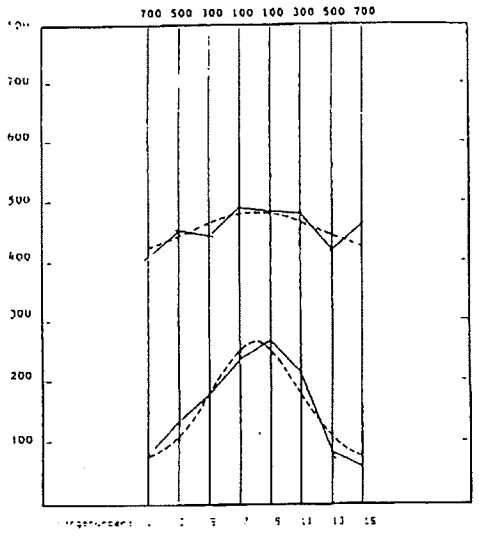

July 30, 1978 after nourishment

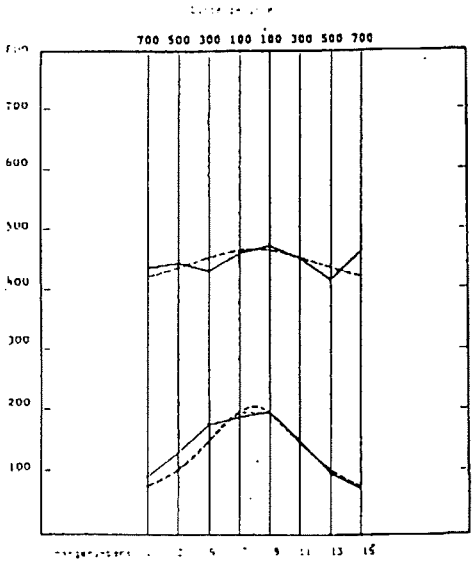

Sept. 7, 1978 after nourishment

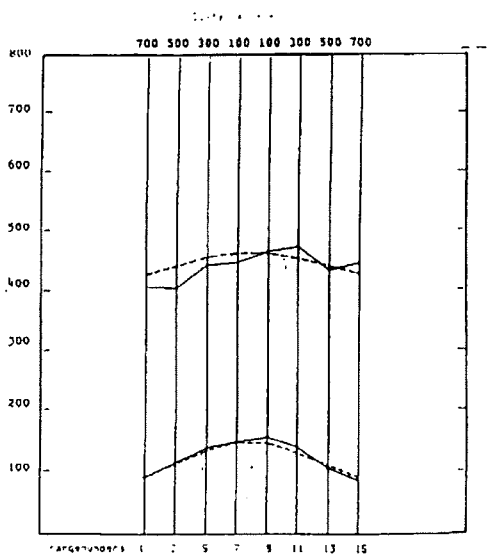

Oct. 1, 1979 after nourishment

Figure 5.41: Comparison of measured and calculated line of beach and inshore using the numerical two-line theory

	one-line theory		two-line theory		
number of schematization (option)	1	2	3	4	5
treated in Section Figure	2.5.2 2.12	2.5.3 2.14	2.5.4 2.15	2.5.5 2.16	2.5.6 2.17
way of computation	analytical				numerical
schematization coastal area: MSL +4 m -2 m -8 m	coastline	beach	beach inshore	as in 3	as in 3
additional assumptions	coastline	line of beach	line of beach and inshore		initial: line of beach and inshore
	has (have) the shape of a Gauss-curve ($\hat{y}$, σ)				
		no sand loss from beach to inshore	beach and inshore have same shape as coastline found in 1 shifted in on/offshore direction	σ for beach and inshore as coastline, found in 1 $\hat{y}_{beach}$* $\hat{y}_{inshore}$	coastal shape follows from numerical computation
initial value(s) of $\hat{y}_{beach}$ and $\hat{y}_{inshore}$ in m (before initial loss)	$\hat{y}$ = 132.87	$\hat{y}_b$ = 192.5	$\hat{y}_b$ = 132.87 $\hat{y}_i$ = 132.87	$\hat{y}_b$ = 170.0 $\hat{y}_i$ = 80.4	$\hat{y}_b$ = 192.5 $\hat{y}_i$ = 68.3
initial value(s) of σ_{beach} and $\sigma_{inshore}$ in m	σ = 294	σ_b = 276	σ_b = 294 σ_i = 294	σ_b = 294 σ_i = 294	σ_b = 276 σ_i = 398
initial inaccuracy (m)	S_{di} = 15.55	beach: 21.25	beach: 41.95 inshore: 39.83 S_{di} = 39.51	beach: 22.45 inshore: 23.20 S_{di} = 22.05	beach: 21.25 inshore: 21.06 S_{di} = 20.44
inaccuracy of calculation (m)	S_d = 11.31	beach: 11.77	beach: 20.23 inshore: 27.33 S_d = 23.65	beach: 9.62 inshore: 21.71 S_d = 16.51	beach: 10.20 inshore: 19.16 S_d = 15.10

Tabel 5. 5: Summary of results

5.2.4 Cadzand

5.2.4.1 General

In the framework of the extension of the harbour of Zeebrugge, a beach fill of $8.4 \cdot 10^6$ m^3 of sand has been placed between this harbour and the border between Belgium and The Netherlands over a distance of approximately 8 km. This beach nourishment project was carried Out between December 1977 and March 1979.

Prior to the execution of the beach nourishment various studies have been carried out, among which a series of coastline computations with the one-line coastal model. On the basis of wave observations the coastal constant s in the diffusion equation $\frac{\partial y}{\partial t} - \frac{s}{h}\frac{\partial^2 y}{\partial x^2} = 0$ was determined. It was found that the value varied strongly along the coast, but the average value was approximately $1.5 \cdot 10^6$ m^3/yr/rad.

In the present analysis the deformation of the eastern limit of the beach fill has been considered. Assuming that the original coastline in 1977 was straight and that the original schematized coastline of the beach fill is rectangular (see Figure 5.42), the following analytical solution of the one-line equation can be applied:

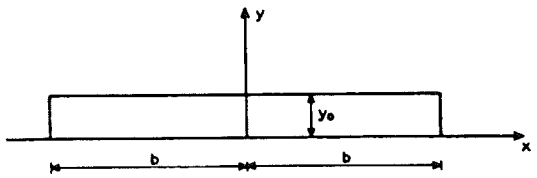

Figure 5.42: Schematization of beach-fill

$$y = \frac{y_0}{2} erf\left(\frac{b - x}{\sqrt{4\frac{s}{h}(t + t_0)}}\right) \qquad (5.39)$$

where t_0 is a constant and *erf* is the error function, y_0 is the width of the fill and b is half of the length of the fill.

From the measured coastal profiles it was found that the height of the active profile h = 12 m. The optimum values of y_0 and b were determined by comparing the computational results with the measured schematized coastlines in the period 1978-1983. With y_0 = 77 m and b = 3970 m found in this way, the optimum value of $\sqrt{4(s/h)t_0}$ was determined for the year 1979, taking t_0= 1 year. It was found that $\sqrt{4(s/h)t_0}$ = 402.5 m and thus s= 0.5 x 10^6 m^3/yr/rad.
With this value of s, the coastlines for the years 1980 to 1983 were computed, and the results agreed reasonably well with the measured schematized coastlines.

5.2.4.2 Description of the area

5.2.4.3 One-line theory

Computation of beach fill deformation

For the analysis of the deformation of the eastern limit of the beach fill the area between km. 15.0 and km. 16.8 has been considered (see Figure 5.43). On the basis of beach levellings and sounding charts the coastal profiles for the yea 1978, 1979, 1980, 1981, 1982 and 1983 have been schematized according to the one-line theory. For that the average height of the active profile is 12 m. Figure 5.44 shows the schematized coastlines plotted with respect to the 1977-position of the coast. The development is rather irregular, in particular in the section

km 5.4 and eastward thereof, where the morphologic evalutions are influenced by the tidal area Zwin. Therefore it was decided to restrict the analysis to the coastal zone between km. 15.6 and km. 16.8.

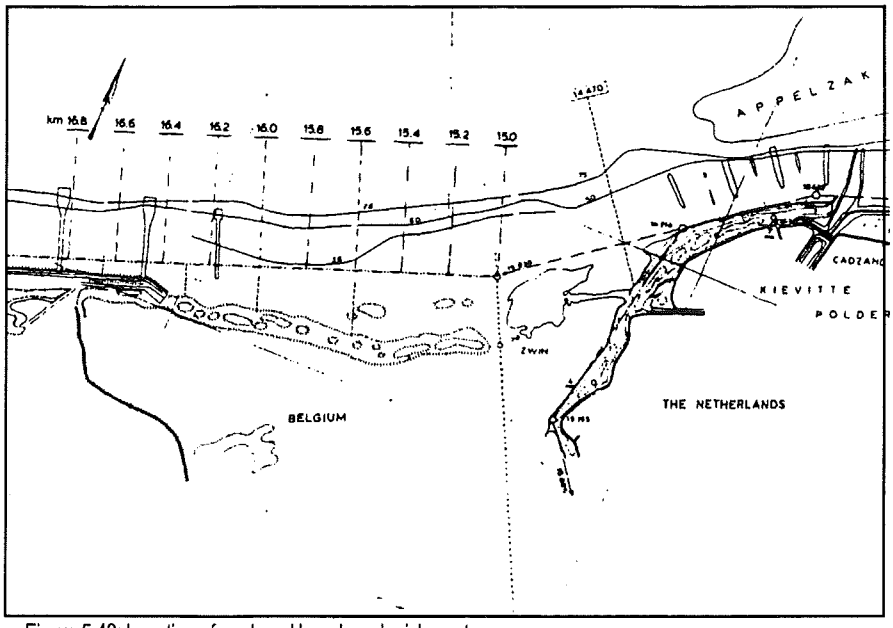

Figure 5.43: Location of analyzed beach replenishment

It is assumed that the coastline of 1977 was straight and that the original schematized coastline of the beach fill was rectangular. In that case the following analytical solution of the one-line equation can be applied:

$$y = \frac{y_0}{2}\{erf(\frac{b-x}{\sqrt{4at}}) + erf(\frac{b+x}{\sqrt{4at}}) \qquad (5.40)$$

where:

y	= position of schematized coastline
y_0	= initial width of the fill in seaward direction
b	= initial length of the fill, measured from the centre in along-shore direction
x	= position along the coast with respect to the centre of the fill
t	= time
a	= coefficient in diffusion equation = s/h
s	= coastal constant
h	= height of schematized profile

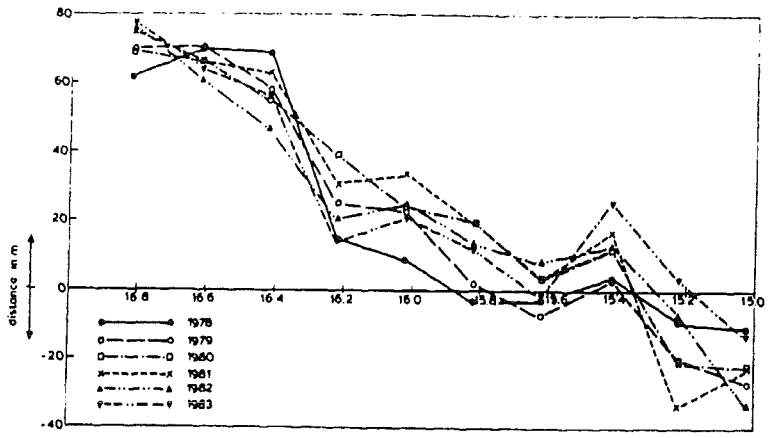

Figure 5.44: Schematized coastlines with repect to coastline 1977

Figure 5.45 shows the schematic geometry of beach fill

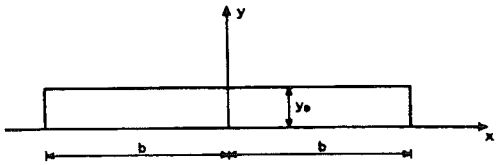

Figure 5.45: Schematic geometry of beach fill

It has been assumed that the deformation of the eastern limit of the beach fill is not affected by its western limit. In that case the analytical solution reduces to

$$y = \frac{y_0}{2} erf(\frac{b-x}{\sqrt{4at}}) \qquad (5.41)$$

In first instance the optimum values of y_0 and b were determined by comparing the computational results with the schematized coastlines in 1978, 1979, 1980, 1981, 1982 and 1983. For the considered coastal area between the sections km 15.6 and km 16.8, which correspond with the model coordinates 4600 and 3400, the following values were found

y_0 = 77 m
b = 3970 m

With these figures the optimum value of $\sqrt{(4at)}$ was determined for the year of 1979, for which it was assumed that t = 1 year, since the eastern part of the beach fill was placed in the period July 1977-June 1978. The optimization for this year yielded the following value $\sqrt{(4at)}$ = 402.5 m

Since t = 1 year it follows that a = 40.500 m^2/year.
The average value of h = 12 m and then the coastal constant $s \approx$ 500,000 m^3/year/radian.

With the above values of y_0 = 77 m, b = 3970 m and a = 40500 m^2/year the coastlines for the subsequent years have been computed and compared with the measured, schematized coastlines. The results are shown in Figure 5.46 for the years 1979, 1980, 1981, 1982 and 1983. It should be observed that the measured positions of the coast east of km 15.6 have not been taken into account.

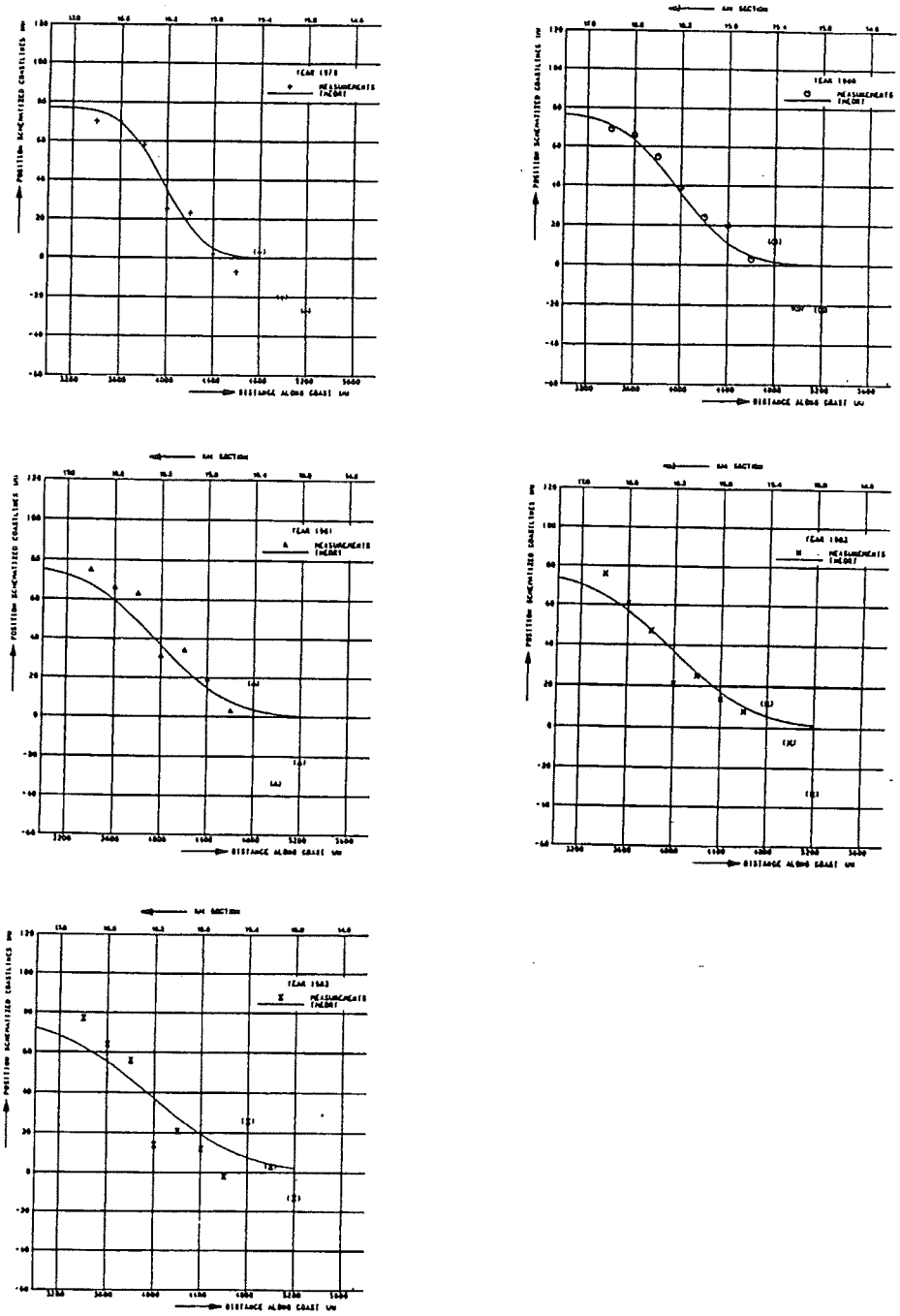

Figure 5.46: Comparison of measured and predicted coastlines

Evaluation

The predicted coastlines for the years 1980 through 1983 agree reasonably well with the measured position of the coast. It should be borne in mind that the analysis has been limited to a relatively short coastal stretch and that only the alongshore deformation of the coast has been considered. In line with other cases it might be concluded that the theory gives a fair estimate.

As far as the coastal constants concern, again large variations are encountered. In a previous study [1] the coastal constant s was determined on basis of the longshore transports computed with the CERC-formula. It was found that $s \approx 1{,}500{,}000$ m^3/year/radian, but according to the computations the value varied strongly along the coast. If this value is introduced in the present computations instead of $s = 500{,}000$ m^3/year/radian, then the predicted coastline position y would differ with roughly 20% from the results presented in Figure 5.46.

5.2.4.4 Two-line theory

The beach nourishment project at Zeebrugge has been used as a second example of the application of the two-line theory. As the two-line theory is more detailed than the one-line theory, it requires more detail with respect to the initial conditions and the boundary conditions. Therefore, in the two-line approach for Zeebrugge, the real situation is approximated better than in the case of the one-line theory (see Section 5.2.4.3). The attention has been focussed on the east-boundary of the fill, which is located near the Dutch-Belgian border, as shown in Figure 5.43.

It may be revealed, that a good prediction of the behaviour of the supply, especially at the eastward boundary, was of great importance for the Belgian Government, since expensive additional coastal protection works, such as groynes with a length of 1 km, were taken into consideration to prevent longshore losses in an eastward direction. With the aid of coastline theories, it has been possible to predict, that these groynes were not necessary. After the execution of the nourishment project, it appeared that the losses were even less than predicted.

The area between km 15.6 and 16.8 has been considered in detail (see Figure 5.43). However, in a more approximative way, also the area between km 14.2 and 15.6, where the ancient, 15th century entrance to the harbour of Bruges, the "Zwin" debouches, has also been taken into consideration, as well as the discontinuity at the most easterly groyne along the Belgian coast. The supply originally ended at km 16.2.

The coast near the Dutch-Belgian border consists of two groyne-protected areas, one on the Dutch and one on the Belgian side. These areas are connected by an unprotected area. In the deeper regions, the bottom topography is to a large extent determined by currents in the tidal channel, the so-called Appelzak. The wave influence is especially important at the beach. In the computations, only waves have been taken into account.

The line of the beach has been defined by the region between MSL +4 m and MSL-2 m, while the region between MSL -2 m and MSL -8 m defines the line of the inshore. The initial situation before nourishment has been modeled by superposition of three stable situations:

- The macro-coastline, where the resultant wave-driven longshore transport (Q) in eastward direction is decreased due to the groynes in the protected area, and by the turning of the coast to the direction of the wave crests in the unprotected area (see Figure 5.47a).
- The unprotected part of the coast is rnodeled by a line of the beach and a line of the inshore between the groynes (see Figure 5.47b and Bakker, 1968a). Just eastward of the last Belgian groyne, sand is transported to the beach, because the profile is flatter than the equilibrium profile. Just westward of the first Dutch groyne, the beach is located moreoffshore. The profile is here steeper than the equilibrium profile.
- The Zwin has been schematized by a sink at the beach and a source at the inshore. Sink and source have the same strength (see Figure 5.47c and Bakker, 1968b). The reason for this schematization is, that during storm conditions the sand is dumped into the Zwin channel, where it is transported by tidal currents from the beach to the inshore zone. Since the lines of beach and inshore are located at a larger distance from each other than the equilibrium distance, an onshore transport results, returning the material from the inshore to the beach.

In this way, the coastline of 1977 between km 16.8 and 15.6 (before nourishment), as shown in the upper part of Figure 5.48, could be reproduced with an accuracy of 12 m. In order to model the fill just after nourishment, the two-line solution for the evolution of a rectangular beach nourishment ha been applied (see Background Report, Annex VI).
It has been assumed, that in 1978 the inshore was not yet affected by the fill, while along the beach already a certain deformation of the rectangular shape had taken place.

According to the theory, the deformation of the fill can be described by an error function. The optimal shape of the error function, found from curve fitting, gave an initial inaccuracy of 10.5

m (7.5 m for the beach and 13.5 m for the inshore). Starting from this initial condition and taking the transport constants for the beach and inshore as $s_1 = s_2 = 250{,}000$ m^3/yr/rad (thus resulting in $s = 500{,}000$ m^3/yr/rad, as found in Section 9.2.2), the lines of beach and inshore of 1980 and 1983 were calculated. The results are shown in Figure 5.48. An overall accuracy of 17 m was found.

The value of the cross-shore sediment transport constant s_y =3 m/yr was chose in such a way, that the behaviour of beach and inshore at the western boundary (km 16.8) corresponds with the behaviour observed in nature. This value has also been used for the modeling of the stationary line of beach and inshore along the unprotected area and for the modeling of the Zwin.

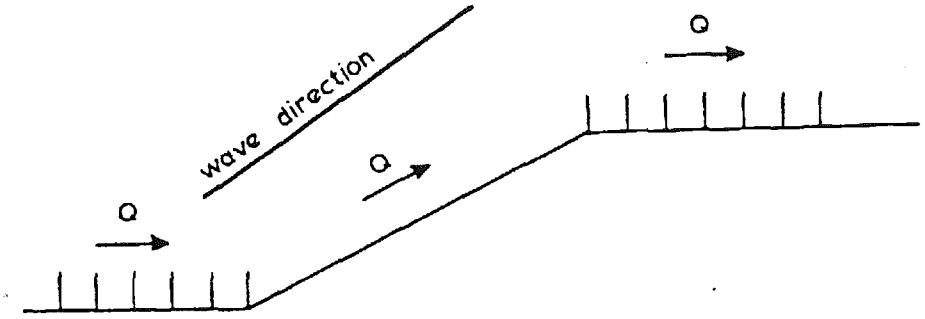

Figure 5-47a: A stable macro-coastline (the transport Q should be everywhere the same)

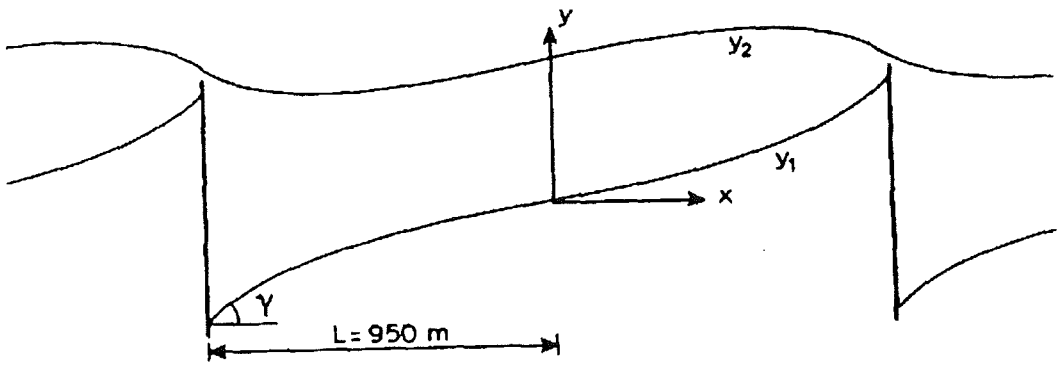

Figure 5-47b: Schematization of the unprotected area between the Belgian and Dutch groynes

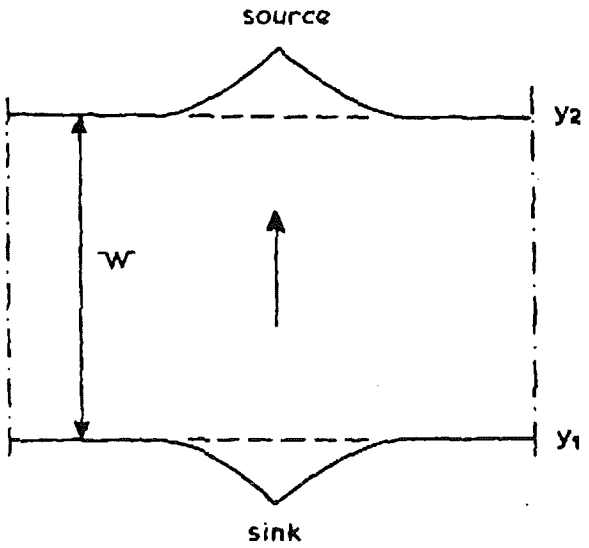

Figure 5-47c: Schematization of the Zwin

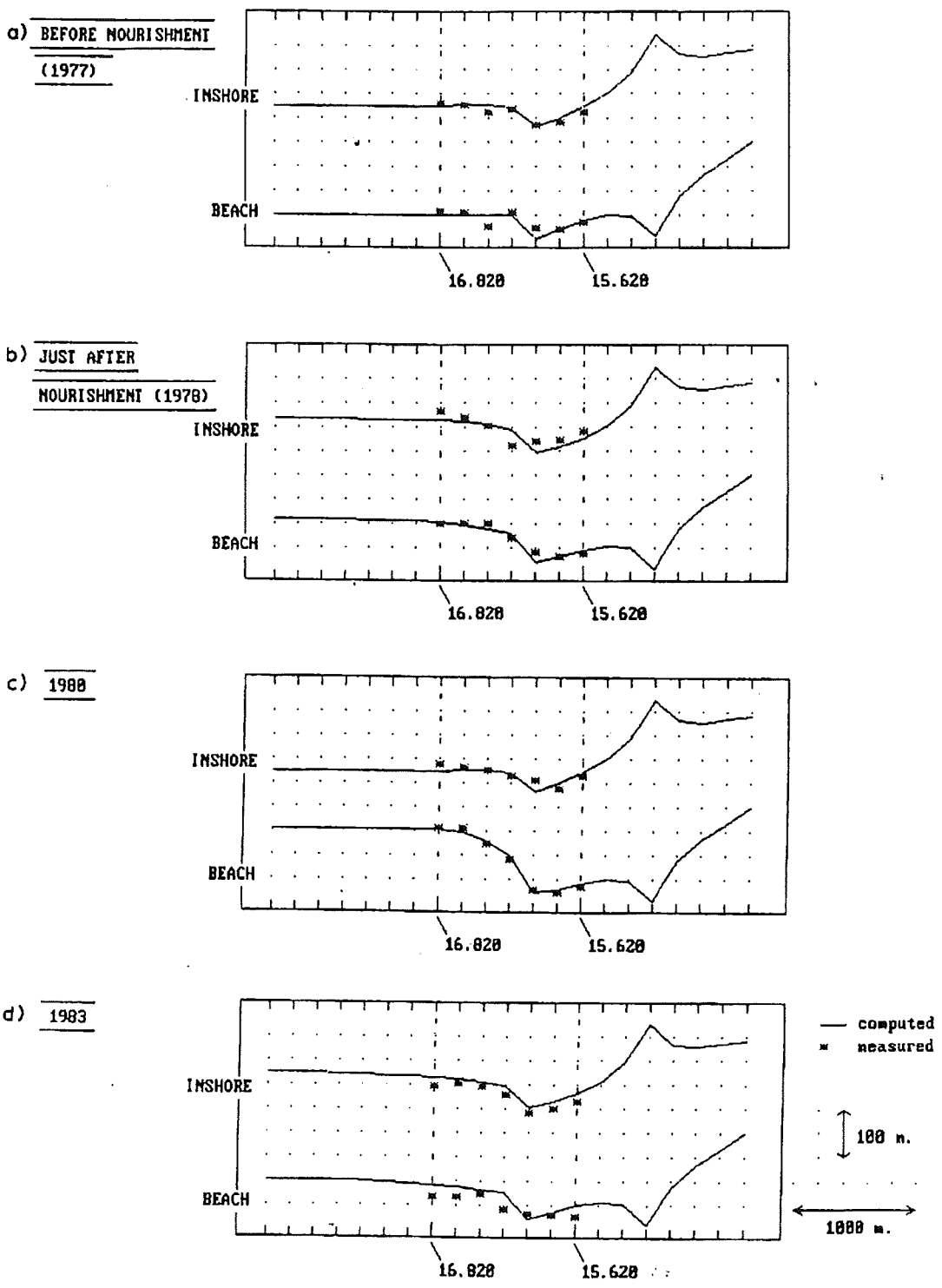

Figure 5-48: Results of two-line computations for Zeebrugge

5.2.5 Holland coast

Abstract
The Coastal Defence Study, as executed in the Netherlands, involved a 100-year prediction for the Coastline evolution of Specific parts of the Holland coast. In order to create this prediction a mathematical two-line model was used. In this model the effects of wave driven as well as tidal transports are incorporated, also cross-shore transport is implemented. The model is calibrated using sand balances, derived from measurements of coastal profiles. Qualitatively correspondence is reached, but quantitative differences between model and nature remain.

5.2.5.1 Introduction

The mathematical prediction of the coastline evolution of the Holland coast for the Coastal Defence Study is based on a two-line model, as described by Bakker (1968) and in the Manual on Beach Nourishment (Pilarczyk,ed.,1986). The way of prediction is described by Dijkman Ct al. (1989); the present paper gives a condensed version of this report.
The Holland coast is the central one of the three parts (Rhine/Scheldt estuary, uninterrupted Holland coast; Wadden islands) into which the Dutch coast can be divided (see figure 5.49). Three harbors (Hook of Holland, Scheveningen and Ijmuiden) partition the Holland coast. The harbor moles of Hook of Holland and Ijmuiden have a length of 3 km and therfore have a dominating effect on the coastal behaviour.

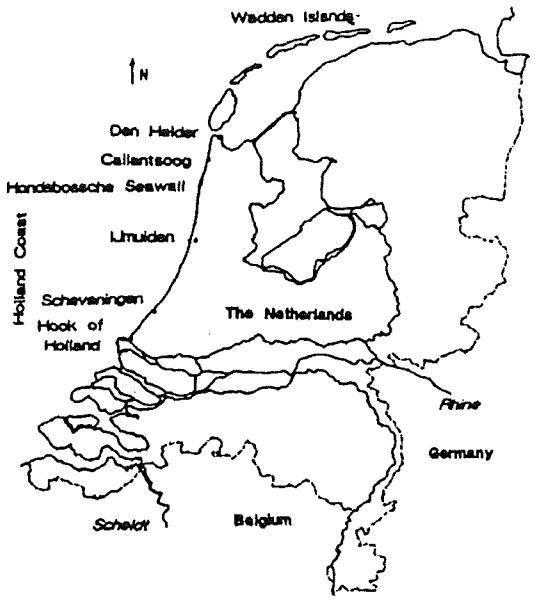

Figure 5.49: The Holland coastt

5.2.5.2 Model boundaries

For the model the Holland coast was divided into three areas:

- Callantsoog to IJmuiden
- IJmuiden to Scheveningen
- Scheveningen to Hook Holland

These areas all stretch from one harbor mole to the other, except for the most Nortern border. Here the model was limited to Callantsoog, because of the influence of the tidal inlet near Den Helder becoming to strong in the more Northern region.

5.2.5.3 Model parameters

- Wave climate
The wave climate used is derived from measurements in the period 1978-1984. These measurements lack direct information on the direction of wave propagation, only the wind direction is given. To overcome this problem a correction to the directions has been applied based on the correlation as proposed by Hokke and Roskam (1987), who found this correlation between the wind direction and the wave direction from measurements using Wavec-buoys. The so corrected wave climate significantly differs from the original 'uncorrected' one.
Wave data originating from three different sites (Eierland, Ilmuiden and LE Goeree) have been used. A comparison between these three sites gives an impression of the variation of the wave climate along the Holland coast, see figure 5.50.

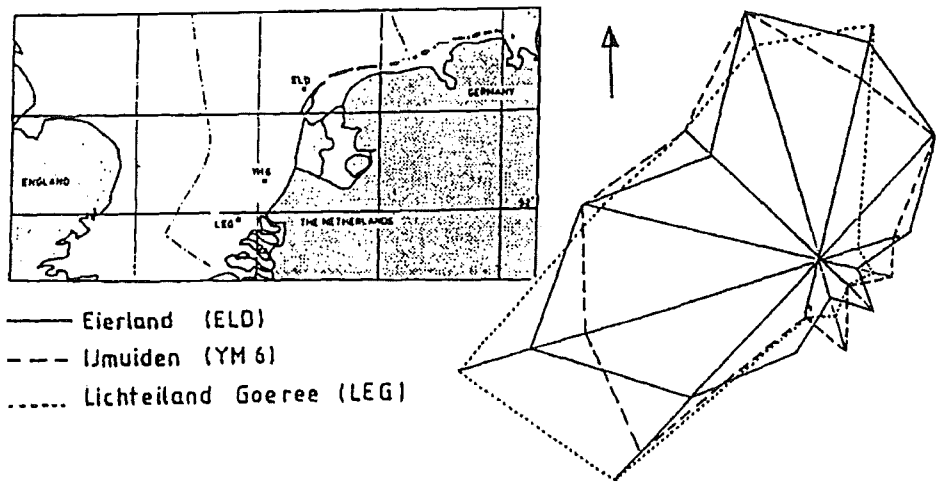

Figure 5.50: Variation of the wave climate

Furthermore the wave climat as now determined is valid for deep water with a depth of appr. 20-25m. In order to obtain the required wave climate at shallower water (of appr. 10 m depth) the ENDEC program (Energy DECay, Delft Hydraulics, 1988) was used. This program incorporates the effects of breaking waves, refraction, shoaling, bottom friction and wind.

-Tidal influence

The tidal data have been taken from the HOKU model (HOllandse KUst, which stands for Holland Coast) (Delft Hydraulics,Hartsuiker, 1988). The non-linear relation between tidal velocities and sediment transports has been compensated by using a morphological tide, which is found by multiplying the average tide with a 'tidal factor' (here taken to be 1.1).
In the direct surroundings of the harbors the influence of the tidal effects can be expected to be much more noticeable than at some distance from those harbors. This as a result of the converging/ diverging tidal flows, causing sediment transport gradients and accessory erosion/accretion patterns. Qualitatively the formation of an eddy at the leeside of a harbor mole causes a reversal of the longshore transport in this region. For the opposite tide the longshore transport directed to the mole will remain constant until a much smaller distance from the mole. The resulting effect of a complete tidal sequence will therefore be an accretion at a small distance to the mole, followed by an erosion that at growing distance from the mole becomes less noticeable.
The tidal effects are calculated in the vicinity of the harbors up to the point where the effect of the harbor mole is negligible. In between the harbours a linear interpolation has been used. The tidal velocities at the points in the grid are calculated for an interval of 30 mm. (25 in total, covering 12 hours). The probabilityfunction for the orbital velocities caused by waves is determined for each grid point. For the fraction of time waves are breaking in this point there is assumed to be no contribution to the tidal transport for that particular combination of waterdepth, wave direction and wave height. Then with the Bijker formula, using both the orbital velocity distributions and the tidal velocities, a resulting tidal sediment transport is calculated. This tidal transport is assumed to be time independent. The results are shown in figure 4.

- Diffraction near the harbors

In the direct vicinity of the harbors the effect of diffracting waves around the harbor moles is an important factor. This effect is implemented in the model, however in a somewhat limited manner: the diffraction and refraction effects have been calaculated seperately. For the method used see Bakker et al. (1989).

- Coastal constants
  These are the constants (constant only in time, but varying along the coast as a result of a variation of the wave conditions along the coast) which determine the longshore wave driven sediment transport ($S_{0,i}$ and S_i in eq. 2.1). Calculation of these constants is done using the following assumptions:

- The wave driven longshore transport between two depth contours is proportional to the longshore component of the energy-loss of the driving wave between those depth contours.

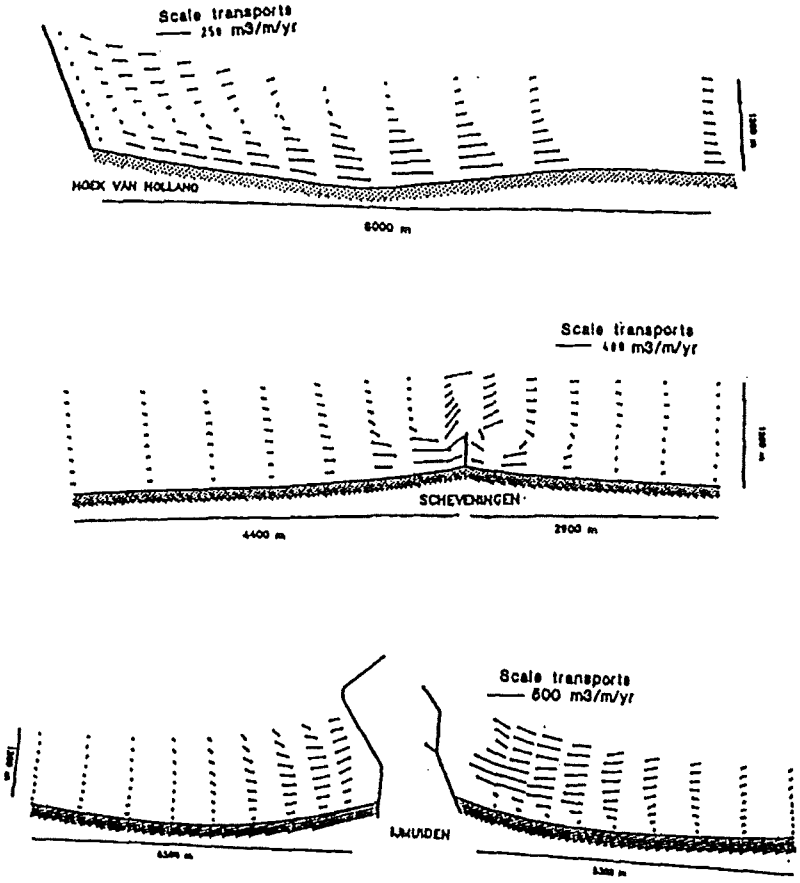

Figure 5.51: Resulting tidal sediment transports near the harbors

The equation used to calculate the longshore transport is a variation of the CERC formula

$$S = A \cdot (n_{br} H_{br}^2 c_{br} \sin(\varphi_{br}) \cos(\varphi_{br}) \qquad (5.42)$$

With S : longshore sediment transport (m^3/yr)
A : proportionality constant (-)
the wave characteristics at the breaker line:
n (-), H (m), c (m/s), φ (rad)

For a more detailed description of the method used see Svasek (1968), Ballker (1969) and Bakker et al.(1989).
The calculations were performed using the KC program (Kust Constanten, which stands for Coastal Constants, by Casteleyn, 1975) which includes diffraction and refraction effects. In order to compensate for the overestimated diffraction effects, caused by using monochromatic waves, a reduction factor for the calculated diffraction effect has been applied, this factor is taken to be 0.75. (The difference between the calculated values in the diffraction zone and the value outside this zone is multiplied by the reduction factor).
Originally the KC program gives values for the coastal constants for a one-line model, the necessary two line values are derived from the one-line values by assuming a constant ratio between the values for beach and inshore respectively. From calculations a ratio (beach : inshore) of 1 : 4 was found.
The only remaining unknown in the coastal constants is the proportionality constant A (see eq. 4.42). This will be determined in the calibration of the model, just like the cross-shore coastal constants s_y and W (see eq. 2.2).

5.2.5.4 The coastal defence works

There are three different defence methods in use along the Holland coast groynes, the Hondsbossche Seawall and sand supplies.
The groynes partially block the longshore sediment transport. The effectiveness of the groynes has been roughly estimated by considering the depth to which they reach, in relation to the sediment transport distribution over the depth as found by Bakker (1969). In the model this has been accounted for by using a reduction factor for the coastal constants. Note that this method implies neglecting the impact the groynes may have on the tidal sediment transports : the tidal transports mainly take place at greater depths than the depths to which the groynes reach.
The Hondsbossche Seawall is a rigid seawall, below MSL-1m it is covered by sediment. At both sides of the seawall there are several groynes preventing this area from eroding too severely. In front of the Hondsbossche Seawall the beach zone does not really exist, in the model this has been accounted for by taking the coastal constants in this area equal to zero. In the inshore zone there can be some sediment transport. However, at both sides of the Hondsbossche seawall very strong curves in the coastlines occur, which are not varying too much in time. Therefore the coastal constant s_2 must also be taken equal to zero for this area. This assumption can be backed up by the geological consistency of the bottom material in front of the Hondsbossche Seawall: there are some almost baring clay layers present there (de Mulder, 1983). This implies there can only be a constant transport along the Hondsbossche Seawall: what goes in on one side must go out the other. The model does not implement the sand supplies, but does take these into account in the calibration of the model, see the next paragraph.

5.2.5.5 Calibration and output

The proportionality constant A, used in the calculation of the coastal constants (see eq 5.42), is used as the instrument to calibrate the model. The calibration is based on the measurements of the coastal profiles of the Dutch Coast on a yearly basis, as stored in the JARKUS database. These measurements are used to create sand balances for the specific parts of the Holland Coast. Some results are shown in figure 5.52, showing the relative amount of sand (relative to the first year) for three subareas.

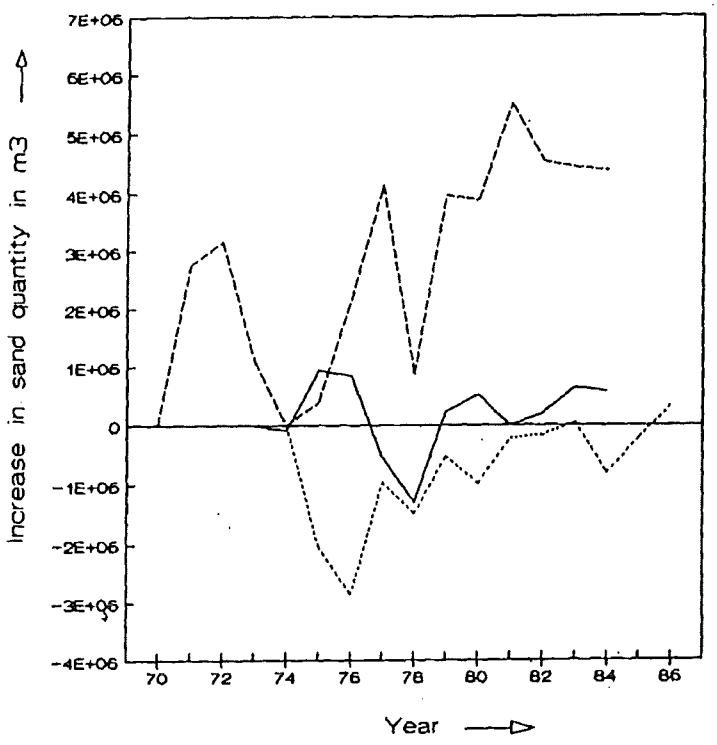

Figure 5.52: Sand balance for the Dutch coast

By making some assumptions these sand balances can be used to give an idea of theaverage sediment transports in the considered areas. The necessary assumptions:

- No sand leaking around the harbor mole near Hook of Holland.
- No sand from above the MSL-5m passes from one side of the harbor moles of Scheveningen and IJmuiden to the other.
- Equally distributed sand supply from deeper water over the MSL-5m line for an area between two harbors.

With these assumptions the following conclusions can be derived:

- Accretion of the area Hook of Holland-IJmuiden of 370.103 m^3/yr, or 6 m^3/m/yr.(=p2 in eq 2.3).
- For the area IJmuiden-callantsoog this accretion is 40.103 m^3/yr, or 0.9 m^3/m/yr. This value has been neglected in eq 2.3). This relatively low value (relative to the value in the area Hook of Holland-IJmuiden) can be explained by the increase (going Northward from IJmuiden) of the Northward tidal flow in deeper water, consuming' the sediment which would otherwise come to benefit the area above the MSL-5m level.
  The onshore transports found here compare reasonably well to those found by Stive (1990). The value Stive proposes, is a bit larger: approximately 10 m^3/mlyr, almost constant over the entire Holland coast. However this value is derived for an onshore transport over the MSL-8m line, where in this paper the transport over the MSL-5 line is considered.
- The optimum value for the proportionality constant A is 500, determined for the area Hook of Holland IJmuiden. This value is about a third of the conventional values! With the proportionality constant A now determined, the longshore transports can be calculated, the results are shown in figure 5.53.
- Again, comparing the so found longshore transports to those found by Stive (1990) a reasonable agreement is found, see Dijkman et al.(1989).

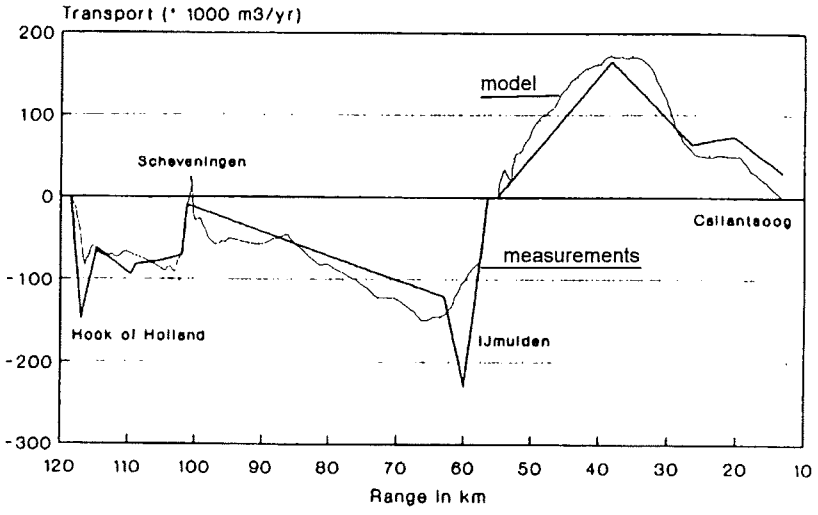

Figure 5.53: Calibration of the coastal constants

- The coastal constant for the cross-shore transport, s_y (at a depth of MSL-1m) is found to be in the order of 0.05 m/yr (for the region Hook of Holland - Scheveningen) tom/yr (for Scheveningen - IJmuiden). These results were found by using a value of 280 m for the equilibrium distance between beach and inshore line. In the modela constant value of 0.10 m/yr is used.

Other scenarios, for instance large offshore transport caused by rip-currents and tidal currents in the immediate vicinity of the harbor moles, have been elaborated with respect to their consequences for the coastal development. (The report by Dijkman et al. (1989) shows

results). However, these scenarios had to be rejected because of the coastal behavior according to these scenarios proved to be unrealistic.

5.2.5.6 Results

Figure 5.54 shows the calibrated coastal development between 1973 and 1984, for the area Callantsoog to IJmuiden. On the left-hand side one observes the effect of the harbor mole of IJmuiden, and between the ranges 20 to 25 the effect of the Hondsbossche Seawall.
Figure 5.55 shows predictions found in this way for the years 2020 and 2090. Finally the same results are presented in a different manner, namely with the reference as the initial situation. Figure 5.56 shows the development of the beach-line, figure 5.57 that of the inshore line.
Results for the area IJmuiden to Hook of Holland are not presented here, they can be found in the report by Dijkman et al.

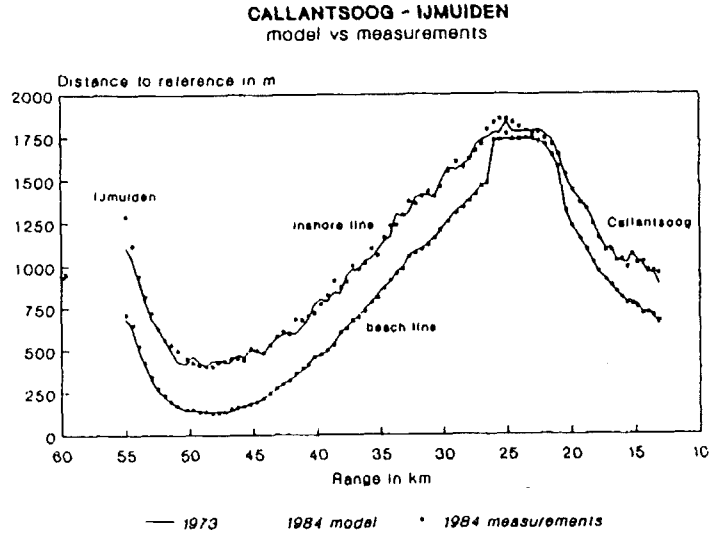

Figure 5-54: calibrated coastal development for Callantsoog to IJmuiden

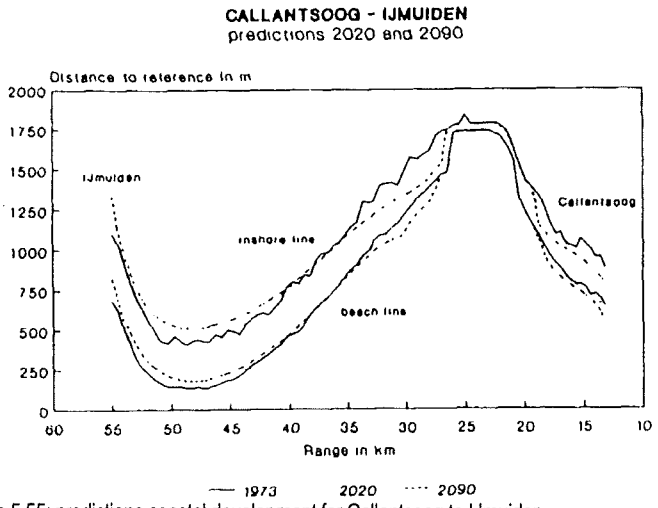

Figure 5.55: predictions coastal development for Callantsoog to IJmuiden

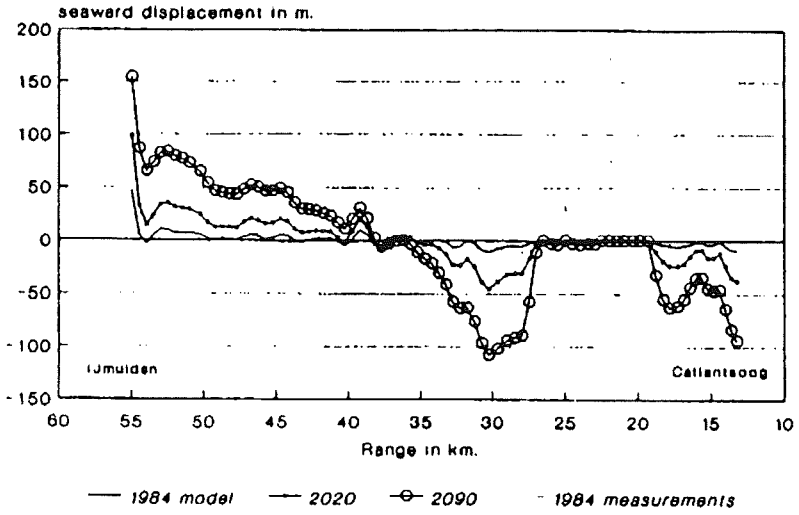

Figure 5.56: development of the beach-line

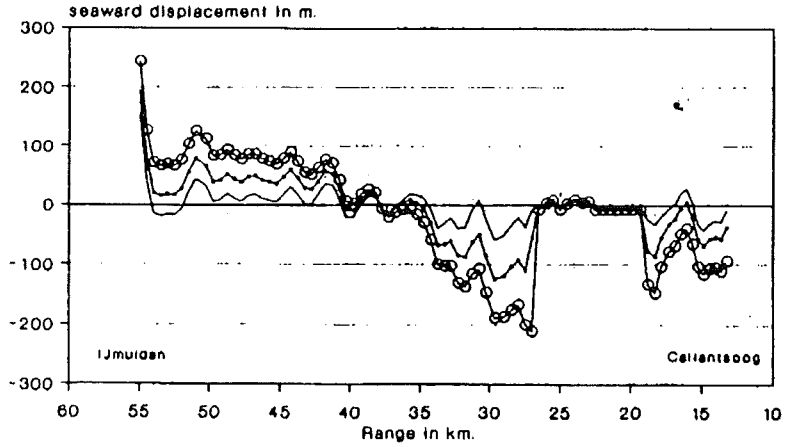

Figure 5.57: development of the shore-line

5.2.5.7 Conclusions

- The results (certainly for an area with harbor moles) strongly depend on the wave climate used (Dijkman et al, 1989). Therefore not only the accuracy, with which the present wave climate is known, but also the accuracy, with which the future wave climate can be predicted highly determines the accuracy of a prediction of the coastline evolution. Accurate wave data (especially concerning wave directions) are vital for accurate coastal prediction.
- The proportionality constant A (giving the ratio between the sediment transport and the longshore component of the wave energy flux, see eq 5.42) found here, is much lower (about a third) than more conventional values.
- The use of the two-line model as an instrument to create a prediction of a coast-line evolution is in creating a qualitative picture giving eroding and accreting areas, but limited in its quantitative accuracy.

5.2.6 The NOURTEC cases (Terschelling; Norderney; Thorsminde)

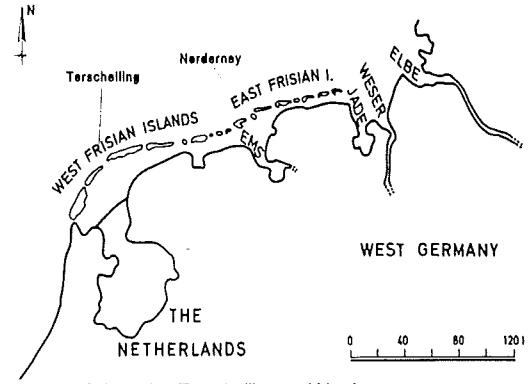

Figure 5.58: Location Terschelling and Norderney

The NOURTEC- project is an EU-research project in the scope of the program for Marine Science and Technology (MAST II). Purpose is Innovative Nourishment Techniques Evaluation. For aim and scope is referred to Mulder et al.(1994). National coastal authorities in three different countries around the North Sea (Germany, the Netherlands and Denmark) have carried out full-scale experiments with alternative coastal nourishment techniques (i.e. shoreface nourishments and combinations of shoreface and beach nourishments). These experiments are implemented under a range of environmental conditions. Extensive modelling and monitoring programmes form an essential part of the projects.
One kind of models used for this goal are line-models. These will be applied on all selected supply sites in the three participating countries.
The present paper deals with the prediction of the coastal behaviour with the aid of those models and comparison with prototype data for the Dutch and German supply: at Terschelling and Norderney (fig.5.58) respectively. In the future, also an analysis of the Danish supply will be given. A more detailed description of the investigations is given by Bakker & Kersting (1994) and by Kersting, Bakker & Niemeyer (1995) respectively.

5.2.6.1 Terschelling

Situation

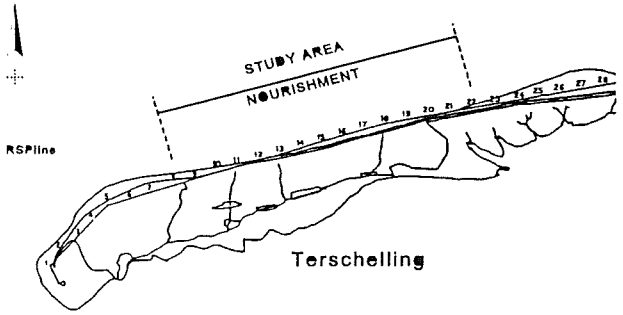

Figure 5.59: Location study area Terschelling

An underwater supply of ca. 2 Mm3 has been carried out in spring and summer of 1993 on the Dutch Wadden isle of Terschelling. Fig. 5.59 shows the site.
Three breaker bars are gradually moving seaward along the whole stretch; motion is periodic; the mutual distance between the breaker bars is 500 m; seaward propagation velocity is 50 m and period 10 years. Depth-averaged (between NAP + 3m and NAP - 2.75m; "NAP" denotes a level, which is about mean sea level) the area under consideration shows a coastal retreat of about 2.75 m/year.

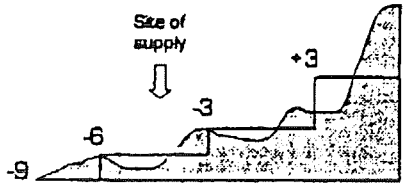

Figure 5.60: Schematization 3-line theory

Three-line model

For the principles of line modeling is referred to the literature (Bakker, 1968 etc.).
In the three-line model (used here) the coastal zone is schematized in three zones (fig. 5.60), which will be called: "beach", "inshore" and "deeper part".

In each zone it is assumed that all contour lines remain parallel and that the profile in this zone only moves horizontally. It is sufficient to compute only an average line in each zone, because it characterizes this zone. There is assumed to be a horizontal separation plane between the zones.
The sediment transport between the lines is assumed to be proportional to the difference between the equilibrium distance and the actual distance between the characterizing lines. In the present application an initial equilibrium position (before any supply takes place) is assumed, where the three lines are straight and parallel (fig.5.60a). Distances y_1, y_2, y_3 are the deviations of the lines of the beach, inshore and deeper part, compared with this initial position. The y-value is computed by dividing the surplus volume in a zone (with respect to the initial position) by its height. In case $y_1 = y_2 = y_3$, the profile again is an equilibrium slope. If longshore transport could be neglected (see Appendix) then the coast would tend to this equilibrium, if for instance sand on the inshore would have been supplied (fig. 5.60a).

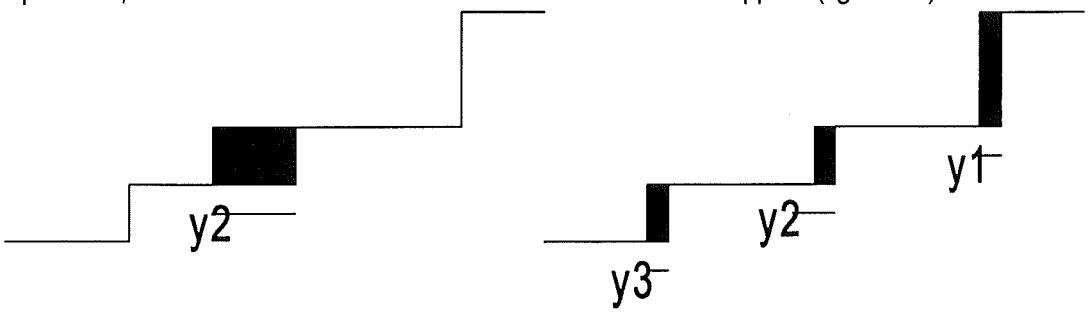

Figure 5.60a: Definition y_1, y_2, y_3

The process, sketched in the previous section results in cross-shore diffusion of sand. Adding longshore diffusion to the cross-shore diffusion, following the approach of Pelnard-Considere (1954) and Bakker (1968), the following dynamic equations can be derived:

$$\frac{dy_1}{dt} = \frac{s_1}{h_1} * \frac{\delta^2 y_1}{\delta x^2} - \frac{s_{y_1}}{h_1} * (y_1 - y_2) \qquad (5.43a)$$

$$\frac{dy_2}{dt} = \frac{s_2}{h_2} * \frac{\delta^2 y_2}{\delta x^2} + \frac{s_{y_1}}{h_2} * (y_1 - y_2) - \frac{s_{y_2}}{h_2} * (y_2 - y_3) \qquad (5.43b)$$

$$\frac{dy_3}{dt} = \frac{s_3}{h_3} * \frac{\delta^2 y_3}{\delta x^2} + \frac{s_{y_2}}{h_3} * (y_2 - y_3) \qquad (5.43c)$$

On the lefthand side is the accretion of line of beach, inshore and deeper part respectively. On the righthand side the longshore transport is determined by the constants s_1, s_2 and s_3 respectively; the cross-shore transport ("beach to inshore" and "inshore to deeper part") by s_{y1} and s_{y2} respectively. $h_{1,2,3}$ denotes the depth allotted to the three zones.
Fig 5.61 shows the diffusion of the (originally rectangular) supply shape in longshore direction in the course of time.

Figure 5.61: Diffusion of supply

5.2.6.2 Coastal constants

Cross-shore constants
From the supply (between two breaker bars; fig. 5.60) the breaker bars get an "antropogenic distortion". It is assumed, that by a diffusion process the sand, involved in this distortion will diffuse to the neighbouring breaker bars. Furthermore, it is assumed, that the velocity of diffusion is related to the time laps between the replacement of one bar by the next landward

bar. Per cycle, a certain percentage (determined by "engineering judgement") is retained; the rest of the sand is transported to the two adjacent breaker bars.
The engineering judgement is based upon the solution of Smit (1987) for the cross-shore diffusion, reproduced in the Appendix.
From his equations it can be derived, that in a period T_{01} (defined in Appendix) the process of spreading the supply evenly over the profile is almost 80 % completed. It seems logical to assume, that the diffusion process to a similar rate is accomplished during the propagation period of the bars. The periods T_{01} and T_{02} are therefore chosen both equal to 10 years. With values for $h_{1,2,3,}$ as shown in fig. 5.60 (6m, 3m,3m), values of s_{y1} and s_{y2} of .2 and .15 m/year respectively are found. A higher cross-shore diffusitivity. At the upper part is found than at the lower part, which seems reasonable.
It is assumed that processes, dominated by the diffusion of the supply can be linearly superponed to the natural longshore and cross-shore coastal processes. The latter processes are implemented by assuming an autonomous erosion of 2.75 m/yr for the zone between NAP -9m and NAP + 3m.
In the mathematical model it is assumed that cross-shore transport of supply below a level of NAP -9m is neglegible (during the time of consideration) compared to the transport above this level. Thus, in the model no period averaged cross-shore transport by the periodical motion of the breaker bars is assumed.

Longshore coastal constants.

To determine the longshore constants for the line-model use is made of the CERC-formula and the assumptions of Svasek (1968): the local sediment transport between two contour lines is proportional to the longshore component of the decrease of the energy flux between those two lines.
For detailed description is referred to Svasek (1968), Svasek & Bijker (1969), Bakker (1969), Bakker, ten Hoopen & Grieve (1972), Ten Hoopen & Bakker (1974) and to Bakker, V.d.Kerk & De Vroeg (1988).

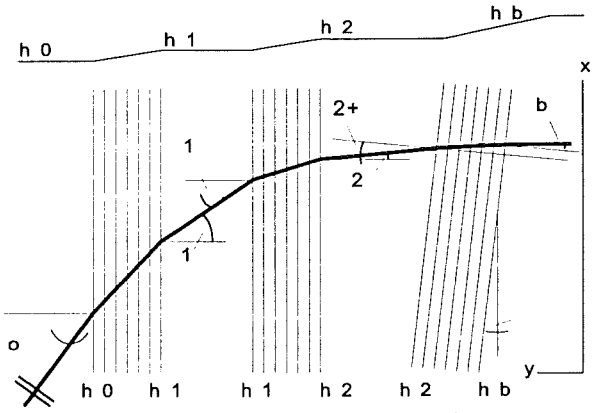

Figure 5.62: Schematization used for transport computations

Sloping shores have been assumed between terraces, separating beach, inshore and deeper zone; local wave height is taken proportional to local depth.
Total wave climate has been taken into account, taking discrete wave classes, each defined by a certain wave height *H*, period *T* and direction ϕ and a probability of occurrence:

$$S_\phi = S_{H.T.\phi} \cdot P_r(H,T,\phi) \qquad (5.44)$$

Fig. 5.63 shows the various classes of wave direction, translated into angles of incidence.

Vertical tide has been taken into account by discretization in a number of levels, combined with probabilities; furthermore it has been taken into account, that high waves from certain directions are linked with water level rise (storm surge height). The black arrows in fig. 5.64 give the transport rates when all contour lines are parallel. Under those circumstances the method results in a total depth-integrated longshore transport for a certain *H, T,* ϕ

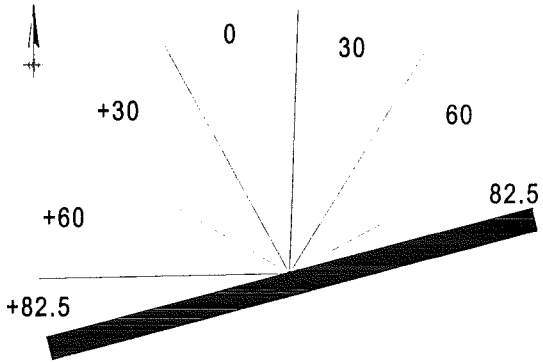

Figure 5.63: Directions of wave approach

as given by the CERC-formula:

$$S_x = 0.040 * H_{b,sig}^2 * n_b * c_b * cos(\varphi_b) * sin(\varphi_b) \qquad (5.45)$$

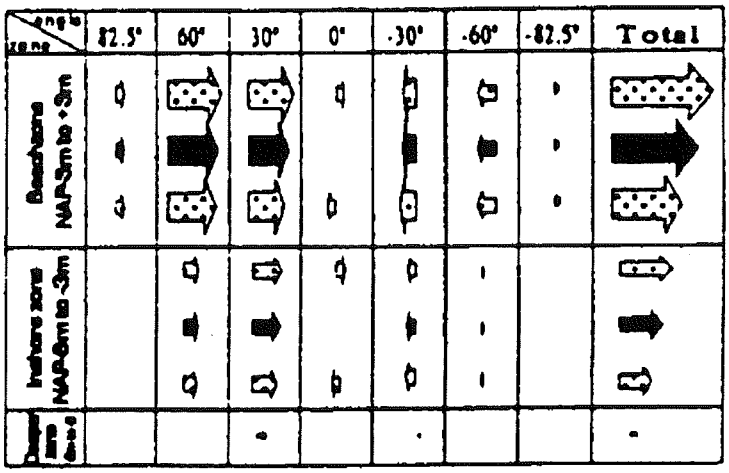

Figure 5.64: Transport rates along the three zones as a function of the angle of approach of the waves at deep water and the effect of $\delta = \pm 2°$.

	82.5°	60°	30°	0°	-30°	-60°	-82.5°	Σ
+2°	41.42	500.4	431.4	40.53	-116.6	-86.03	-10.14	804.2
0°	40.55	478.3	387.3	0	-128.7	-87.91	-10.25	679.3
-2°	39.46	453.8	341.2	-40.53	-142.1	-90.54	-10.30	551.0
+2°	0.004	68.36	161.9	15.22	-38.16	-0.830	0	196.5
0°	0.004	67.57	148.5	0	-41.98	-0.818	0	165.3
-2°	0.004	66.30	134.4	-15.22	-45.56	-0.712	0	131.2
0°	0	0	5.518	0	-1.428	0	0	4.09

Tabel: 5-6: Transport rates (10^3 m³/yr) The volumes of the arrows in figure 5.64 are proportional to numbers in table 5-6

The columns in fig.5.64 denote the various angles of wave incidence; the "rules" the three zones. The volumes of the arrows are proportional to the transport (weighted with its probability of occurrence) integrated over all classes of H and T. Probability of occurrence has been derived from SON, a measurement station in the vicinity of Schiermonnikoog. Wave data have been made available by Rijkswaterstaat (Roskam 1988).

Calculated numerical values of transport rates (in thousands m^3 /year) are depicted in table 5-6 (the lines "0 degree "; for beach, inshore and deeper zone respectively).

For both upper zones the longshore transport has been computed three times for each wave direction: apart from assuming parallel depth contours also the angle of the beach (inshore) has been turned over an angle delta with respect to the other contour lines. For instance: in fig 5.62 the angle of the beach is turned. The gray arrows in fig 64 show the effect, where delta has been chosen ± 2°. Table 5-6 shows the numerical results.
The constants s_1 and s_2, which can be shown theoretically (Pelnard Considere, 1954) to be the derivative of the longshore transport to the coastal direction, are calculated from:

$$s_i = \frac{\sum_{+82.5°}^{-82.5°} [S_i(\varphi_i + \delta) - S_i(\varphi_i - \delta)]}{2 * \delta}$$

$$s_1 = \frac{804.2 - 551}{2 * 2 * \frac{\pi}{180}} * 10^6 = 3.63\,10^6 \quad m3/year/rad \qquad (5.46)$$

$$s_2 = \frac{198.5 - 131.2}{2 * 2 * \frac{\pi}{180}} * 10^6 = 0.964\,10^6 \quad m3/year/rad$$

Results.
For s_1 and s_2 values of $3.63*10^6$ and $.96*10^6$ m^3/year/rad were found; the calculation of the total longshore transport gave $.85*10^6$ m^3/year as result. it was found, that diffusitivity in longshore direction along the deeper part could be neglected. Effect of curvature of the inshore on the coastal constant for the beach (the inshore turns more or less in the same way at the same time as the beach) has not been taken into account. Neglecting this effect can give a rather important overestimate of the coastal constant of the beach (Bakker & Delver, 1986; Bakker et al., 1988).
Another extreme (no longshore diffusion) is given by the formulae of Smit (1987) (Appendix)

Fig 5.65a,b,c shows (extreme high diffusitivity) a plan view of the expected development of beach, inshore and deeper part (mind the different vertical scales). The autonomous erosion of the coast is depicted on the righthand side of the figure.

Figure 5.65:a,b,c: Lines of beach, inshore and deeper part $y_{1,2,3}$

Figure 5.66a,b,c Site of beach, inshore, deeper part in the course of time (in center of supply)

Fig.5.65a,b,c show the expected position (in the course of time) of the line of the beach, inshore and deeper part, in the center of the supply area.
Both extremes (no c.q. extreme longshore diffusitivity) are shown, where autonomous erosion is not taken into account. A more seaward position is indicated in positive direction. The drawn lines show the development, if one ignores the autonomous coastal erosion. The beach would increase, the inshore (where the supply was applied at *t= 0*) would retreat from its exposed position. Finally, supply sand would spread evenly over the profile.

The interrupted lines in fig. 5.66a,b,c show the rate of autonomous coastal erosion at the same scale, more exactly: the amount of cumulative supply, necessary to balance this kind of erosion. During the time the drawn line lies above (c.q. below) the interrupted line, the beach, c.q. inshore has a more seaward (c.q. landward) position than just before the application of the supply. It shows, that according to the computations the supply will stop the erosion of the beach during the order of a decennium, without causing considerable accretion.

5.2.6.3 Norderney

Conditions at the site of supply.

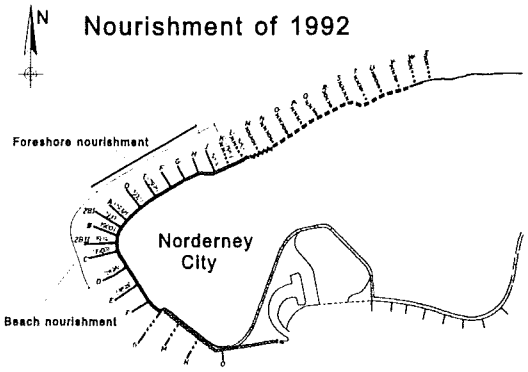

Figure 5.67: Combined beach and shoreface nourishment. Coastal protection.

Near the west point of the German Wadden island of Norderney, 450.000 m^3 of sand has been supplied in 1992 to the beach and the shore-face (fig. 5.67).
The seaward limit of the nourishment coincides with the 5 m depth contour. The coastline is protected by groynes, revetments and sea-walls. For the largest part the area is inside the "Riffbogen" (bars formed by the outer delta). Wave attack is important on the North West side.
At the South West side (Norderneyer Seegat) current dominates (cf. Thilo & Kurzak (1952), Luck (1977) and Niemeier (1986 a,b,c, 1990 and 1992)).

Since the first artificial nourishment (1.25 Mm^3 in 1951/52) (major) sand supply in this area and its vicinity was repeated 6 times (incl.1992). Fig. 5.67 shows the area of coastal nourishment in 1992: an amount of ..5m^3, of which 5O % supplied above NN-1m (as NAP the level NN is about mean water level). Ca. 20% was supplied between NN-3m and NN-Sm.

Wave climate and wind set-up

The outer delta largely shelters the considered area from the deep water wave field. However, even more than at Terschelling, high waves and high surge levels are often linked together. Kersting et al. (1995) compute the sand transport using the SON deep water wave climate as well .for Norderney as well as Terschelling. However, storm surge levels at Norderney are higher than at Terschelling. Thus, if Norderney would have been located near Terschelling, its (present) outer delta would give better protection; it would reduce wave height at the Westpoint shore more than in the present situation. Kersting et al. estimate that the effect of location on the surf height results (for the same wind, i.e. offshore wave height) in surge top water level rises, being 22% higher at Norderney than at Terschelling. They use as well theoretical considerations (Schalkwijk (1947) and Weenink (1958)) as well as analysis of the SON wind and wave data.

Sand transport computations

Schematization

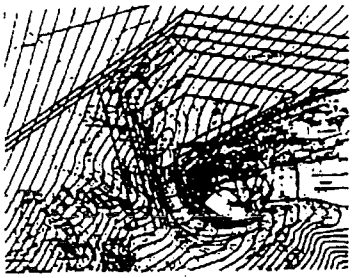

Figure 5.67a: Refraction pattern

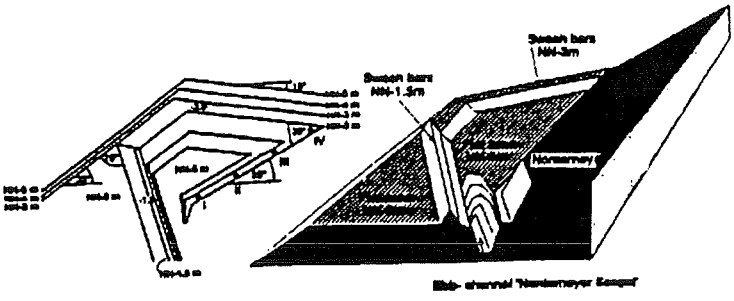

Figure 5.67b: Schematization and points I to IV

Figure 5.67c: Schematization (3D)

Investigations concern the coastal area with a length of ca 5 km between the tidal inlet and the site where the outer delta merges with the island (between point I to IV; fig 5.67b).The wave climate on the inshore and the beaches in this area is strongly influenced by the bars of this outer delta. These bars reduce the energy of the incoming waves and also influence the propagation direction of the waves by refraction.
Fig 5.67b,c shows the schematization chosen; contour lines are schematized to sets of parallel straight lines. Furthermore, fig. 5.67a displays the real contour lines and a refraction diagram, from Niemeyer (1986), which idicates an analogy in similarity of hydraulic response between schematization and prototype. Further research with respect to this aspect is proceeding. Convergence and divergence of wave rays are, in the schematization, partially taken into account: difference in direction of beach and inshore is implemented. However, the effect of the curvature of beach and inshore on the refraction coefficient is not taken into account. By the chosen schematization, the three parts of the outer delta together act as a convex lens, focussing the wave rays. From the refraction diagram of fig.5.67a the same picture arises. Because of this, a convex beach, making everywhere (about) the same angle with the wave crests will be stable, where for an offshore topography with totally straight contour lines, parallel to the beach, a straight beach would have been stable. This explains the convex character of the Westend of the island.
Up to now, only the transport along the shore (beach and inshore) of the island has been calculated. The transport along the seaward shoreface of the outer delta will be calculated in the future. Again, the Svasek method of computation has been used (cf. ch.2 for literature). Effects of current are not taken into account. Preliminary computations concerning diffusitivity constants $s_{1,2}$ vhave been carried out (for point IV; fig. 5.67b) by varying the direction of beach or inshore as done in ch.2. Apart from this, diffusitivity constants for Norderney will be calculated from measured data.

Results

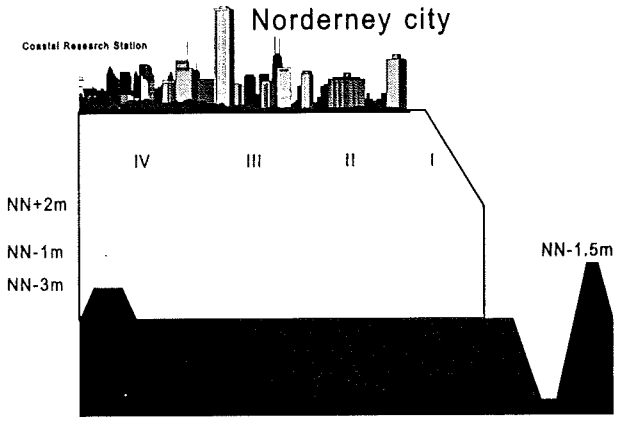

Figure 5.68: Transport capacity (without groynes) if the coast is assumes straight

Fig. 5.68 shows the calculated transport capacities in the points I to IV , which would occur, if the coastline is assumed straight. It shows£ that accretion in the coastal area between points I and IV would result (according to the computations). Longshore diffusitivity constants s_1 and s_2 in point IV are $.6*10^6$ and $2.8*10^6$ m^3/year/rad for beach and inshore respectively. From the values calculated one would find, that a convex coast with a difference in coastal direction of ca.9° to 12° between point I and point IV (fig. 5.67b) would give a stable coast. The present difference in coastal direction is ca 15° (which is greater) thus erosion (as occurs) can be expected the computations Referred to Kersting et al. (1995) As the accuracy is low, the result has only qualitative importance.
Because of the existing groynes the real transport, along the inshore, will be much less than the transport capacity. Bakker & Joustra (1970), comparing coastal erosion along the dutch coast before and after the construction of groynes, indicate, that groynes might reduce coastal transport with a factor of 4. This would reduce the value of s_2 case of erosion) in the same way.

Line modeling

Coastal constants; relation between curvature~and erosion

Bakker (1968b) describes another way find the coastal constants: from coastal measurements. The data for volumetric change and curvature are related; latter taken as difference of coastal direction $\Delta\phi$ between left side and right side of the stretch. In order to obtain uniformity of data, a stretch of (only) 890 m (between groynes "A" and "H1") near the Western end of Norderney has been analyzed. Fig. 5.69 displays this relationship; from this figure Kersting et al. (1995) derive values of s_1= 1.2·10^6 and s_2=.9·106 m^3/year/rad. As for the first observation (encircled in fig.14b) leading to s_2 the groynes will have been less effective (the supply extended further seaward than the groynes), this observation has been discarded, leading to s_2=.2·10^6 m^3/year/rad. Based upon fig. 69d, s_3 has been taken zero. The constants $s_{y1,2}$ (both assumed as 4 m/year) have been found by estimating T_{01} from the measurements and by iterative approximation, using the numerical three-line model (ch.2.2). Initial- and boundary conditions are imposed by prototype data.

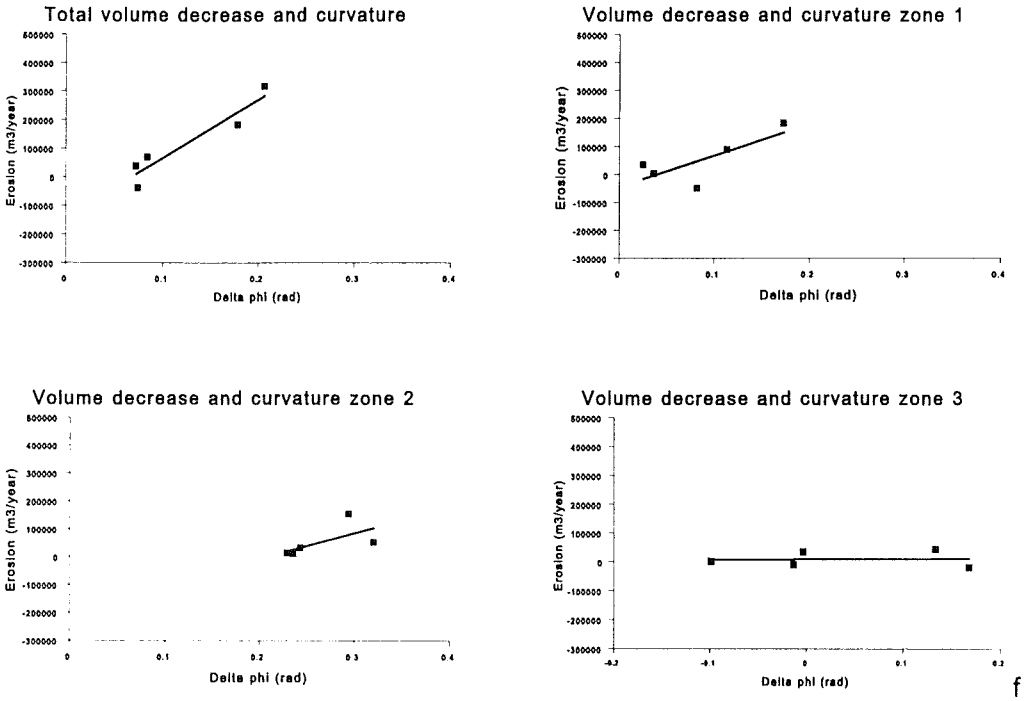

Figure 5.69a,b,c,d: volume decrease & curvature

Results

In the Norderney case, "$y_{1,2,3}$" will be defined as the surplus volume remaining after the supply, (expressed in m^3/m'/m depth) between 2 successive separation planes (see fig.68). Comparison between measurement and computation gives ($y_{1,2,3}$=$f(x)$; t as parameter) and fig 5.70 ($y_{1,2,3}$= $f(t)$; x in the center of the field). For y_1 and y_2 good agreement is found; y_3, which in the model can only change because of cross-shore transport, appears to remain too large in the model. This suggests scour by current in the area below the groynes.

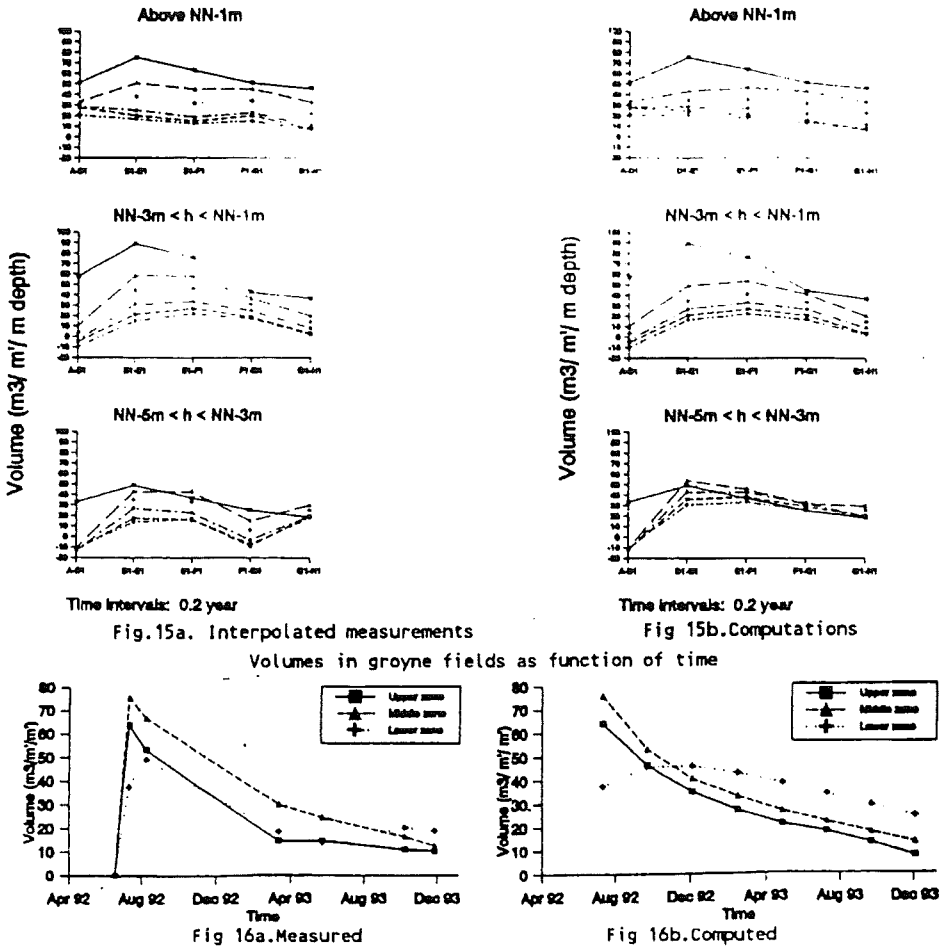

Figure 5.70a,b,c,d: Volumes in central groyne section

5.2.6.4 Discussion and conclusions.

Terschelling

Depending on the assumptions (of which the extremes are: "only cross-shore diffusitivity" and "cross-shore plus unfavorable high value of longshore diffusion", a "life time" of the supply can be estimated, This varies respectively between 13 and 7 years (estimating the autonomous erosion as 2.75 m/year).

Norderney

- Concerning Norderney only preliminary conclusions and some indications can be given. Comparing longshore coastal constants.derived from transport formulae and from evaluation of topographic field data the s_2-value, found from those field data is lower than expected (even considering the effect of the groynes), where the s_1- value is considerably larger. The total of s_1+s_2) is in the expected range.
- The coastal measurements indicate much larger longshore diffusitivity on the beach (above NN - 1 m) than on the inshore (NN-3 m<h<NN-1 m).
- In the future effects of currents should be carefully examined, especially concerning the zone seaward of the groynes. Three-line model (which is able to reproduce the development of beach and inshore rather well) underestimates (without current effects) the erosion of the deeper zone.

General

- Comparison of coastal constants in general for various stretches of coast is given by Bakker et al. (1988). In that scope, the maximum values of the longshore diffusitivity assumed for Terschelling are rather high: values of 1 to $2 \cdot 10^6$ are more common.
- The cross-shore transport constants $s_{y1.2}$ are (physically) strongly dependent upon the depth of the separation plane, as well on the schematization. Compared to the values, mentioned by Bakker et al. (1988), the cross-shore transport constants assumed for Terschelling are somewhat low. For instance, using Kalman filtering, de Vroeg (1987) finds $s_y \approx .7$ m/year at NAP
- .72m ($T_{01} \approx 7$ years) for the Dutch Rijnland-coast. Compared to this, the value of $y_{1.2}$ of 4 m/year at NAP
- -3m ($T_{01} = 0.4$ year and $T_{02} = 0.25$ year) seems extremely high. Up to now, T_0-values of the order of 1 year were the smallest ever found (in Cadzand, CUR et al.,1986; $s_y = 3$ m/year at NAP -2m). As in Norderney, in Cadzand a tidal channel is near to the coastal area. In the Norderney case, the wave attack is probably larger than in Cadzand.

The difference in character between the supplies of Terschelling and Norderney is remarkable

- Supplying high on the beach instead of on the inshore would have been favorable for the Terschelling case if the costs of supplying on beach or inshore would have been equal. In Norderney however this is different because (most probably) the groynes largely reduce the longshore diffusitivity of the inshore (compared to the beach).
- Probably the deeper zone in Norderney will show to be more active (current effects near to the Norderneyer Seegatt) than at Terschelling.
- Different as well is the goal of both supplies, which emphasizes the importance of the offshore nourishment in Norderney::Were the supply forms an essential part as a maintenance measure for the coastal protection by reducing the damage to the coastal defence works (sea-walls and groynes). This goal was formulated in 1952 (Arbeitsgruppe Norderney) and it has been shown to be very cost effective since then.

5.3 Literature

1. BAKKER W.T.;
   The dynamics of a coast with a groyne system.
   11th Conf. on Coastal Engineering, Ch. 31, London 1968

2. BAKKER W.T., KLEIN BRETELER, E.H.J. and ROOS, A., The dynamics of a coast with a groyne system. 12th Conf. on Coastal Engineering, Ch. 64, Washington
3.
4. DELFT HYDRAULICS LABORATORY;
   The influence of groynes on the coast, Report M 918 part I (experiments) March 1976 (in Dutch)

5. BARCELO, J.P.;
   Experimental study of the hydraulic behaviour of groyne Systems.
   11th Conf. on Coastal Engineering, Ch. 13, London 1968

6. BIJKER, EW.;
7. Longshore transport computations.
   Proc. A.S.C.E., vol. 97, ww 4, pp. 687-701, November 1971

8. SWART, D.H.;
   A schematization of onshore-offshore transport.
   14th Conf. on Coastal Engineering, Chapter 51, Copenhagen 1974

9. DELFT HYDRAULICS LABORATORY;
   Comparison of theoretical and experimental coast lines, Report N 918 partIII, 1976 (in Dutch)

10. BOCHOVE, C. van;
    Elaborations of a model test conducted by Barcelo. Memo 72-2! of Rijkswaterstaat, Dir. Water Management and Water Movements, Section Coastal Research, The Hague 1972

11. BAKKER, W.T.;
    The influence of longshore variation of the wave height on the littoral current.
    Study-Report WWK 71-19 of Rijkswaterstaat, Dir. Water Management and Water Movements, Section Coastal Research, The Hague 1971

12. HULSBERGEN, C.H.;
    Origin, effect and suppression of secondary waves.
    14th Conf. on Coastal Engineering, Chapter 22, Copenhagen 1974

13. BYRNE, R.J.;
    Field occurrences of induced multiple gravity waves.
    Journ. of Ceoph. Res., vol. 74, 1969, no. 10, May 15, pp. 2590-2596

14. CALVIN, C.J.;
    Classification of breaking waves on three laboratory beaches.
    Res. Divn, 1967.

15. Patzold (1980

16. Bakker,W.T. & J.H. de Vroeg (1987)
    Coastal modeling and coastal measurements in the Netherlands
    Proc. Seminar SOGREAI': Prototype measurements to validate numencal models of coastal processes, Grenoble.

17. Bakker,W.T, (1969)
    Calculation of the longshore wave driven transport using the method of parallel depth

contours, (in Dutch).
Dutch ministry of public works, repon WWK 69-7.

18. Casteleyn. A. (1975)
Numerical calculations of coastal changes...(in Dutch)
Delft University of technology, technical report 75-1

19. Dijkman,M.J., W.T. Bakker & J.IL de Vroeg (1989)
Two-line model for the Holland Coast (in Dutch). Voorspelling ontwikkeling kustlijn 1990-2090,
Fase 3, deelrapport 3.2 (van Technisch rapport 5).
Dutch ministry of public works (Rijkswaterstaat)

20. Dorrestein,R. (1964)
Wind and wave data of the Netherlands Lightvessels.
Royal Dutch Meteorological Institute, 'Mededelingen', nr.90

21. Dutch Ministry of Public Works (1989)
Kustverdediging na 1990 (Coastal Defense after 1990),

22. Hartsuyker,G. (1988)
Tidal flow niodel for the holland coast (in dutch).
Delft Hydraulics

23. Hokke,A.W. & A.P.Roskam (1987)
Measured deep water wave climate (in dutch)
Rijkswaterstaat, Tidal Waters Division, GWAO 87.291

24. de Mulder,E.J.F. (1983);
Geological history of the Hondsbossche Seawall (in Dutch)
'vrienden van de Hondsbossche', 3 edition
Rijks geologische dienst

25. Pilarczyk, K.W. and J.v.Overeem (ed.) (1986);
Manual on Artificial Beach Nourishment

26. Stive,MJ.F.,J.A.Roelvink & H.J. de Vriend (1990);
Large scale coastal evolution concept.

27. De Vroeg J.H., E.S.P. Smit & W.T. Bakker (1988);
Coastal Genesis
21st int. Conf. On Coastal Engng., Malaga

28. Bakker, W.T. (1968a);
"The dynamics of a coast with a groyne system-" Proc. 11th cong. on coastal engng., London

29. Bakker, W.T. (1968b);
"A mathematicaL theory about sand waves and its application on the Dutch wadden Isle of vlieland" Shore and Beach

30. Bakker, W.T. & D. Sj. Joustra (1970);
"The History of the Dutch coast in the Last century"
Proc. 12th cont. on coastal Engng., Washington

31. Bakker W.T., N.G.H ten Hoopen & G.R.K.Grieve (1971);
"Berekening van het zandtransport volgens de methods Svasek bij een strand en een vooroever, die een hoek met elkaar maken."(Computation of the sand transport according to the Svasek method, when beach and inshore make an angle with each other (in dutch)

Rijkswaterstaat, Dir. for Water Management and hydraulic Res., Dept. for coastal Res. Study Rep WICK 71-18

32. Bakker, W.T. & G.Delver (1986);
"Coastal changes, caused by a shallow water sanddam in front of the Delfland coast."
Delft university of Technology; coastal Engineering Group.

33. Bakker,W.T., C.v.d.Kerk & J.H. de vroeg (1988);
"Detemination of coastal constants in mathematical line modeLs." 2nd European workshop on coastal zones, as related to Physical Processes and coastal structures

34. Bakker, W.V. & N.F.Kersting (1994);
"Pilot study concerning the behaviour of coastal supply on the Dutch Wadden island of Terschelling."
Delft University of Technology; coastal Engineering Group.

35. CUR. Rijkswaterstaat. Delft Hydr.Lab. (1986);
Manual on Artificial Beach Nourishment.

36. ten Hoopen. H.G.H & W.T.Bakker (1974);
"Erosion problem of the Dutch IsLand of Goeree" Proc. 14th mt. Conf. on coastal Engng., Copenhagen, 1974

37. Kersting, N.F., W.T.Bakker & H.D.Niemeyer (1995);
"Evaluation of a combined foreshore and beach nourishment at the German wadden Island of Norderney
Delft University of Technology; coastal Engineering Group and coastal Research Station Norderney

38. Kroon, A., P.Hoekstra, J.P.M.Mulder, D.Roelvink, K.T. Houwan & B.G. Ruessink (1994);
"Process-oriented monitoring of a shoreface nourishment; NOURTEC experiment at Terschelling, the NetherLands"
Proc. 24th Int.conf.on Coastal Engng-, Kobe, Japan.

39. Luck, G. (1977);
"Inlet changes of the East Frisian Islands"
Proc. 15th Int.Conf.on Coastal Engng., HonoluLu

40. Mulder, J.P.M., J.v.d.Kreeke. P.van Vessem (1994);
"Experimental shoreface Nourishment. Terschelling (NL)."
Proc. 24th Int.conf.on coastal Engng.. Kobe, Japan.

41. Niemeyer. H.D. (1986);
"Ausbreitung and Dampung des seegangs im See- und Wattengebied von Norderney"
(Spreading and attenuation of swell around Sea and Wadden of Norderney, in german)

42. Niemeyer, H.D. (1990);
"Morphodynamics of tidal inlets" course "CoastaL Morphology" Delft University of Technology; Proc. COMETT-course

43. Pelnard considere, R. (1954);
44. "Essai de theorie a l'evoLution des forms de rivages en plages de sable et de galets.
"Quatrieme Journees de 'I Hydraulique, Paris 13-15 Juin 1954. Les Energies de La Mer Question 3

45. Roskam, A.P. (1988);
"Golfklimaten langs de NederLandse kust" (Wave climates along the dutch coast; in dutch) Rijkswaterstaat, Dienst Getijdewateren

46. Schalkwijk, N. (1947);
"A contribution of the study of storm surges on the Dutch coast."

K.N.M.I. Med. & verh. Series B, part I, no.7

47. Smit, E.S.P. (1987);
"De rol van het sediment dwarstransport in de ontwikkeling van de Hollandse kust." (The effect of cross-shore transport for the development of the Dutch coast; in dutch) Delft university of Technology; Coastal Engineering Group.

48. Svasek, J.N. & E.w.Bijker (1969);
"Two methods for determination of morphological changes induced by coastal structures." XXIInd Int.Mav. congress Paris, Section II, item 4.

49. Thilo, R. & G.Kurzak (1952);
"Die Ursachen der Abbrucherscheinungen am West- und Nordwest-Strand der Insel Norderney" (the causes of erosion at the West- und North-west-beach of the island Norderney; (in Gernan) Die Kuste

50. van Vessem, P. (1992);
"Morfologische analyse kustvak Terschelling, raai 13 tot 20." (Morphological analysis coastal area Terschelling; range 13 to 20; in dutch)
Rijkswaterstaat. Tidal waters Division

51. de Vroeg, J.H. (1987);
"The use of Kalman filtering for investigation of coastal behaviour."
Delft University of Technology; coastal Engineering Group.

52. Weenink, M.P.H., (1958);
"A theory and method of calculation of wind effect on sealevels in a partly enclosed sea, with special application to the southern coast of the North sea."
K.N.M.I. Med. & Verh. no. 73